

Sustainable Concrete for the Green Construction Industry

Lead Guest Editor: Md. Akter Hosen

Guest Editors: Huzaifa Hashim and Imran Hosen





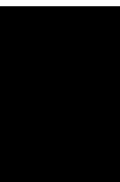
Sustainable Concrete for the Green Construction Industry

Advances in Civil Engineering

Sustainable Concrete for the Green Construction Industry

Lead Guest Editor: Md. Akter Hosen

Guest Editors: Huzaifa Hashim and Imran Hosen



Copyright © 2023 Hindawi Limited. All rights reserved.

This is a special issue published in "Advances in Civil Engineering." All articles are open access articles distributed under the Creative Commons Attribution License, which permits unrestricted use, distribution, and reproduction in any medium, provided the original work is properly cited.






Chief Editor

Cumaraswamy Vipulanandan, USA














Associate Editors

Chiara Bedon , Italy
Constantin Chalioris , Greece
Ghassan Chehab , Lebanon
Ottavia Corbi, Italy
Mohamed ElGawady , USA
Husnain Haider , Saudi Arabia
Jian Ji , China
Jiang Jin , China
Shazim A. Memon , Kazakhstan
Hossein Moayedi , Vietnam
Sanjay Nimbalkar, Australia
Giuseppe Oliveto , Italy
Alessandro Palmeri , United Kingdom
Arnaud Perrot , France
Hugo Rodrigues , Portugal
Victor Yepes , Spain
Xianbo Zhao , Australia

Academic Editors

José A.F.O. Correia, Portugal
Glenda Abate, Italy
Khalid Abdel-Rahman , Germany
Ali Mardani Aghabaglou, Turkey
José Aguiar , Portugal
Afaq Ahmad , Pakistan
Muhammad Riaz Ahmad , Hong Kong
Hashim M.N. Al-Madani , Bahrain
Luigi Aldieri , Italy
Angelo Aloisio , Italy
Maria Cruz Alonso, Spain
Filipe Amarante dos Santos , Portugal
Serji N. Amirkhanean, USA
Eleftherios K. Anastasiou , Greece
Panagiotis Ch. Anastasopoulos , USA
Mohamed Moafak Arbili , Iraq
Farhad Aslani , Australia
Siva Avudaiappan , Chile
Ozgur BASKAN , Turkey
Adewumi Babafemi, Nigeria
Morteza Bagherpour, Turkey
Qingsheng Bai , Germany
Nicola Baldo , Italy
Daniele Baraldi , Italy

Eva Barreira , Portugal
Emilio Bastidas-Arteaga , France
Rita Bento, Portugal
Rafael Bergillos , Spain
Han-bing Bian , China
Xia Bian , China
Huseyin Bilgin , Albania
Giovanni Biondi , Italy
Hugo C. Biscaia , Portugal
Rahul Biswas , India
Edén Bojórquez , Mexico
Giosuè Boscato , Italy
Melina Bosco , Italy
Jorge Branco , Portugal
Bruno Briseghella , China
Brian M. Broderick, Ireland
Emanuele Brunesi , Italy
Quoc-Bao Bui , Vietnam
Tan-Trung Bui , France
Nicola Buratti, Italy
Gaochuang Cai, France
Gladis Camarini , Brazil
Alberto Campisano , Italy
Qi Cao, China
Qixin Cao, China
Iacopo Carnacina , Italy
Alessio Cascardi, Italy
Paolo Castaldo , Italy
Nicola Cavalagli , Italy
Liborio Cavaleri , Italy
Anush Chandrappa , United Kingdom
Wen-Shao Chang , United Kingdom
Muhammad Tariq Amin Chaudhary, Kuwait
Po-Han Chen , Taiwan
Qian Chen , China
Wei Tong Chen , Taiwan
Qixiu Cheng, Hong Kong
Zhanbo Cheng, United Kingdom
Nicholas Chileshe, Australia
Prinya Chindaprasirt , Thailand
Corrado Chisari , United Kingdom
Se Jin Choi , Republic of Korea
Heap-Yih Chong , Australia
S.H. Chu , USA
Ting-Xiang Chu , China


Zhaofei Chu , China
Wonseok Chung , Republic of Korea
Donato Ciampa , Italy
Gian Paolo Cimellaro, Italy
Francesco Colangelo, Italy
Romulus Costache , Romania
Liviu-Adrian Cotfas , Romania
Antonio Maria D'Altri, Italy
Bruno Dal Lago , Italy
Amos Darko , Hong Kong
Arka Jyoti Das , India
Dario De Domenico , Italy
Gianmarco De Felice , Italy
Stefano De Miranda , Italy
Maria T. De Risi , Italy
Tayfun Dede, Turkey
Sadik O. Degertekin , Turkey
Camelia Delcea , Romania
Cristoforo Demartino, China
Giuseppe Di Filippo , Italy
Luigi Di Sarno, Italy
Fabio Di Trapani , Italy
Aboelkasim Diab , Egypt
Thi My Dung Do, Vietnam
Giulio Dondi , Italy
Jiangfeng Dong , China
Chao Dou , China
Mario D'Aniello , Italy
Jingtao Du , China
Ahmed Elghazouli, United Kingdom
Francesco Fabbrocino , Italy
Flora Faleschini , Italy
Dingqiang Fan, Hong Kong
Xueping Fan, China
Qian Fang , China
Salar Farahmand-Tabar , Iran
Ilenia Farina, Italy
Roberto Fedele, Italy
Guang-Liang Feng , China
Luigi Fenu , Italy
Tiago Ferreira , Portugal
Marco Filippo Ferrotto, Italy
Antonio Formisano , Italy
Guoyang Fu, Australia
Stefano Galassi , Italy

Junfeng Gao , China
Meng Gao , China
Giovanni Garcea , Italy
Enrique García-Macías, Spain
Emilio García-Taengua , United Kingdom
DongDong Ge , USA
Khaled Ghaedi, Malaysia
Khaled Ghaedi , Malaysia
Gian Felice Giaccu, Italy
Agathoklis Giaralis , United Kingdom
Ravindran Gobinath, India
Rodrigo Gonçalves, Portugal
Peilin Gong , China
Belén González-Fonteboa , Spain
Salvatore Grasso , Italy
Fan Gu, USA
Erhan Güneyisi , Turkey
Esra Mete Güneyisi, Turkey
Pingye Guo , China
Ankit Gupta , India
Federico Gusella , Italy
Kemal Hacıfendioglu, Turkey
Jianyong Han , China
Song Han , China
Asad Hanif , Macau
Hadi Hasanzadehshooiili , Canada
Mostafa Fahmi Hassanein, Egypt
Amir Ahmad Hedayat , Iran
Khandaker Hossain , Canada
Zahid Hossain , USA
Chao Hou, China
Biao Hu, China
Jiang Hu , China
Xiaodong Hu, China
Lei Huang , China
Cun Hui , China
Bon-Gang Hwang, Singapore
Jijo James , India
Abbas Fadhil Jasim , Iraq
Ahad Javanmardi , China
Krishnan Prabhakan Jaya, India
Dong-Sheng Jeng , Australia
Han-Yong Jeon, Republic of Korea
Pengjiao Jia, China
Shaohua Jiang , China

MOUSTAFA KASSEM , Malaysia
Mosbeh Kaloop , Egypt
Shankar Karuppannan , Ethiopia
John Kechagias , Greece
Mohammad Khajehzadeh , Iran
Afzal Husain Khan , Saudi Arabia
Mehran Khan , Hong Kong
Manoj Khandelwal, Australia
Jin Kook Kim , Republic of Korea
Woosuk Kim , Republic of Korea
Vaclav Koci , Czech Republic
Loke Kok Foong, Vietnam
Hailing Kong , China
Leonidas Alexandros Kouris , Greece
Kyriakos Kourousis , Ireland
Moacir Kripka , Brazil
Anupam Kumar, The Netherlands
Emma La Malfa Ribolla, Czech Republic
Ali Lakirouhani , Iran
Angus C. C. Lam, China
Thanh Quang Khai Lam , Vietnam
Luciano Lamberti, Italy
Andreas Lampropoulos , United Kingdom
Raffaele Landolfo, Italy
Massimo Latour , Italy
Bang Yeon Lee , Republic of Korea
Eul-Bum Lee , Republic of Korea
Zhen Lei , Canada
Leonardo Leonetti , Italy
Chun-Qing Li , Australia
Dongsheng Li , China
Gen Li, China
Jiale Li , China
Minghui Li, China
Qingchao Li , China
Shuang Yang Li , China
Sunwei Li , Hong Kong
Yajun Li , China
Shun Liang , China
Francesco Liguori , Italy
Jae-Han Lim , Republic of Korea
Jia-Rui Lin , China
Kun Lin , China
Shibin Lin, China

Tzu-Kang Lin , Taiwan
Yu-Cheng Lin , Taiwan
Hexu Liu, USA
Jian Lin Liu , China
Xiaoli Liu , China
Xuemei Liu , Australia
Zaobao Liu , China
Zhuang-Zhuang Liu, China
Diego Lopez-Garcia , Chile
Cristiano Loss , Canada
Lyan-Ywan Lu , Taiwan
Jin Luo , USA
Yanbin Luo , China
Jianjun Ma , China
Junwei Ma , China
Tian-Shou Ma, China
Zhongguo John Ma , USA
Maria Macchiaroli, Italy
Domenico Magisano, Italy
Reza Mahinroosta, Australia
Yann Malecot , France
Prabhat Kumar Mandal , India
John Mander, USA
Iman Mansouri, Iran
André Dias Martins, Portugal
Domagoj Matesan , Croatia
Jose Matos, Portugal
Vasant Matsagar , India
Claudio Mazzotti , Italy
Ahmed Mebarki , France
Gang Mei , China
Kasim Mermerdas, Turkey
Giovanni Minafò , Italy
Masoomah Mirrashid , Iran
Abbas Mohajerani , Australia
Fadzli Mohamed Nazri , Malaysia
Fabrizio Mollaioli , Italy
Rosario Montuori , Italy
H. Naderpour , Iran
Hassan Nasir , Pakistan
Hossein Nassiraei , Iran
Satheeskumar Navaratnam , Australia
Ignacio J. Navarro , Spain
Ashish Kumar Nayak , India
Behzad Nematollahi , Australia

Chayut Ngamkhanong , Thailand
Trung Ngo, Australia
Tengfei Nian, China
Mehdi Nikoo , Canada
Youjun Ning , China
Olugbenga Timo Oladinrin , United Kingdom
Oladimeji Benedict Olalusi, South Africa
Timothy O. Olawumi , Hong Kong
Alejandro Orfila , Spain
Maurizio Orlando , Italy
Siti Aminah Osman, Malaysia
Walid Oueslati , Tunisia
SUVASH PAUL , Bangladesh
John-Paris Pantouvakis , Greece
Fabrizio Paolacci , Italy
Giuseppina Pappalardo , Italy
Fulvio Parisi , Italy
Dimitrios G. Pavlou , Norway
Daniele Pellegrini , Italy
Gatheeshgar Perampalam , United Kingdom
Daniele Perrone , Italy
Giuseppe Piccardo , Italy
Vagelis Plevris , Qatar
Andrea Pranno , Italy
Adolfo Preciado , Mexico
Chongchong Qi , China
Yu Qian, USA
Ying Qin , China
Giuseppe Quaranta , Italy
Krishanu ROY , New Zealand
Vlastimir Radonjanin, Serbia
Carlo Rainieri , Italy
Rahul V. Ralegaonkar, India
Raizal Saifulnaz Muhammad Rashid, Malaysia
Alessandro Rasulo , Italy
Chonghong Ren , China
Qing-Xin Ren, China
Dimitris Rizos , USA
Geoffrey W. Rodgers , New Zealand
Pier Paolo Rossi, Italy
Nicola Ruggieri , Italy
JUNLONG SHANG, Singapore





Nikhil Saboo, India
Anna Saetta, Italy
Juan Sagaseta , United Kingdom
Timo Saksala, Finland
Mostafa Salari, Canada
Ginevra Salerno , Italy
Evangelos J. Sapountzakis , Greece
Vassilis Sarhosis , United Kingdom
Navaratnarajah Sathiparan , Sri Lanka
Fabrizio Scozzese , Italy
Halil Sezen , USA
Payam Shafigh , Malaysia
M. Shahria Alam, Canada
Yi Shan, China
Hussein Sharaf, Iraq
Mostafa Sharifzadeh, Australia
Sanjay Kumar Shukla, Australia
Amir Si Larbi , France
Okan Sirin , Qatar
Piotr Smarzewski , Poland
Francesca Sollecito , Italy
Rui Song , China
Tian-Yi Song, Australia
Flavio Stochino , Italy
Mayank Sukhija , USA
Piti Sukontasukkul , Thailand
Jianping Sun, Singapore
Xiao Sun , China
T. Tafsirojjaman , Australia
Fujiao Tang , China
Patrick W.C. Tang , Australia
Zhi Cheng Tang , China
Weerachart Tangchirapat , Thailand
Xiixin Tao, China
Piergiorgio Tataranni , Italy
Elisabete Teixeira , Portugal
Jorge Iván Tobón , Colombia
Jing-Zhong Tong, China
Francesco Trentadue , Italy
Antonello Troncone, Italy
Majbah Uddin , USA
Tariq Umar , United Kingdom
Muahmmad Usman, United Kingdom
Muhammad Usman , Pakistan
Mucteba Uysal , Turkey

Ilaria Venanzi , Italy
Castorina S. Vieira , Portugal
Valeria Vignali , Italy
Claudia Vitone , Italy
Liwei WEN , China
Chunfeng Wan , China
Hua-Ping Wan, China
Roman Wan-Wendner , Austria
Chaohui Wang , China
Hao Wang , USA
Shiming Wang , China
Wayne Yu Wang , United Kingdom
Wen-Da Wang, China
Xing Wang , China
Xiuling Wang , China
Zhenjun Wang , China
Xin-Jiang Wei , China
Tao Wen , China
Weiping Wen , China
Lei Weng , China
Chao Wu , United Kingdom
Jiangyu Wu, China
Wangjie Wu , China
Wenbing Wu , China
Zhixing Xiao, China
Gang Xu, China
Jian Xu , China
Panpan , China
Rongchao Xu , China
HE YONGLIANG, China
Michael Yam, Hong Kong
Hailu Yang , China
Xu-Xu Yang , China
Hui Yao , China
Xinyu Ye , China
Zhoujing Ye, China
Gürol Yildirim , Turkey
Dawei Yin , China
Doo-Yeol Yoo , Republic of Korea
Zhanping You , USA
Afshar A. Yousefi , Iran
Xinbao Yu , USA
Dongdong Yuan , China
Geun Y. Yun , Republic of Korea






Hyun-Do Yun , Republic of Korea
Cemal YİĞİT , Turkey
Paolo Zampieri, Italy
Giulio Zani , Italy
Mariano Angelo Zanini , Italy
Zhixiong Zeng , Hong Kong
Mustafa Zeybek, Turkey
Henglong Zhang , China
Jiupeng Zhang, China
Tingting Zhang , China
Zengping Zhang, China
Zetian Zhang , China
Zhigang Zhang , China
Zhipeng Zhao , Japan
Jun Zhao , China
Annan Zhou , Australia
Jia-wen Zhou , China
Hai-Tao Zhu , China
Peng Zhu , China
QuanJie Zhu , China
Wenjun Zhu , China
Marco Zucca, Italy
Haoran Zuo, Australia
Junqing Zuo , China
Robert Černý , Czech Republic
Süleyman İpek , Turkey

Contents






Assessing the Quality of Concrete Tunnel Lining Exposed to Tunnel Fire through Residual Compressive Strength

Husen Alhawat, R. Hamid , Shahrizan Baharom , M. R. Azmi , and A. B. M. A. Kaish 
Research Article (9 pages), Article ID 9735496, Volume 2023 (2023)





Flexural Behavior of Graphite Tailings RC Beams in Chloride Environment

Bo-Ya Feng , Xun-Guo Zhu , Hong-Chun Xia , Lin Yang , and Te Xie 
Research Article (13 pages), Article ID 1427007, Volume 2023 (2023)



The Impact of Molar Proportion of Sodium Hydroxide and Water Amount on the Compressive Strength of Slag/Metakaolin (Waste Materials) Geopolymer Mortar

Fatimah N. Al-Husseinawi , William Atherton , Zainab Al-Khafaji , Monower Sadique , and Zaher Mundher Yaseen 
Research Article (14 pages), Article ID 5910701, Volume 2022 (2022)



Sustainable Concrete Columns with GGBS and Industrial Sand: A Comparative Study on Destructive and Nondestructive Tests on Damaged Columns Strengthened with GFRP Jacketing

G. I. Gunarani , B. Karthikeyan , A. Priyadharshini, Senthil Kumaran Selvaraj , S Jose, D. Vincent Herald Wilson, and Tezeta Moges Adane 
Research Article (11 pages), Article ID 6716511, Volume 2022 (2022)

Study on Fresh and Mechanical Properties of Polyblend Self-Compacting Concrete with Metakaolin, Lightweight Expanded Clay Aggregate, and SAP as Alternative Resources

S. S. Vivek, B. Karthikeyan, G. Ragul Kanna, Senthil Kumaran Selvaraj , Jose S, Ponnusamy Palanisamy, and Tezeta Moges Adane 
Research Article (13 pages), Article ID 2350447, Volume 2022 (2022)

Comparative Study on Mechanical Properties of Concrete Blended with *Costus englerianus* Bagasse Ash and Bagasse Fibre as Partial Replacement for Lime and Cement

Naraindas Bheel , Charles Kennedy, Paul Awoyera , Samiullah Sohu, and Suhail Ahmed Abbasi
Research Article (8 pages), Article ID 8900167, Volume 2022 (2022)


An Experimental Study on the Strength and Crack Healing Performance of *E. coli* Bacteria-Induced Microbial Concrete

Md. Mahfuzul Islam, Nusrat Hoque , Moinul Islam , and Imteaz Ibney Gias
Research Article (13 pages), Article ID 3060230, Volume 2022 (2022)

Shrinkage and Mechanical Properties of Fibre-Reinforced Blast Furnace Slag-Steel Slag-Based Geopolymer

Shengtang Xu , Chaofan Wu , Jinchao Yue , and Zikai Xu 
Research Article (10 pages), Article ID 8931401, Volume 2022 (2022)

Impacts of Addition of Palm Kernel Shells Content on Mechanical Properties of Compacted Shale Used as an Alternative Landfill Liners

Clement A. Amagu , Beatrice O. Enya, Jun-ichi Kodama, and Mostafa Sharifzadeh
Research Article (13 pages), Article ID 9772816, Volume 2022 (2022)

Force-Deformation Study on Glass Fiber Reinforced Concrete Slab Incorporating Waste Paper

S. Praburanganathan , N. Sudharsan, Yeddula Bharath Simha Reddy, Chukka Naga Dheeraj Kumar Reddy , L. Natrayan , and Prabhu Paramasivam 

Research Article (10 pages), Article ID 5343128, Volume 2022 (2022)

Research Article

Assessing the Quality of Concrete Tunnel Lining Exposed to Tunnel Fire through Residual Compressive Strength

Husen Alhawat, R. Hamid , Shahrizan Baharom , M. R. Azmi , and A. B. M. A. Kaish 

Department of Civil Engineering, Faculty of Engineering and Built Environment, Universiti Kebangsaan Malaysia (UKM), Bangi 43600, Selangor, Malaysia

Correspondence should be addressed to R. Hamid; roszilah@ukm.edu.my

Received 5 July 2022; Revised 7 December 2022; Accepted 23 March 2023; Published 7 April 2023

Academic Editor: Md. Akter Hosen

Copyright © 2023 Husen Alhawat et al. This is an open access article distributed under the Creative Commons Attribution License, which permits unrestricted use, distribution, and reproduction in any medium, provided the original work is properly cited.

Compressive strength performance of concrete after exposure to the elevated temperature is important for evaluating and repairing concrete structures. This paper presents an experimental study to determine the residual compressive strength of concrete used in tunnel lining after exposed to tunnel fire. Two types of concrete tunnel lining segments are evaluated in this study. One of it was constructed using a patented fire-resistant concrete (MYC) containing high volume fly ash and nanosilica (HVFANS). Another concrete tunnel lining segment was constructed using concrete containing silica fume normally used in the current construction, coded as SPC concrete. The drilled core results show that, after exposure to tunnel fire temperature up to around 1045°C, the compressive strength of MYC has dropped to 66% of the design strength. In comparison, the SPC concrete showed a decrease in compressive strength to 62% of design strength. The experimental results confirmed that the SPC segments have shown slightly lower residual compressive strength compared to the MYC segments. However, the MYC tunnel segment shows high resistance to the spalling of cover concrete compared to the SPC tunnel segment. Therefore, it can be said that the residual strength alone is not sufficient to compare the damage of concrete exposed to tunnel fire; the spalling damage observation is similarly important as it is one of the important serviceability criteria for designing concrete structures.

1. Introduction

A massive number of concrete structures have been constructed all over the world, and this number is increasing day by day. Concrete compressive strength is the main property among the mechanical and physical properties, which is necessary for the design of constructional element or determination of its load-bearing capacity. At high temperatures, the properties of hardened concrete are more complex as the physical and mechanical properties of concrete are changed, compared to those at ambient temperature. The concrete undergoes physical and chemical modifications at high temperatures, which primarily triggers mechanical changes. The free water and the bonded water evaporate when the concrete is heated at about 100–110 degree Celsius [1]. In view of the internal vapour heat conditions resulting from high heat and evaporation of the water, hydration of

cement particles is improved when the temperature exceeds 300°C. As the temperature increases to 400°C, concrete hydroxide starts to decompose to calcium oxide and water [2]. As the calcium silicate hydrate (C-S-H) plays a significant role in the hardness and efficiency of the hardening process, it starts to crumble when it reaches up to 600°C [3–6].

Some researchers studied the effect of fire on the mechanical characteristics of concrete such as compressive strength, elastic modulus, and tensile strength, and the majority of them found that the mechanical characteristics decrease with the increase in temperature during a fire event [5, 7].

In the construction sector, high strength concrete (HSC) and high performance concrete (HPC) are commonly used, while silica fume [8, 9] is one of the key materials for the production of this type of concrete, because it improves the

mechanical features of the concrete. Some researchers have indicated that nanosilica performs better than silica fume in improving the compressive strength of the concrete [10] while its price is identical to that of silica fume [11]. Several researchers have discovered that nanosilica particles increase the hydration of the material and effectively increase the pozzolanic activity instead of acting as a simple filler for the structure of calcium silicate hydrate which makes it denser and more compact [12, 13]. This is why nanosilica is used in high strength or performance concrete construction [14].

Previous study had shown that, at all curing periods, all samples containing nanosilica showed substantial increases in strength, where higher nanosilica contents show greater strength [15]. Nanosilica is able to increase the strength of fly ash concrete by accelerating the process of hydration [13]. After exposure to 400°C, the compressive strength of all specimens had increased, which was more effective for nanosilica-containing specimens. When the samples are heated to this temperature, the hydration process can be increased by generating dense calcium silicate hydrate by increasing nanosilica reactivity that enhances the strength properties. Exposure to 700°C leads to a significant reduction in compressive and bending strength for these specimens, primarily due to the overbuilding of vapour pressure, which led to large cracks. Furthermore, at this temperature, the binding products in the concrete paste became dehydrated causing a decrease in the strength properties. However, the residual resistance of specimens containing nanosilica was increased [13, 15]. This was primarily because of the filling effect of nanosilica and the higher content of fly ash in the specimens [15]. Additionally, 2.5% of nanosilica and 52.5% of fly ash as cement replacement were able to produce fire-resistant concrete that can retain 94% of its strength in temperatures of up to 700°C [16].

Tunnel linings can suffer heavy structural damage or even collapse when exposed to tunnel fire temperature curves. Previous studies showed that tunnel fire temperature curve is different from normal temperature curve [17, 18]. An assessment of postfire damage is the most important thing when evaluating the structural safety of a tunnel's concrete lining [17]. Wang et al. [17] studied the residual compressive strength (RCS) of small-scale lining concrete blocks and detection of inner defects in the lining structure through combined ultrasonic pulse velocity (UPV) and ultrasonic shear-wave tomography. Previous studies on concrete cube and drilled cores from small-scale slab test have reported the residual compressive strength of concrete at a maximum temperature around 700°C and compared the fire-resistant performance based on residual strength solely [8, 15, 16]. Alhawati et al. [18] studied the spalling behaviour of tunnel lining segments exposed to high temperatures. High temperature behaviour of concrete tunnel lining was also studied by Yan et al. [19, 20] through destructive testing of concrete core sample. Hua et al. [21] evaluated the spalling behaviour of concrete tunnel segment under high temperature. They proposed a simplified concrete cover spalling model based on the rate of spalling during the initiation to finishing of tunnel fire with the help of mathematical and numerical modelling. Qiao et al. [22, 23] investigated the

thermomechanical damage behaviour of tunnel lining subjected to modified RABT fire loading. They utilized residual stress criterion to quantify the spalling damage depth in concrete tunnel lining. Abraham and Dérobert [24] studied the nondestructive evaluation of concrete tunnel (Mont-Blanc tunnel) after the true fire event on March 26, 1999. Ground penetrating radar and the seismic refraction method was used in their investigation. Zhai [25] also performed the nondestructive method of evaluation to quantify the damage in concrete tunnel lining after fire hazard. Most of these studies determined the residual strength of concrete through destructive or nondestructive methods, spalling mechanism, extent of spalling, and spalling rate under low-to-long-term fire events. Therefore, it can be said that both the residual strength and spalling behaviour of concrete are important to assess the condition of concrete tunnel lining after a fire event.

EFNARC [26] provides a guideline for testing of passive fire protection for concrete tunnel linings based on destructive testing of concrete core sample. Other than that, no established procedure or code provisions are available to quantify the damage and risk assessment of concrete tunnel subjected to devastating fire [20]. For realistic assessment of the fire damage of concrete tunnels, an established method would be necessary to capture the potential damage scenarios [27]. Some researchers provided emphasis on determining the residual strength and some others emphasized on spalling behaviour of cover concrete [17, 18, 20, 24, 25]. However, in reality, both parameters are important for determining the service life of the concrete tunnel after a fire event. Therefore, this study is conducted to understand the relationship between these two factors for assessing the fire damage of tunnel lining made of two different types of concrete.

2. Experimental Method

2.1. Materials. Materials and mix design proportions for MYC and SPC tunnel lining segments are shown in Tables 1 and 2.

2.2. Testing Setup for Attaining Tunnel Fire Temperature. To attain tunnel fire temperature to study its effect on the concrete tunnel linings, an innovative testing setup is designed and described by Alhawati et al. [18]. Two rings of tunnel lining were constructed, one using MYC and the other using SPC. Figure 1(a) shows the typical arrangement of tunnel lining segments to form the tunnel ring and Figure 1(b) shows the assembling process during the construction of tunnel ring. Brick walls with opening are constructed covering the both tunnel rings to provide confinement effect. This helped to achieve the desired tunnel fire time-temperature curve of RABT-ZTV [18].

All the details for the test and the temperature measurement during the test were described in the previous study [18]. Figures 2(a) and 2(b) show the peak fire and maximum temperatures during the test measured by a thermal image camera. The time temperature curves for this test compared with the RABT-ZTV car is shown in Figure 3.

TABLE 1: Physical properties of the materials and mix design proportion for MYC (reinforced concrete segments using HVFANS concrete, Malaysian patent code MY-163281-A) (18).

Material	Proportion	Type (class)	Specific gravity	Size	Weight (kg/m ³)
Fly ash	52.5%	F	2.1	—	278
Nano silica	2.5%	Cembinder 8	—	—	26.56
Portland cement	45%	Type 1	—	—	225.8
Polypropylene fibre	1%	—	0.9	Length 12 mm	1
Coarse aggregate	—	—	2.07	Max. 10 mm	942.6
Fine aggregate	—	—	2.75	Max. 4.75	682.01
Water	0.34 (W/C)	Normal tap water	—	—	154.85
Superplasticizer	0.4–2%	Darex super 20	—	—	5.31

TABLE 2: Physical properties of the materials and mix design proportion for SPC.

Material	Proportion (%)	Type (class)	Specific gravity	Size
Cement including fly ash	90	Fly ash type F	2.1	—
Silica fume	10	—	—	—
Polypropylene fibre	1	—	0.9	Length 12 mm

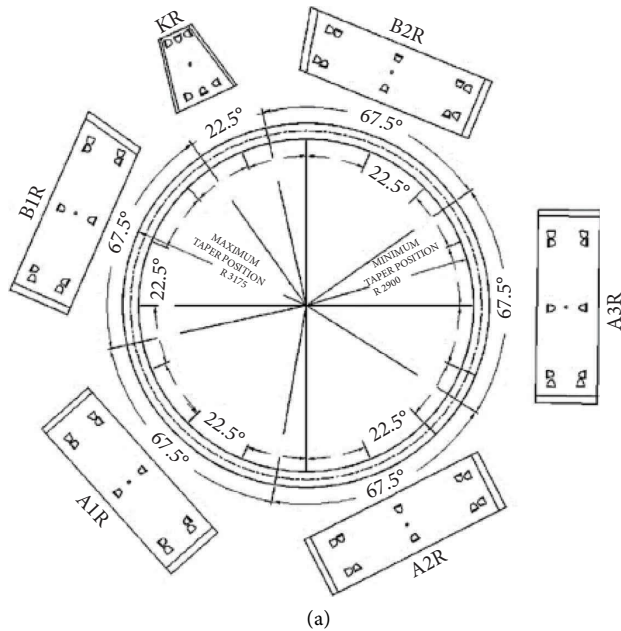


FIGURE 1: (a) Elevation of the ring and (b) assembling the segments into rings (18).

2.3. Drilling and Coring Method. After the fire test, concrete cores with a diameter of 100 mm were drilled in the entire 275 mm depth of the MYC and SPC full-scale segments to determine their residual compressive strength. All the drilled concrete cores were obtained according to the standard procedures [28, 29]. In the SPC and MYC segments, the reinforcing steel was mapped before obtaining the concrete core with the intent of preventing the extraction of the rebar in the recovered cores. Drilled cores were extracted and sealed in plastic bags. These cores were transported to the lab for further tests. The length of the cores was further adjusted at both ends to be approximately 200 mm to meet the standard guidelines [29, 30].

Core drilling was performed in different locations depending on the spalling area on the segments for both types of concrete tunnels, considering the drilling locations to be representing the damaged areas as shown in Figure 4. Six cores were drilled in this study from the segments for both types of concrete tunnels according to the standard procedure [31].

Core samples were extracted from the structural portion of the tunnel using core drilling equipment that has diamond bits added to the drilling barrel. Since any movement could lead to a spoiled core during the drilling process, the rig was securely fixed to the concrete segment. To prevent cutting out a twisted core, the rig was set up perpendicular to

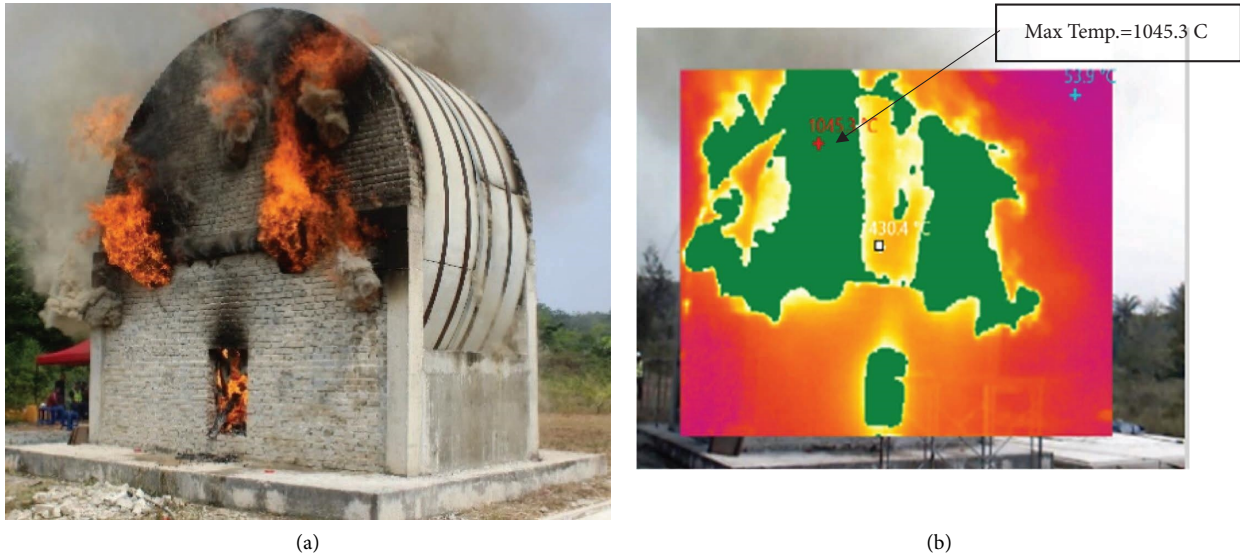


FIGURE 2: The tunnel ring fire test (a) during the peak fire at 15 minutes and (b) infrared photos for maximum temperature.

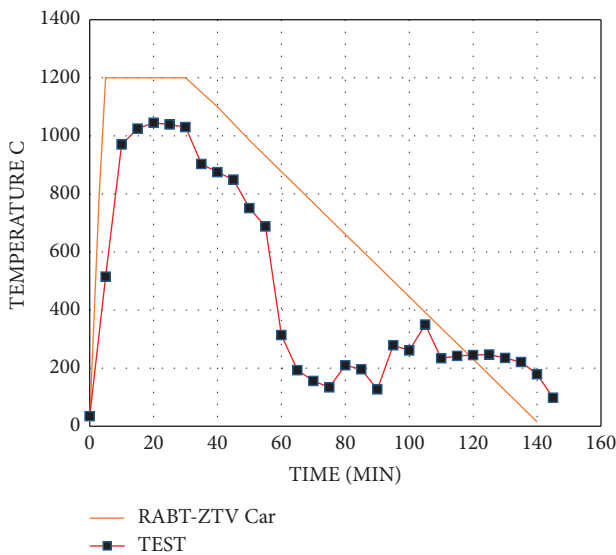


FIGURE 3: Time-temperature curves produced by test setup and the RABT-ZTV.

the surface on which the core would be extracted. Figure 5 shows the core drilling process in the full-scale tunnel segment, and Figure 6 shows the core samples after being extracted from the tunnel segments.

In the laboratory, the drilled cores were visually tested to verify their state and to investigate their condition to better

interpret the cores' compressive strength. All core specimens were prepared by grinding their ends to obtain appropriate length, smooth ends, and perpendicular shape to the longitudinal core axis before measuring the compression strength [29].

3. Experimental Results

The concrete cores were tested to use these values in the measurement of L/D ratio and to conform to the criteria for the cross-sectional area of the core compression test [32]. For compliance, both ends of the cores were shortened to approximately 200 mm. Thus, the diameter to height ratio is equal to $1/2$; thus, there is no need to apply any factors to reduce the obtained value [30]. The core compressive strength is calculated dividing the peak load by the core cross-sectional area depending on the average core diameter [29].

The compressive strengths of MYC and SPC concrete segments before and after exposure to the elevated temperature are presented in Table 3. The compressive strength before heating was obtained using cubes. Thus, there is a need to make adjustment to cylinder compressive test value (f_c) equivalent to the cube compressive test values (f_{cu}). Therefore, to gain the f_{cu} after heating, the formula $f_c = 0.8 f_{cu}$ was used, as referred in the standard guidelines [33]. The percentage of residual compressive strength was calculated using the following equation:

$$\text{residual compressive strength (\%)} = \frac{f_c \text{ (before exposure to heating)}}{f_c \text{ (after exposure to heating)}} \times 100. \tag{1}$$

The test results indicated that for tunnel fire temperature, compressive strength had reduced greatly for both types of

concrete mix. The MYC tunnel concrete showed a little bit higher residual strength. The strength of MYC concrete

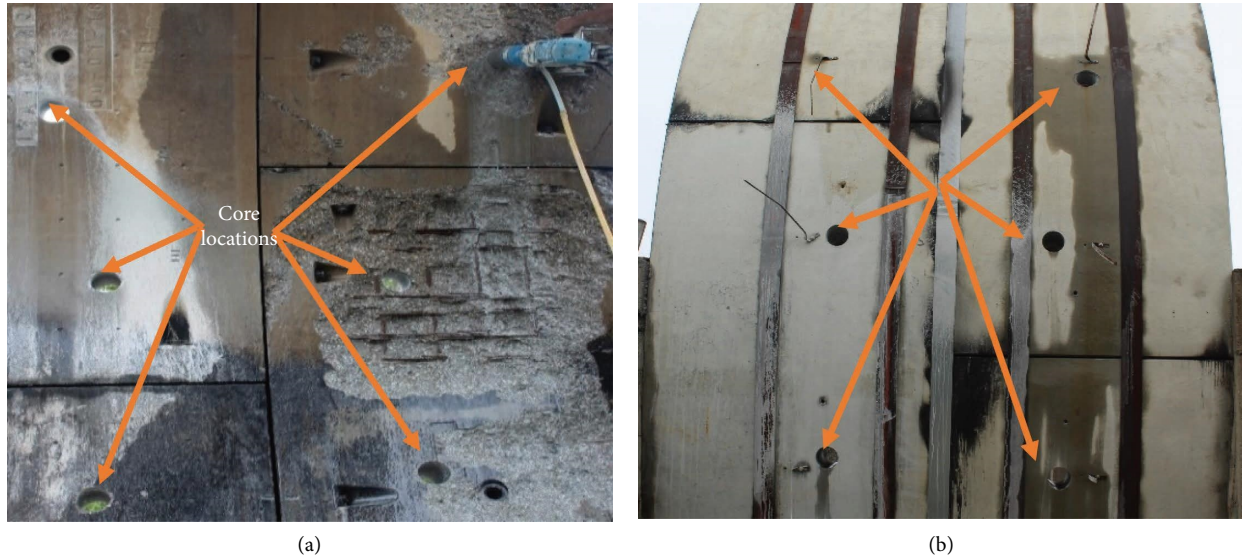


FIGURE 4: Coring drill locations in the full-scale segments for MYC and SPC concrete tunnels; (a) inner surface view and (b) outer surface view.

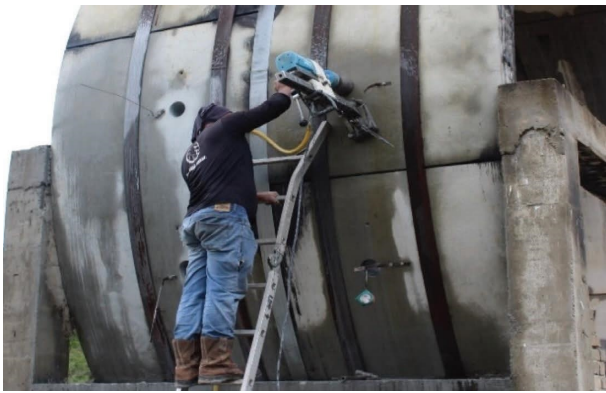


FIGURE 5: Drilling cores in the full-scale segments for MYC and SPC concrete.



FIGURE 6: Extracted core samples from the tunnel segments.

decreased and remained at 66.04% after exposure to an elevated temperature of 1000°C and above, whereas the SPC concrete strength was decreased to 62.46% after exposure to tunnel fire.

Therefore, the residual compressive strength of MYC concrete was reduced and dropped to 48 MPa, which meant it was reduced by 33.96% after exposure to a 1000°C tunnel fire. Figure 7 shows the comparison of the residual compressive strengths between MYC and SPC concrete.

This reduction in strength was due to more vapour pressure and more cracks than when the concrete was exposed to 700°C and above, which affected the strength of concrete. The elevated temperature also affected the cement paste binder. These results were also compared with the results obtained by a previous researcher [34]. It was noticed that there difference in the compressive strength between both types of concrete was not large, although there was significant difference in spalling behaviour between them. Such differences are because the components for MYC concrete have more resistance to spalling and fire than on the compressive strength and static loading. The MYC concrete's behaviour after exposure to temperature up to 1000°C can be reflected by both pozzolanic and filler influences of NS in the mixture, which enhanced the concrete microstructure and increased the content of calcium silica hydrate.

Figure 8 shows the failure of the SPC and MYC core samples after compression test. From the fire test, it can be seen that explosive spalling occurred mostly in the SPC tunnel lining as shown in Figure 9. Moreover, some of the concrete covers had been scalded off, exposing the steel reinforcements, which greatly influence the load-bearing performance of the tunnel linings. However, in both concrete mixes, the PP fibre had melted due to the very high temperatures, reducing the amount of pore pressure build-up [35]. Spalling contours show how much damage has been occurred in a particular point, as well as how much of the surface area has been damaged. Spalling patterns for SPC and MYC segments are depicted in Figures 9 and 10. Some patterned cracks were appeared in one of the MYC

TABLE 3: Compressive strength of the MYC and SPC concrete segments.

Samples	Before exposure to fire, f'_{cu} (MPa)	After exposure to fire of higher than 1000°C			Average residual strength (%)
		f'_c (MPa)	f'_{cu} (MPa)	Residual compressive strength (%)	
MYC 1	72.30	37.3	46.63	64.5	66.04
MYC 2	72.30	38.4	48	66.39	
MYC 3	72.30	38.9	48.63	67.25	
SPC 1	72.45	36.37	45.46	62.75	62.46
SPC 2	72.45	34.5	43.13	59.53	
SPC 3	72.45	37.75	47.19	65.1	

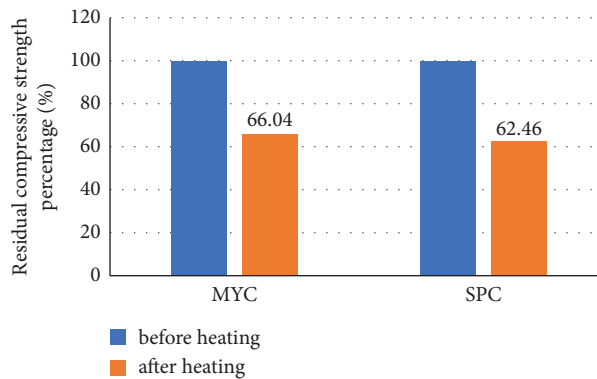


FIGURE 7: Comparison of residual compressive strengths between MYC and SPC concrete.



FIGURE 8: Failure of coring SPC and MYC sample after compression.

segments, but the ring itself showed no signs of spalling as shown in Figures 9 and 10. The SPC segments displayed a variety of severe spalling patterns and had exposed the reinforcing steel that could have weakened the structure. Spalling patterns are random and not related to the boundary conditions.

The volume of spalling was used to calculate the depths of the spalling. Each segment's spalled area was measured and converted to a percentage. Segments BR1, AR1, AR3,

BR2, and KR have a spalling rate of 45.36%, 40.7%, 36.84%, 49.16%, and 7.92%, respectively, in the SPC tunnel segments. On the other hand, segments BR1, AR1, AR3, BR2, and KR had spalling volumes of 1.65%, 4.76%, 4.88%, 7.15%, and 0.283%, respectively, in the MYC tunnel segment. Cracking in the MYC segments was analysed by. However, visual inspection shows that 16.56% of the MYC segments had cracked due to high temperature exposure.



FIGURE 9: Spalling at different locations of SPC and MYC segments.

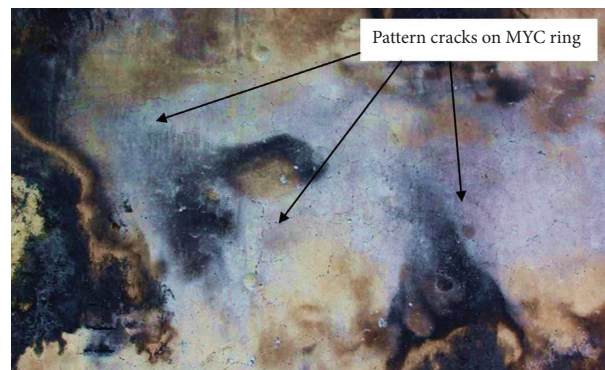


FIGURE 10: Cracking on the MYC segment.

4. Discussion

The experimental outcome of this study showed that the spalling was totally different on the SPC segments and MYC segments. Severe spalling occurred in the SPC segments, whereas there was no spalling in the MYC segments. This might be due to the presence of silica fume in the SPC that reduced the permeability and thus increased the vapour pressure during the fire leading to more spalling occurrence. However, the design strengths for MYC and SPC were the same. The residual strengths after fire exposure were almost the same at different locations on the tunnel rings. Therefore, it is difficult to judge the health of fire exposed concrete

tunnel only based on the design and residual strengths of concrete.

For a concrete structure, satisfying the serviceability requirements is as necessary as satisfying the strength requirements. Even though historic events rarely observed a tunnel failure due to a fire event [21, 36], severe damage in terms of spalling was observed in such events. Therefore, serviceability requirement in terms of concrete spalling is an important criterion for assessing the health of a concrete tunnel. Characterizing concrete spalling in terms of the spalling starting time is also important to understand the degradation pace of the tunnel concrete in a fire event. Hua et al. [21] mentioned that the spalling normally starts when

gas temperature inside the tunnel lining reaches the spalling starting temperature. However, spalling starting times for MYC and SPC segments were not being able to be determined in this study as the tunnel was closed from both ends as shown in Figure 2. Furthermore, depth of spalling together with the area of spalling plays a vital role to understand the depth of damage in the tunnel lining [36]. This also helps to understand the condition of reinforcing steels inside the tunnel lining.

5. Conclusion

The main objective of this study was to assess the health of concrete tunnel lining after exposed to tunnel fire. Based on the experimental results, the following conclusions are drawn:

- (i) The findings revealed that, after exposed to high temperature, the compressive strength of MYC concrete tunnel lining dropped to 66.04% of design strength, whereas the conventional concrete for the current construction of tunnels (SPC concrete) decreased to 62.46% of design strength.
- (ii) It is also observed that the spalling of SPC segments was severe where the reinforcing steel also exposed in most of the SPG segments that could have weakened the tunnel structure. However, the MYC segments only show the patterned surface cracking, even though the residual strengths of both types of concrete were almost the same after exposure to the standard fire.

This concludes that determining the performance of different types of concrete tunnel lining with different material components drilled cores is not enough to know the after fire health of a concrete tunnel. Spalling behaviour including the spalling rate and depth of spalling are also important to assess the health of the tunnel lining. A particular mix design may produce good concrete in terms of the residual strength; however, surface spalling may cause severe damage resulting in failure to meet the serviceability requirement of the tunnel structure. Therefore, this study concludes that the residual strength of concrete spalling behaviour should be evaluated to assess the condition of fire-exposed concrete tunnel lining.

Data Availability

The datasets used in this study are available from the authors upon request.

Conflicts of Interest

The authors declare that they have no conflicts of interest.

Acknowledgments

The authors acknowledge the financial contribution of the Ministry of Higher Learning through project nos. DIP-2019-002 and PRGS/2/2015/TK08/UKM/02/1. The authors also

acknowledge the financial, technical, and expertise contribution of the UKM industry and government body collaborators (SPC Industries Sdn. Bhd. and Fire and Rescue Department, Malaysia).

References

- [1] J. Geng, Q. Sun, W. Zhang, and C. Lü, "Effect of high temperature on mechanical and acoustic emission properties of calcareous-aggregate concrete," *Applied Thermal Engineering*, vol. 106, pp. 1200–1208, 2016.
- [2] M. Li, C. X. Qian, and W. Sun, "Mechanical properties of high-strength concrete after fire," *Cement and Concrete Research*, vol. 34, no. 6, pp. 1001–1005, 2004.
- [3] J. P. Ingham, "Application of petrographic examination techniques to the assessment of fire-damaged concrete and masonry structures," *Materials Characterization*, vol. 60, no. 7, pp. 700–709, 2009.
- [4] B. Georgali and P. E. Tsakiridis, "Microstructure of fire-damaged concrete. A case study," *Cement and Concrete Composites*, vol. 27, no. 2, pp. 255–259, 2005.
- [5] W. Zheng, H. Li, and Y. Wang, "Compressive behaviour of hybrid fiber-reinforced reactive powder concrete after high temperature," *Materials and Design*, vol. 41, pp. 403–409, 2012.
- [6] B. Zhang, "Effects of moisture evaporation (weight loss) on fracture properties of high performance concrete subjected to high temperatures," *Fire Safety Journal*, vol. 46, no. 8, pp. 543–549, 2011.
- [7] R. Felicetti, "The drilling resistance test for the assessment of fire damaged concrete," *Cement and Concrete Composites*, vol. 28, no. 4, pp. 321–329, 2006.
- [8] R. K. Ibrahim, R. Hamid, and M. R. Taha, "Strength and microstructure of mortar containing nanosilica at high temperature," *ACI Materials Journal*, vol. 111, no. 2, pp. 163–170, 2014.
- [9] Z. Li, H. Wang, S. He, Y. Lu, and M. Wang, "Investigations on the preparation and mechanical properties of the nano-alumina reinforced cement composite," *Materials Letters*, vol. 60, no. 3, pp. 356–359, 2006.
- [10] Y. Qing, Z. Zenan, K. Deyu, and C. Rongshen, "Influence of nano-SiO₂ addition on properties of hardened cement paste as compared with silica fume," *Construction and Building Materials*, vol. 21, no. 3, pp. 539–545, 2007.
- [11] U. Skarp, R. Troli, R. T. M. Collepardi, and S. Collepardi, "Optimization of silica fume, fly ash and amorphous nanosilica in superplasticized high-performance concretes," *Optimization*, vol. 221, 2004.
- [12] T. Ji, "Preliminary study on the water permeability and microstructure of concrete incorporating nano-SiO₂," *Cement and Concrete Research*, vol. 35, no. 10, pp. 1943–1947, 2005.
- [13] J. J. Gaitero, I. Campillo, and A. Guerrero, "Reduction of the calcium leaching rate of cement paste by addition of silica nanoparticles," *Cement and Concrete Research*, vol. 38, no. 8–9, pp. 1112–1118, 2008.
- [14] J. Vera-Agullo, D. Portillo-Rico, M. J. García-Casas, A. Gutiérrez-Martínez, J. M. Mieres-Royo, and J. Grávalos-Moreno, "Mortar and concrete reinforced with nanomaterials," *Nanotechnology in Construction* 3, pp. 383–388, Springer, Berlin, Germany, 2009.
- [15] R. K. Ibrahim, R. Hamid, and M. R. Taha, "Fire resistance of high-volume fly ash mortars with nanosilica addition," *Construction and Building Materials*, vol. 36, pp. 779–786, 2012.

- [16] R. K. Ibrahim, *The strength and micro structures of sustainable high strength high-volume fly ash concrete with nano materials exposed to high temperature*, Ph.D. thesis, UKM, Kuala Lumpur, Malaysia, 2013.
- [17] Q. Wang, D. Chen, K. Zhu et al., "Evaluation residual compressive strength of tunnel lining concrete structure after fire damage based on ultrasonic pulse velocity and shear-wave tomography," *Processes*, vol. 10, no. 3, p. 560, 2022.
- [18] H. Alhawati, R. Hamid, S. Baharom, M. R. Azmi, and A. B. M. A. Kaish, "Thermal behaviour of unloaded concrete tunnel lining through an innovative large-scale tunnel fire experimental testing setup," *Construction and Building Materials*, vol. 283, Article ID 122718, 2021.
- [19] Z. G. Yan, H. H. Zhu, J. Woody Ju, and W. Q. Ding, "Full-scale fire tests of RC metro shield TBM tunnel linings," *Construction and Building Materials*, vol. 36, pp. 484–494, 2012.
- [20] Z. G. Yan, H. H. Zhu, and J. W. Ju, "Behavior of reinforced concrete and steel fiber reinforced concrete shield TBM tunnel linings exposed to high temperatures," *Construction and Building Materials*, vol. 38, pp. 610–618, 2013.
- [21] N. Hua, A. Tessari, and N. Elhami Khorasani, "Characterizing damage to a concrete liner during a tunnel fire," *Tunnelling and Underground Space Technology*, vol. 109, Article ID 103761, 2021.
- [22] R. J. Qiao, Z. S. Shao, F. Liu, and W. Wei, "Damage evolution and safety assessment of tunnel lining subjected to long-duration fire," *Tunnelling and Underground Space Technology*, vol. 83, pp. 354–363, 2019.
- [23] R. J. Qiao, Z. S. Shao, W. Wei, and Y. Y. Zhang, "Theoretical investigation into the thermo-mechanical behaviours of tunnel lining during RABT fire development," *Arabian Journal for Science and Engineering*, vol. 44, no. 5, pp. 4807–4818, 2018.
- [24] O. Abraham and X. Dérobert, "Non-destructive testing of fired tunnel walls: the Mont-Blanc Tunnel case study," *NDT and E International*, vol. 36, no. 6, pp. 411–418, 2003.
- [25] Z. T. Zhai, "Ultrasonic testing and experimental study on damage of lining structure concrete after tunnel fire," M.Sc. thesis, China Jiliang University, Hangzhou, China, 2020.
- [26] Efnarc, *Guidelines for Testing of Passive Fire protection for concrete Tunnels Linings*, European federation dedicated to specialist construction chemicals and concrete systems, Brussels, Belgium, 2006.
- [27] F. Souza, M. Rosignuolo, S. Andreini, C. La Mendola, and Knaust, "Probabilistic thermo-mechanical analysis of a concrete tunnel lining subject to fire," in *Proceedings of the IFireSS 2017–2nd International Fire Safety Symposium*, pp. 997–1004, Naples, Italy, June 2017.
- [28] Aci Committee 214, *214 4R-03 Guide for Obtaining Cores and Interpreting Compressive Strength Results*, ACI, Toronto, Ontario, 2003.
- [29] M. F. A. Alwash, "Assessment of concrete strength in existing structures using nondestructive tests and cores: analysis of current methodology and recommendations for more reliable assessment," L'Université De Bordeaux, Bordeaux, France, Docteur De, 2017.
- [30] AMST, "C 42/C 42M – 04 Obtaining and testing drilled cores and sawed beams of concrete 1," *Practice*, vol. 23, no. 11, pp. 4–8, 2001.
- [31] J. H. Bungey and S. G. Millard, *Testing of Concrete in Structures*, Taylor and Francis, Milton Park, UK, 1995.
- [32] Astm C39, "Standard test method for compressive strength of cylindrical concrete specimens: C39/C39m-18," *Am. Soc. Test. Mater.*, vol. 4, p. 8, 2018.
- [33] M. H. Mussa, A. A. Mutalib, R. Hamid, and S. N. Raman, "Dynamic properties of high volume fly ash nanosilica (HVFANS) concrete subjected to combined effect of high strain rate and temperature," *Latin American Journal of Solids and Structures*, vol. 15, no. 1, pp. 1–19, 2018.
- [34] Bs En 206-1, "Concrete - Part 1: specification, performance, production and conformity," *Eurocode*, vol. 3, pp. 1–72, 2000.
- [35] M. Saeidpour and L. Wadsö, "Moisture equilibrium of cement based materials containing slag or silica fume and exposed to repeated sorption cycles," *Cement and Concrete Research*, vol. 69, pp. 88–95, 2015.
- [36] N. Hua, A. Tessari, and N. Elhami Khorasani, "Quantifying uncertainties in the temperature-time evolution of railway tunnel fires," *Fire Technology*, vol. 57, no. 1, pp. 361–392, 2020.

Research Article

Flexural Behavior of Graphite Tailings RC Beams in Chloride Environment

Bo-Ya Feng , **Xun-Guo Zhu** , **Hong-Chun Xia** , **Lin Yang** , and **Te Xie** 

College of Architecture and Engineering, Dalian University, Dalian 116622, Liaoning, China

Correspondence should be addressed to Xun-Guo Zhu; zhu_xunguo@hotmail.com

Received 28 June 2022; Revised 30 September 2022; Accepted 28 November 2022; Published 31 January 2023

Academic Editor: Md. Akter Hosen

Copyright © 2023 Bo-Ya Feng et al. This is an open access article distributed under the Creative Commons Attribution License, which permits unrestricted use, distribution, and reproduction in any medium, provided the original work is properly cited.

This paper investigates the mechanical properties of graphite tailings concrete beams under various curing environments. The results show that the concentration of graphite tailings has an important influence on the mechanical properties of concrete. Finally, the bending characteristics of the beam and the modified bearing capacity calculation formula are obtained, which provides a theoretical basis and the reference value for the construction of green building materials. Through research, the main innovations and main findings of this paper are as follows: (1) In the three kinds of concrete experimental environment, the fracture load and ultimate load of concrete beams with graphite tailings replacement rate of 20% are the largest. (2) In the three kinds of concrete test environment, when the concrete test beams under the same load, with the increase of graphite tailings replacement rate, the mid-span deflection of concrete beams showed a trend of decreasing first and then increasing. When the replacement rate of graphite tailings sand is 20%, the mid-span deflection of the test beam is the smallest. (3) Through experiments, it is found that the normal section bearing capacity of graphite tailings concrete beams after chloride salt erosion conforms to the plane section assumption. After chlorine salt erosion, the strain of the longitudinal tensile steel bar of concrete beams with different graphite tailings sand replacement rates is the same as that of ordinary concrete beams, and the slope of the strain curve is the same, showing a linear trend. The experimental results show that the replacement rate of graphite tailings sand has an insignificant effect on the strain of steel bars. (4) The Gauss function is used to fit the experimental value of normal section bearing capacity of concrete beam, and the calculation formula of normal section ultimate bearing capacity of graphite tailings sand concrete beam under chloride environment is established. The research results of this paper have significant reference value for the study of mechanical properties of graphite tailings sand concrete components.

1. Introduction

In recent years, with the development of the Chinese economy, the construction of coastal cities has developed rapidly [1]. Large-scale infrastructure construction needs a lot of concrete materials, which will consume a lot of natural stone and cause serious ecological problems [2–5]. To effectively reduce the use of natural stone, alternative raw materials must be found. After years of research, it has been found that graphite tailings sand can be used as a substitute for natural sand [6, 7]. A rational use of graphite tailings sand can not only effectively reduce the use of natural sand but also solve the problem of environmental pollution [8–10]. Coastal buildings are faced with salt-ion erosion due to their service environment, which leads to the durability

failure of concrete structures [11–13]. Once the buildings are damaged, it will inevitably cause huge economic losses. To avoid the failure of concrete structures, it is necessary to study the mechanical properties of concrete structures in coastal environments.

There are many factors contributing to the failure of concrete structures. Among them, chloride ion erosion is the main cause of steel corrosion, which directly leads to the durability failure of concrete structures [14, 15]. When chloride ions penetrate the concrete, they will destroy the steel passivation film, resulting in steel corrosion [16, 17]. Shang-Qin [18] conducted bending tests on concrete beams under chloride erosion conditions. The test results show that with the increase in service time, the ultimate bearing capacity of concrete beams increases first and then decreases.

At the same time, based on the test results and the existing specifications, the formula for calculating the bearing capacity of concrete beams suitable for marine environment is obtained. Yin et al. [19] also conducted similar tests. The test results show that with the increase of the number of dry and wet cycles, the crack width and mid-span deflection of the test beam gradually increases, and the ultimate bearing capacity of the test beam gradually decreases.

Chloride corrosion is the main cause of steel corrosion, and steel corrosion is the first factor affecting the durability of concrete structures [20–22]. Chloride penetrates concrete, destroys steel passive film, and causes steel corrosion [23–25]. In recent years, Hong-Bo et al. [26–30] studied the influence of graphite tailings on the properties of cement-based materials and concrete blocks. The results show that the mechanical properties of cement-based materials can be improved by adding an appropriate amount of graphite tailings. Compared with ordinary concrete, low-content of graphite tailings concrete has better compressive strength, compressive sensitivity, and impermeability. Sun [31] studied the influence of graphite tailings incorporation ratio on the mechanical properties of foamed concrete, and the results show that the appropriate amount of graphite tailings incorporation can improve its compressive strength.

In summary, the research on the durability of graphite tailings concrete focuses on the permeability and resistance to chloride ion erosion of concrete test blocks under chloride salt erosion, while the mechanical properties of graphite tailings concrete components in a chloride salt environment such as bending resistance are less studied. The authors of this paper and their research team have conducted research on related issues and have achieved certain results [32]. To better improve the research paper, in this paper, the bending test of graphite tailings concrete beams with different substitution rates under three curing environments of air, water, and chloride salt is conducted. The failure mode, crack propagation law, load characteristic value, mid-span deflection, and strain of the concrete and steel bar of the test beams under three curing environments are analyzed. According to the above experimental values, a new calculation formula has been established. The above research results will provide good guidance value for similar research on graphite tailings concrete members.

2. Test Overview

2.1. Materials and Mixtures Ratio

- (1) Cement: P.O42.5 ordinary Portland cement.
- (2) Stone: particle size of 5~20 mm, good gradation, apparent density of 2650 kg/m³.
- (3) Natural river sand: river sand with a fineness modulus of 2.49.
- (4) Graphite tailings: graphite tailings from the graphite tailings reservoir.
- (5) Poly carboxylic water reducer: MZ-10C poly-carboxylic high performance water reducer is selected from Table 1.

- (6) Steel bar: HRB400 bar is used. And its diameter is 10 mm, and its yield strength is 415 MPa.

The physical characteristics of natural sand and graphite tailings is shown in Table 1.

2.2. Proportion Relation of Concrete Component Materials.

According to the mix proportion in Table 2, graphite tailings concrete beams with substitution rates of 0, 10%, 20%, 30%, and 40% were prepared. It should be noted that the sand ratio in the table is 30%, which is significantly lower than that of the common pumping concrete in the project. This is because the fineness modulus of sand is small, and there are many particles in the sand, and the cohesion of the concrete is easy to be guaranteed. Therefore, small sand ratio is adopted, and this test is nonpumping concrete. The sand ratio of pumping concrete is 2%–5% higher than that of nonpumping concrete, so the sand ratio used in this test is lower than that of pumping concrete in the project.

2.3. Experimental Design. In this experiment, three groups of graphite tailings concrete beams (air, fresh water, and chloride environment, respectively, expressed by SMK, FE, and CE) were designed, and five concrete beams were made in each group. One of the beams was a natural sand concrete beam as the contrast beam, and the four roots were graphite tailings concrete beams, with substitution rates of 10%, 20%, 30% and 40%, respectively. The number of graphite tailings concrete beams in chloride environment was CE-0, CE-10, CE-20, CE-30, and CE-40. The number of graphite tailings concrete beams in air and freshwater environment was the same. The test beam size is length 1600 mm, section size is 120 mm × 180 mm, and net span is 1500 mm. To study the flexural performance of graphite tailings concrete beams in three environments, all test beams adopt the same reinforcement ratio. The reinforcement ratio of longitudinal tensile reinforcement is 1.257%, and the thickness of the longitudinal reinforcement protective layer is 20 mm. Specimen production and environmental erosion processes are shown in Figure 1. The size and reinforcement of the beam are shown in Figure 2. Each reinforced concrete beam was made, and three cube test blocks were prepared at the same time. After the same condition of maintenance, the same environmental corrosion was conducted with the same group of test beams.

2.4. Test Scheme and Measurement Content. Chlorine salt erosion test using 10% NaCl solution, natural immersion 120 d. The loading test adopts a three-point loading mode, forming a 500 mm pure bending section in the middle of the span. The loading device and the layout of the measuring points are shown in Figure 3. According to the standard of concrete structure test method, the bending test of concrete beams after environmental action is conducted [33]. The concentrated load is applied by a hydraulic press, and the pressure sensor is placed in the span of the distribution beam to realize the loading mode of two concentrated forces and three points. Before the test loading, the test beam is

TABLE 1: Physical properties of graphite tailings sand and natural sand.

Physical property	Grain size (mm)	Apparent density (kg·m ⁻³)	Bulk density (kg·m ⁻³)	Fineness modulus	Water absorption (%)	pH value
Natural sand	0.16~5	2620	1540	2.49	21.87	8
Graphite tailings	0.01~3	2855	1630	0.90	30.10	10

TABLE 2: Mix ratio and mechanical properties of 1 m³ graphite tailing sand concrete.

Test specimen number	Volume of concrete materials (kg/m ³)					Water reducing admixture	Water cement ratio	Percentage of sand (%)
	Water	Cement	Natural sand	Pebble	Graphite tailings			
SMK-0	180.00	409.09	535.48	1294.45	0	15.68	0.44	30
SMK-10	180.00	409.09	481.93	1294.45	53.55	15.68	0.44	30
SMK-20	180.00	409.09	428.38	1294.45	107.10	15.68	0.44	30
SMK-30	180.00	409.09	374.84	1294.45	160.64	15.68	0.44	30
SMK-40	180.00	409.09	321.29	1294.45	214.19	15.68	0.44	30

Note. Specimen number SMK-*n*, SMK represents test beam, *n* represents graphite tailings replacement rate value. For example, SMK-20 represents the test beam with graphite tailings replacement rate of 20%. Among them, SMK-0 is the ordinary concrete control beam.

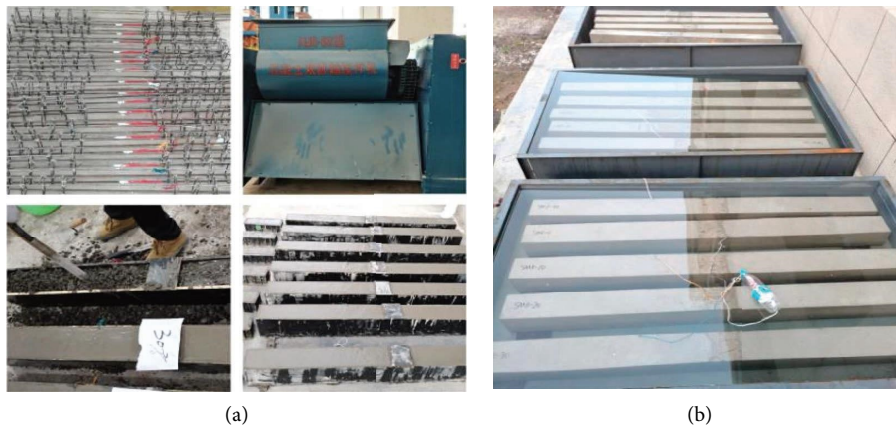


FIGURE 1: Specimen production and environmental erosion process. (a) The specimen-making process. (b) Environmental erosion process.

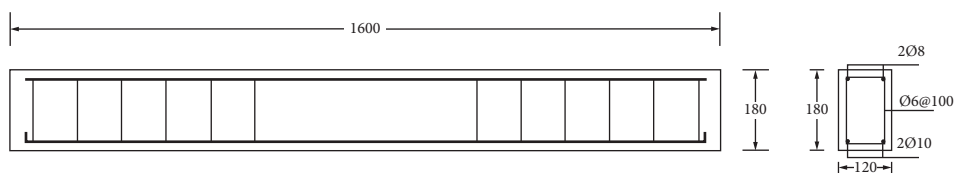


FIGURE 2: Size and reinforcement diagram of the test beam (unit: mm).

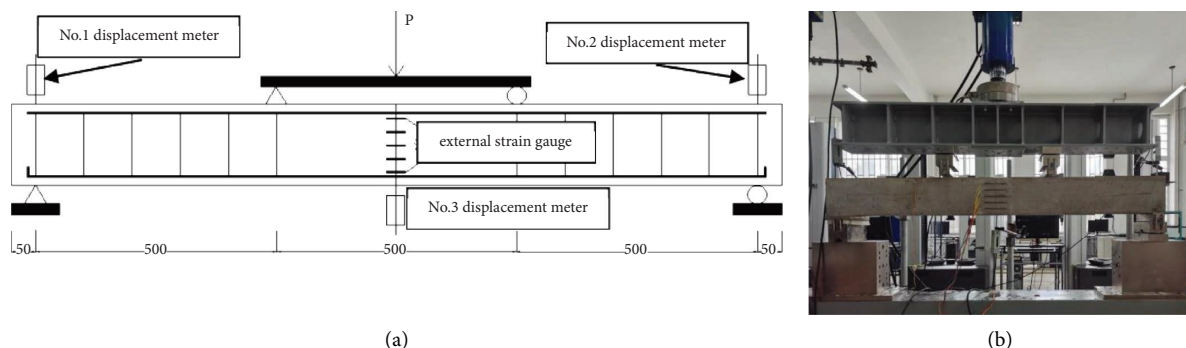


FIGURE 3: Layout of measuring points and loading device diagram. (a) Layout of measuring points. (b) Loading device.

preloaded to ensure the normal operation of the instrument and the normal contact of each point. At the beginning, the loading mode was according to each level of 3 kN loading, each loading stayed for 3 minutes, and then the change of cracks on the surface of the beam was observed, when the specimen's first crack appeared, with each level of 5 kN for differential loading and gradual increase of load, the number of cracks gradually increased, cracks continued to extend upward and the crack width increased, with the pen to thicken the cracks of the test beam, in order to more clearly see the cracks of the test beam, and record the stress load and crack width.

The main measurement contents of the test are as follows: (1) Cracking load, ultimate load and crack development process of the test beam, and the crack development process is observed by the DJCK-2 crack width meter. (2) The strain of reinforcement and concrete is measured by sticking strain gauges in the middle of the tensile reinforcement, and five concrete strain gauges are evenly arranged along the height of the beam in the middle of the beam span to measure the strain of concrete; (3) Load-deflection changes, YHD-50 displacement gauges arranged at both ends of the beam and the middle of the beam to measure the deformation of the specimen.

3. Experiment Results and Analyses

3.1. Crack Propagation Distribution Law. Through the bending load test of the test beam, it is found that the failure process and crack development process of the graphite tailings concrete beam in the three environments are consistent with those of the ordinary concrete beam. The failure mode and crack development process of each test beam in the fresh water and chloride environments are also basically consistent with those in the air environment, but the characteristic load changes slightly. The bending failure mode and crack distribution of the test beam in the fresh water and chloride environment, are shown in Figure 4.

3.2. Cracking Load and Ultimate Load of Beam. The test results of the cracking load P_{cr} and ultimate load P_u of each test beam under air, water and chloride environment are shown in Table 3. The effects of different variation parameters on cracking load and ultimate load of test beam are shown in Figures 5 and 6. It can be seen from Table 3 and Figures 5 and 6.

3.2.1. Effects of Different Graphite Tailings Replacement Ratios on Cracking Load and Ultimate Load of Test Beams. It can be seen from Table 3 and Figure 5 that with the increase of graphite tailings replacement rate, the variation laws of cracking load and ultimate load of test beams in air, water, and chlorine salt are the same, showing a trend of first increase and then decrease. Among them, in the chloride environment, the cracking loads of CE-10 and CE-20 increased by 12.64% and 15.97%, respectively, compared with CE-0, and the ultimate load increased by 6.78% and 8.93%, respectively. The cracking load and ultimate load of CE-40

decreased by 8.39% and 5.00% compared with CE-0. The results show that with the increase of graphite tailings replacement rate, the performance of test beams in different environments is better than that of ordinary concrete beams at the replacement rate of 10%~20%, and the bearing capacity is lower than that of ordinary concrete beams at the replacement rate of 40%. The reason is that when the replacement rate of graphite tailings is 10%~20%, the diameter of graphite tailings is smaller than that of natural sand, which makes the distribution of particles in concrete more uniform, increases the compactness of concrete materials and improves the bearing capacity of graphite tailings concrete beams.

3.2.2. Influence of Different Erosion Environment on Cracking Load and Ultimate Load of Graphite Tailings Concrete Beam.

It can be seen from Table 3 and Figure 6 that the bearing capacity of the test beam under a clear water environment is the highest under the same replacement rate of graphite tailings, and the bending bearing capacity of the test beam after chlorine salt erosion is lower than that in an air (noncorrosion) environment. Taking the replacement rate of graphite tailings 20%, as an example, the cracking load and ultimate load of graphite tailings concrete beams in a clear water environment are increased by 6.74% and 4.87%, respectively, compared with those in an air environment. This is because the hydration reaction can continue to occur in the test beam in a clear water environment, and the hydration products are generated to make the concrete denser, thus enhancing the bearing capacity of the test beam. However, the cracking load and ultimate load of graphite tailings concrete beams after chloride corrosion are 3.82% and 2.03% lower than those in an air environment, respectively. It is also found that the cracking load is more affected by environmental erosion than the ultimate load, indicating that the bearing capacity of reinforced concrete beams immersed in a 10% NaCl solution for 120 days is more affected by concrete damage.

3.3. Mid-Span Deflection. The load-deflection curves of concrete beams with different graphite tailings replacement rates in air, water, and chloride environments are shown in Figures 7(a)–7(c). To compare the change law of mid-span deflection of concrete beams with the same graphite tailings replacement rate after erosion in different environments with load, the load-deflection curves of concrete beams with a 20% graphite tailings replacement rate after erosion in air, water, and chloride environments are plotted, as shown in Figure 7(d). From Figure 7, it can be seen that the load-deflection curve trend of a graphite tailings concrete beam and an ordinary concrete beam is similar, which can be divided into three stages: (1) The noncracking stage of the test beam: at the initial stage of loading, the test beam is not cracked, the load-deflection curve is approximately linear change, and the deflection increment is small. (2) The test beam cracked at the yield stage of reinforcement. After the test beam cracked, the load-deflection curve showed a turning point, and the growth rate of deflection gradually accelerated.

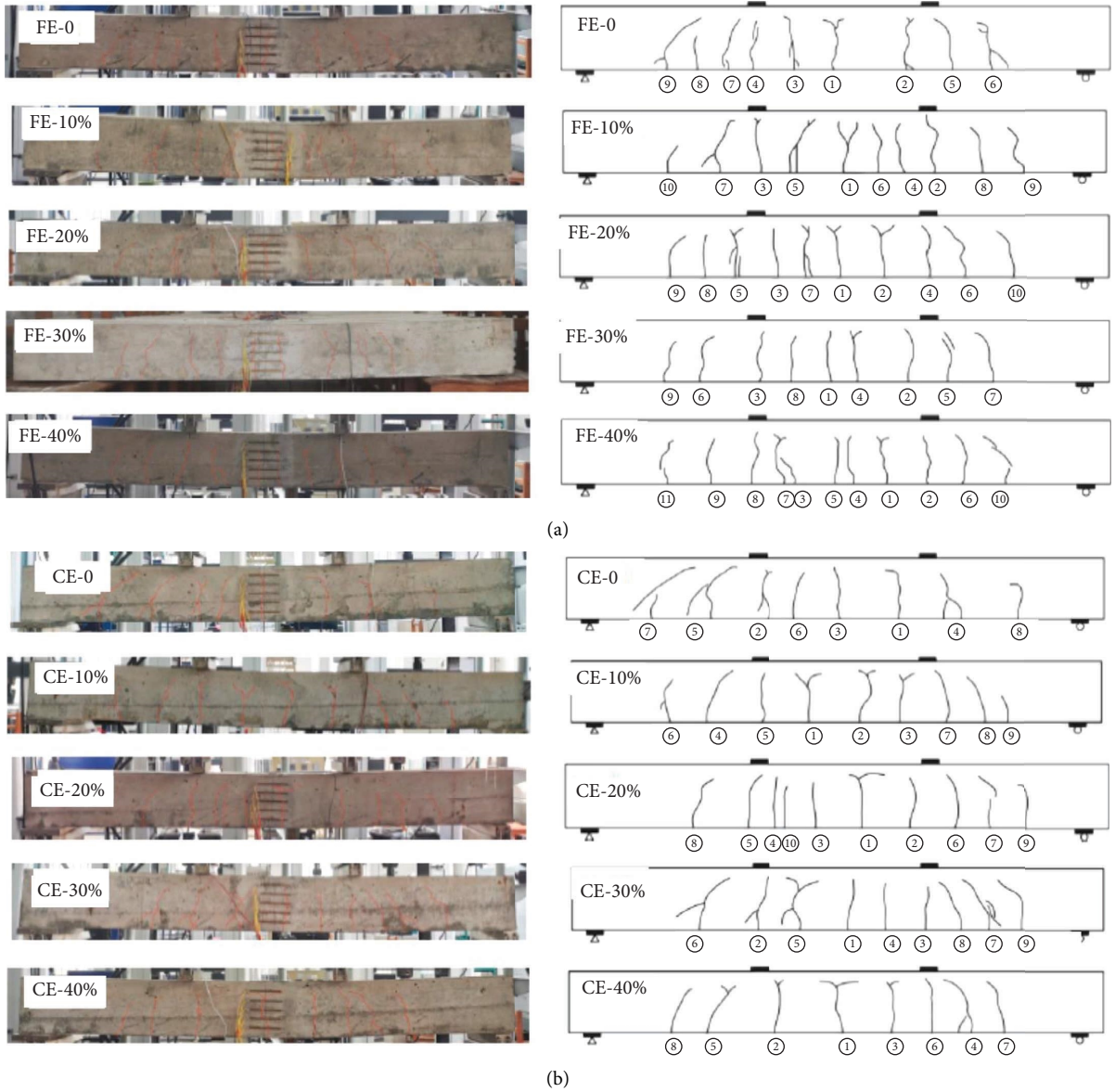


FIGURE 4: Bending failure mode and crack distribution map of test beam under water and chloride environment. (a) Fresh water environment and (b) chloride environment.

TABLE 3: Test values of cracking load and ultimate load of test beams in three environments.

Graphite tailings sand replacement rate (%)	Air environment		Clear water environment		Chlorine environment	
	P_{cr} (kN)	P_u (kN)	P_{cr} (kN)	P_u (kN)	P_{cr} (kN)	P_u (kN)
0	12.12	49.25	12.42	50.85	11.08	47.81
10	13.25	52.01	13.37	53.17	12.48	51.05
20	13.36	53.16	14.26	55.75	12.85	52.08
30	12.43	50.33	13.17	52.42	11.51	49.26
40	11.21	47.01	12.12	49.17	10.15	45.42

The load-deflection curve gradually developed nonlinearly after cracking. (3) The steel bar yield to the failure stage: after the steel bar yield, the load-deflection curve appears the second turning point, and the deflection of the beam increases sharply after yield. The load-deflection curve is also close to a horizontal straight line, and the final test beam is damaged.

Specifically, it can be seen from Figures 7(a) and 7(b) that when the test beam bears the same level of load in an air and clear water environment, with the increase of the graphite tailings replacement rate, the mid-span deflection of the test beam decreases first and then increases. When the replacement rate is 20%, the mid-span deflection of the test

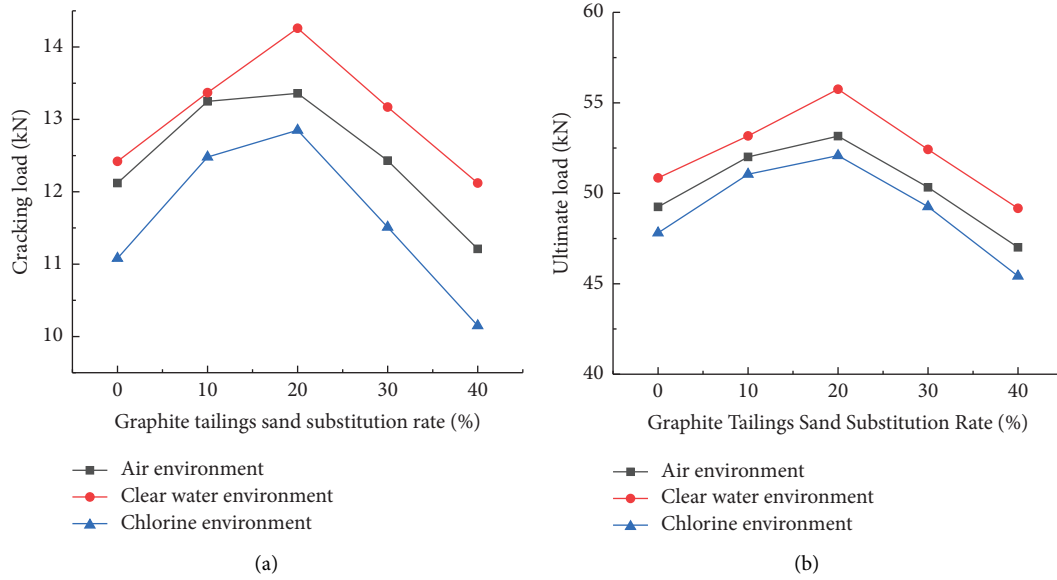


FIGURE 5: Influence of graphite tailing sand replacement rate on cracking load and ultimate load of test beam. (a) Cracking load and (b) Ultimate load.

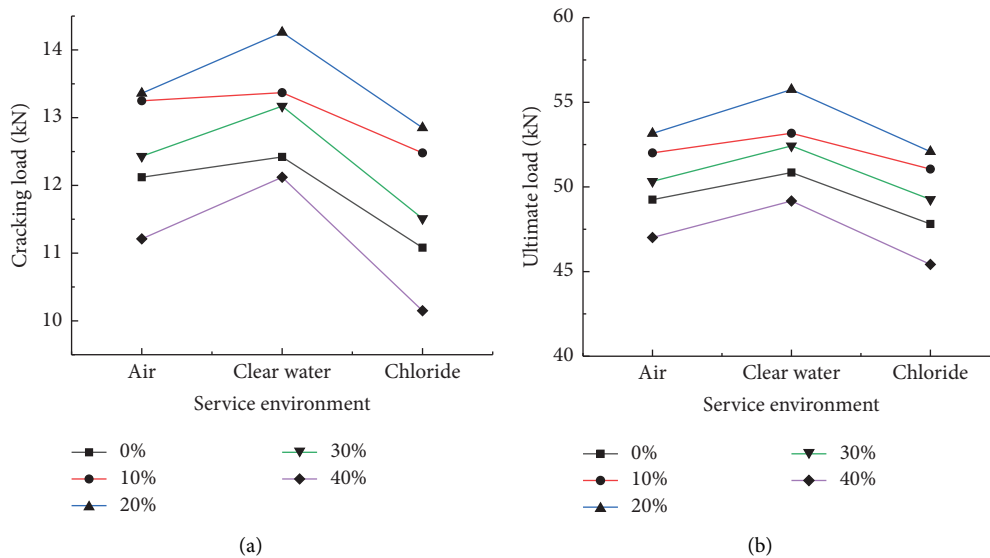


FIGURE 6: Influence of service environment on cracking load and ultimate load of test beam. (a) Cracking load and (b) Ultimate load.

beam is small. It can be seen from Figure 7(c) that after chlorine salt erosion of graphite tailings concrete beams, when the replacement rates of graphite tailings are 10% and 20%, the mid-span deflection growth rate of the test beam is slower than that of the ordinary concrete beam. When the replacement rate of graphite tailings is 40%, the mid-span deflection growth of the test beam is faster than that of the ordinary concrete beam, indicating that a small amount of graphite tailings can improve the flexural performance of reinforced concrete beams after chlorine salt erosion. It can be seen from Figure 7(d) that under the same load, the mid-span deflection of the graphite tailings concrete beam presents the law of clear water < air < chlorine salt.

3.4. *The Variation of Mid-Span Concrete Strain.* The mid-span concrete strain curves of concrete beams with different graphite tailings content under different loads in clear water and chlorine salt environment are shown in Figures 8 and 9. It can be seen from Figures 8 and 9 that with the increase of load, the concrete strain of each test beam shows an increasing trend. When the load is 20 kN, the concrete strain of the test beam CE-10 is larger than that of the FE-10, indicating that the resistance to deformation of the graphite tailings concrete beam decreases after being corroded by chloride. Under the environment of clear water and chloride salt, when the test beam was subjected to the same load, the cross-

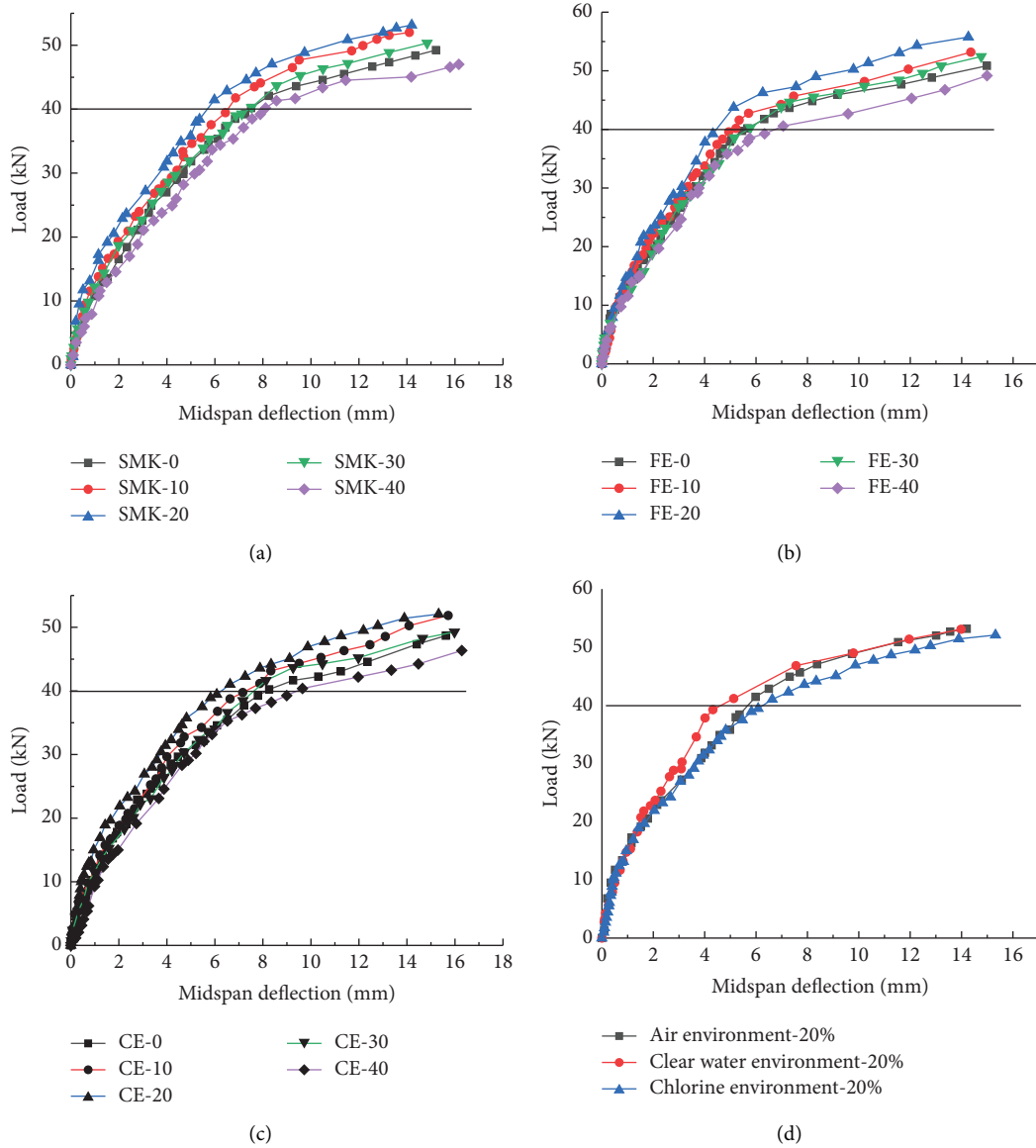


FIGURE 7: Load-deflection curve. (a) Air environment; (b) fresh water environment; (c) chloride environment; and (d) the replacement rate of graphite tailings is 20%.

sectional strain of concrete beams with different graphite tailings content was not significantly different, and the strain of concrete beams with 40% graphite tailings content was slightly higher. However, regardless of the amount of graphite tailings, the strain at each measuring point on the normal section is proportional to the distance from the point to the neutral axis, and the concrete strain of each measuring point on the mid-span section is linearly distributed. Therefore, in a clear water and chloride environment, the graphite tailings concrete beam still conforms to the plane section assumption. The test results show that the cross section of a graphite tailings concrete beam conforms to the plane section assumption under the three test environments listed above, which provides the experimental basis for the theoretical calculation of bearing capacity.

3.5. Longitudinal Steel Strain in the Mid-Span. The variation trend of the longitudinal tensile reinforcement strain in the mid-span of the test beam under different environments with the increase of load is shown in Figure 10. The load-steel strain curve of graphite tailings concrete beam can be divided into three parts: (1) In the early stage of loading, the test beam has not yet cracked elastic stage. In this stage, the tensile force is borne by concrete and steel, and the strain value of steel increases slowly and linearly. (2) From the cracking stage of the test beam to the yield stage of the steel bar, the tensile force of the test beam after cracking is transferred to the steel bar. In this stage, the steel bar strain is still linearly increased, but the growth rate is faster than that before cracking, and the slope of the steel bar strain-load curve is reduced. (3) When the steel bar yields to the failure stage, the load increases slightly and the strain increases sharply.

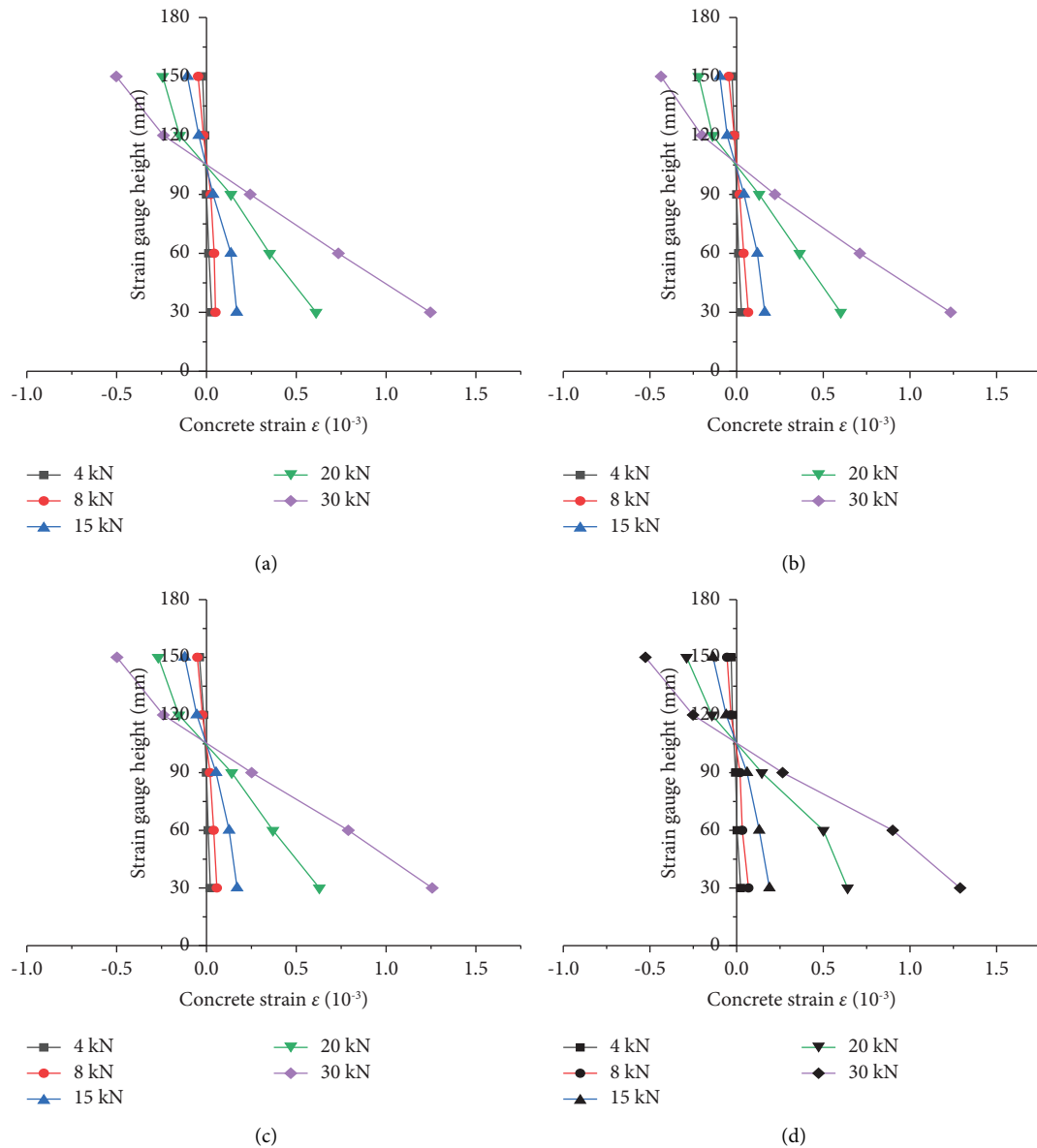


FIGURE 8: Strain distribution of different section heights in the middle of the test beam in a freshwater environment. (a) FE-10; (b) FE-20; (c) FE-30; and (d) FE-40.

It can be seen from Figure 10 that after water and chloride erosion, the longitudinal tensile steel strain of concrete beams with different graphite tailings replacement rates is consistent with that of ordinary concrete beams, and the slope of the curve is the same, indicating that the graphite tailings replacement rate has an insignificant effect on the steel strain. In the chloride environment, when each test beam bears the same load, the strain of the steel bar of the graphite tailings concrete beam with the replacement rate of 20% is smaller than that of the ordinary concrete beam and is smaller than that of the other graphite tailings replacement rate test beams. The reason is that when the replacement rate of graphite tailings is 20%, the porosity of the test beam is the smallest and the densest, and the influence of chloride ions into the concrete on the steel bar is the smallest, so the steel

bar strain is small. This shows that the pore structure of concrete beams with graphite tailings is better than that of ordinary concrete beams with a small amount of graphite tailings, which is more conducive to the resistance of concrete beams to chloride corrosion damage.

Taking the replacement rate of graphite tailing sand of 20% as an example, the strain-load curve of the mid-span longitudinal tensile steel bar of 20% graphite tailing concrete beam in clear water and chloride environment is drawn, as shown in Figure 11. It can be seen from the diagram that chloride salt erosion has a slight effect on the strain of steel bars of graphite tailings concrete beams, but due to the short immersion time and low corrosion degree, chloride salt erosion has no significant effect on steel bars.

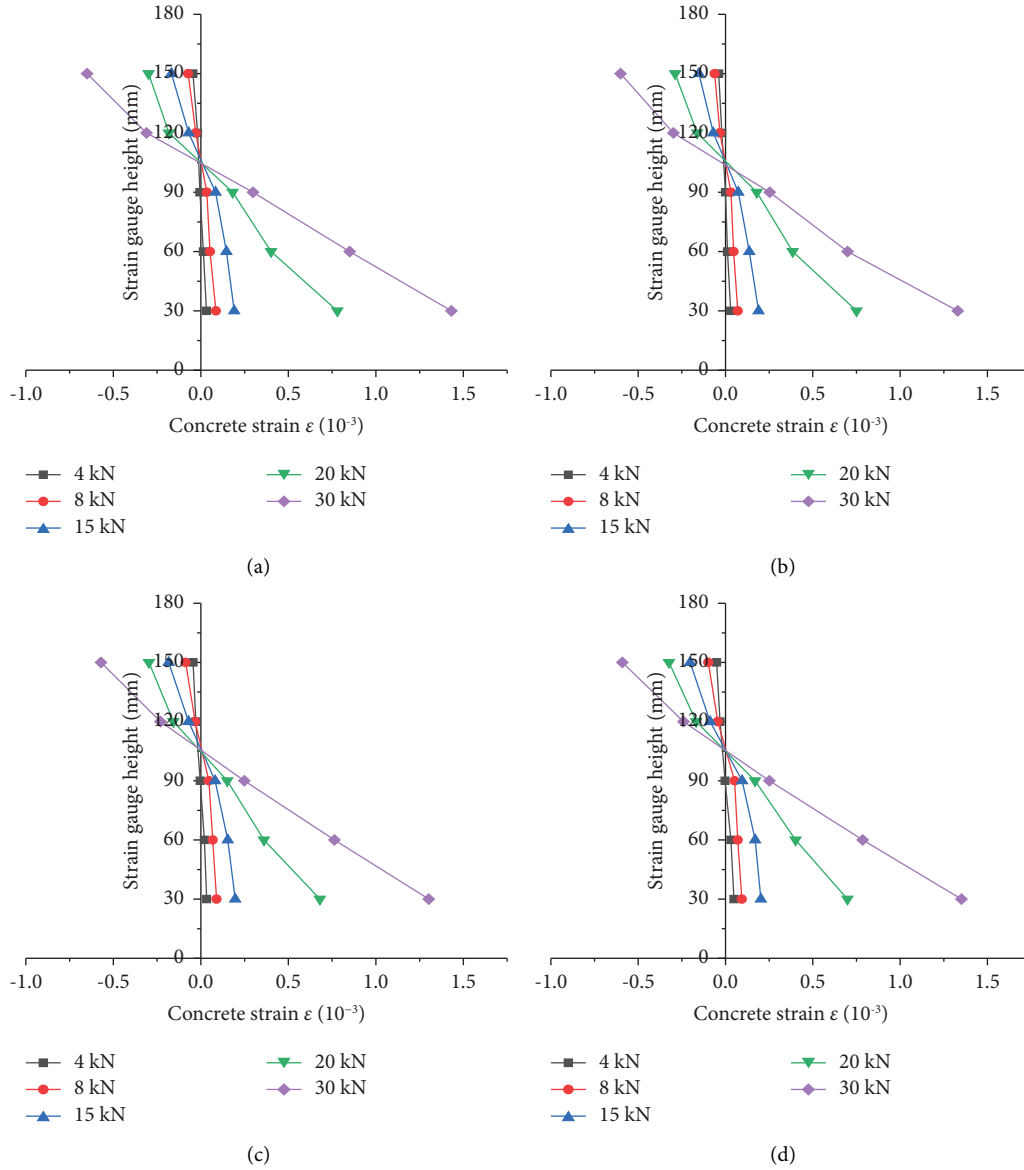


FIGURE 9: Strain distribution of different section heights in the middle of test beam in a chlorine environment. (a) CE-10; (b) CE-20; (c) CE-30; and (d) CE-40.

4. Analysis of Bearing Capacity of Graphite Tailings Concrete Beam Normal Section Under Chloride Erosion Environment

After chlorine salt erosion, the internal damage of graphite tailings concrete makes the strength of graphite tailings concrete decrease. The degradation of concrete’s mechanical properties is the main factor affecting the bending performance of graphite tailings-reinforced concrete beams under the salt erosion environment. Therefore, in this section, the formula for calculating the ultimate bearing capacity of test beams after chlorine salt erosion is derived, and the influence of concrete strength changes with different graphite tailings contents on the bending bearing capacity of reinforced concrete beams after salt erosion is emphatically discussed. The theoretical value of the ultimate bearing capacity of the graphite tailings concrete beam after

chloride corrosion is calculated by using the bearing capacity calculation formulas (1) and (2) of the normal section of the reinforced concrete beam [34]. The calculation results are shown in Table 4. In the table, M_c^y represents the ultimate bending moment test value of the graphite tailings concrete beam after salt corrosion, and M_u^y represents the theoretical calculation value of the ultimate bending moment of the graphite tailings concrete beam after salt corrosion.

$$M_u = \alpha_1 f_c b x \left(h_0 - \frac{x}{2} \right), \tag{1}$$

$$\alpha_1 f_c x = f_y A_s, \tag{2}$$

where, α_1 is the simplified stress figure coefficient of the concrete in the compression zone, taking 1.0; f_c is the measured compressive strength of graphite tailings concrete

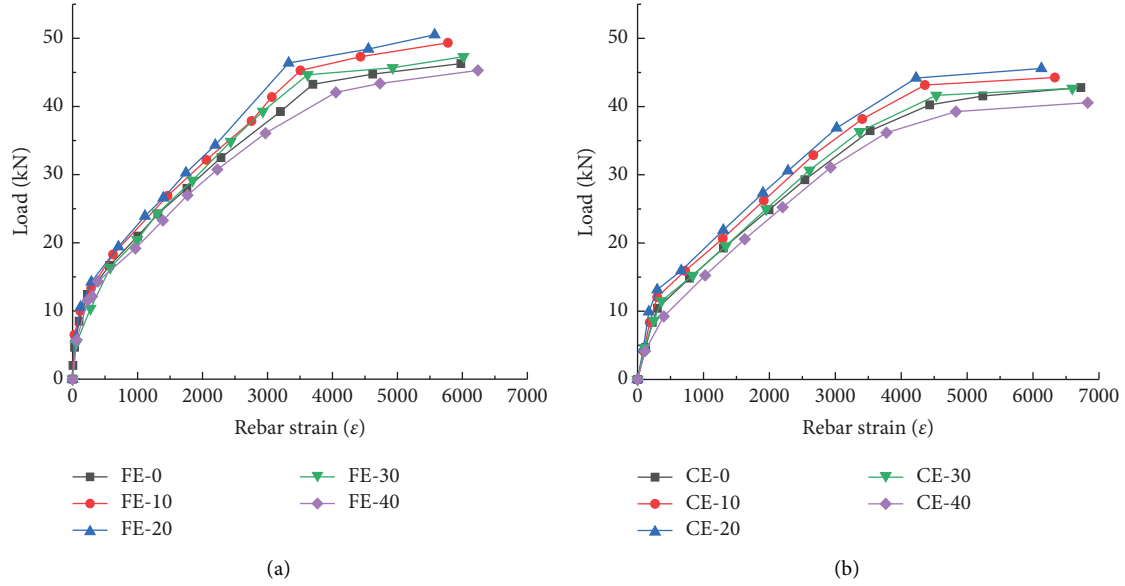


FIGURE 10: Strain-load curve of the longitudinal tensile steel bar in the middle of each test beam. (a) Fresh water environment and (b) chloride environment.

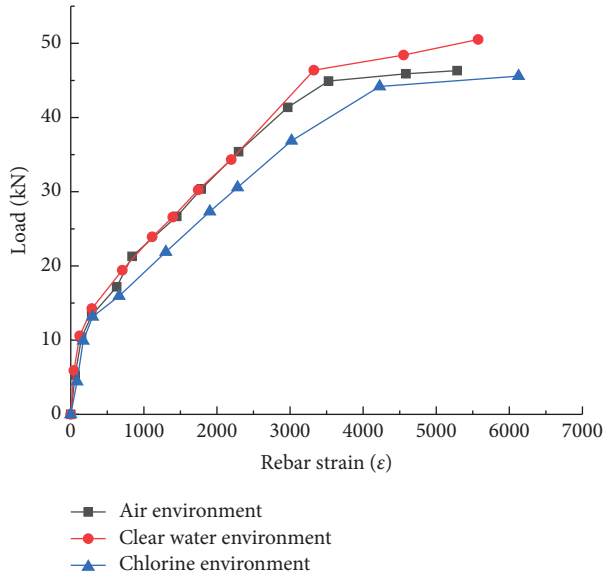


FIGURE 11: Strain-load curves of 20% graphite tailings concrete beams in different environments.

after chloride erosion, and takes the measured value, MPa; b is the beam width, mm; x is the height of the compression zone of the section, mm; h_0 is the effective height of the section, mm; f_y is the yield strength of longitudinal bars, and takes the measured value, MPa; and A_s is the effective cross-sectional area of the longitudinal reinforcement under tension, mm^2 . The table is the comparison of calculated and experimental values of ultimate bearing capacity of graphite tailings concrete beams after chloride salt erosion.

From Table 4, the experimental values of graphite tailings concrete beams and ordinary concrete beams after chlorine salt erosion are greater than the calculated values, indicating that the ultimate bearing capacity of graphite

TABLE 4: Comparison of experimental and computational results according to formulas (1) and (2).

Specimen number	f_c (MPa)	M_c^y (MPa)	M_u^y (MPa)	M_c^y/M_u^y
CE-0	35.2	11.95	9.206	1.298
CE-10	36.1	12.76	9.218	1.384
CE-20	36.9	13.02	9.229	1.411
CE-30	35.1	12.32	9.204	1.339
CE-40	34.6	11.36	9.197	1.235

tailings concrete beams after chlorine salt erosion is feasible to calculate according to concrete specifications. To obtain the ultimate bearing capacity of concrete beams with different replacement rates of graphite tailings after chlorine salt erosion more accurately, two different fitting functions are used, and the correction coefficient of graphite tailings replacement rate is introduced. The data of concrete beams with different replacement rates of graphite tailings after chlorine salt erosion are numerically fitted.

4.1. Polynomial Fitting. To express the ultimate bearing capacity of graphite tailings concrete beams more accurately, the test results in Table 4 are fitted by polynomial function, and the fitting formula (3) and the fitting curve in Figure 12 are obtained. According to the fitting curve, the correlation coefficient of the fitting curve is 0.9879.

$$M^y = \gamma M_u^y = (Ax^2 + Bx + C)M_u^y, \quad (3)$$

where x is the replacement rate of graphite tailings sand, (%); γ is the correction factor; M_u^y is the theoretical calculation value of the ultimate bearing capacity of the test beam after chloride corrosion, MPa; and M^y is the corrected ultimate bearing capacity of the test beam after chloride corrosion, MPa; $A = -3.42143E - 4$, $B = 0.01198$, $C = 1.29917$. Table 5 is

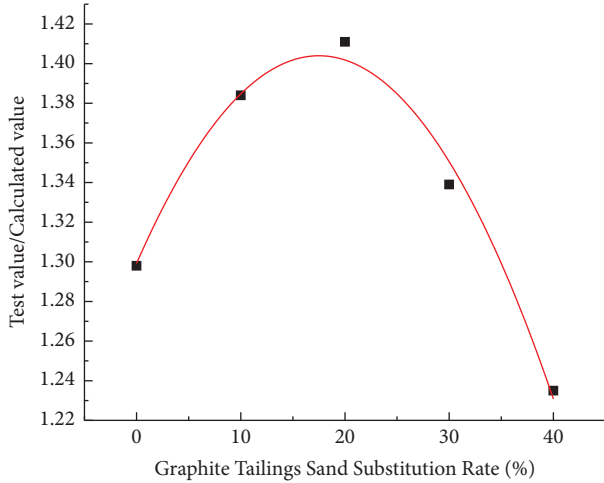


FIGURE 12: Polynomial fitting curve of ultimate bearing capacity of concrete beams with different replacement rates of graphite tailings after chloride erosion.

TABLE 5: Comparison of experimental and computational results according to formula (3).

The number of specimens	M^y (MPa)	M_c^y (MPa)	M_c^y/M^y
CE-0	12.02	11.95	0.9942
CE-10	12.82	12.76	0.9953
CE-20	13.00	13.02	1.0015
CE-30	12.50	12.32	0.9856
CE-40	11.40	11.36	0.9965

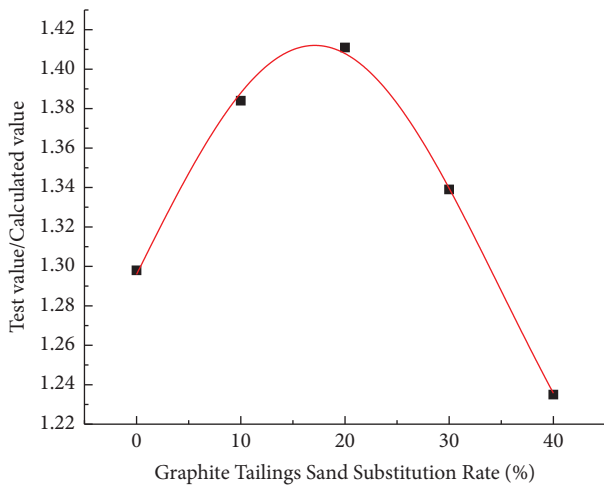


FIGURE 13: Gaussian function fitting curve of ultimate bearing capacity of concrete beams with different replacement rates of graphite tailings after chloride erosion.

a comparison of calculated and experimental values from formula (3).

4.2. Gaussian Function Fitting. The Gauss function fitting curve is shown in Figure 13. According to the fitting curve, the formula for calculating the ultimate bearing capacity of a normal section of graphite tailings concrete beam after

TABLE 6: Comparison of experimental and computational results according to formula (4).

The number of specimens	M^y (MPa)	M_c^y (MPa)	M_c^y/M^y
CE-0	11.93	11.95	1.0017
CE-10	12.78	12.76	1.0016
CE-20	12.96	13.02	1.0046
CE-30	12.33	12.32	0.9992
CE-40	11.38	11.36	0.9984

chloride salt erosion is (4) and (5), and the correlation coefficient of the fitting curve is 0.9985. Compared with the polynomial fitting curve, the correlation coefficient of the Gaussian function fitting curve is closer to one, and the degree of coincidence is higher, indicating that the calculation formula of ultimate bearing capacity modified by the Gaussian function is more suitable for the calculation of ultimate bearing capacity of graphite tailings concrete beams after chlorine salt erosion. The axial compressive strength in the calculation formula needs to use the measured compressive strength value of graphite tailings concrete block after chlorine salt erosion. In practical engineering application, the compressive strength can be determined according to the empirical data or through experiments. At the same time, the modified formula can estimate the ultimate bearing capacity of the graphite tailings concrete beams with other mass replacement rates after chloride attack.

$$M^y = yM_u^y, \quad (4)$$

$$y = y_0 + \frac{A}{w \times \sqrt{\pi/2}} \times \exp \left[-2 \frac{x - w_0}{w} \right]^2, \quad (5)$$

where M^y is the corrected ultimate bearing capacity of the test beam after chloride corrosion, MPa; y is the correction factor; M_u^y is the theoretical calculation value of the ultimate bearing capacity of the test beam after chloride corrosion, MPa; and x is the replacement rate of graphite tailings sand, (%); $y_0 = 1.10078$; $A = 13.81231$; $w = 35.40572$; $w_0 = 17.10824$. Table 6 is a comparison of calculated and experimental values from formula (4).

5. Conclusion

Graphite tailings are solid waste produced in the process of graphite mining, which has caused great damage to the natural ecological environment. Partial replacement of graphite tailings with construction sand is one of the effective ways to reuse solid waste. This paper studies the crack propagation law and bearing capacity of graphite tailings concrete beams under load. The following conclusions can be drawn from this study:

- (1) Through experiments, it is found that the failure process and crack development process of graphite tailings concrete beams under three curing environments are the same, but the failure load of graphite tailings concrete beams under a chloride curing environment is small.

- (2) In the three kinds of concrete curing environment, the fracture load and ultimate load of concrete beams with graphite tailings sand replacement rate of 20% are the largest. When the replacement rate of graphite tailings sand is the same, the fracture load and ultimate load of concrete beams under a chloride curing environment are the smallest.
- (3) In three kinds of concrete experimental environment, when the concrete test beam under the same load, with the increase of graphite tailings replacement rate, the mid-span deflection of concrete beam decreases first and then increases. When the replacement rate of graphite tailings sand is 20%, the mid-span deflection of the test beam is the smallest; when the replacement rate of graphite tailings sand is 10% and 20%, the growth rate of the mid-span deflection of the test beam is slower than that of the ordinary concrete beam.
- (4) Under the same load, the mid-span deflection of a graphite tailings sand concrete beam under the water experimental environment < the mid-span deflection of the graphite tailings sand concrete beam under the air experimental environment < the mid-span deflection of a graphite tailings sand concrete beam under the chloride experimental environment.
- (5) The test results show that the cross section of a graphite tailings concrete beam conforms to the plane section assumption under the above three test environments, which provides the experimental basis for the theoretical calculation of bearing capacity.
- (6) The experimental results show that the replacement rate of graphite tailings sand has negligible effect on the strain of steel bar. Comparing the strain values of the steel bars, it is found that the strain value of the steel bars in the graphite tailings sand concrete beam changes little than in the clear water experimental environment. In the chloride salt experimental environment, due to concrete and steel by chloride ion erosion, steel strain value changes large.
- (7) Through the data fitting of the bearing capacity test results of graphite tailings concrete beams, the modified Gauss bearing capacity calculation formula is obtained. This conclusion has great reference value for the study of mechanical properties of concrete beams under chloride environment.

Data Availability

The data used to support the findings of this study are included within the article.

Disclosure

The manuscript was already published as a preprint based on the link https://papers.ssrn.com/sol3/papers.cfm?abstract_id=4033145.

Conflicts of Interest

The authors declare that they have no conflicts of interest.

Acknowledgments

The authors would like to thank the National Natural Science Foundation of China (51374045) and Key Laboratory Platform of Dalian University (202101ZD02) and Research Innovation and Entrepreneur-Ship Team of Dalian University (XQN202002) and Teaching Reform Foundation of Dalian University (JG2022031) for supporting this work. The authors gratefully acknowledge the financial support from the organization.

References

- [1] L. En-Ping, "Analysis on the development of Offshore cities under the new development Pattern of double Circulation[J]," *Enterprise Economy*, vol. 40, no. 11, pp. 5–14+2, 2021.
- [2] X. Jian-Zhuang, J.-Y. Shen, and Q. Gao, "Current situation and innovative technology for recycling of engineering waste soil[J]," *Journal of architecture and civil engineering*, vol. 37, no. 04, pp. 1–13, 2020.
- [3] S. Fang-Zhi and X.-J. Li, "Summary of energy-saving and emission-reduction of road engineering," *Road Machinery & Construction Mechanization*, vol. 28, no. 11, pp. 30–35+45, 2011.
- [4] X.-Fu Han, "Improving Industrial development environment and Adhering to low Carbon green road-Thoughts on the present situation and development trend of concrete Industry in China," *China Concrete*, vol. 4, pp. 42–46, 2011.
- [5] H. Su, "Construction waste recycled concrete application," *Building Technology Development*, vol. 36, no. 11, pp. 19–20, 2009.
- [6] P. N. Hiremath and S. C. Yaragal, "Effect of different curing regimes and durations on early strength development of reactive powder concrete," *Construction and Building Materials*, vol. 154, pp. 72–87, 2017.
- [7] A. A. Mokhtar, R. Belarbi, and F. B. Jema, "Experimental investigation of the variability of concrete durability properties [J]," *Cement and Concrete Research*, vol. 1, no. 25, pp. 21–36, 2013.
- [8] Y. Guo, Z. Chen, and X. Qin, "Evolution mechanism of microscopic pores in pavement concrete under multi-field coupling," *Construction and Building Materials*, vol. 173, pp. 381–393, 2018.
- [9] C. Zhang, L. Ben, Y. Yu, and Y.-J. Zhao, "Effect of graphite tailings on mechanical properties of recycled coarse aggregate concrete," *Journal of Foshan University (Social Science Edition)*, vol. 39, no. 4, pp. 9–15, 2021.
- [10] H. Liu, X.-F. Wang, and Z.-H. Yang, "Potential ecological Risk Assessment of Heavy Metals in Abandoned mining areas in Eastern Heilongjiang Province," *Journal of Engineering*, vol. 9, no. 1, pp. 40–45, 2018.
- [11] J. Thomas, N. N. Thaickavil, and P. M. Wilson, "Strength and durability of concrete containing recycled concrete aggregates," *Journal of Building Engineering*, vol. 19, pp. 349–365, 2018.
- [12] J. De Brito, J. Ferreira, J. Pacheco, D. Soares, and M. Guerreiro, "Structural, material, mechanical and durability properties and behaviour of recycled aggregates concrete," *Journal of Building Engineering*, vol. 6, pp. 1–16, 2016.

- [13] S.-Y. Wang, T.-H. Jiang, and X.-C. Zhang, "Study on chloride ion penetration resistance of high-performance concrete under double deterioration mechanism," *Transportation Science & Technology*, vol. 5, pp. 149–152, 2021.
- [14] W.-M. Qian, J. Su, L. I. Yang, J. I. Wei, and J.-Y. Zhao, "Effect of ultra-low temperature and chloride on carbonation performance of ultra-high toughness cement-based composite," *Acta Materiae Compositae Sinica*, 2022.
- [15] D.-X. Cai, B. I. Wen-Yan, and X.-M. Guan, "Simulation and experiments of the effect of coarse aggregates on the diffusion of chloride ions in concrete," *Journal of Building Materials*, 2022, <https://kns.cnki.net/kcms/detail/31.1764.TU.20220902.1720.002.html>.
- [16] M. Qing, J. Chang, and B.-Y. Sun, "Research on sulfate corrosion resistance and Microstructure characteristics of Iron tailings concrete," *Multipurpose Utilization of Mineral Resources*, 2022, <https://kns.cnki.net/kcms/detail/51.1251.td.20220831.1653.002.html>.
- [17] D. Shang-Qin, *Experimental study on Mechanical Properties of sea sand concrete Beams in marine Environment*, Guangxi University, Guangxi, China, 2020.
- [18] S.-P. Yin, Y. Yu-Lin, and N. Ming-Wang, "Bending performance analysis of TRC reinforced beams under chloride erosion[J]," *Journal of Huazhong University of Science and Technology (Natural Science Edition)*, vol. 47, no. 02, pp. 7–13, 2019.
- [19] S. Qing-Bo, J.-J. Zhang, and F.-N. Zhou, "Experimental study on chloride ion erosion of Joints in concrete Bridge[J]," *Railway Construction Technology*, vol. 8, pp. 30–34+110, 2022.
- [20] X.-Y. Mou, Y.-W. Wang, and L. Shi-Bao, "Prediction of effective chloride diffusion coefficient of recycled aggregate concrete based on multiscale analysis," *Acta Materiae Compositae Sinica*, 2022.
- [21] Z.-G. Sun, L. Xiao-Kui, and L. Hong-Biao, "Flexural strengthening Effectiveness of chloride corrosion damaged RC beams by using PVA-ECC," *Journal of Basic Science and Engineering*, vol. 30, no. 04, pp. 963–973, 2022.
- [22] H. Liu, Q. Zhang, V. Li, H. Su, and C. Gu, "Durability study on engineer cementitious composites (ECC) under sulfate and chloride environment," *Construction and Building Materials*, vol. 133, no. 15, pp. 171–181, 2017.
- [23] M. Sahmaran, V. C. Li, and C. Andrade, "Corrosion resistance of steel-reinforced engineer cementitious composite beams," *ACI Materials Journal*, vol. 105, no. 3, pp. 243–250, 2008.
- [24] Y. Zhang, N. Ueda, H. Nakamura, M. Kunieda, and H. Nakamura, "Behavior investigation of reinforced concrete members with flexural strengthening using strain-hardening cementitious composite," *ACI Structural Journal*, vol. 114, no. 2, pp. 417–426, 2017.
- [25] A. S. Shanour, M. Said, A. I. Arafa, A. Maher, and A. I. Arafa, "Flexural performance of concrete beams containing engineered cementitious composites," *Construction and Building Materials*, vol. 180, no. 20, pp. 23–34, 2018.
- [26] L. Hong-Bo, Yu-X. Zhang, and Z.-R. Wang, "Research on compressive strength and impermeability of graphite tailings cement mortar [J]," *Engineering Journal of Heilongjiang University*, vol. 10, no. 04, pp. 16–20, 2019.
- [27] H. Liu, B. Li, J. Xue, J. Hu, and J. Zhang, "Mechanical and Electroconductivity properties of graphite tailings concrete," *Advances in Materials Science and Engineering*, vol. 2020, Article ID 9385097, 20 pages, 2020.
- [28] Z.-R. Wang, B. Li, and L. Hong-Bo, "Degradation characteristics of graphite tailings cement mortar subjected to freeze-thaw cycles," *Construction and Building Materials*, vol. 234, pp. 132–133, 2020.
- [29] L. Hong-bo, D.-S. Zhang, and L. Xiao-li, "Research on the Compress-ion sensitivity of graphite tailings concrete," *Journal of Engineering of Heilongjiang University*, vol. 6, no. 01, pp. 22–27, 2015.
- [30] S. Xiao-wei, W.-qi. Zhang, and Qi. Wang, "Research on the performance of graphite tailings foamed concrete," *Nonmetallic Minerals*, vol. 43, no. 03, pp. 9–13, 2020.
- [31] W.-X. Sun, *Study on Durability of Graphite Tailings Concrete*, Heilongjiang-ang University, Heilongjiang, China, 2019.
- [32] F. Bo-Ya, X. Xia, Z. Zhu, and X. Zhu, "Experimental study on flexural behaviour of graphite tailings concrete beam in chloride environment," 2022, https://papers.ssrn.com/sol3/papers.cfm?abstract_id=4033145.
- [33] National Standard of the People's Republic of China, *GB/T 50152-2012 Standard for Test Methods of concrete structure*, China Architecture & Building Press, Beijing, 2012.
- [34] National Standard of the People's Republic of China, *GB 50010-2010 Code for Design of concrete structures*, China Architecture & Building Press, Beijing, 2010.

Research Article

The Impact of Molar Proportion of Sodium Hydroxide and Water Amount on the Compressive Strength of Slag/Metakaolin (Waste Materials) Geopolymer Mortar

Fatimah N. Al-Husseinawi ^{1,2}, William Atherton ³, Zainab Al-Khafaji ⁴,
Monower Sadique ³ and Zaher Mundher Yaseen ⁵

¹Liverpool John Moores University, Department of Civil Engineering, Liverpool L3 3AF, UK

²Al-Turath University College, Baghdad, Iraq

³Liverpool John Moores University, Department of Civil Engineering, Peter Jost Enterprise Centre, Byrom Street, Liverpool L3 3AF, UK

⁴Building and Construction Techniques Engineering Department, AL-Mustaqbal University College, Hillah 51001, Iraq

⁵Civil and Environmental Engineering Department, King Fahd University of Petroleum & Minerals, Dhahran 31261, Saudi Arabia

Correspondence should be addressed to Zaher Mundher Yaseen; yaseen@alayen.edu.iq

Received 28 June 2022; Accepted 21 September 2022; Published 6 October 2022

Academic Editor: Md. Akter Hosen

Copyright © 2022 Fatimah N. Al-Husseinawi et al. This is an open access article distributed under the Creative Commons Attribution License, which permits unrestricted use, distribution, and reproduction in any medium, provided the original work is properly cited.

This investigation aimed to improve great early geopolymer mortar strengths under various parameters with various binder proportions to reduce the use of cement since the OPC production process leads to high emissions of CO₂. Hence, to solve this problem, alternative materials were used. In this research, metakaolin (MK) and ground-granulated blast-furnace slag (GGBFS) waste materials were utilized and mixed together with the sodium hydroxide and alkaline activator sodium silicate (NaOH and Na₂SiO₃). The performance of the various mixtures was assessed via compressive strength testing based on British standards. The compressive strength was found to be highly affected by molar proportion and water amount. The optimum strength was 77.8 MPa for a mix design of 95% GGBFS +5% MK and a 2.5 mass proportion between Na₂SiO₃ and NaOH (12 Molar), together with a 0.2 water/binder proportion.

1. Introduction

Owing to its excellent strength and durability, concrete seems to be the most extensively used material in building, with an expected current usage of 1 m³ per person annually [1]. Concrete is produced mostly of cement, gravel, sand, and water, which has been used in the building of tunnels, skyscrapers, airports, residences, and other constructions. However, there are several challenges associated with the usage of ordinary Portland cement (OPC), including durability issues, including concrete disintegration when attacked by aggressive substances such as acids, sulphates, and chlorides [2–4]. In addition, the environmental

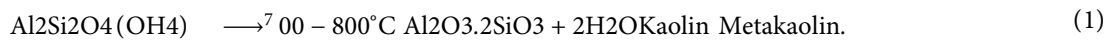
concerns were raised by the release of around 5–7% of total global CO₂ emissions throughout the OPC manufacturing process and the usage of 5% of natural resources owing to the widespread use of cement in building [5–9]. The high percentage of CO₂ emissions in the OPC manufacture process is associated with the limestone calcination process that is considered as one of the major cement ingredients [10]. The consumption of heat energy resulting in temperatures greater than 1400°C during the manufacturing process of the raw materials in the kiln has led to a high release of CO₂ [11–15].

Geopolymer cement has been used over the past decade as an alternative solution to cement because it provides a

suitable use for industrial wastes by converting them into cementitious products via the alkali-activation process [16]. The use of geopolymer technology in building has greatly reduced cement consumption, cutting carbon pollution by up to 80 percent and therefore decreasing the cement industry's environmental impact. Also, to resolve concerns arising from the disposal of industrial materials by processing and repurposing them in geopolymer production [17], geopolymer cements improve structural performance by enhancing durability and compressive strength, improving resistant against acid, and structural performance under elevated temp curing conditions. The kind and quantity of binder ingredients employed, the alkaline activator utilized, and the curing conditions utilized influence

and govern these qualities [17]. Geopolymers seem to be inorganic alumina-silicate materials that have been formed into three-dimensional polymeric chains using alkaline activator solutions [18]. GGBFS, a granular by-product, nonmetallic, and glassy from the iron producing industry, is one of the most frequently utilized alumina-silicate components in the preparation of geopolymer cement. Alumina, silicates, and calcium, as well as other bases, make up the majority of it [19, 20].

Metakaolin (MK) is an amorphous alumina-silicate clay that is formed thermally by calcining kaolinite clay at 500–800 degrees centigrade in a dehydroxylation process [21]:



Kaolin clay seems to be a fine, white clay mineral that is often used in porcelain production [22]. The type and chemical composition of these basic minerals greatly depend on their source. In addition to other elements such as alkaline activators and curing conditions, this variation has a significant influence on the pace of strength development and chemical processes of geopolymer cement [23]. As a result, in terms of generating a product with consistent precise desirable qualities, the manufacturing process of geopolymers necessitates a higher level of quality control than that of traditional Portland cement [24]. Once Portland cement is completely substituted by alkaline activated cements, Bernal and Provis [25] and Juenger et al. [26] found that GGBFS-based geopolymer concretes have strong mechanical performance and generate durable concrete with a low environmental impact. Despite this, the alkali-activated GGBFS-based geopolymer sets quickly and has poor workability significant microcracks, efflorescence drying shrinkage, and dry shrinkage [27, 28], and low carbonation resistant [29]. MK was employed in the early geopolymers improvement owing to its strong reactivity with alkaline activators and pure alumina-silicate amount that aids create a greater degree of geopolymerisation since its high amorphous phase amount and finer particle size [24]. Once heated, the geopolymer-based MK caused more matrix degradation than the fly ash geopolymer. The major source of the damage was discovered to be the prominent mesopores in the geopolymer-based MK matrix, which prevent moisture from escaping when heated. Although in the situation of fly ash, the geopolymer matrix has a significant number of micropores that allow moisture to escape once heated, causing little degradation to the geopolymer matrix [30, 31]. The fly ash-based geopolymer, on the contrary, revealed a problem with the curing conditions. To establish structural integrity and increase strength, a high-temperature curing process is required [32].

Owing to the facts presented throughout the introductory section, several researchers have investigated the formulations of novel blended binders made from two different

materials in order to overcome the aforementioned shortcomings of such binders [33–35]. The new binders have been created by mixing aluminosilicate elements with the slag binder, including MK and fly ash (FA). In comparison to binders in which only the aluminosilicate precursors have been activated, the activation of these two materials leads to enhancements in several characteristics; additionally, such mixed binders advance an original microstructure with the coexistence of Ca-rich and Na-rich reaction products [25]. Once comparison with binders made from a raw material, including geopolymer-based-MK, laminar structures composition, and blending GGBFS with alumina-silicate substances under great alkalinity situations resulted in a greater dissolution rate of siliceous structures, thus enhancing the system's durability and stability [24].

A study conducted on the mechanical properties of GGBFS and MK geopolymer mortar found that the mixture of 20% GGBFS and 80% MK gave the highest compressive strength [36], while the difference in NaOH amount had affected the resultant compressive strength in relation to GGBFS amount; it has been detected that increasing the NaOH amount from 2.0 M to 1.2 M reduces compressive strength unless more GGBFS amount is added to the mixture. Whilst Bernal [25] discovered that the addition of MK caused a substantial increase in the compressive strength. Burciaga-Díaz et al. [37] detected that the compressive strength for the GGBFS and MK geopolymer pastes increased with high GGBFS amounts up to 100%, and Rao and Raja [38] found the same for GGBFS and MK geopolymer concrete. The maximum compressive strength was also obtained at 0% MK + 100% GGBFS of 52.0 N/mm². Nevertheless, studies looked only at the impact of a low molar proportion of NaOH, but they did not investigate the strength of the results under a high molar proportion such as 12 M.

Thus, this investigation aimed to determine the molarity impact of sodium hydroxide on strength under low and high alkalinity. It also focused on the significant role that water plays in the dissolution stage of the geopolymerisation

TABLE 1: Chemical analysis of undisturbed materials used using EDXRF.

Ingredients	CaO	Al ₂ O ₃	SiO ₂	Na ₂ O	MgO	K ₂ O	TiO ₂	Fe ₂ O ₃	BaO	SO ₃
OPC	65.829	1.704	24.476	1.414	1.342	0.688	0.405	2.524	0.177	—
GGBFS	38.744	4.673	36.467	3.124	4.056	0.528	0.808	0.064	0.150	—
MK	0.166	41.720	41.193	—	—	0.088	1.402	0.331	0.121	0.067

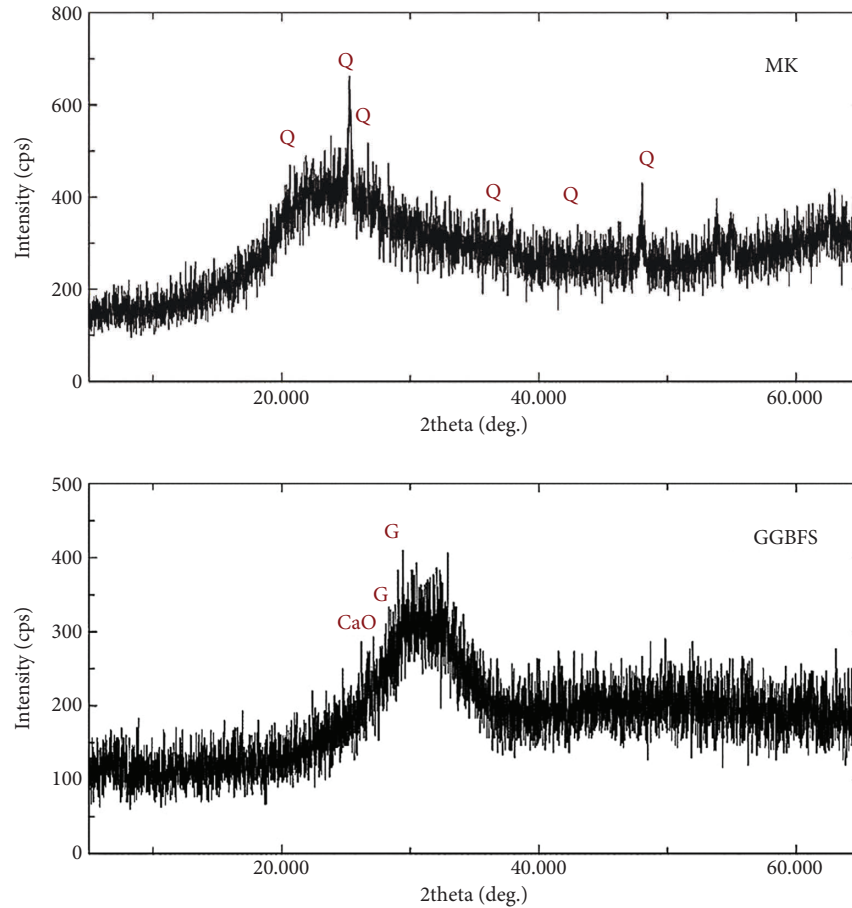


FIGURE 1: XRD diffractions forms for the utilized materials, GGBFS and MK. G = gypsum and Q = quartz.

process and, consequently, the compressive strength. The work sets out to investigate various water amounts that were added to various binder proportion mixes. The study also aimed to discover the influence of combined factors (molar proportion, water amount, and binder proportion) on the strength of the mix to optimize the mix design proportions. This research focuses on finding how far can geopolymer replace cement by studying the compressive strength, setting time, and microstructure of the produced samples.

2. Research Methodology

2.1. Materials Used and Mix Constituents. Commercially, GGBFS powder was obtained from Hanson Cement Ltd. in the UK on January 11, 2017, whilst MK powders were obtained from BASF Chemical Company, Canada. GGBFS and MK at chemical analysis demonstrated in Table 1 were utilized as the main raw materials. MK consists mainly of 41.193 percent silica and 41.720 percent alumina with just

0.166 percent CaO, though GGBFS consists mostly of calcium oxides with a ratio of 38.744 percent and silica amount of 36.467 percent with just 4.673 percent alumina. The powder XRD pattern of raw materials demonstrated that both MK and GGBFS are amorphous with only a noticeable semi-crystalline peak of quartz (Q) was detected at 25° (2 theta) in MK, whereas gypsum (G) and lime (CaO) at around 28° (2 theta) were detected in GGBFS, as shown in Figure 1. Alternatively, SEM analysis of the raw materials (Figure 2) illustrates that GGBFS consists primarily of angular particles, whereas MK seems to have a platy particle shape; additionally, the MK particle seems to have a large surface area with a small size, which increases its water requirements and reactivity when compared to GGBFS.

To make the geopolymer mortar-based slag/metakaolin, GGBFS was chosen as the primary binder (b) in this research, and it has been partially substituted by MK, as indicated in Table 2. The reference mixtures (C refers to the reference sample with cement only, while CS refers to the

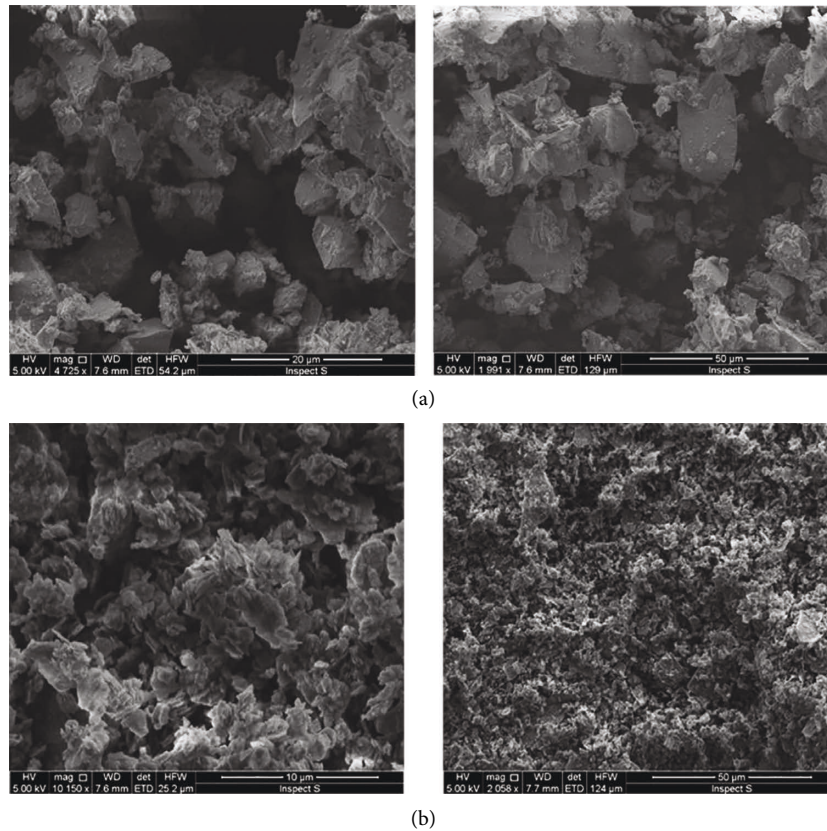


FIGURE 2: SEM observations for powders (a) GGBFS and (b) MK.

reference sample with cement and superplasticizer) for the comparison with geopolymer mortar were made with ordinary Portland CEM II (32 grade). In the preparation of the mortar mixes, natural dry sand with a specific gravity = 2.62 Mg/m^3 and a particle size = 0/2 FP washed plastering sand Gf85 [39] has been utilized as fine aggregate. As an alkaline solution (Al), a combination of sodium silicate (SS) and sodium hydroxide (SH) has been employed to prepare the geopolymer specimens. The sodium silicate solutions had a molar ratio of $\text{SiO}_2 : \text{Na}_2\text{O}$ of 2:1, a water content of 60%, and a specific gravity of 1.5. Sodium hydroxide has been created from pellets (98 percent pureness) dissolved in water (w) at two different molar amounts, 12 M and 0.3 M, which have been selected after conducting many trials to obtain the best molar amount (12 percent amount of solutions) to see the impact of concentrations in different molarities and percentages on the compressive strength. Distilled water was added to all mixtures, and to keep on workability, superplasticizer (S) has been utilized at 1% in select mixtures, as indicated in Table 2.

2.2. Specimen Synthesis and Experimental Procedures

2.2.1. Preparation of Alkaline Activator Solutions.

Sodium silicate and sodium hydroxide were used to make the alkaline solutions. Sodium hydroxide has been initially made by dissolving NaOH granules in distilled water and

letting it cool for 24 hrs at room temp. To test the effect of solution molar ratio on compressive strengths, the NaOH solution has been produced in two amounts: 12 molar solution and 12 percent (0.3 molar). To make the 12 molar solution, 480 gm of NaOH solid granules ($12 \times 40 = 480$) have been dissolved in one litre of pure water (in which 40 was the NaOH molecular weight). The 12 percent NaOH solution has been made by dissolving 12 gm of NaOH granules in a litre of water. Sodium silicate has been applied in two various proportions. First, it has been applied at mass proportion of 2.5 (sodium silicate mass to sodium hydroxide mass) and then added at 2.0 mass ratio. After that, water has been inserted into the alkaline activator solutions in two different quantities as given in Table 2, and the mixture has been allowed to sit for a few minutes before being used in the geopolymer mixture.

2.2.2. Mix Proportions of Specimens.

The raw materials have been mixed at specific mass proportions of GGBFS/(GGBFS + MK) to make the cubic mortar samples as shown in Table 2, and all mixtures were made with a total binder amount of 775 kg/m^3 . Dried sand was added at a mass proportion of 1.5 sand to the binder (GGBFS + MK), while activator was added at a mass proportion of 0.4 activator/binder, while water/binder ratio was first 0.4 and then decreased to 0.2 with the addition of 1% superplasticizer, as shown in Table 2.

TABLE 2: Combination composition of mortars OPC and slag/MK-based geopolymer utilized in the current investigation.

MixID	Ingredients' quantity (kg/m ³)										
	Binder	OPC	GGBFS	MK	Sand	SH (12%)	SH (12 M)	SS	w/b	S	Al/b
100 G	775	0	775	0	1162.5	88.57	0	221.43	0.4	0	0.4
90 G	775	0	697.5	77.5	1162.5	88.57	0	221.43	0.4	0	0.4
80 G	775	0	620	151	1162.5	88.57	0	221.43	0.4	0	0.4
70 G	775	0	542.5	232.5	1162.5	88.57	0	221.43	0.4	0	0.4
60 G	775	0	465	310	1162.5	88.57	0	221.43	0.4	0	0.4
50 G	775	0	387.5	387.5	1162.5	88.57	0	221.43	0.4	0	0.4
100 GM	775	0	775	0	1162.5	0	88.57	221.43	0.4	0	0.4
90 GM	775	0	697.5	77.5	1162.5	0	88.57	221.43	0.4	0	0.4
80 GM	775	0	620	151	1162.5	0	88.57	221.43	0.4	0	0.4
70 GM	775	0	542.5	232.5	1162.5	0	88.57	221.43	0.4	0	0.4
60 GM	775	0	465	310	1162.5	0	88.57	221.43	0.4	0	0.4
50 GM	775	0	387.5	387.5	1162.5	0	88.57	221.43	0.4	0	0.4
100 GS	775	0	775	0	1162.5	88.57	0	221.43	0.2	7.75	0.4
90 GS	775	0	697.5	77.5	1162.5	88.57	0	221.43	0.2	7.75	0.4
80 GS	775	0	620	151	1162.5	88.57	0	221.43	0.2	7.75	0.4
70 GS	775	0	542.5	232.5	1162.5	88.57	0	221.43	0.2	7.75	0.4
60 GS	775	0	465	310	1162.5	88.57	0	221.43	0.2	7.75	0.4
50 GS	775	0	387.5	387.5	1162.5	88.57	0	221.43	0.2	7.75	0.4
100 GMS ¹	775	0	775	0	1162.5	0	88.57	221.43	0.2	7.75	0.4
95 GMS	775	0	736.25	38.75	1162.5	0	88.57	221.43	0.2	7.75	0.4
90 GMS	775	0	697.5	77.5	1162.5	0	88.57	221.43	0.2	7.75	0.4
85 GMS	775	0	658.75	116.25	1162.5	0	88.57	221.43	0.2	7.75	0.4
80 GMS	775	0	620	151	1162.5	0	88.57	221.43	0.2	7.75	0.4
75 GMS	775	0	581.25	193.75	1162.5	0	88.57	221.43	0.2	7.75	0.4
100 C	775	775	0	0	1162.5	0	0	0	0.4	0	0
100 CS ²	775	775	0	0	1162.5	0	0	0	0.2	7.75	0

100 refer to the GGBFS proportion used in relation to the total binder; G is GGBFS; M refers to the use of 12 molar NaOH solution, S refers to the use of superplasticiser. C is cement and S refers to the use of superplasticiser.

TABLE 3: The average compressive strengths in MPa after seven days.

Mix ID	GGBFS/(GGBFS + MK) (%)	Compressive strength (MPa)			Mix ID	GMS	Mix ID	Control mixes
		G	GM	GS				
100		30.0	56.6	64.3	100	63.5	C	31.8
90		23.8	32.7	55.9	95	77.8	CS	8.4
80		4.0	8.6	49.6	90	60.4		
70		2.0	7.3	15.1	85	69.1		
60		1.8	7.5	9.2	80	61.8		
50		1.8	8.5	4.8	75	69.4		

Note: the mix designs given are found by the number in the first column with the letter in the first row above to have the same mix design in Table 3.

2.2.3. Mixing and Casting Procedure. The alkali activators were first prepared a few minutes earlier and blended together. After that, the free water was inserted to blend well. GGBFS and MK were first weighted separately and then blended together for approximately 2 min. The alkali activator solution was then added to the blended mixture of GGBFS and MK and all mixed together for 2-3 minutes. Next, dried fine aggregates are applied to the previous combination and blended well for another 120 seconds. Eventually, the samples have been poured into PVC cubic moulds of 4 × 4 × 4 cm dimensions, left uncovered at a temp (27 ± 2°C with 0% RH) for 24 hours, and then demoulded and cured under different temperature conditions.

TABLE 4: Masses and compressive strengths for 95 percent GMS amount at 28 curing days.

Specimens	Compressive strengths (MPa)	Masses (g)
1	86.1	133.5
2	70.5	133.3
3	91.7	134.3

Hardened geopolymer mortar: the average strength of concrete of three 4 cm side cubes has been evaluated in the laboratory utilizing a universal testing machine (UTM) in line with BS EN 196-1 2005 [40] at a loading rate of 0.40 MPa/sec.

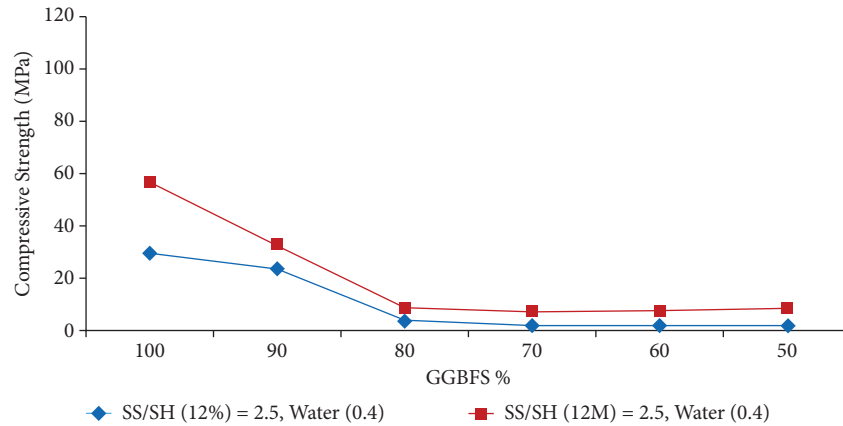


FIGURE 3: The impact of NaOH molar proportion on the compressive strengths at 7 curing days.

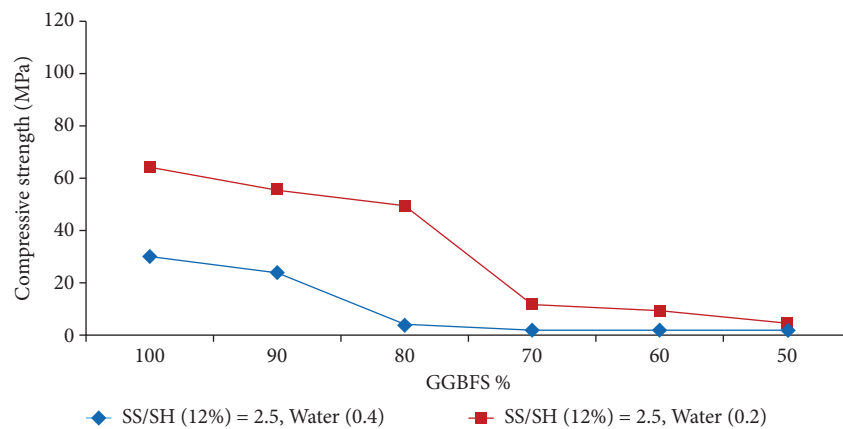


FIGURE 4: The impact of superplasticiser and low water amount on compressive strengths at 7 curing days.

Analytical analysis of geopolymer: the MK and GGBFS microstructure geopolymer combinations have been studied using a scanning electron microscope (SEM). To ensure that specimens seem to be fully free from water, small pieces have been hammered from the paste's core and dried at 40 degrees centigrade for four hours. The basic chemical analysis of OPC, MK, and GGBFS, and the XRD forms for both GGBFS and MK, have been determined using powder X-ray fluorescent and X-ray diffraction examinations.

3. Results and Discussion

In this section of the research, we present, through the tables, the compressive strength results for each of the previously pelleted samples in Table 3, in which we used GGBS and MK as alternative materials for cement, adding to them solutions of sodium hydroxide and sodium sulphate in order to activate the reaction between them. Also, tests were conducted on two samples of cement as a binder in order to compare with the previous samples. Therefore, the results showed the following.

Table 3 shows the compressive strength obtained after 7 days for different mix designs.

In Table 4, the masses have been taken for the mix design of 95 GMS since it is the optimum mix design that gives the highest compressive strength among the other mixes. And, as shown in Table 4, the mass with a small amount can change the compressive strength of the geopolymer.

3.1. The NaOH Molar Proportion Influence. Increasing sodium hydroxide concentration from 12% to 12 M enhanced the compressive strengths of the geopolymer (Figure 3). The compressive strengths at seven curing days increased significantly from 30 MPa for the 100G mix to 56.6 MPa for the 100 GM mix and from 23.8 MPa for the 90G mix to 32.7 MPa for the 90 GM mix, which have all been greater than 31.8 MPa for that of mix C (Table 3).

The great amount of NaOH in alkaline solutions boosts silica and alumina particle dissolution and promotes the development of both CSH and geopolymer gels, which enhances compressive strengths. Once the calcium content is low, as in 80–50 percent GGBFS, the content of hydroxyl ions rises, preventing Ca^{2+} dissolution. As a result, the dissolved aluminum and silicate particles form geopolymer gel, inhibiting CSH production and resulting in poor compressive strength. However, once the calcium

TABLE 5: Various GGBFS amount with various water proportions.

Mix ID	Masses (g)		
	G	GS	GMS
100	127.5	136.6	138.8
90	126.8	134.6	136.9

Note: the mix designs mentioned are found by the number in first column with the letter in the first row above to have the same mix design in Table 3.

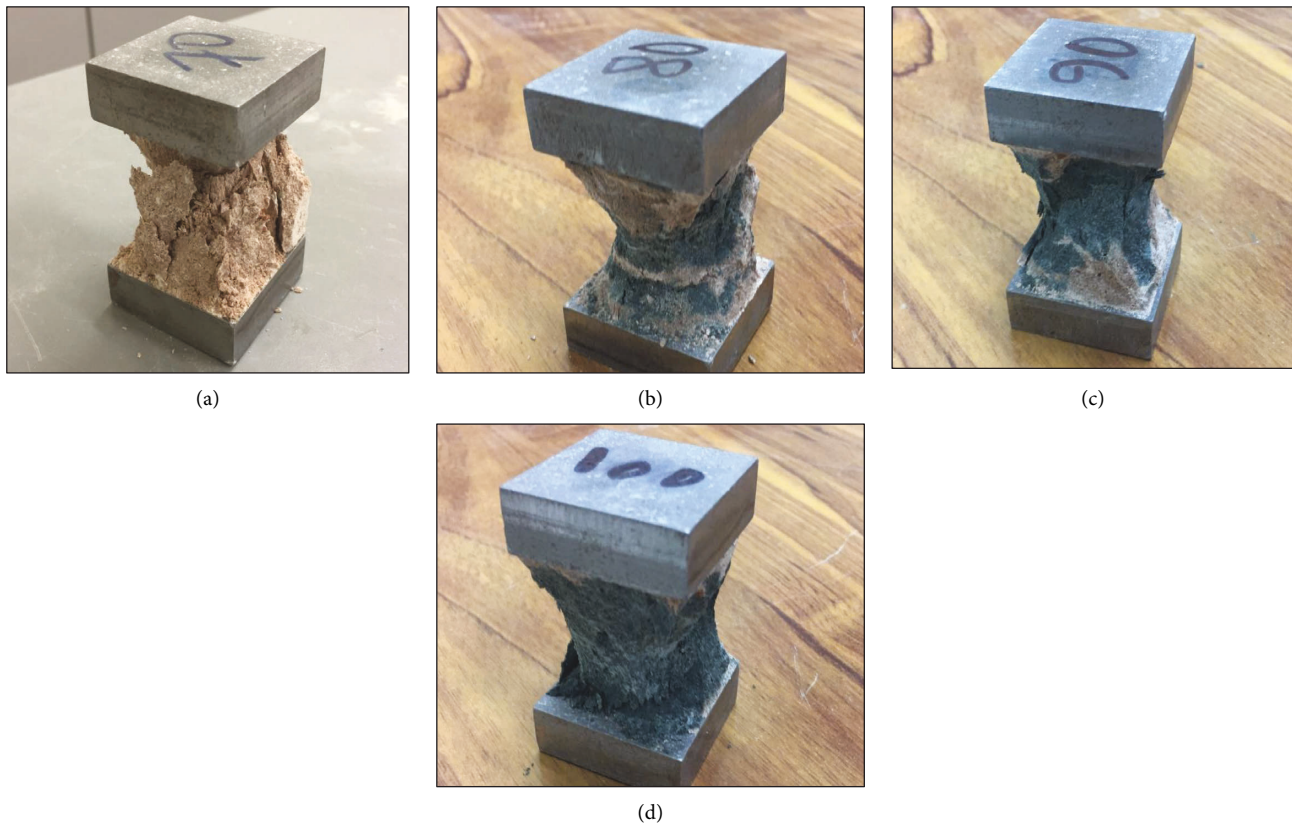


FIGURE 5: The impact of water amount and super plasticisers on different GGBFS amount mixture's structure.

concentration is sufficient, as in 90 and 100 percent GGBFS, there might be enough dissolved Ca^{2+} to produce CSH and geopolymer gels, leading to increased strengths. Once the NaOH content is lower (12 percent), less hydroxyl ions have been generated, causing more dissolved Ca^{2+} and less dissolved aluminum and silicates particles owing to the low alkalinity environment, leading in more CSH gel and less geopolymer gel, which lead to poor compressive strength [36, 41]. Furthermore, as the amount of alumina-silicate rises, the potential for Si-O-Si and Si-O-Al bonding increases and, therefore, does the necessity for high alkali content solutions to enhance the dissolution of Si-O-Al and Si-O-Si bonds and thus the precipitation of cementitious reactions [42]. The requirement for activator is substantially lower at low MK concentrations (90–100 percent GGBFS).

Furthermore, a progressive rise in compressive strength was from 35.3 MPa at 50 percent GGBFS to the optimal magnitude of 44.0 MPa at 100 percent GGBFS, utilizing a

8 M sodium hydroxide solution at ambient curing temps [38]. Although there was no substantial increase in compressive strength between 50 and 80 percent GGBFS in Figure 3, there had been a considerable rise once GGBFS was increased to 90 and 100 percent.

3.2. The Impact of Low Water Amount. Figure 4 shows the impact of low water content with 1% superplasticizer on the compressive strength of geopolymer mortar cubes.

The compressive strength was enhanced by halving the quantity of water (0.2 water/binder proportion). It boosted the strength of specimens 100GS = 64.3 MPa and 90GS = 55.9 MPa, which is two times higher than the strength of specimens 100G and 90G (Table 3), while it increased the strength from 3.97 MPa at 80 G to 49.60 MPa at 80 Gs with enough workability for moulding, which is higher than the control mix C. Decreasing water amount

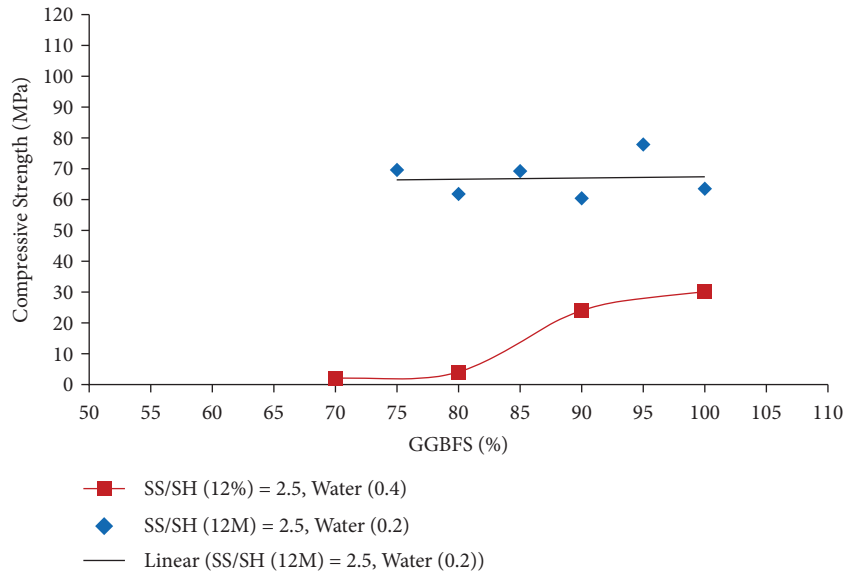


FIGURE 6: Boosting the mixture ratio after 7 curing days without RH.

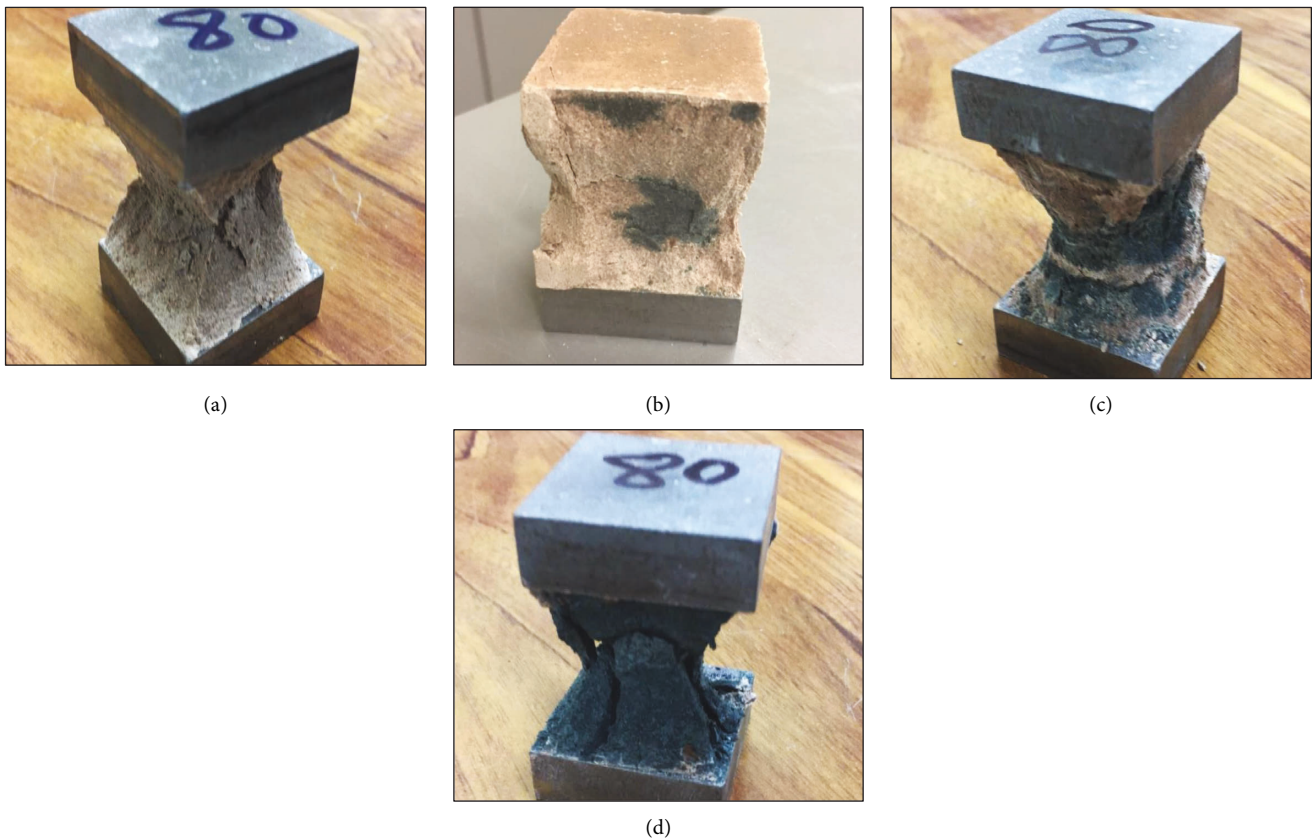


FIGURE 7: The impacts of various NaOH molar proportion and water amount on the geopolymerisation processes (specimens with 80 and 20 percent of GGBS and MK, respectively) the pictures have been lected after conducting compressive strengths test; (a). 40% water proportion, 12% NaOH; (b). 12 M NaOH, 40% water proportion (c). 1% SP, 20% water proportion, 12% NaOH; (d). 12 M NaOH, 20% water proportion, 1% SP.

aided reduce pores and voids in the systems leads to higher density structures (Table 5). The introduction of a superplasticizer helped give adequate workability for the reactions

by dispersing the particles and releasing entrapped water by separating the agglomeration through the repulsion of similar charges [42]. However, raising the MK amount to

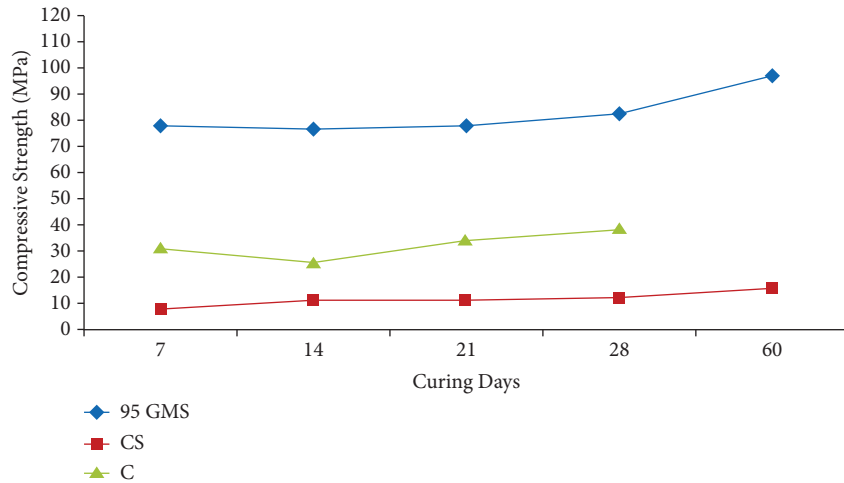


FIGURE 8: Compressive strength results for optimal mixture design and OPC reference mixtures during 7, 14, 21, 28 and 60 curing days.

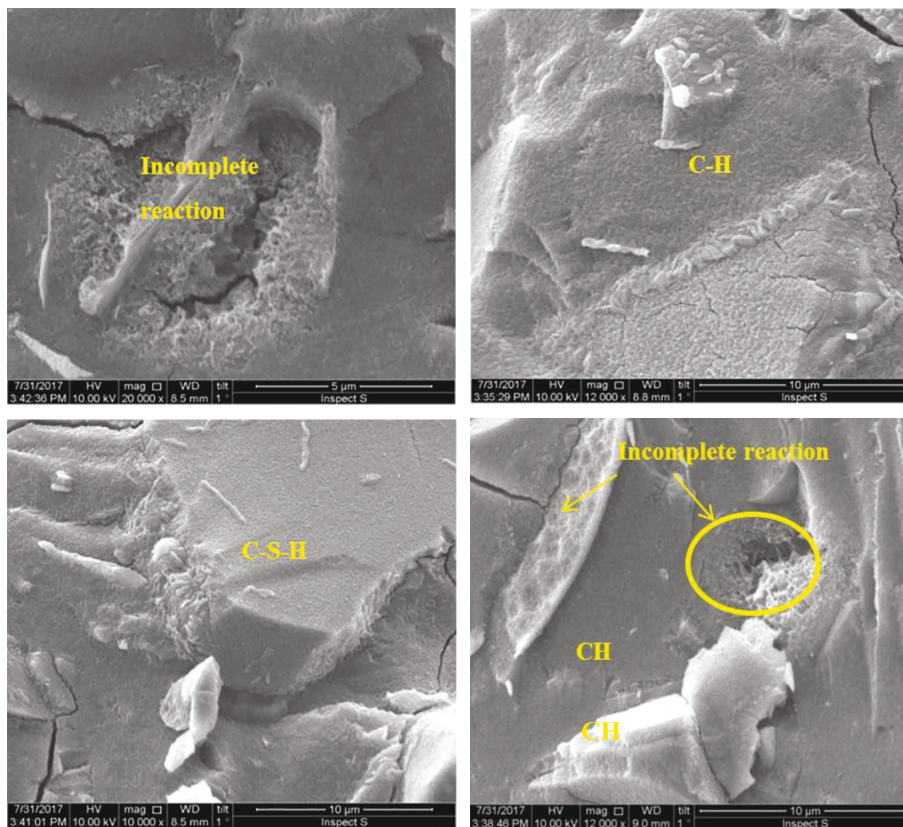


FIGURE 9: The SEM images for 95 GMS geopolymer paste at 7 curing days.

more than 30 percent (70 percent GGBFS or less) lowered strength magnitudes even after lowering the water quantity and applying 1% SP. It has been found that, at 30 percent MK, the mixture gets extremely dry despite the inclusion of superplasticizer. This is due to the increased surface area of MK, which necessitates a larger water amount so as to maintain sufficient water quantity and workability for the dissolving process.

Figure 5 demonstrates four specimens blended with various GGBFS amounts and constant water to binder

proportions of 0.2. As samples gave various coloured areas, as shown in Figure 5, the darker sections relate to the reacted areas while the light-coloured sections relate to unreacted materials. Figure 5(a) demonstrates that the 70% GGBFS specimen had light-coloured sections that indicate unreacted areas. The sample failure seemed brittle in contrast to those with greater GGBFS levels, and this was attributable to a lack of water necessary to dissolve alumina-silicate owing to the higher MK content in the combination. As a result of the large number of open holes, it created a

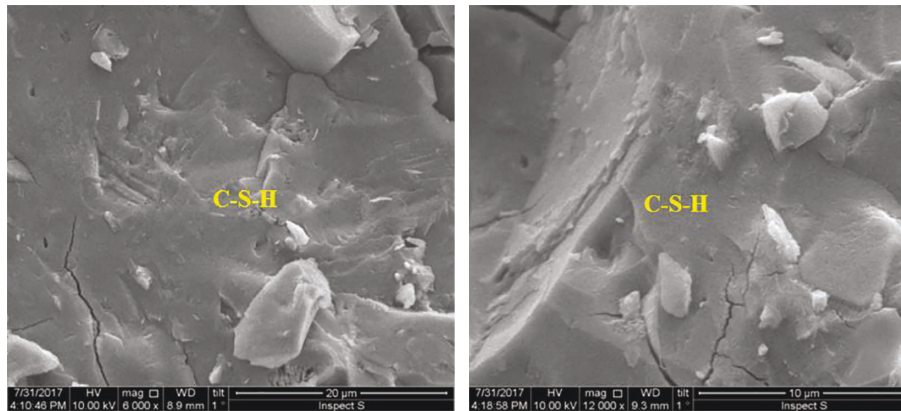


FIGURE 10: The SEM images for 90 GMS geopolymer paste at 7 curing days.

low-density geopolymer. Moreover, since MK possesses properties comparable to clay, it expands and contracts once exposed to water. As a consequence, specimens containing a high-level of MK had more open pores [43].

In contrast, the reaction process improved and formed more dark areas in samples with lower MK and higher GGBFS amounts, as shown clearly on the 80% GGBFS (Figure 5(b)), while it totally turned dark at 90 and 100% GGBFS amount (Figures 5(c) and 5(d)). Though several specimens lacked consistency in dark area distribution, it can be seen in the centre of the 80 percent specimen and around the margins of the 90 percent specimen. This indicates that the geopolymerisation process is nonuniform, as shown by the fact that the cubes' masses from the same mixture have been detected to be almost similar, despite the compressive strength of each cube being considerably different (Table 4).

3.3. The Impact of Both Low Water Amount and High Molar Proportion. As illustrated in Figure 6, the combined impact of 12 M and 0.2 water amount with superplasticiser resulted in a considerable improvement in compressive strength. For the GGBFS amounts 100, 95, 90, 80, 85, and 75 percent, the compressive strength of cubes with low water amount and high molar proportion was spread around the magnitude 67 MPa. The overall impact of a 12 M sodium hydroxide solution and a little quantity of water increased the geopolymer's compressive strength and doubled it, notably for GGBFS and MK blended mixes, confirming MK's preferential dissolving in high alkaline solutions [25]. Due to the obvious high quantity of MK that has a large surface area and results in a dry mix owing to the high water requirements, the compressive strength cannot be evaluated at GGBFS levels lower than 75%. This resulted in inadequate workability to pour and compact the mixture in the mould.

The influence of both a large molar percentage of NaOH solutions and a small quantity of water on the geopolymerisation processing in terms of compressive strength and reaction products is shown in Figure 7. Increasing the molar proportions from 0.3 M to 12 M lead to production of dark grey colored patches in the cubic specimen (as shown in Figures 7(a) and 7(b)), which also caused a significant

increase in compressive strength, especially at high GGBFS levels (Table 3). Decreasing the quantity of water to half the original value, on the contrary, resulted in substantially greater compressive strength, as seen by bigger dark regions in Figure 7(c). Despite this, the distribution of dark-colored patches was uneven across the specimen, indicating a nonuniform reaction process. Once the impacts of both low water quantity and high molar proportion were combined, the specimen fully changed color to a dark grey color (Figure 7(d)), and the compressive strength increased to greater levels (Table 3). As a consequence, the dark grey spots represent reaction products of the geopolymerisation process, which contribute to the high compressive strength.

3.4. Comparison between Optimized and OPC Control Mix.

In contrast to the two OPC reference mixtures, Figure 8 depicts the evolution of the optimal design proportions. The 95 GMS mix design produced much more strength in comparison with the two OPC mixtures. It possessed a compressive strength of 77.8 MPa at 7 curing days, which hovered around that amount till 21 days; then, the strength slightly improved to reach 82.7 MPa at 28 days, and it continued to increase till it reached 97.3 MPa at 60 curing days. The OPC mixture specimen of 0.2 (water/cement proportion) showed a little increase from 8.4 to 11.5 MPa between 7 and 14 days. After that, it held relatively stable strength at 12 MPa at 28 days and climbed to 15.9 MPa at 60 days. At the same time, the OPC mixes with 0.4 w/c proportion provide higher strength, reaching to 31.8 MPa at 7 days, while at 14 days the strength was 26 MPa since the cubes that were tested at 14 days were not from the same batch of the seven days' mix (same mix design with various cast dates); thus, the progress in the strength was not as expected. Subsequently, there was a gradual increase in strength to reach 38.4 MPa at 28 days.

3.5. The SEM Analysis. Figures 9–11 illustrate the microstructure analysis of the three various blends at seven curing days, involving the optimal one (depending on compressive strength). The major reactions produced by GGBFS/MK binder with alkali activation lead to the creation of CH

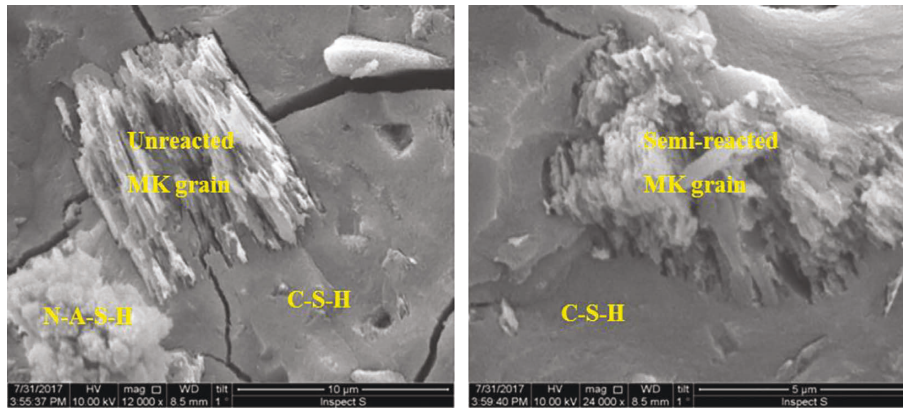


FIGURE 11: The SEM images for 85 GMS geopolymer paste at 7 curing days.

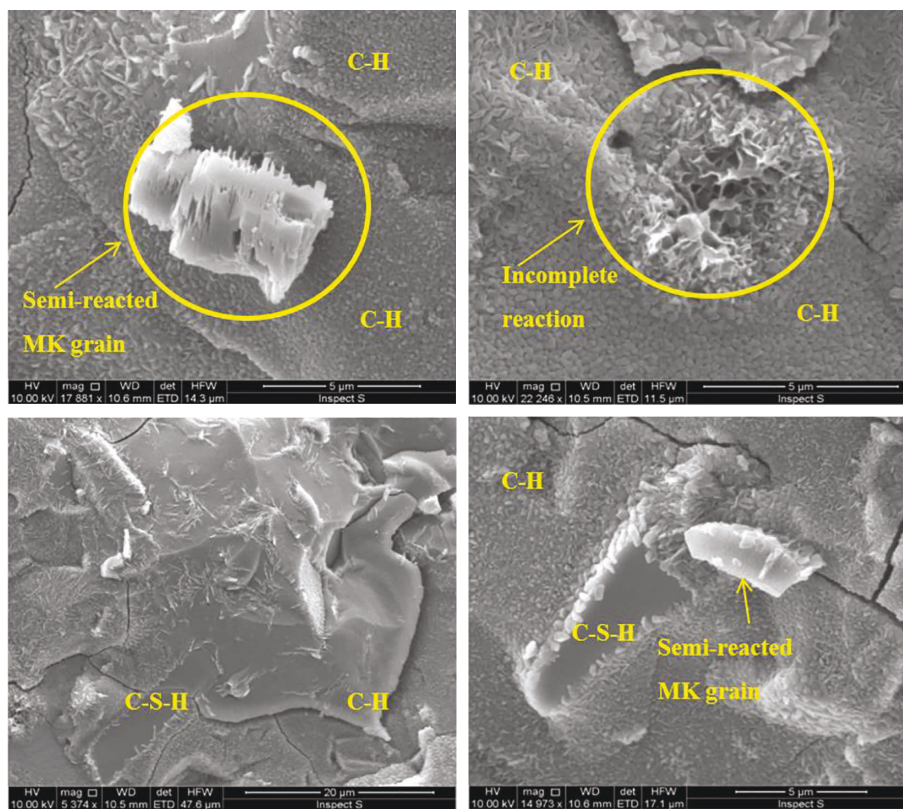


FIGURE 12: The SEM images for 95 GMS geopolymer paste at 35 curing days.

crystals and C-S-H gel, as shown in these images. The 85 GMS specimen microstructure is clearly illustrated in (Figure 11) the N-A-S-H gel as identified in [44]. Nonetheless, some unreacted MK particles and incomplete reaction regions have been found in the specimens with the produced gels, revealing the nonuniform reaction process distribution (Figure 11) that explains the large variance in the consequent compressive strength for the identical mixtures (as observed in Table 4).

Based on the lack of technicians available to do the test on that day, the SEM analysis for the next 28 days cannot be acquired; as a result, it was postponed until the next available day, that was 35 curing days after curing.

Figure 12 shows that, after 35 curing days, more C-H crystals emerged inside the microstructure, whereas at high MK amounts, more C-S-H gel and sodium aluminosilicate hydrated gel (N-A-S-H) have been created (Figures 13 and 14). Because MK seems to be the main silicate and alumina source, increasing MK concentration increased the likelihood of more N-A-S-H gel formation rather than CH for the 90 GMS and 85 GMS specimens. C-H, as well as C-S-H, has been the primary products at lower MK levels (95 percent GGBFS). In the SEM pictures, microcracks were seen on the structural surface of all specimens. The external force applied by the hammer to create small parts appropriate for testing and the uncombined water

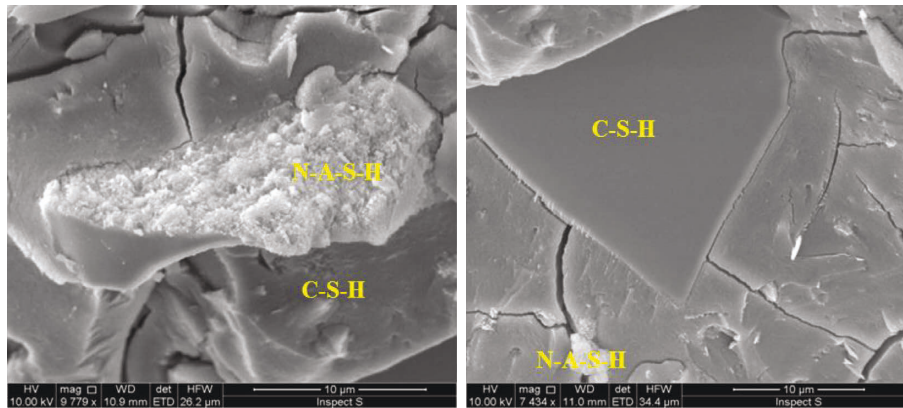


FIGURE 13: The SEM images for 90 GMS geopolimer paste at 35 curing days.

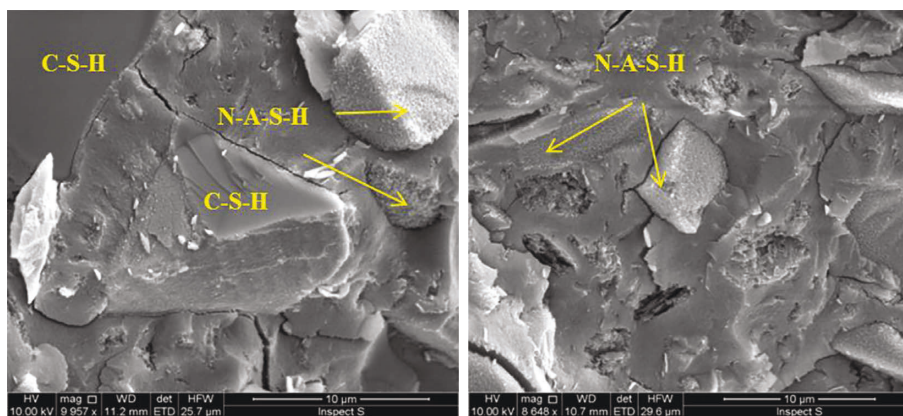


FIGURE 14: The SEM images for 85 GMS geopolimer paste at 35 curing days.

evaporated from the specimens when dried sample at 40 degrees centigrade in the furnace and then put in the microscope column vacuum, resulting in substantial shrinkage and thus microcracking, have all been reasons for their presence. Furthermore, the use of a low water/binder ratio in the mixture seems to be blamed.

4. Conclusion

In this research, different mix designs of GGBS and MK were prepared to seek the amount of compressive strength in comparison with OPC samples as well as the optimum mix design in terms of the compressive strength. The findings were as follows:

- (i) In terms of optimized aluminosilicate dissolution species leading to the produced geopolimer, the high molar fraction of sodium hydroxide increased the cubes' compressive strength.
- (ii) Alternatively, using a superplasticiser to reduce the quantity of water in the solution resulted in a denser structure by eliminating gaps and holes generated by leftover water and thereby increasing the mechanical qualities.
- (iii) As a result of the combined influence of low water amount and high molar proportion with low curing temp, the optimal mixture (95 percent GGBFS + 5 percent MK) had been achieved.
- (iv) The alkali-activated slag/MK geopolimer had a solid microstructure with no holes or cavities but some microcracks, according to SEM examination.
- (v) C-S-H gel and CH crystals seemed to be prominent in the structure after 7 curing days, whereas (N-A-S-H) gel was found in the microstructure of greater MK amounts (85 GMS), along with some unreacted MK particles and incomplete reaction regions.
- (vi) More C-H crystals grew inside the microstructure at 35 curing days, and more hydrated (N-A-S-H) gel and C-S-H gel have been created at great MK levels (90 GMS and 85 GMS).
- (vii) Because MK was the primary silicate and alumina source, increasing MK concentration increased the likelihood of more N-A-S-H gel formation rather than C-H for the 90 GMS and 85 GMS specimens. C-H, as well as C-S-H, was the dominating product at lower MK amounts (95 GMS).

Data Availability

Most datasets generated and/or analysed in this study are included within the article. The other datasets can be obtained from the corresponding author upon request.

Conflicts of Interest

The authors declare that they have no conflicts of interest.

Acknowledgments

This work was supported by Al-Mustaqbal University College (Grant number: MUC-E-0122). Mr Anmar Dulaimi and Mr Hassnen M Jafer are gratefully acknowledged for their help in providing the raw materials. This research was conducted in the labs of Liverpool John Moores University with the help of the technical staff.

References

- [1] Y. Chen, F. Veer, and O. Copuroglu, "A critical review of 3D concrete printing as a low CO₂ concrete approach," *Heron*, vol. 62, pp. 167–194, 2017.
- [2] A. A. Adam, *Strength and Durability Properties of Alkali Activated Slag and Fly Ash-Based Geopolymer concrete*, RMIT Univ Melbourne, Melbourne Australian Forestry, 2009.
- [3] K. Chen, D. Wu, L. Xia, Q. Cai, and Z. Zhang, "Geopolymer concrete durability subjected to aggressive environments—A review of influence factors and comparison with ordinary Portland cement," *Construction and Building Materials*, vol. 279, Article ID 122496, 2021.
- [4] W. Li, E. D. Shumuye, T. Shiyang, Z. Wang, and K. Zerfu, "Eco-friendly fibre reinforced geopolymer concrete: a critical review on the microstructure and long-term durability properties," *Case Studies in Construction Materials*, vol. 16, Article ID e00894, 2022.
- [5] D. N. Huntzinger and T. D. Eatmon, "A life-cycle assessment of Portland cement manufacturing: comparing the traditional process with alternative technologies," *Journal of Cleaner Production*, vol. 17, no. 7, pp. 668–675, 2009.
- [6] W. K. Tuama, M. M. Kadhum, N. A. Alwash, Z. S. Al-Khafaji, and M. S. Abdulaheem, "RPC effect of crude oil products on the mechanical characteristics of reactive-powder and normal-strength concrete," *Periodica Polytechnica: Civil Engineering*, 2020.
- [7] X. S. Shi, F. G. Collins, X. L. Zhao, and Q. Y. Wang, "Mechanical properties and microstructure analysis of fly ash geopolymeric recycled concrete," *Journal of Hazardous Materials*, vol. 237, pp. 20–29, 2012.
- [8] G. F. Huseien, J. Mirza, M. Ismail, S. K. Ghoshal, and M. A. M. Ariffin, "Effect of metakaolin replaced granulated blast furnace slag on fresh and early strength properties of geopolymer mortar," *Ain Shams Engineering Journal*, vol. 9, no. 4, pp. 1557–1566, 2018.
- [9] M. Su, Q. Zhong, and H. Peng, "Regularized multivariate polynomial regression analysis of the compressive strength of slag-metakaolin geopolymer pastes based on experimental data," *Construction and Building Materials*, vol. 303, Article ID 124529, 2021.
- [10] A. Naqi and J. G. Jang, "Recent progress in green cement technology utilizing low-carbon emission fuels and raw materials: a review," *Sustainability*, vol. 11, no. 2, p. 537, 2019.
- [11] E. Gartner, "Industrially interesting approaches to "low-CO₂" cements," *Cement and Concrete Research*, vol. 34, no. 9, pp. 1489–1498, 2004.
- [12] H. S. Majdi, A. A. Shubbar, M. S. Nasr et al., "Experimental data on compressive strength and ultrasonic pulse velocity properties of sustainable mortar made with high content of GGBFS and CKD combinations," *Data in Brief*, vol. 31, Article ID 105961, 2020.
- [13] A. A. Shubbar, M. Sadique, M. S. Nasr, Z. S. Al-Khafaji, and K. S. Hashim, "The impact of grinding time on properties of cement mortar incorporated high volume waste paper sludge ash," *Karbala International Journal of Modern Science*, vol. 6, no. 4, 2020.
- [14] A. A. Shubbar, H. Jafer, M. Abdulredha et al., "Properties of cement mortar incorporated high volume fraction of GGBFS and CKD from 1 day to 550 days," *Journal of Building Engineering*, vol. 30, Article ID 101327, 2020.
- [15] D. N. Jabbar, A. Al-Rifaie, A. M. Hussein, A. A. Shubbar, M. S. Nasr, and Z. S. Al-Khafaji, "Shear behaviour of reinforced concrete beams with small web openings," *Materials Today Proceedings*, vol. 42, 2021.
- [16] S. A. Bernal, E. D. Rodríguez, A. P. Kirchheim, and J. L. Provis, "Management and valorisation of wastes through use in producing alkali-activated cement materials," *Journal of Chemical Technology and Biotechnology*, vol. 91, no. 9, pp. 2365–2388, 2016.
- [17] S. Akçaözoglu and C. D. Atiş, "Effect of granulated blast furnace slag and fly ash addition on the strength properties of lightweight mortars containing waste PET aggregates," *Construction and Building Materials*, vol. 25, no. 10, pp. 4052–4058, 2011.
- [18] M. H. Al-Majidi, A. Lampropoulos, A. Cundy, and S. Meikle, "Development of geopolymer mortar under ambient temperature for in situ applications," *Construction and Building Materials*, vol. 120, pp. 198–211, 2016.
- [19] M. Kaur and M. S. Naval, "Performance of ground granulated blast furnace slag concrete with partial replacement of sand by saw dust," *IOSR Journal of Mechanical and Civil Engineering*, vol. 2, no. 6, pp. 26–30, 2012.
- [20] B. W. Tomkins, *Chemical Resistance of Geopolymer concrete against H₂SO₄ & NaOH*, University of Southern Queensland, Queensland, Australia, 2011.
- [21] P. White, "Summary for policymakers," in *Intergovernmental Panel on Climate Change, editor. Clim Chang 2013 - Phys Sci Basis*, pp. 1–30, Cambridge University Press, Cambridge England, 2009.
- [22] R. Siddique and M. I. Khan, *Supplementary Cementing Materials* Springer Science & Business Media, Heidelberg, Germany, 2011.
- [23] S. M. A. Kabir, U. J. Alengaram, M. Z. Jumaat, A. Sharmin, and A. Islam, "Influence of molarity and chemical composition on the development of compressive strength in POFA based geopolymer mortar," *Advances in Materials Science and Engineering*, vol. 2015, pp. 1–15, 2015.
- [24] S. A. Bernal, "Effect of the activator dose on the compressive strength and accelerated carbonation resistance of alkali silicate-activated slag/metakaolin blended materials," *Construction and Building Materials*, vol. 98, pp. 217–226, 2015.
- [25] S. A. Bernal and J. L. Provis, "Durability of alkali activated materials: progress and perspectives," *Journal of the American Ceramic Society*, vol. 97, no. 4, pp. 997–1008, 2014.
- [26] M. C. G. Juenger, F. Winnefeld, J. L. Provis, and J. H. Ideker, "Advances in alternative cementitious binders," *Cement and Concrete Research*, vol. 41, no. 12, pp. 1232–1243, 2011.

- [27] Z. S. Al-Khafaji, Z. Al Masoodi, H. Jafer, A. Dulaimi, and W. Atherton, "The effect of using fluid catalytic cracking catalyst residue (FC3R) as A cement replacement in soft soil stabilisation," *International Journal of Civil Engineering & Technology*, vol. 9, pp. 522–533, 2018.
- [28] T. Bakharev, J. G. Sanjayan, and Y.-B. Cheng, "Resistance of alkali-activated slag concrete to carbonation," *Cement and Concrete Research*, vol. 31, no. 9, pp. 1277–1283, 2001.
- [29] D. L. Y. Kong, J. G. Sanjayan, and K. Sagoe-Crentsil, "Comparative performance of geopolymers made with metakaolin and fly ash after exposure to elevated temperatures," *Cement and Concrete Research*, vol. 37, no. 12, pp. 1583–1589, 2007.
- [30] D. A. J. Hussain, "The fields of applying the recycled and used oils by the internal combustion engines for purposes of protecting the environment against pollution," *Journal of Advanced Research in Dynamical and Control Systems*, vol. 12, no. 01, pp. 698–706, 2020.
- [31] A. Wardhono, D. W. Law, and A. Strano, "The strength of alkali-activated slag/fly ash mortar blends at ambient temperature," *Procedia Engineering*, vol. 125, pp. 650–656, 2015.
- [32] F. Puertas and A. Fernández-Jiménez, "Mineralogical and microstructural characterisation of alkali-activated fly ash/slag pastes," *Cement and Concrete Composites*, vol. 25, no. 3, pp. 287–292, 2003.
- [33] S. A. Bernal, J. L. Provis, B. Walkley et al., "Gel nanostructure in alkali-activated binders based on slag and fly ash, and effects of accelerated carbonation," *Cement and Concrete Research*, vol. 53, pp. 127–144, 2013.
- [34] S. Kumar, R. Kumar, and S. P. Mehrotra, "Influence of granulated blast furnace slag on the reaction, structure and properties of fly ash based geopolymer," *Journal of Materials Science*, vol. 45, no. 3, pp. 607–615, 2010.
- [35] R. Arellano Aguilar, O. Burciaga Díaz, and J. Escalante García, "Lightweight concretes of activated metakaolin-fly ash binders, with blast furnace slag aggregates," *Construction and Building Materials*, vol. 24, no. 7, pp. 1166–1175, 2010.
- [36] C. K. Yip, G. C. Lukey, and Van Deventer Jsj, "Effect of blast furnace slag addition on microstructure and properties of metakaolinite geopolymeric materials," *Ceramic Transactions*, vol. 153, pp. 187–209, 2004.
- [37] O. Burciaga-Díaz, L. Y. Gómez-Zamorano, and J. I. Escalante-García, "Influence of the long term curing temperature on the hydration of alkaline binders of blast furnace slag-metakaolin," *Construction and Building Materials*, vol. 113, pp. 917–926, 2016.
- [38] P. M. Rao and K. H. Raja, "Study of the properties of metakaolin and GGBS based geopolymer concrete," *International Journal of Civil Engineering & Technology*, vol. 8, 2017.
- [39] S. Naganathan, S. Silvadanan, T. Y. Chung, M. F. Nicolasselvam, and S. Thiruchelvam, "Use of wastes in developing mortar—a review," *Advanced Materials Research*, vol. 935, pp. 146–150, 2014.
- [40] B. Standard, *Methods of Testing Cement*, Determ Strength, 2005.
- [41] E. Kim, *Understanding Effects of Silicon/aluminum Ratio and Calcium Hydroxide on Chemical Composition, Nanostructure and Compressive Strength for Metakaolin Geopolymers*, University of Illinois at Urbana-Champaign, Urbana, IL, 2012.
- [42] M. Heikal, M. S. Morsy, and I. Aiad, "Effect of polycarboxylate superplasticizer on hydration characteristics of cement pastes containing silica fume," *Ceram Silikat*, vol. 50, p. 5, 2006.
- [43] P. Risdanareni, P. Puspitasari, E. Santoso, and E. P. Adi, "Mechanical and physical properties of metakaolin based geopolymer paste," *MATEC Web Conf*, vol. 101, p. 1021, 2017.
- [44] Á Palomo, E. Kavalerova, A. Fernández-Jiménez, P. Krivenko, I. García-Lodeiro, and O. Maltseva, *A Review on Alkaline Activation: New Analytical Perspectives*, CSIC-Instituto de Ciencias de la Construcción Eduardo Torroja (IETCC), Madrid, Spain, 2015.

Research Article

Sustainable Concrete Columns with GGBS and Industrial Sand: A Comparative Study on Destructive and Nondestructive Tests on Damaged Columns Strengthened with GFRP Jacketing

G. I. Gunarani ¹, B. Karthikeyan ¹, A. Priyadharshini,¹ Senthil Kumaran Selvaraj ², S Jose,³ D. Vincent Herald Wilson,³ and Tezeta Moges Adane ⁴

¹SASTRA Deemed to be University, Thanjavur 613401, Tamil Nadu, India

²Department of Manufacturing Engineering, School of Mechanical Engineering (SMEC), Vellore Institute of Technology (VIT), Vellore 632014, Tamil Nadu, India

³School of Mechanical Engineering (SMEC), Vellore Institute of Technology (VIT), Vellore 632014, Tamil Nadu, India

⁴School of Civil Engineering, Engineering and Technology College Dilla University, P.O.Box. 419, Dilla, Ethiopia

Correspondence should be addressed to Senthil Kumaran Selvaraj; senthilkumaranselvaraj82@gmail.com and Tezeta Moges Adane; tezeta@du.edu.et

Received 23 March 2022; Accepted 11 August 2022; Published 10 September 2022

Academic Editor: Md. Akter Hosen

Copyright © 2022 G. I. Gunarani et al. This is an open access article distributed under the Creative Commons Attribution License, which permits unrestricted use, distribution, and reproduction in any medium, provided the original work is properly cited.

This paper presents the experimental investigation of the load-resisting characteristics of damaged columns repaired with glass reinforced polymer (GFRP) jacketing. The high-strength columns were made with ground granulated blast furnace slag (GGBS) used at 15%, 25%, and 35% as a partial substitute for cement. Cube specimens of size 100 mm × 100 mm × 100 mm and columns of size 600 mm × 120 mm were cast to perform the study. Considering the practical difficulties in the construction field in obtaining river sand, industrial sand was used for making the specimens eco-friendly. On completion of the prescribed curing period of 28 days, the cube specimens were subjected to a compression test to ensure the grade of the mix design, and the column specimens were subjected to axial loading and were tested in two categories, with and without wrapping of GFRP sheets' split tensile strength. Compression tests on cubes and columns were done. The nondestructive test was also performed with the ultrasonic pulse velocity (UPV) method to check the dense nature of the concrete before and after wrapping with GFRP. On comparing the results, it was observed that it is possible to obtain a higher strength using industrial sand when supported with suitable admixtures and strengthening processes.

1. Introduction

The use of natural resources in concrete is unavoidable in concrete mix, and it is a combination of cement, fine aggregate, mainly river sand, and coarse aggregate. However, the uncontrolled population growth has led to rapid urbanization, which indeed has led to the depletion of natural resources and an increase in the disposal of industrial, agricultural, and construction wastes [1]. Present work aims at developing suitable concrete with other sources from industrial waste so that the natural resources can be preserved to some extent. In this regard, the use of two industrial wastes, one for cementitious material and another for river sand, was

followed in this research to develop high-strength concrete. Furthermore, to check the practical application, column elements were made with the obtained mixes and the behavior of the structural elements was studied, in addition to which the techniques for repairing the concrete columns made with such industrial wastes were also discussed.

1.1. Use of Industrial Waste in Construction. Researchers have already reported the use of such wastes in construction as a partial replacement for cement or in the form of fine aggregates. Fly ash, silica fume, ground granulated blast furnace slag (GGBS), and waste glass are some of the

industrial wastes that are frequently preferred by researchers to be used in concrete as a partial replacement for cement [2–6]. In the present research, GGBS was used as a partial replacement for cement, GGBS is an industrial by-product obtained during the manufacture of pig iron as a chemical. As the chemical composition of GGBS resembles that of cement, it was chosen as a partial replacement for cement in the present work. Since sand occupies a larger quantity than cement in concrete and also as it plays a major role in making the concrete a solid one by reducing volume changes and filling up the pores or voids in the concrete, its demand is also very high. This demand for sand, if not controlled, will result in the nonavailability of good quality sand. To avoid such a situation, it is a good practice to use artificial sand for the construction process. In the construction field, agricultural wastes such as rice-husk ash, sugar cane bagasse ash, oyster nutshell, and sawdust were some of the few known wastes that were being used as a partial replacement for river sand [7–11]. Sivakumar et al, [12] have used Garnet and Al-fly ash in their work and other industrial wastes such as copper slag, steel slag, and iron ore tailings have also been utilized as a partial substitute for fine aggregates [13–16].

In this paper, the use of industrial sand as a full replacement for natural river sand has been discussed. Industrial sand is obtained by crushing stone or rock particles into finer particles, and these particles contain mostly rock dust rather than silt and clay [17]. Researchers have already experimented with M-sand for various types of concrete and have stated that good quality concrete can be achieved by using industrial sand with high micro fine particles [18, 19]. Guan et al., [20] tested the bond behavior of concrete-filled tubular columns made with M-Sand and mentioned in their results that a higher bond strength existed between specimens made with M-Sand. In the current research, experimental investigations were conducted using 100% artificial sand for casting structural columns, and the observations were reported.

1.2. Repair and Rehabilitation: Necessity and Techniques Adopted. Reinforced concrete structures, though made with river sand and other conventional natural materials, face several engineering problems such as dampness, formation of cracks, corrosion of rebars, and also insufficient bearing capacity [21], and the repairing and strengthening of such structures has gained lot of attraction in recent decades. It becomes essential to study the effects of the structure when alternate resources and the techniques to strengthen them are used. Fiber reinforced polymers (FRP) are widely preferred for retrofitting.

Confinement of structural elements using fiber reinforced polymer (FRP) is a commonly adopted technique and many studies have reported on using FRP to strengthen conventional concrete. Researchers have reported that wrapping of columns with FRP is one of the most effective applications [22–25]. Experimental investigations by earlier researchers report that FRPs are preferred due to their lightweight, low thermal conductivity, resistance to corrosion, great mechanical properties, and high ductility compared with reinforced columns [22, 26–28]. Glass fiber reinforced polymer (GFRP) and carbon fiber reinforced

polymer (CFRP) are the most commonly used forms of FRP for retrofitting. Hadi et al. [29] have discussed the effects of using CFRP in hollow-core concrete columns and reported that CFRP confinement improved the ductility of the column than the strength. The use of CFRP has extended to ultra-high-performance concrete (UHPC) too. Lam et al. [30] presented the experimental investigations of UHPC columns confined by FRP. Researchers have reported many works related to GFRP. Kumudha et al. [31] presented the experimental investigations on rectangular concrete columns confined with GFRP wrapping and stated that better improvement in compressive strength was achieved when the numbers of GFRP layers were increased. Rahul and Urmil in 2013 [32] reported the experimental results of GFRP wrapped columns in different sections, namely, circular and rectangular sections. Rodsin [33] investigated the confinement effects of using a low-cost GFRP in columns made with clay bricks as coarse aggregates. The authors reported that circular columns had undergone more axial deformation than other sections, and it was controlled effectively by GFRP confinement.

1.3. Research Significance. The novelty of the current research is to estimate the damage assessment on structural elements made with industrial waste and artificial sand and to discuss the techniques to repair the damaged structural elements. Even though many focused research works are available for strengthening of circular columns, relatively less work has been performed on columns with industrial or artificial sand as fine aggregate used 100% as a replacement for natural river sand. Due to the depletion of natural resources and also the urbanization process, the scarcity of natural sand will become a major problem in the future, and it is time to try other alternatives. This paper tries to fulfil this endeavor.

Considering the literature details mentioned above, this paper discusses the following:

- (1) Strength of cube specimens cast with cement partially replaced with GGBS in 0%, 15%, 25%, 35%, and industrial sand used fully as a replacement for river sand
- (2) Axial strength of column specimens cast with the abovementioned combination
- (3) Axial strength of damaged columns after retrofitted with GFRP layers
- (4) Axial strength of GFRP columns directly without subjecting them to any damage before comparison

2. Materials Used

2.1. Cementitious Materials and Aggregates. Ordinary Portland Cement (OPC) of 43-grade cement conforming to IS 8112 [34] was used. The specific gravity of cement is 3.15.

In this study, artificial sand was used as a fine aggregate. Artificial sand, also known as industrial sand or M-sand, is manufactured by crushing large stones, boulders, and fewer grains of sand. The fineness modulus and specific gravity of sand are 3.8 and 2.63, respectively, which are consistent with

Zone II as per IS 383-1970 [35]. The advantages of M-sand are its high-compressive strength. It has fewer impurities, which results in a better quality of concrete. The artificial sand used in the present research is shown in Figure 1. The gradation curve of the artificial sand obtained from sieve analysis is shown in Figure 2. Though it is slightly coarser than river sand, the particles are distributed and proper packing can be ensured if the material is used in the concrete.

A crushed coarse aggregate of 16 to 20 mm in size was used. The modulus of the degree of fineness and the specific gravity is 3.8 and 2.63, respectively, which is consistent with Zone II as per IS 383-1970.

Ground granulated blast slag furnace (GGBS) shown in Figure 3 was used as a partial replacement of cement at different percentages. The specific gravity of GGBS is 2.85 to 2.95 as received from the manufacturer, and the size was analyzed using a zeta analyzer and is found to be 0.1 to 0.6 micron which is presented in Figure 4. To check the nature of the GGBS used, XRD analysis was performed from which it was noted that the material is not fully crystalline and it possesses amorphous nature. Figure 5 shows the XRD pattern of the GGBFS used.

Superplasticizer- CONPLAST SP 430 was used to achieve a workable concrete mix.

2.2. GFRP Sheets. Glass fiber reinforced polymer is used as a retrofitting material and also for strengthening purposes in this investigation. It is a unidirectional glass fiber with a size of 1.37 × 45.72 m roll. The elastic modulus of the sheet is 72.4 GPa and its tensile strength is 3240 MPa. These values are as per manufacturer specifications. Figure 6 shows the sample GFRP sheet used in the current research.

2.3. Mix Proportion. A nominal concrete mix possessing a compressive strength of 30 MPa was designed as per IS 10262- 2019 [36] and the mix proportion arrived was 1 : 1.7 : 2.5. A total of 4 mixes, including one control (C) mix, were made. C, GG15, GG25, and GG35 represent the mixes in which GGBFS was replaced for cement in 0, 15, 25, and 30 percentages. Cubes of size 100 mm × 100 mm × 100 mm were cast to check the compressive strength of the mix. Mix proportion details are listed in Table 1.

2.4. Casting and Repairing of Column. The same mix proportions were used for preparing the column specimens too with and without wrapping. Reinforced concrete columns of size 600 × 120 mm were made with 4 numbers of 8 mm longitudinal bars and 6 mm stirrups. For each mix proportion, two categories, namely, with and without wrapping of GFRP, were made, thus making a total of 7 combinations including control. Figures 7 and 8 show the reinforcements used and the columns after casting.

2.5. Rehabilitation of Column. The rehabilitation process was proceeded with the jacketing process using GFRP wrap. The surface of the concrete column was prepared by grinding the rough surface, followed by removing all the sharp corners. Epoxy resin was coated on the surface of the columns, and



FIGURE 1: M-sand.

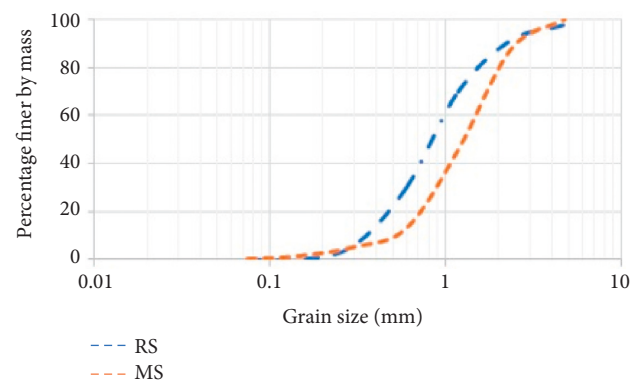


FIGURE 2: Particle size distribution of river sand and M-sand.



FIGURE 3: GGBS.

the specimens were left to stick to the surface. Thermax max-treat epoxy resin is prepared by mixing 125 g of max-treat saturant hardener with 1 kg of max-treat saturant resin. The GFRP sheet was then wrapped around the column with 2 layers and was pressed well. Epoxy resin was applied again to the GFRP wrap and the specimens were left to dry.

3. Testing Methods

3.1. Compression Test. Specimens of size 100 × 100 × 100 mm were cast and tested till failure. Preliminary testing on cubes

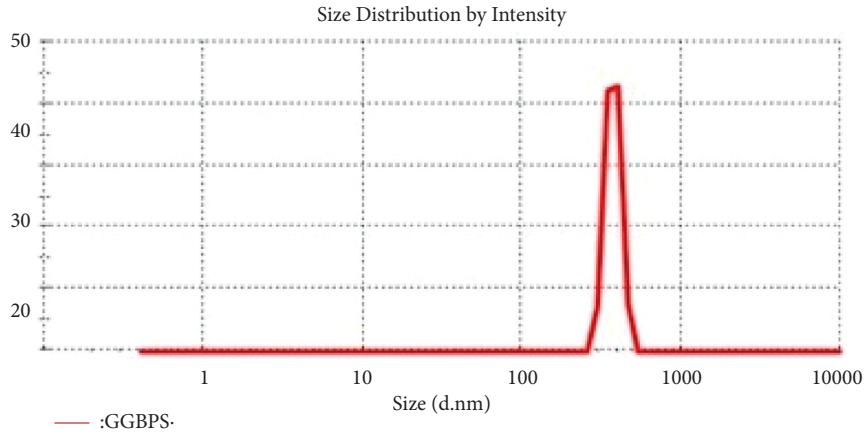


FIGURE 4: Size analysis using zeta analyzer.

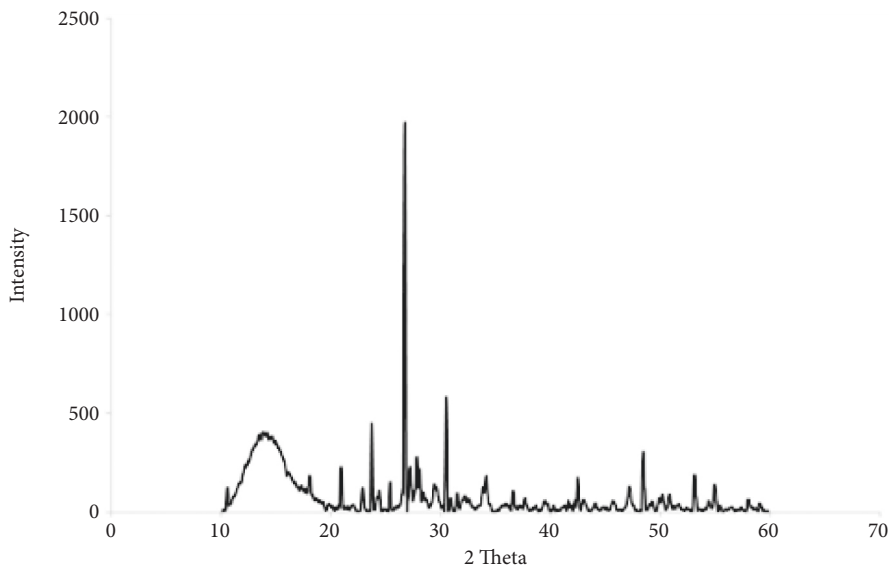


FIGURE 5: XRD pattern for GGBS.



FIGURE 6: GFRP sheets.

for compressive strength has been carried out. The test was done as per IS 516-1959 [37] till failure using a compression testing machine (CTM) of 3000 kN capacity.

3.2. *Ultrasonic Pulse Velocity (UPV)*. The ultrasonic pulse velocity (UPV) test is a nondestructive test to check the quality of concrete. In this test, ultrasonic pulses are used to

TABLE 1: Mix proportion.

Mix ID	C	GG15	GG25	GG35
GGBS, replacement percentage	—	15	25	35
Fine aggregate (industrial sand), kg/m ³		544.18		
Coarse aggregate, kg/m ³		1113.84		
Superplasticizer	1.5 l per 100 kg of cement			
w/c	0.36			
Mix ratio	1 : 1.04 : 1.3			

check the quality of concrete and also to ensure that the concrete is denser. The depth and width of the cracks, if any, in the pores in the concrete can also be detected from this test, and the strength was assessed by measurement of the velocity of an ultrasonic pulse passing through the concrete column. Ultrasonic pulse velocity test as per IS:13311(Part 1), 1992 [38], has been carried out to compare the crack velocity in the column before repairing and after the process of rehabilitation. The details of the test being conducted are illustrated in Figure 9.



FIGURE 7: Reinforcements used in column casting.



FIGURE 9: UPV test being conducted on column specimens.



FIGURE 8: Columns' specimens.

3.3. *Axial Loading in UTM.* A 1000T column testing machine was used for performing the axial load testing. An axial load is applied along the longitudinal or centroidal axis of a structural member such that it produces no moment. The crack and ultimate load failure due to axial loading were noted. The test setup shown in Figures 10 and 11 shows the damaged column after testing. Figure 12 shows the specimens wrapped with GFRP.

4. Results and Discussion

4.1. *Compressive Strength.* Figure 13 illustrates the comparison of the compressive strength results of all mixes with control concrete. The compressive strength increased with an increase in replacement levels of GGBS. However, since no significant variation in strength was found after 25% replacement, replacement levels up to 35% were considered.



FIGURE 10: Test set up for axial loading.

GG35 has shown the highest compressive strength among all combinations, and C has registered the least strength. Except for C, all specimens have shown strength either equal to or



FIGURE 11: Column after being subjected to damage.



FIGURE 12: Column specimens wrapped with GFRP.

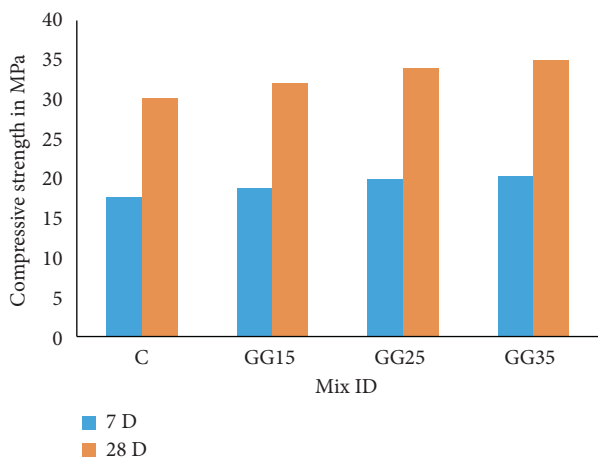


FIGURE 13: Compressive strength test.

more than the mean target strength required for M30. Though the mean target strength for M30 grade should be more than 30 MPa, the values obtained for the mix are closer to 30 MPa or slightly more because this project aims to use industrial sand and the results obtained on using it were found to be slightly less. Since it was decided to study the

axial load carrying capacity of columns with 100% replacement of industrial sand for river sand, the same was tried with the cubes to check the possible strength, and the mix showed a promising strength equivalent to that of an M30 grade.

4.2. Axial Load Resistance of Unwrapped Columns. Figures 14–Figure 17 show the load vs. deflection details of the unwrapped columns for different combinations of GGBS. Control specimens possessed the lowest axial load resistance. All the specimens with GGBS have possessed a reasonable increase in axial strength. GG35 specimen, which possessed better compressive characteristics, has shown better performance in axial strength resistance too and has shown a peak resisting value of 375.6 kN which is 10.76% more than the load resisting characteristics of the control specimens.

4.3. Axial Load Resistance of Columns Repaired with Wrapping. The load-deflection details of the column specimens which were tested without wrapping and later tested once again after rehabilitating them with two layers of GFRP specimens are illustrated in Figures 14 to 17. Also, it is observed from the results that there is a significant improvement in the load resistance in the column specimens after wrapping. Even without wrapping, the columns showed a considerable increase in the axial loads with the increase in the replacement levels of GGBS; after being repaired with GGBS sheets, their load resisting capability increased by 23.7%, 42.2%, 59.6%, and 66.27% for control, GG15, GG25, and GG35 specimens. It is understood that the inner core of the concrete has not been damaged much, and the mix along with GGBS and industrial sand has put up a better resistance against the axial load. The pozzolanic action of GGBS, proper bonding of the mix with the aggregates, and better wrapping techniques have led to the high load resisting capability for the specimens.

4.4. Axial Compression Test on Columns after Strengthening with GFRP. Strengthening of the column is a process to restore or add the ultimate load-bearing capacity of the column. Though strengthening of the column is a process of adding or restoring the ultimate load capacity of a damaged reinforced concrete column, the GFRP wrap column strengthening technique has been adopted in present work on normal columns before they are subjected to any load conditions to observe the variations in the load carrying capacities of a normal column without wrapping and after strengthening with GFRP. The reinforced concrete column in each mix has been strengthened and tested for ultimate load failure by giving axial load to the column. The axial load carrying capacity has increased as the percentage of partial replacement of GGBS increases with GFRP wrap. The damaged columns, after being retrofitted with GFRP wrapping and with partial replacement of GGBS, have shown a drastic improvement in load carrying capacity. The

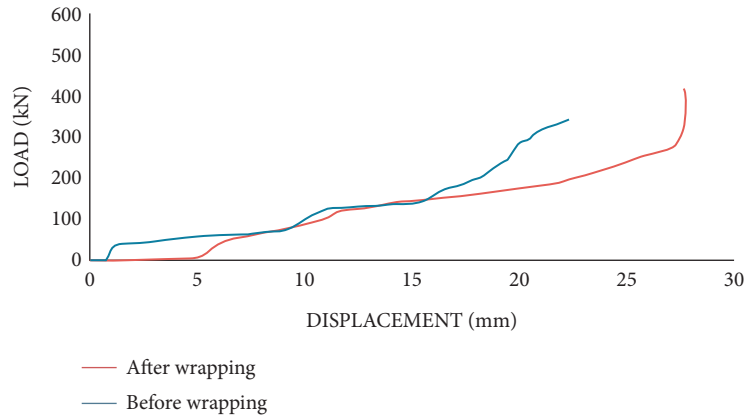


FIGURE 14: Load-deflection behavior of C specimens before and after wrapping.

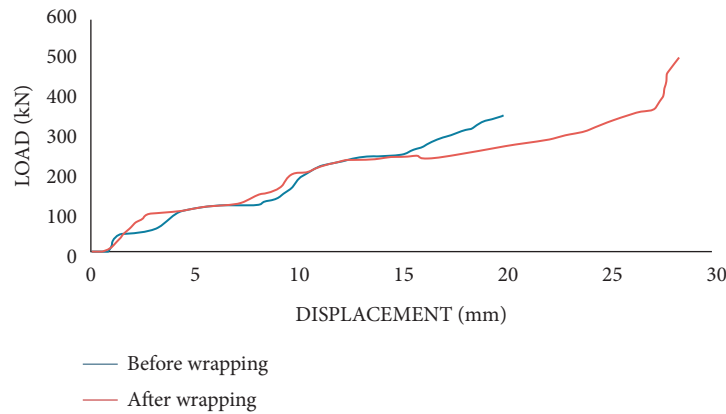


FIGURE 15: Load-deflection behavior of GG15 specimens before and after wrapping.

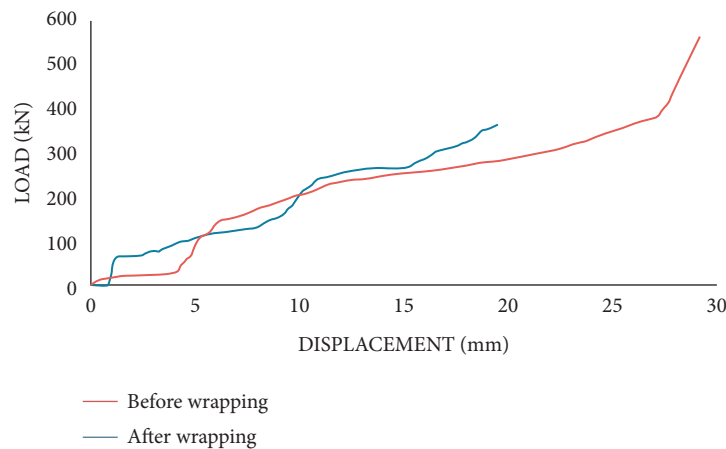


FIGURE 16: Load-deflection behavior of GG25 specimens before and after wrapping.

peak load carrying capacities of the columns have increased to 625.1 kN for GG35 specimens which is the maximum among all and is 66.42% more than the peak load carrying capacity of the specimen without any wrapping. Other specimens have also shown considerable improvement in load carrying capacity. The results are illustrated in Figures 18 to 21.

4.5. *Ultrasonic Pulse Velocity Test.* Table 2 shows the ultrasonic pulse velocity values of column specimens tested with wrapping and without wrapping. It is observed that the UPV values increase with the increase in the replacement levels of GGBS. Earlier researchers have also confirmed that use of supplementary materials will help improving the UPV values as the microcracks developed are properly filled by

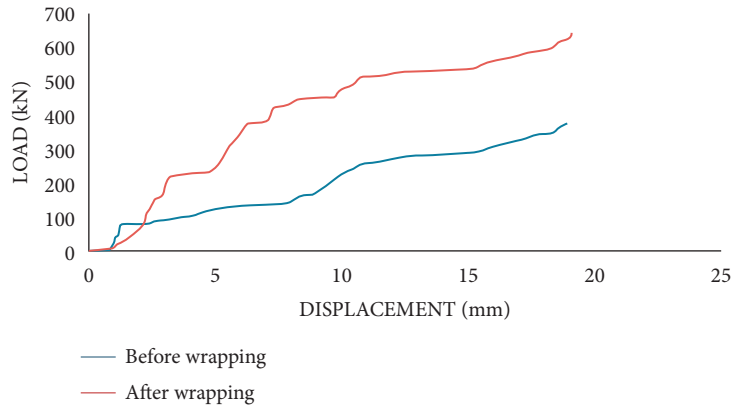


FIGURE 17: Load-deflection behavior of GG35 specimens before and after wrapping.

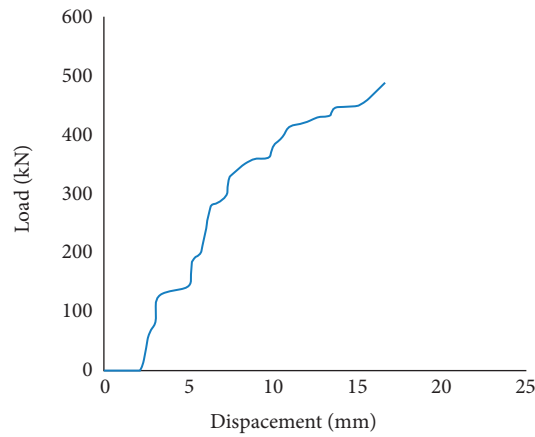


FIGURE 18: Load-deflection behavior of C specimens strengthened with wrapping.

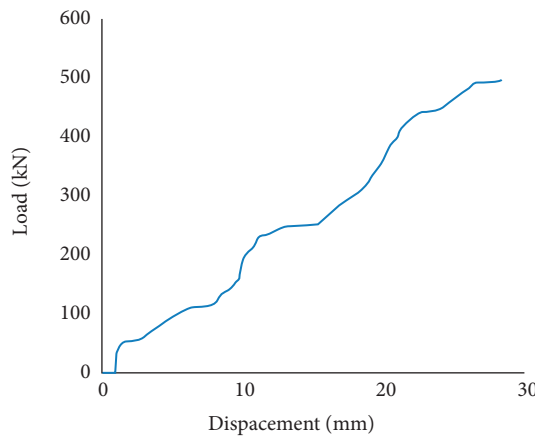


FIGURE 19: Load-deflection behavior of GG15 specimens strengthened with wrapping.

them. Yang et al. [9] reported the compressive strength results of concrete with oyster shells as fine aggregate and reported that the concrete showed an increase in compressive strength by 5% without admixture and suggested that it can be improved to 10% with proper admixture usage in concrete. They mentioned regarding the UPV values that it was higher for 5% replacement and stated that the lower

UPV values were due to the weakness of the C-S-H gel. Iam and Makul [10] in their research stated that the UPV values usually increased when the concrete is made with supplementary cementitious mineral admixtures as the micropores in the concrete structures get filled due to the pozzolanic effect. They also mentioned that better relation existed between the compressive strength of concrete and UPV of self-

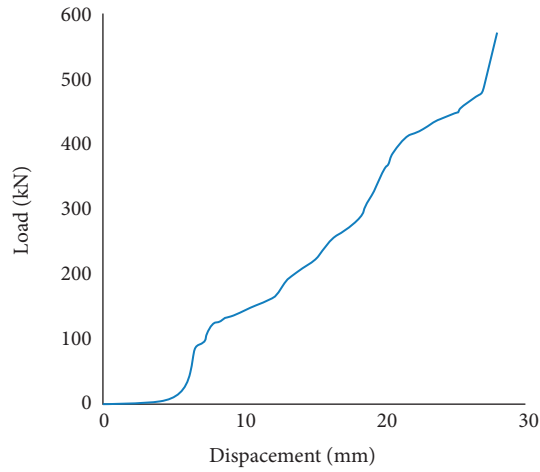


FIGURE 20: Load-deflection behavior of GG25 specimens strengthened with wrapping.

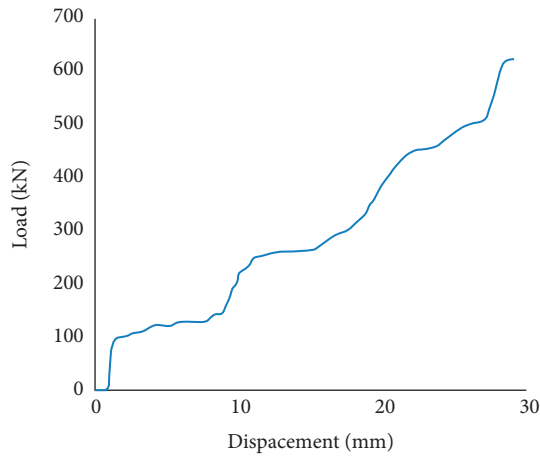


FIGURE 21: Load-deflection behavior of GG35 specimens strengthened with wrapping.

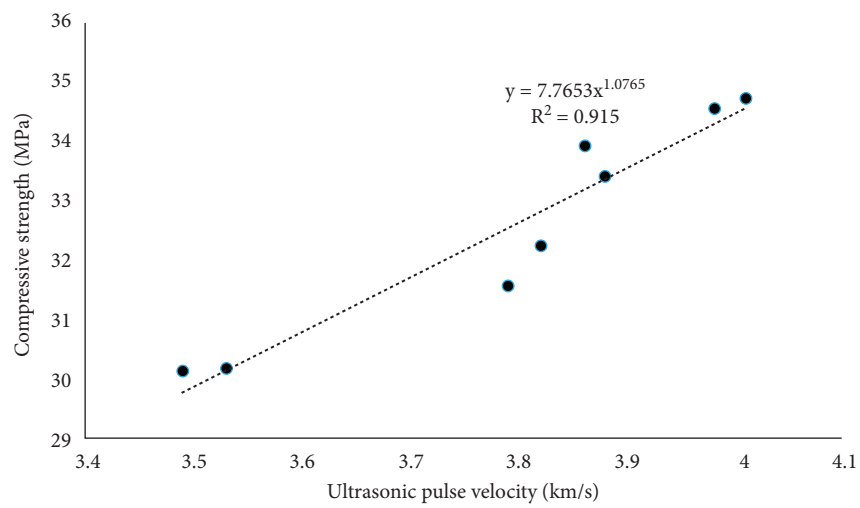


FIGURE 22: Comparison between compressive strength and UPV values.

compacting concrete made with rice husk. The same works well here too that the UPV values are higher for GG35% which possessed the highest compressive strength in cubes.

The relation between the compressive strength and ultrasonic pulse velocity of the unwrapped column specimens is presented in Figure 22. A regression analysis has been

TABLE 2: Ultrasonic pulse velocity test results.

Sample ID	1st crack occurrence velocity (km/s)	
	Before wrapping	After wrapping
C	3.53	4.12
C	3.49	4.08
GG15	3.79	4.26
GG15	3.82	4.35
GG25	3.88	4.56
GG25	3.86	4.48
GG35	3.98	4.51
GG35	4.01	4.63

performed and from which a relation between the compressive strength of concrete made with industrial sand and GGBS and the ultrasonic pulse velocity can be derived.

5. Conclusions

The following conclusions were derived from the experiments:

- (i) All the specimens cast with the industrial sand have achieved a strength closer to the mean target strength required for M30 concrete
- (ii) The partial replacement of cement with GGBS has gradually increased the compressive strength up to 35%
- (iii) The axial load resisting capacity of the columns with industrial sand as fine aggregate increased with an increase in the replacement level of GGBS
- (iv) A massive improvement was observed in the load resisting behavior of the columns after they are retrofitted with GFRP wrapping
- (v) Finally, the combined action of the pozzolanic reaction by GGBS and the effective wrapping by GFRP provided adequate strength to the concrete to overcome structural failures

6. Future Scope

This report presents the discussion on the macrostudies or the mechanical strength details of concrete columns made with industrial waste and artificial sand. The strength of cube specimens was nearer to the design strength of 30 MPa and not very much greater than that. One of the reasons may be due to the large replacement of 35% cement with an industrial waste such as GGBS and another reason may be due to the utilization of industrial waste fully for the work. The study can further be expanded by performing microstructure analysis after analyzing the samples from the low- and high-strength cubes and by suitably modifying the mixed proportions of cement and GGBS. Further improvement can also be made by utilizing river sand along with the industrial sand instead of using industrial sand fully for the research.

Data Availability

All data are included within the article.

Conflicts of Interest

The authors declare that they have no conflicts of interest.

References

- [1] J. K. Prusty, S. K. Patro, and S. S. Basarkar, "Concrete using agro-waste as fine aggregate for sustainable built environment-A review," *International Journal of Sustainable Built Environment*, vol. 5, no. 2, pp. 312–333, 2016.
- [2] P. Kara De Maeijer, B. Craeye, R. Snellings et al., "Effect of ultra-fine fly ash on concrete performance and durability," *Construction and Building Materials*, vol. 263, Article ID 120493, 2020.
- [3] B. Karthikeyan and G. Dhinakaran, "Influence of ultrafine TiO₂ and silica fume on performance of unreinforced and fiber reinforced concrete," *Construction and Building Materials*, vol. 161, pp. 570–576, 2018.
- [4] A. Oner and S. Akyuz, "An experimental study on optimum usage of GGBS for the compressive strength of concrete," *Cement and Concrete Composites*, vol. 29, no. 6, pp. 505–514, 2007.
- [5] B. Karthikeyan and G. Dhinakaran, "Strength and durability studies on high strength concrete using ceramic waste powder," *Structural Engineering & Mechanics*, vol. 61, no. 2, pp. 171–181, 2017.
- [6] G. S. Islam, M. H. Rahman, and N. Kazi, "Waste glass powder as partial replacement of cement for sustainable concrete practice," *International Journal of Sustainable Built Environment*, vol. 6, no. 1, pp. 37–44, 2017.
- [7] P. Shafiq, H. B. Muhmud, M. Z. Jumat, and M. Zargar, "Agricultural wastes as aggregates in concrete mixtures-A Review," *Construction and Building Materials*, vol. 53, p. 110, 2014.
- [8] S. A. Khawaja, U. Javed, T. Zafar, M. Riaz, M. S. Zafar, and M. K. Khan, "Eco-friendly incorporation of sugarcane bagasse ash as partial replacement of sand in foam concrete," *Cleaner Engineering and Technology*, vol. 4, Article ID 100164, 2021.
- [9] E. I. Yang, M. Y. Kim, H. G. Park, and S. T. Yi, "Effect of partial replacement of sand with dry oyster shell on the long term-performance of concrete," *Construction and Building Materials*, vol. 24, no. 5, pp. 758–765, 2010.
- [10] G. S. Iam and N. Makul, "Utilization of lime stone powder to improve the properties of self-compacting concrete incorporating high volumes of untreated rice husk ash as fine aggregate," *Construction and Building Materials*, vol. 38, p. 455, 2013.
- [11] R. Siddique, M. Singh, S. Mehta, and R. Belarbi, "Utilization of treated saw dust in concrete as partial replacement of natural

- sand," *Journal of Cleaner Production*, vol. 261, Article ID 121226, 2020.
- [12] S. Sivakumar, S. Senthil Kumaran, M. Udayakumar, and A. Daniel Das, "Garnet and Al-fly ash composite under dry sliding condition," *Journal of Composite Materials*, vol. 52, no. 17, pp. 2281–2288, 2018.
- [13] W. Wu, W. Zhang, and G. Ma, "Optimum content of copper slag as a fine aggregate in high strength concrete," *Materials & Design*, vol. 31, no. 6, pp. 2878–2883, 2010.
- [14] K. S. Al-Jabri, M. Hisada, A. H. Al-Saidy, and S. K. Al-Oraimi, "Performance of high strength concrete made with copper slag as a fine aggregate," *Construction and Building Materials*, vol. 23, no. 6, pp. 2132–2140, 2009.
- [15] X. Huang, R. Ranade, W. Ni, and V. C. Li, "Development of green engineered cementitious composites using iron ore tailings as aggregates," *Construction and Building Materials*, vol. 44, pp. 757–764, 2013.
- [16] B. Karthikeyan, R. Kathyayini, V. Aravindh Kumar, V. Uthra, and S. Senthil Kumaran, "Effect of dumped iron ore tailing waste as fine aggregate with steel and basalt fibre in improving the performance of concrete," *Materials Today Proceedings*, vol. 46, pp. 7624–7632, 2021.
- [17] P. Nanthagopalan and M. Santhanam, "Fresh and hardened properties of self-compacting concrete produced with manufactured sand," *Cement and Concrete Composites*, vol. 33, no. 3, pp. 353–358, 2011.
- [18] B. Li, J. Wang, and M. Zhou, "Effect of limestone fines content in manufactured sand on durability of low- and high-strength concretes," *Construction and Building Materials*, vol. 23, no. 8, pp. 2846–2850, 2009.
- [19] T. Shanmuga Priya and S. Thirumalini, "Evaluation of strength and durability of natural fibre reinforced high strength concrete with M-sand," *Romanian Journal of Materials*, vol. 48, p. 483, 2018.
- [20] M. Guan, Z. Lai, Q. Xiao, H. Du, and K. Zhang, "Bond behavior of concrete-filled steel tube columns using manufactured sand (MS-CFT)," *Engineering Structures*, vol. 187, pp. 199–208, 2019.
- [21] D. Li, J. Zhou, and J. Ou, "Damage, nondestructive evaluation and rehabilitation of FRP composite-RC structure-A review," *Construction and Building Materials*, vol. 271, Article ID 121551, 2021.
- [22] Y. Wei, X. Zhang, G. Wu, and Y. Zhou, "Behaviour of concrete confined by both steel spirals and fiber-reinforced polymer under axial load," *Composite Structures*, vol. 192, pp. 577–591, 2018.
- [23] A. Siddika, M. A. A. Mamun, R. Alyousef, and Y. M. Amran, "Strengthening of reinforced concrete beams by using fiber-reinforced polymer composites: a-review," *Journal of Building Engineering*, vol. 25, Article ID 100798, 2019.
- [24] L. Biolzi, C. Ghittoni, R. Fedele, and G. Rosati, "Experimental and theoretical issues in FRP-concrete bonding," *Construction and Building Materials*, vol. 41, pp. 182–190, 2013.
- [25] N. Nistico and G. Monti, "RC square sections confined by FRP: Analytical prediction of peak strength," *Composites Part B: Engineering*, vol. 45, no. 1, pp. 127–137, 2013.
- [26] Y. Wei, X. Zhang, J. Wu Bai, G. Wu, and Z. Dong, "Behaviour of concrete confined with steel spirals and fibre reinforced polymer under axial load," *Composite Structures*, vol. 246, p. 577, 2020.
- [27] S. Lin, Y. G. Zhao, and J. Li, "An improved wrapping scheme of axially loaded fiber-reinforced polymer confined concrete columns," *Composite Structures*, vol. 226, Article ID 111242, 2019.
- [28] M. N. S. Hadi, "The behaviour of FRP wrapped HSC columns under different eccentric loads," *Composite Structures*, vol. 78, no. 4, pp. 560–566, 2007.
- [29] M. N. S. Hadi and A. Hussam, T. Goaz Yu, "Experimental investigation of CFRP confined hollow core Reactive Powder Concrete columns," *Construction and Building Materials*, vol. 174, pp. 343–355, 2018.
- [30] L. Lam, L. Huang, J. H. Xie, and J. F. Chen, "Compressive behavior of ultra-high performance concrete confined with FRP," *Composite Structures*, vol. 274, Article ID 114321, 2021.
- [31] R. Kumutha, R. Vaidyanathan, and M. S. Palanichamy, "Behaviour of reinforced concrete rectangular columns strengthened using GFRP," *Cement and Concrete Composites*, vol. 29, no. 8, pp. 609–615, 2007.
- [32] R. Rahul and D. Urmil, "Behaviour of GFRP wrapped coulmns in different sections," *Procedia Engineering*, vol. 51, p. 240, 2013.
- [33] K. Rodsin, "Confinement effects of glass FRP on circular concrete columns made with crushed fired clay bricks as coarse aggregates," *Case Studies in Construction Materials*, vol. 15, Article ID e00609, 2021.
- [34] *IS 8112:2013 Ordinary Portland Cement,-43 Grade Specification*, Bureau of Indian Standards, Manak Bhavan, 9 Bahadur Shah Zafar Marg, New Delhi, 110002.
- [35] *IS 383-1970, Specification for Coarse and fine Aggregates from Natural Sources for concrete*, Bureau of Indian Standards, Manak Bhavan, 9 Bahadur Shah Zafar Marg, New Delhi, 110002.
- [36] *IS 10262- 2019, Guidelines to concrete Mix Design*, Bureau of Indian Standards, Manak Bhavan, 9 Bahadur Shah Zafar Marg, New Delhi, 110002.
- [37] *IS 516-1959, Methods of Test for Strength of concrete*, Bureau of Indian Standards, Manak Bhavan, 9 Bahadur Shah Zafar Marg, New Delhi, 110002.
- [38] *I. S. As, 13311(Part 1)- 1992, Ultrasonic Pulse Velocity, Non-destructive Testing of concrete Methods of Test*, Bureau of Indian Standards, Manak Bhavan, 9 Bahadur Shah Zafar Marg, New Delhi, 110002.

Research Article

Study on Fresh and Mechanical Properties of Polyblend Self-Compacting Concrete with Metakaolin, Lightweight Expanded Clay Aggregate, and SAP as Alternative Resources

S. S. Vivek,¹ B. Karthikeyan,¹ G. Ragul Kanna,¹ Senthil Kumaran Selvaraj¹ ,² Jose S,³ Ponnusamy Palanisamy,³ and Tezeta Moges Adane⁴ 

¹School of Civil Engineering, SASTRA Deemed to be University, Thanjavur-613401, Tamilnadu, India

²Department of Manufacturing Engineering, School of Mechanical Engineering (SMEC), Vellore Institute of Technology (VIT), Vellore-632014, Tamil Nadu, India

³School of Mechanical Engineering, Vellore Institute of Technology (VIT), Vellore 632014, India

⁴School of Civil Engineering, Engineering and Technology College, Dilla University, P. O. Box. 419, Dilla, Ethiopia

Correspondence should be addressed to Senthil Kumaran Selvaraj; senthilkumaranselvaraj82@gmail.com and Tezeta Moges Adane; tezeta@du.edu.et

Received 9 April 2022; Revised 17 May 2022; Accepted 24 June 2022; Published 15 July 2022

Academic Editor: Md. Akter Hosen

Copyright © 2022 S. S. Vivek et al. This is an open access article distributed under the Creative Commons Attribution License, which permits unrestricted use, distribution, and reproduction in any medium, provided the original work is properly cited.

This paper discusses the possibility of developing a lightweight self-compacting concrete (SCC) with self-curing capabilities. In this regard, a supplementary cementitious material metakaolin, a presoaked lightweight expanded clay aggregate (LECA), and a chemical agent, superabsorbent polymer (SAP), were incorporated in developing a self-compacting self-curing concrete possessing a target strength of 60 MPa through experimental investigations, and the results are reported. The research includes an analysis of basic material properties of constituent materials including fresh properties of concrete and mechanical properties such as compressive and splitting tensile strength. It was inferred from the experimental results that utilization of self-curing agents in SCC has enhanced the mechanical properties when compared with conventional SCC mix. In particular, a combination of 0.3% SAP and 15% LECA gave the optimum strength values. The optimum usage limit of both the materials is presented in this study, and the results prove that SCC can be used as an alternate resource without disturbing the natural resources.

1. Introduction

Self-compacting concrete (SCC) is a special concrete having notable advantages such as high flowability and self-compaction with less segregation and is preferred in places of congested reinforcements. In spite of the advantages that SCC possesses, the cost involved in preparing it is higher than conventional concrete as the quantity of cement used is larger and also due to the usage of chemical admixtures to maintain the flowability [1]. In this section, a thorough literature review has been presented in three broad subcategories, namely (i) use of supplementary cementitious materials in SCC, (ii) significance of lightweight aggregate in SCC, and (iii) advantages of initiating self-curing process in SCC.

1.1. Use of Supplementary Cementitious Materials in SCC. SCC can be prepared economically by replacing partially cement with industrial wastes, namely fly ash (FA), ground granulated blast furnace (GGBS) slag, and limestone powder. Not only the supplementary cementitious materials will make the concrete preparation economical but will also help in reducing the autogenous shrinkage and higher heat hydration developed due to higher usage of cement in SCC [2–4].

Mineral admixtures in addition to reducing the total economy when used as an alternative cementitious material in SCC also enhance the workability and help in reducing the segregation of concrete [5]. Metakaolin, silica fume, GGBS, limestone powder, and fly ash are the usual supplementary

cementitious materials that are used in conventional as well as SCC mixes. Among the various mineral admixtures available, metakaolin is preferred by many researchers due to the benefits it possesses such as less economic than micro-silica, having a higher alumina and silica content than FA and GGBS that results in the development of additional C-S-H gel [6].

Metakaolin has been used in the preparation of SCC, and various researchers have reported the fresh and hardened properties of concrete made using SCC [7–10]. Özcan and Kaymak [11] in their research on SCC reported that incorporating metakaolin along with calcite improved the long-term compressive strength and also enhanced the durability properties. Ashish and Verma [12] have performed an optimal metakaolin-based SCC mix design using particle packing, efficiency, and compressive strength methods by varying W/C ratios and reported that it was possible to produce the target strength up to 120 MPa when tested at early ages. Also, in another report, the same authors worked using waste foundry sand and metakaolin to prepare an economical and environmentally friendly SCC and revealed the advantages of using both in SCC [13]. In the present investigation also, a suitable SCC is prepared using metakaolin as an alternative cementitious material for cement. Investigations of earlier researchers state that the performance of concrete is indeed improved when metakaolin is used as a substitute for cement in normal and high-strength conventional concrete [14, 15]. Ashish et al. [16] have compared the cementing efficiencies of flash and rotary calcined metakaolin in concrete and reported that the MK can be replaced up to 30%, and flash calcined metakaolin showed enhanced strength properties compared with rotary calcined metakaolin. Kavitha et al. [17, 18] reported that the incorporation of metakaolin in SCC improves micro and macro properties and enhances durability. Vivek et al. [19–22] researched SCC using various mineral admixtures, namely silica fume, metakaolin, and GGBS in the binary mix and ternary combinations and also with natural and artificial fibers, and concluded that mineral admixtures had shown better performance when compared with control specimen.

1.2. Significance of Lightweight Aggregate in SCC. Though the cement content is reduced with mineral admixtures, the total cementitious quantity is maintained, and due to this high powder content, the viscosity is also sustained. The presence of high powder content used for modifying the viscosity may affect its density making it higher than the density of conventional concrete [23]. Replacement of fine or coarse aggregate with a suitable material can make the mix economical and also environmentally friendly as the natural resources can be preserved. Qasrawi [4] has tried replacing coarse aggregate with steel slag, and it was reported that a green sustainable SCC can be produced using industrial wastes. But the self-weight of concrete is also significant while designing reinforced concrete structures and executing multistorey frames. Hence, the use of lightweight aggregate in SCC can be a suitable solution for this problem, and in addition to reducing the self-weight, they possess further advantages such as reducing size in structural members, reducing heat absorption,

labour requirement, and more importantly leading to reduced construction time [24].

Experimental results of earlier research works reveal that lightweight aggregate in SCC provides a suitable filling effect with less segregation in concrete [25]; this was confirmed by Kim et al. [26] who investigated the characteristics of semilightweight SCC using two different artificial lightweight aggregates and found that the flowability increased and segregation decreased. Adhikary et al. [27, 28] presented detailed reviews on using various materials such as expanded clay as a lightweight aggregate and aerogel in SCC. Juradin et al. [29] have researched SCC using silica fume, fly ash, and filler material to understand the effect on self-compacting lightweight concrete. The authors reported that the silica fume has enhanced SCC fresh properties, and the compressive strength was influenced by the expanded clay and the crushed aggregate. Ofuyatan et al. [30] implemented waste utilization in lightweight SCC with palm ash and reported that using 20% palm ash as partial substitution yielded optimum results. Nepamuceno et al. [31] proposed a grading curve of the lightweight aggregates based on the flow property of mortar. Li et al. [32] proposed a simple design mix method for using lightweight aggregates in SCC using ceramsite, a shale-type and spherical-shaped mineral whose particle size values were satisfactory for being used as a coarse aggregate. Afzali Naniz and Mazloom [33] discussed the effect of using lightweight mineral admixtures such as micro-silica, colloidal nano-silica, and their combinations in SCC and inferred that 10% silica fume and 3% colloidal nano-silica showed better fresh and strength properties. In the present work, lightweight expanded clay aggregate (LECA) was used as the lightweight aggregate.

1.3. Advantages of Initiating Self-Curing Process in SCC. Next to the large cement usage and self-weight, the other problem that the construction industry faces frequently is requiring sufficient water for curing. Improper curing may result in strength loss and stability and may also affect the performance of the reinforced concrete structures. The internal curing process could be an appropriate alternative for conventional curing techniques as it will increase the retention of water within self-compacting concretes with satisfactory fresh and hardened state concrete properties. Curing agents escalate the water retaining capability of SCC by dwindling water evaporation from SCC and help them possess sufficient hardened concrete properties. By employing a proper curing agent for concrete, defensibility and saving in water can be achieved in places of water scarcity. Azari Jafari et al. [34] reported that the use of presoaked superabsorbent polymers SAP in nonvibrated LWC mixtures enhanced the flowability of concrete up to a certain extent. Ali and Marzieh [35] have researched SCC using acrylic polymer and micro-SiO₂ to investigate the fresh properties, compressive strength, and water absorption test. It was inferred that the workability properties were improved and the high quality of SCC was produced using acrylic polymer of about 1–2% and 10% of micro-SiO₂.

Kamal et al. [36] studied the chances of developing a self-curing SCC possessing normal and high strength. The

authors indicated in their results that it is possible to develop both normal and high-strength self-curing SCC and both perform well as structural elements. Chaitanya et al. [37] tried lightweight clay aggregate as self-curing agents for water detention and stated that the internal-curing agent LECA in concrete considerably gave better mechanical properties to concrete. Doha et al. [38] indicated in their report that the internal curing of concrete developed a denser hydrated cement paste and the interfacial transition zone (ITZ) had undergone suitable changes by becoming closer and dense, thereby upgrading the strength of concrete.

1.4. Research Gap. Although SCC with metakaolin, lightweight aggregates, and self-curing agents have been studied by earlier researchers, from the literature survey, it is clear that most of the mineral admixtures and lightweight components were added individually, and the research works focused on the effect of each mineral admixture in SCC. Very limited works were done implementing all the components together to prepare an SCC. So, as an upgrade to the earlier researches, here, a novel mix is proportioned using metakaolin, LECA, and a self-curing agent, namely superabsorbent polymer (SAP), and the physical and mechanical properties are discussed in this paper.

1.5. Research Significance. The novelty of this research is to prepare self-curing SCC with LECA as a partial substitute for fine aggregate to reduce the self-weight along with SAP as an internal curing agent and partially replace cement at a constant level of 10% metakaolin to develop a polyblend combination. LECA acts as an internal storing source in concrete and increases the water reattaining capability of SCC. Lightweight aggregates act as water retainers inside the concrete and ensure sufficient water is available for cement hydration in concrete. Along with the reduction in self-weight aspects, self-curing is also attributed to the current research. Hence, the modern method in today's construction process does not need to provide further moisture within concrete for more efficacious cement hydration along with lightweight aggregates for weight reduction and does not need to use conventional curing methods.

2. Material Proportions, Methodology, and Mix Design

2.1. Materials. OPC 53 grade cement and metakaolin were the basic cementitious materials used. Coarse aggregate of 12.5 mm downgraded size and fine aggregate M-sand (zone II) confirmed to IS 383-1970 [39] were the natural aggregates utilized for the current work. Table 1 shows the chemical composition of cement and metakaolin obtained from the x-ray fluorescent method. Figure 1 shows the XRD pattern of the metakaolin used from which it is understood that the sample possesses amorphous nature mostly though some narrow peaks are obtained at a certain angle due to the presence of silica. The microstructure of the MK used is also shown in Figure 2. Superabsorbent polymer (SAP) is a copolymer added as an additive in SCC as it acts as an internal curing agent in concrete.

TABLE 1: Chemical composition of cementitious materials used.

Formula	Concentration in percentage	
	Cement	Metakaolin
SiO ₂	25.91	53.67
Al ₂ O ₃	5.85	43.34
CaO	68.05	0.37
Fe ₂ O ₃	0.12	0.46
MgO	0.07	0.09
TiO ₂	—	1.19
SO ₃	—	0.27
K ₂ O	—	0.17
Na ₂ O	—	0.12
P ₂ O ₅	—	0.12
PbO	—	0.04
CeO ₂	—	0.04
V ₂ O ₅	—	0.04
Cl	—	0.02
Cr ₂ O ₃	—	0.02
ZrO ₂	—	0.01
Pd	—	96 ppm
NiO	—	95 ppm
ZnO	—	60 ppm
CuO	—	56 ppm
SrO	—	53 ppm

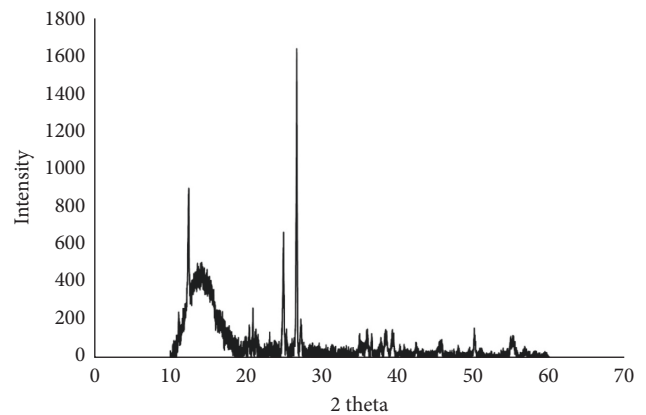


FIGURE 1: XRD image of Metakaolin.

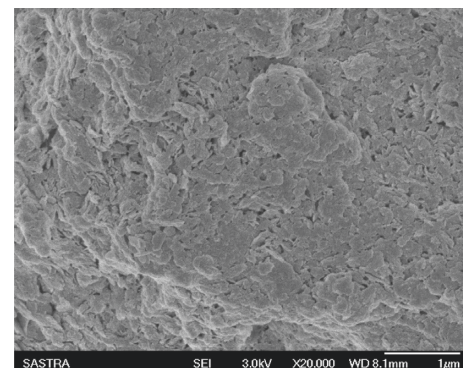


FIGURE 2: Microstructure of Metakaolin.

Lightweight expanded clay aggregate (LECA), which is porous, having less bulk density than the normal aggregate and size less than 5 mm as indicated by the supplier, was used as a partial substitute for fine aggregate. TEC MIX 640 a polycarboxylic ethers type superplasticizer (SP) and Glenium-2, a viscosity modifying agent, were the chemical agents used for maintaining the workability and flowability. The relevant initial tests required were conducted on the constituent materials of SCC, and Table 2 presents these.

2.2. Methodology. The methodology involves preparing SCC using constant 10% MK as a partial substitute for cement and using LECA as a partial replacement for river sand in various proportions along with an additive SAP. As a preliminary research study, the physical and chemical properties of the materials were examined, and their results were reported. After conducting the basic tests on constituents used in SCC, trial design mixes were prepared in the laboratory until the desired flowability of the SCC mix was met as per EFNARC guidelines. While examining fresh properties the mix proportions, W/C ratio and superplasticizer dosages were adjusted, and the slump flow trial tests were repeated. The cube and cylinder specimen moulds were made ready, and the prepared SCC mixes were cast, cured, and tested at the age of 7 days and 28 days to study the hardened state properties. Since the lightweight SCC mixes were prepared and tested, it is significant to compare the weight of all SCC mixes with respect to the control SCC mix. The microstructure studies were performed for the MK and the optimum SAP and LECA mixes. The flow chart on the research methodology adopted is illustrated in Figure 3.

2.3. SCC Mix Design and Material Proportion. Two series of SCC mixes were developed. In the first series, SAP was added as an additive in 0.1%, 0.3%, 0.5%, and 0.7% of cement content, and in the second series, LECA was replaced by fine aggregate from 0% to 25% in an increment of 5%, and totally 10 mixes were made including the control mix. The mix design was done according to IS 10262–2019 [40], and trial mixes were also conducted in the laboratory by slump flow test trials. In SCC, the binder content usually ranges between 400 and 600 kg/m³. Here, 600 kg/m³ is used for better flow and to maintain homogeneity in SCC mixes. W/C ratios have been adopted from the IS 10262-2019 and are kept as 0.35, and the target strength for the present mix is 68.25 N/mm². The fresh properties tests and mechanical properties tests were conducted. The mix proportion is shown in Table 3.

2.4. Trial Mixes. Among the two trial mixes specified in Table 4, the T2 ratio has been considered for casting specimens as it satisfied the requirements of the fresh properties of SCC.

3. Fresh Property Tests

SCC fresh properties tests were performed as per the European Federation of National Associations Representing for Concrete (EFNARC) specifications 2002 and 2005

[41, 42]. The test of the slump was akin to a conventional slump test, but instead of slump height, the diameter of the flow was measured to check whether the slump flow spread diameter is in the range between 650 mm and 800 mm. V-funnel and J-ring tests were used to find the fresh properties of SCC, while the former is used to test the ability to fill and the latter is used to appraise the passing capacity of SCC that tends to flow in critical reinforcements and other hindrances without any separation or blocking. Figures 4–6 illustrate the details.

After performing the fresh properties tests on SCC mixes, the obtained results were compared with the satisfactory limits laid by EFNARC guidelines shown in Tables 5 and 6.

3.1. Specimen Details. After conducting a fresh property test, cube specimens of size 100 mm × 100 mm × 100 mm and cylinder specimens of size 100 mm diameter × 200 mm height were cast to test the compressive and split tensile strength. The specimens were water-cured for the period of 7 days and 28 days to determine the mechanical properties as per IS 516 [43]. Hence, a total of 10 SCC mixes were cast after conducting a fresh properties test.

4. Results and Discussion

4.1. Fresh Properties of LECA, SAP, and Combined SCC Mixes

4.1.1. Flowability. As per EFNARC guidelines, the slump flow values shall be between 650 mm and 800 mm and also subclassified based on the slump flow (SF) class.

From Figure 7, it is apparent that all SCC mixes except 0.7% SAP have obtained the range specified in EFNARC guidelines as the slump values of the mixes are between 550 mm and 650 mm. The reason for the reduction in slump flow value in the 0.7% SAP mix was due to water demand that had affected the higher viscosity characteristics affecting the flowability properties of SCC. On comparing SAP-based SCC mixes slump flow values with SCC control mixes, it was inferred that the increase in the percentage of SAP has shown a reduction in slump flow values. The reason could be the influence of shear stress and plastic viscosity in the SAP-based SCC mixes. Among all SAP-based SCC mixes, the mix containing 0.1% of SAP performed better but the reduction in slump flow spread diameter values by 1.167%. It was inferred from Figure 6 that the slump flow spread diameter values had reduction by the increment of SAP percentages, which was analogous to the results reported by Azari Jafari et al. [34]. The reason for maintaining the flowability of SCC mixes in the presence of SAP (by varying percentages) was governed by the metakaolin of 10% (maintained constant) for all SCC mixes, which was similar to the research performed by Kavitha et al. [17, 18]. This was due to the presence of a higher surface area of MK caused better flowability of SCC mixes.

In LECA-based SCC mixes, a gradual increase in slump flow can be observed values when LECA is increased up to 10% in SCC beyond which, a reduction in slump flow values has occurred. The highest slump flow value was

TABLE 2: Material characteristics.

S. no.	Materials	Size	Water absorption (%)	Specific gravity
1	Cement	—	—	3.15
2	M-sand (fine)	4.75 mm	0.9	2.36
3	Coarse aggregate	12 mm	1.275	2.75
4	Metakaolin	1.5–2.5 microns	—	2.6
5	LECA	Below 10 mm	25	1.07
6	SAP	230–100 mesh	350–500 g/cc	—

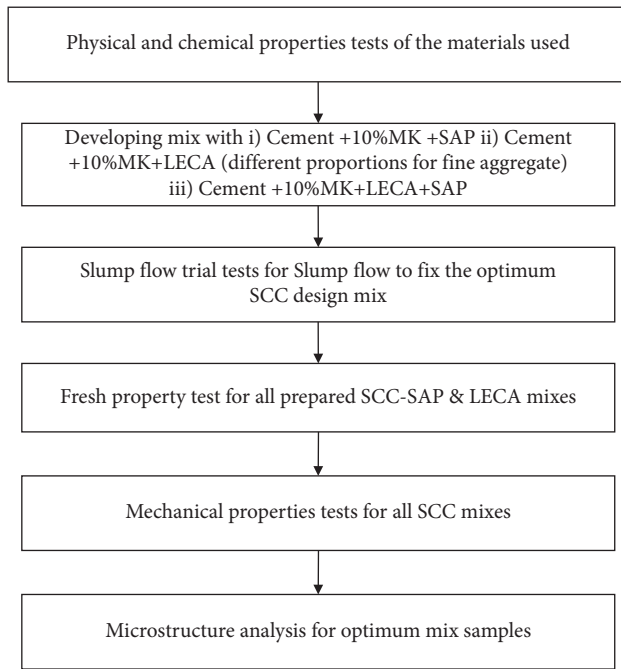


FIGURE 3: Methodology adopted.

obtained for a 10% LECA-based SCC mix when compared with SAP, and it had a flow spread diameter of about 3.357% when compared with the control SCC mix. The reason could be the size effect (less than 10 mm), and the specific gravity of LECA material used in the SCC mix has influenced the flowability property. As the range of slump flow values of LECA-based SCC mixes was between 660 mm and 750 mm, it is categorized as slump flow SF2 class and can be used for concreting of walls and columns. Hence, in LECA based SCC mixes, it is obvious that an increase in aggregate content will hinder the flowing property of SCC slightly as it causes a resistance to the flow because of very tiny holes inside aggregates, which takes over the mixing water and the lower density of light aggregates that creates the particle withstand against fluidity than the control mix. In contrast, LECA SCC mixes had the highest flowability compared to SAP that was inferred from the fresh properties results. The reason could be the presence of an internal curing agent in SAP-based SCC mixes that had the enhanced fluidity, which was similar to the results reported by Kim et al. [26].

The SAP and LECA blend SCC combinations have obtained the slump flow value of 680 mm, which is slightly less than the control SCC mix of about 0.73% but higher than

SAP-based SCC mixes of about 0.44%. This small reduction in slump flow was mainly due to 0.3% SAP, but the homogeneity of SCC flow was enhanced by the presence of MK and LECA as discussed earlier.

4.1.2. T-500 Test. EFNARC guidelines mention that the time taken for T-500 shall be in the range of 2 to 5 seconds. T-500 test measures the flowability rate or viscosity of SCC since the flow time has been measured.

From Figure 8, it is clear that for all SCC mixes, the T-500 time was well within 5 s, whereas for 0.7% of SAP-based SCC mixes, an increase in time by 5.5 s is observed. Among all SAP-based SCC mixes, 0.1% SAP had performed better with the increase in time taken as 4.65% concerning the control SCC mix. Among all LECA-based SCC mixes, 15% of LECA had performed better than the control SCC mix of about 20.93% in terms of flow time gain.

From Figures 7 and 8, a similarity could be observed between obtained slump flow values and flow rates. An increase in flow rate is noted in SAP-based SCC mixes, whereas the flow rate has got decreased in LECA-based SCC mixes. From EFNARC guidelines, the viscosity class has been categorized based on the measured time taken in “seconds.” If the time taken is less than or equal to 2 s, then it belonged to VS1 class, and the value is more than 2 s is referred to as VS2 class. Based on the obtained results, all SCC mixes belonged to VS2 class. Hence, viscosity of SCC mixes increased, and the time delay occurred. For the optimum combinations of LECA and SAP-based SCC mixes, the flow rate has got increased in the mix with the reduction in viscosity.

4.1.3. V-Funnel Test. The V-funnel test measures the flow time in SCC mixes. As per EFNARC guidelines, the flow time ranges between 6 and 12 seconds. The V-funnel test is also used to assess the viscosity and filling ability of SCC mixes. From the obtained results shown in Figure 9, all values are well within the EFNARC specifications.

About 0.7% of SAP-based SCC mixes possessed higher viscosity that increased the flow time by 25.93% compared with the control SCC mix, whereas 15% of LECA-based SCC mix has shown a time gain of about 7.41%. All SCC mixes belonged to the VF2 class whose flow time is more than 8 seconds and between 9 and 25 seconds. Hence, the viscosity is more pronounced in SAP-based SCC mixes when compared to other SCC mixes.

TABLE 3: Mix proportions.

Sl. no	Mix ID	C (kg/m ³)	MK (kg/m ³)	FA (kg/m ³)	LECA (kg/m ³)	SAP (kg/m ³)	CA (kg/m ³)	SP (l/m ³)	VMA (l/m ³)
1	Control SCC	600	—	930	—	—	804	7.2	0.6
2	0.1% SAP	540	60	930	—	0.6	804	7.2	0.6
3	0.3% SAP	540	60	930	—	1.8	804	7.2	0.6
4	0.5% SAP	540	60	930	—	3	804	7.2	0.6
5	0.7% SAP	540	60	930	—	4.2	804	7.2	0.6
6	5% LECA	540	60	883.5	46.5	—	804	7.2	0.6
7	10% LECA	540	60	837	93	—	804	7.2	0.6
8	15% LECA	540	60	790.5	139.5	—	804	7.2	0.6
9	20% LECA	540	60	744	186	—	804	7.2	0.6
10	0.3% SAP + 15% LECA	540	60	790.5	139.5	1.8	804	7.2	0.6

TABLE 4: Trail mix proportions as per IS 10262-2019 code of practice.

Mix ID	Cement	Metakaolin	Coarse aggregate	Fine aggregate	W/P	SP (%)	VMA (%)	Remarks
T1	0.85	0.15	1.34	1.55	0.35	0.9	0.1	Flow is not satisfied <650 mm
T2	0.85	0.15	1.34	1.55	0.33	1.2	0.1	Flow is satisfactory >650 mm



FIGURE 4: Slump flow test.



FIGURE 5: J-ring test.

4.2. Compressive Strength of LECA, SAP, and Combined SCC Mixes. Figure 10 illustrates the compressive strength for SAP, LECA, and their combinations along with the control SCC mix. About 0.3% SAP has obtained the highest compressive strength of about 33.65 MPa and 64.92 MPa when tested at the age of 7 days and 28 days with a strength gain of about 2.59% and 1.23% more than the control SCC mix. The reason could be the internal curing process namely copolymerization exhibited because of the addition of superabsorbent polymer in the SCC mix. Among all SCC mixes, SAP-based SCC mixes performed better than the LECA and control SCC mixes. From Figure 10, it is clear that beyond the addition of 0.3%, SAP has shown a gradual decrease in compressive strength, which was similar to the results reported by Afzali Naniz and Mazloom [33]. The reason was due to the SAP reduced shrinkage that had resulted in the strength loss, which was attributed analogous to the research reported by Chaitanya et al. [37]. In SCC, the polymer blended with mineral admixture had shown a high strength



FIGURE 6: V-funnel test.

TABLE 5: SCC fresh properties tests: satisfactory Limits as per EFNARC 2005 guidelines.

Test methods	Unit	The typical range of values	
Slump flow test by Abrams cone	mm	650	800
J-ring test	mm	0	10
T50 cm slump flow	s	2	5
V-funnel test	s	6	12
L-box test	H ₂ /H ₁ ratio	0.8	1.0
U-box test	H ₂ -H ₁ (mm)	0	30

TABLE 6: SCC fresh properties tests: consistency class as per EFNARC 2005 guidelines.

Test methods	Unit	Consistency class	The typical range of values
Slump flow test	mm	Slump flow class:	
		SF1	550–650
		SF2	660–750
T-500 test	s	Viscosity class:	
		VS1	≤2
		VS2	>2
V-funnel test	s	Viscosity class:	
		VF1	≤8
		VF2	9 to 25
L-box test	H ₂ /H ₁ ratio	Passing ability class:	
		PA1	≥0.80 with 2 rebars
		PA2	≥0.80 with 3 rebars



FIGURE 7: Slump flow spread diameter of all SCC mixes.

and quality, which was similar to the results reported by Azari Jafari et al. [34].

In the second series of mixes consisting of LECA-based SCC, 15% LECA has attained the highest compressive strength among other LECA-based SCC mixes. But it has got a strength reduction of about 11.19% and 2.62% at the age of 7 days and 28 day concerning control SCC mix. The reason for the strength reduction was the fine aggregate replacement. In an SCC mix, the main constituents are the fine aggregates that induce flowability and strength also. The

trend obtained here was similar to the results inferred by Chaitanya et al. [37].

Finally, the optimum percentages of 0.3% SAP and 15% LECA have been blended to study the mechanical properties. From Figure 7, it was inferred that there is a slight strength reduction of about 3.45% and 0.70% at 7 days and 28 days with respect to control SCC. Figures 11–13 show the microstructure of selected optimum mixes. Since much variation was not found in the compressive strengths, the microstructure also did not show much variation; the presence of

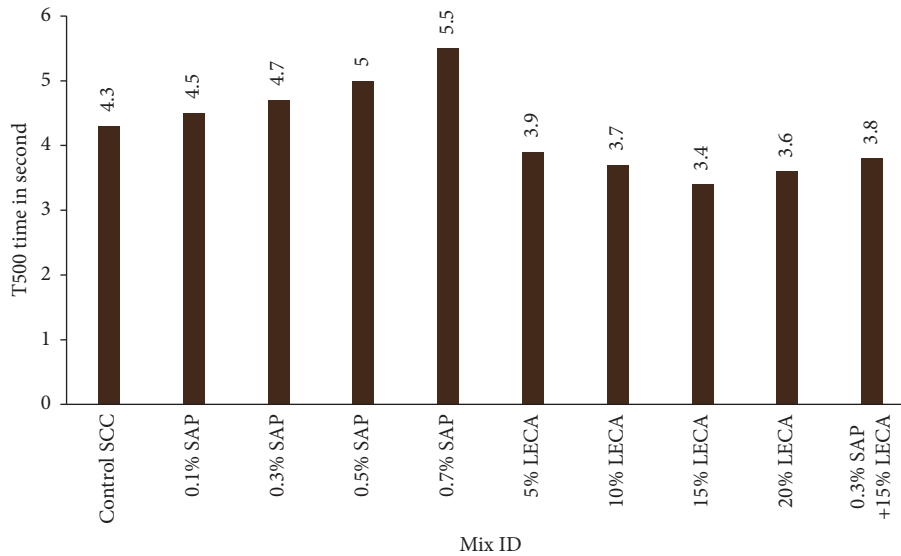


FIGURE 8: T-500 time of all SCC mixes.



FIGURE 9: V-funnel time of all SCC mixes.

voids in 0.3% SAP and 15% LECA was less when compared with the control SCC specimen. Ettringite crystals were also not seen much in the mixes. From the results, it is understood that an equivalent concrete specimen can be made with target strength of about 60 MPa using SAP and LECA instead of normal aggregate in blended combinations along with MK.

4.3. Tensile Strength of LECA, SAP, and Combined SCC Mixes. Control SCC has obtained the highest tensile strength in concern to SAP, LECA, and their blended combinations, which is evident from Figure 14. Here also, much variation is not noted among the tensile strength values, and the same trend observed in compressive strength values followed here too. From Figures 10 and 14, it was inferred that for SAP and LECA SCC mixes, the average percentage ratio between the tensile strength and compressive strength ranges between 6.54 and 8.10 at the age of 28 days and 7 days, respectively. The obtained average compressive strength results for SAP and LECA SCC mixes were

12.4 and 15.4 times more than the respective average tensile strength at the age of 7 days and 28 days, respectively. Also, as the compressive strength increased in the series of mixes, the tensile strength would increase proportionately.

In SAP-based SCC mixes, 0.3% of SAP has the highest tensile strength among other SAP-based SCC mixes. But there is a strength reduction of 6.63% in 28 days compared with the control SCC mix. About 15% of LECA has the highest tensile strength among other LECA-based SCC mixes. A reduction in strength of about 14.86% from the control SCC mix in 28 days was observed. In SAP and LECA blended SCC mixes, at 28 days, the strength reduction noted was about 9.84% compared with the control SCC mix.

4.4. Unit Weight of SCC Mixes. The unit weight of normal weight concrete mixes lies between 2,400 and 2,500 kg/m³, and that of other lightweight concrete mixes almost lies

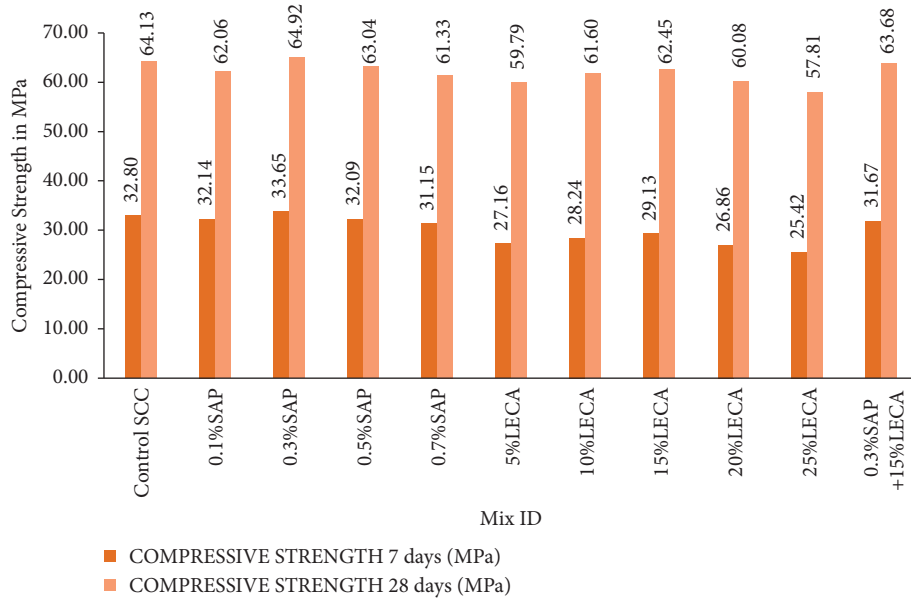


FIGURE 10: Compressive strength of all SCC mixes.

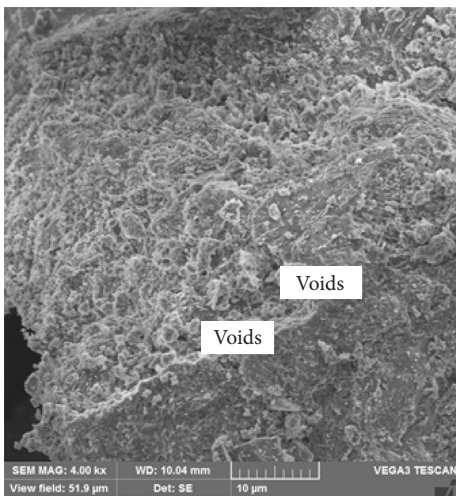


FIGURE 11: Microstructure of control SCC.

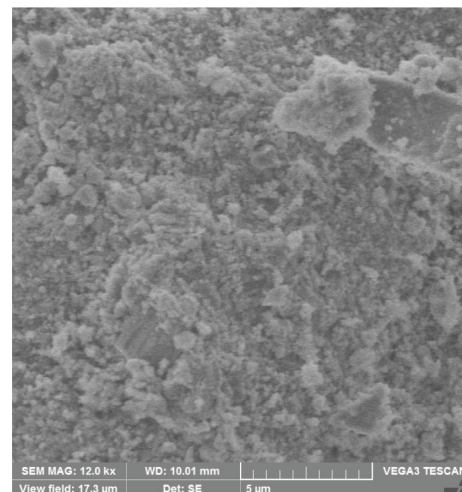


FIGURE 13: Microstructure of 15% LECA.

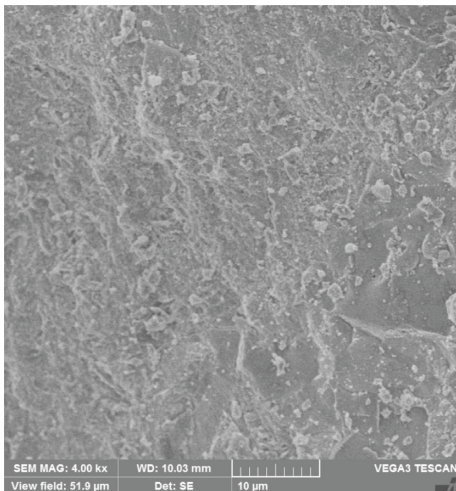


FIGURE 12: Microstructure of 0.3% SAP.

between 1,400 and 1,900 kg/m³ as specified by the code ASTM C 330 [44] and ASTM C 567 [45–54].

Figure 15 shows the unit weight of all SCC mixes. The control SCC mix was analogous to the conventional concrete that obtained a unit weight of 2,562 kg/m³. The first series of mixes containing SAP-based SCC mixes had the unit weight in the range between 2,444 kg/m³ and 2,533 kg/m³. Hence, a slight reduction of about 4.62% in unit weight was attained in SAP-based SCC mixes compared with the control SCC mix. It is also understood that as the percentage of SAP increased from 0.1% to 0.7% in SCC mixes, a gradual decrease in the unit weight took place. In the second series of SCC mixes, when the fine aggregate was substituted with LECA from 5% to 20%, the unit weight had the range between 1,891 kg/m³ and 2,396 kg/m³. The average unit weight of SAP and LECA SCC mixes were 2,293 kg/m³ was 10.5% less than the unit weight of the control SCC mix, in which

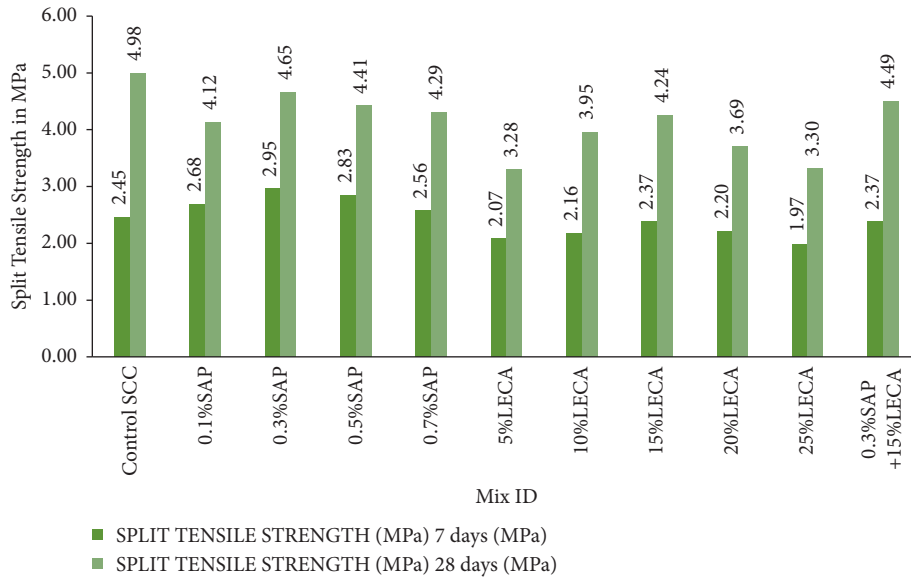


FIGURE 14: Tensile Strength of all SCC mixes.

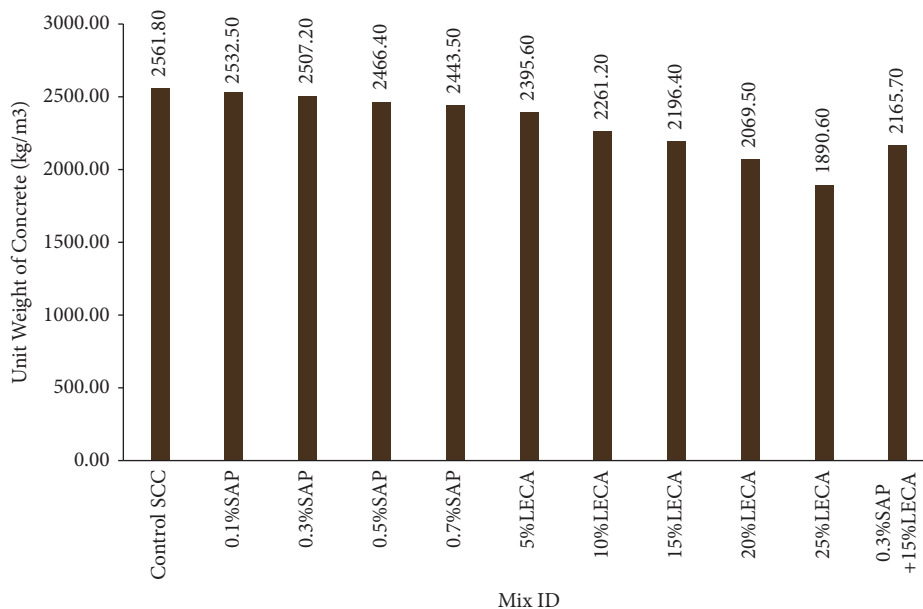


FIGURE 15: Unit weight of all SCC mixes.

the least unit weight was obtained by 0.3% SAP and 15% LECA concerning the control SCC mix. Thus, the unit weight of concrete was reduced by 26.2% when the fine aggregate was replaced by 25% of LECA in the SCC mix. In SAP and LECA blended SCC combinations, the unit weight was also reduced drastically by 15.46% concerning the control SCC mix.

5. Conclusions

The results obtained from the experimental investigations done on the SCC mixes with SAP and LECA individually and together are summarized below:

- (i) The fresh properties test results of mixes made with all combinations indicate that the SCC mixes are well within the specifications of IS code guidelines. In general, it was noted that higher usage of LECA and SAP caused segregation and blocking effects in rheological properties.
- (ii) Among the mixes made with SAP, 0.3% SAP registered the highest strength 28 days strength value with an increase in strength by 1.23% to the control specimen.
- (iii) LECA-based mixes showed higher strength for 15% addition, which was less by 2.62% than the control mix.

- (iv) The combined use of SAP and LECA in 0.3% and 15% showed a considerable reduction in weight, but the strength values were nearer to that of the specimens made with 0.3% SAP and 15% SAP separately, and the addition of SAP or LECA either individually or in combined form did not affect the strength.
- (v) The split tensile strength of SAP mixes 0.3% SAP had the highest tensile strength that showed an increase in strength by 6.62%. About 15% of LECA mixes registered the highest tensile strength among the LECA-based mixes. But both values are less than the control specimen. The combined mix also registered a decrease in values compared to control by 9.84% after 28 days.
- (vi) Also, though the differences in strength values of the SCC mixes prepared were less, it is to be noted that the strength values can be maintained even if part of the fine aggregate is replaced with a lightweight aggregate, and practically, it will be beneficial in saving the natural resources being depleted and in reducing the overall weight of the structure.
- (vii) A considerable reduction in the unit weight of the specimens made with SAP and LECA was observed without affecting the strength properties. So, it is apparent that such a mix can be most preferred for multistorey structures.
- (viii) The optimum blended mix (0.3% SAP and 15% LECA; lightweight) possessed better mechanical properties, and it is apparent from the results that SCC could be produced with both lightweight and self-curing properties.
- (ix) Finally, it is understood SCC specimens can be made with a target strength of about 60 MPa using SAP and LECA instead of normal aggregate in blended combinations along with MK without much affecting the strength due to loss in weight.

Data Availability

All data used to support the findings of the study are included within the article.

Conflicts of Interest

The authors declare that they have no conflicts of interest.

References

- [1] N. Ranjbar, A. Behnia, B. Alsubari, P. Moradi Birgani, and M. Z. Jumaat, "Durability and mechanical properties of self-compacting concrete incorporating palm oil fuel ash," *Journal of Cleaner Production*, vol. 112, pp. 723–730, 2016.
- [2] F. A. Sabet, N. A. Libre, and M. Shekarchi, "Mechanical and durability properties of self consolidating high performance concrete incorporating natural zeolite, silica fume and fly ash," *Construction and Building Materials*, vol. 44, pp. 175–184, 2013.
- [3] M. Benzaid and A. Benmarce, "Behaviour of self-compacting concrete mixed with different additions at high temperature," *Journal of Materials and Environmental Science*, vol. 8, pp. 3081–3092, 2017.
- [4] H. Qasrawi, "Towards Sustainable Self-compacting concrete: effect of Recycled Slag coarse aggregate on the fresh properties of SCC," *Advances in Civil Engineering*, vol. 2018, Article ID 7450943, 2018.
- [5] P. Danish and G. Mohan Ganesh, "Study on influence of Metakaolin and waste marble powder on self-compacting concrete – a state of the art review," *Materials Today Proceedings*, vol. 44, no. Part-1, pp. 1428–1436, 2021.
- [6] R. Prakash, S. N. Raman, N. Divyah, C. Subramanian, C. Vijayaprabha, and S. Praveenkumar, "Fresh and mechanical characteristics of roselle fibre reinforced self-compacting concrete incorporating fly ash and metakaolin," *Construction and Building Materials*, vol. 290, Article ID 123209, 2021.
- [7] A. A. A. Hassan, M. Lachemi, and K. M. A. Hossain, "Effect of metakaolin and silica fume on the durability of self-consolidating concrete," *Cement and concrete Composites*, vol. 34, no. 6, pp. 801–807, 2012.
- [8] R. Madandoust and S. Y. Mousavi, "Fresh and hardened properties of self-compacting concrete containing metakaolin," *Construction and Building Materials*, vol. 35, pp. 752–760, 2012.
- [9] S. Dadsetan and J. Bai, "Mechanical and microstructural properties of self-compacting concrete blended with metakaolin, ground granulated blast-furnace slag and fly ash," *Construction and Building Materials*, vol. 146, pp. 658–667, 2017.
- [10] A. S. Gill and R. Siddique, "Strength and micro-structural properties of self-compacting concrete containing metakaolin and rice husk ash," *Construction and Building Materials*, vol. 157, pp. 51–64, 2017.
- [11] F. Özcan and H. Kaymak, "Utilization of metakaolin and calcite: Working Reversely in workability Aspect—as mineral admixture in Self-compacting concrete," *Advances in Civil Engineering*, vol. 2018, Article ID 4072838, 2018.
- [12] D. K. Ashish and S. K. Verma, "Robustness of self-compacting concrete containing waste foundry sand and metakaolin: a sustainable approach," *Journal of Hazardous Materials*, vol. 401, Article ID 123329, 2021.
- [13] D. K. Ashish and S. K. Verma, "Determination of optimum mixture design method for self-compacting concrete: Validation of method with experimental results," *Construction and Building Materials*, vol. 217, pp. 664–678, 2019.
- [14] B. Karthikeyan, S. K. Selvaraj, G. Dhinakaran, G. Sundaramali, N. Muthuswamy, and V. Paramasivam, "A comparative analysis by experimental investigations on normal and ground ultra-fine mineral admixtures in arresting permeation in high strength concrete," *Advances in Civil Engineering*, vol. 2022, pp. 1–11, Article ID 3831580, 2022.
- [15] B. Karthikeyan and G. Dhinakaran, "Effect of ultra-fine SiO₂ and metakaolin on high Strength concrete in Aggressive environment," *Scientia Iranica*, vol. 24, pp. 1–10, 2017.
- [16] D. K. Ashish, S. K. Verma, and S. K. Verma, "Cementing efficiency of flash and rotary-calcined metakaolin in concrete," *Journal of Materials in Civil Engineering*, vol. 31, no. 12, 2019.
- [17] O. Kavitha, V. Shanthi, G. Prince Arulraj, and P. Sivakumar, "Fresh, micro and macrolevel studies of metakaolin blended self-compacting concrete," *Applied Clay Science*, vol. 114, pp. 370–374, 2015.



- [18] O. Kavitha, V. Shanthi, G. P. Arulraj, and V. Sivakumar, "Microstructural studies on eco-friendly and durable Self-compacting concrete blended with metakaolin," *Applied Clay Science*, vol. 124-125, pp. 143-149, 2016.
- [19] S. S. Vivek and G. Dhinakaran, "Durability characteristics of binary blend high strength SCC," *Construction and Building Materials*, vol. 146, pp. 1-8, 2017.
- [20] S. S. Vivek, R. S. Narayanan, and G. Dhinakaran, "Comparative study on flexural behaviour of RCC beam and SCC ternary beams with mineral admixtures," *Construction and Building Materials*, vol. 152, pp. 57-64, 2017.
- [21] S. S. Vivek and G. Dhinakaran, "Fresh and hardened properties of binary blend high strength self-compacting concrete," *Engineering Science and Technology, an International Journal*, vol. 20, no. 3, pp. 1173-1179, 2017.
- [22] S. S. Vivek, "Fresh and hardened State properties of ternary blend Self compacting concrete using Silica fume and ground granulated blast furnace Slag," *Romanian Journal of Materials*, vol. 51, no. 3, pp. 414-422, 2021.
- [23] A. H. Nahhab and A. K. Ketab, "Influence of content and maximum size of light expanded clay aggregate on the fresh strength and durability properties of self-compacting light weight concrete reinforced with micro steel fibers," *Construction and Building Materials*, vol. 233, Article ID 117922, 2020.
- [24] K. K. Sideris and N. S. Anagnostopoulos, "Durability of normal strength self-compacting concretes and their impact on service life of reinforced concrete structures," *Construction and Building Materials*, vol. 41, pp. 491-497, 2013.
- [25] S. H. Muller and M. Haist, "self-compacting light weight concrete," *Bentonwerk und Fertigteil-Technik*, vol. 12, pp. 8-7, 2004.
- [26] Y. J. Kim, Y. W. Choi, and M. Lachemi, "Characteristics of self-consolidating concrete using two types of lightweight coarse aggregates," *Construction and Building Materials*, vol. 24, no. 1, pp. 11-16, 2010.
- [27] S. K. Adhikary, D. K. Ashish, and Ž. Rudžionis, "Expanded glass as light-weight aggregate in concrete - a review," *Journal of Cleaner Production*, vol. 313, Article ID 127848, 2021.
- [28] S. K. Adhikary, D. K. Ashish, and Z. Ľmantas Rudžionis, "Aerogel based thermal insulating cementitious composites: a review," *Energy and Buildings*, vol. 245, Article ID 111058, 2021.
- [29] S. Juradin, G. Baloević, and A. Harapin, "Experimental testing of the effects of fine particles on the properties of the Self-compacting lightweight concrete," *Advances in Materials Science and Engineering*, pp. 1-8, 2012.
- [30] O. M. Ofuyatan, F. Olutoge, D. Omole, and A. Babafemi, "Influence of palm ash on properties of light weight self-compacting concrete," *Cleaner Engineering and technology*, vol. 4, Article ID 100233, 2021.
- [31] M. C. S. Nepomuceno, L. A. Pereira-de-Oliveira, and S. F. Pereira, "Mix design of structural lightweight self-compacting concrete incorporating coarse lightweight expanded clay aggregates," *Construction and Building Materials*, vol. 166, pp. 373-385, 2018.
- [32] J. Li, Y. Chen, and C. Wan, "A mix-design method for lightweight aggregate self-compacting concrete based on packing and mortar film thickness theories," *Construction and Building Materials*, vol. 157, pp. 621-634, 2017.
- [33] O. Afzali-Naniz and M. Mazloom, "Assessment of the influence of micro- and nano-silica on the behavior of self-compacting lightweight concrete using full factorial design," *Asian Journal of Civil Engineering*, vol. 20, no. 1, pp. 57-70, 2019.
- [34] H. AzariJafari, A. Kazemian, M. Rahimi, and A. Yahia, "Effects of pre-soaked super absorbent polymers on fresh and hardened properties of self-consolidating lightweight concrete," *Construction and Building Materials*, vol. 113, pp. 215-220, 2016.
- [35] H. Ali and Z. Marzieh, "Self-compacting concrete incorporating micro-SiO₂ and acrylic polymer," *Advances in Civil Engineering*, pp. 1-6, 2014.
- [36] M. Kamal, M. Safan, A. Bashandy, and A. Khalil, "Experimental investigation on the behavior of normal strength and high strength self-curing self-compacting concrete," *Journal of Building Engineering*, vol. 16, pp. 79-93, 2018.
- [37] C. V. K. Chaitanya, P. Prasad, D. Neeraja, and A. R. Ravi Theja, "Effect of LECA on mechanical properties of self-curing concrete," *Materials Today Proceedings*, vol. 19, no. Part-2, pp. 484-488, 2019.
- [38] M. A. S. Doha, J. A. S. Aymen, and A. T. Bassam, "Effect of internal curing on behavior of high-performance concrete," *Construction and Building Materials*, vol. 250, pp. 436-448, 2019.
- [39] IS 383, *Specification for Coarse and Fine Aggregates from Natural Sources for Concrete*, 1970.
- [40] IS 10262, *Guidelines for concrete Mix Design Proportioning*, Bureau of Indian Standards, New Delhi, 2019.
- [41] EFNARC, *Specification and Guidelines for Self-Compacting Concrete*, 2002.
- [42] EFNARC, *The European Guidelines for Self-Compacting Concrete Specification, Production and Use*, 2005.
- [43] IS 516, *Methods of Tests for Strength of Concrete*, Bureau of Indian Standards, New Delhi, 1959.
- [44] ASTM C 330, *Standard Specification of Lightweight Aggregates for Structural Concrete*, American Society for Testing Materials, West Conshohocken, PA, 2005.
- [45] ASTM C 567, *Standard Test Method for Determining Density of Structural Lightweight Concrete*, American Society for Testing Materials, West Conshohocken, PA, 2012.
- [46] S. Sivakumar, S. Senthil Kumaran, M. Uthayakumar, and A. Daniel Das, "Garnet and Al-flyash composite under dry sliding conditions," *Journal of Composite Materials*, vol. 52, no. 17, pp. 2281-2288, 2018.
- [47] V. R. NazeeraBanu, S. Rajendran, and S. Senthil Kumaran, "Investigation of the Inhibitive effect of Tween 20 Self-Assembling Nanofilms on Corrosion of Carbon Steel," *Journal of Alloys and Compounds*, vol. 675, pp. 139-148, 2016.
- [48] S. Kannan, S. Senthil Kumaran, and L. A. Kumaraswamidhas, "An investigation on compression strength analysis of commercial Aluminium Tube to Aluminium 2025 Tube Plate by using TIG welding process," *Journal of Alloys and Compounds*, vol. 666, pp. 131-143, 2016.
- [49] S. Kannan, S. Senthil Kumaran, and L. A. Kumaraswamidhas, "An Investigation on mechanical property of commercial copper tube to Aluminium 2025 tube plate by FWTPET process," *Journal of Alloys and Compounds*, vol. 672, pp. 674-688, 2016.
- [50] S. Muthukumar and S. Senthil Kumaran, "Saket Kumar, Friction welding of Cu-tube to Al-tube plate using an external tool," *Transaction of Indian Institute of metals*, vol. 64, pp. 255-260, 2011.
- [51] G. K. Balaji, S. Muthukumar, S. Senthil Kumaran, and A. Pradeep, "Optimization of friction welding of tube to tube plate using an external tool with filler plate," *Journal of*

Materials Engineering and Performance, vol. 21, no. 7, pp. 1199–1204, 2012.

- [52] S. Senthil Kumaran, S. Muthukumaran, D. Venkateswarlu, G. K. Balaji, and S. Vinodh, “Eco- friendly aspects associated with friction welding of tube-to-tube plate using an external tool process,” *International Journal of Sustainable Engineering*, vol. 5, no. 2, pp. 120–127, 2012.
- [53] S. Senthil Kumaran and A. Daniel Das, “An investigation of Boiler Grade tube and tube plate without block by using friction welding process,” *Materials Today Proceedings*, pp. 8567–8576, 2018.
- [54] S. Senthil Kumaran and A. Daniel Das, “Friction welding Joints of SA 213 tube to SA 387 tube plate Boiler Grade materials by using clearance and Interference Fit method,” *Materials Today Proceedings*, vol. 5, pp. 8557–8566, 2018.

Research Article

Comparative Study on Mechanical Properties of Concrete Blended with *Costus englerianus* Bagasse Ash and Bagasse Fibre as Partial Replacement for Lime and Cement

Naraindas Bheel ¹, Charles Kennedy,² Paul Awoyera ³, Samiullah Sohu,⁴ and Suhail Ahmed Abbasi⁴

¹Department of Civil and Environmental Engineering, Universiti Teknologi PETRONAS, Bandar Seri Iskandar, Tronoh, Perak 32610, Malaysia

²Department of Civil Engineering, Rivers State University, Port Harcourt, Nigeria

³Department of Civil Engineering, Covenant University, Ota, Nigeria

⁴Department of Civil Engineering, Quaid-e-Awam University of Engineering, Science and Technology Campus Larkana, Larkana, Sindh, Pakistan

Correspondence should be addressed to Naraindas Bheel; naraindas_20001014@utp.edu.my

Received 2 February 2022; Revised 26 April 2022; Accepted 17 May 2022; Published 1 June 2022

Academic Editor: Xia Bian

Copyright © 2022 Naraindas Bheel et al. This is an open access article distributed under the Creative Commons Attribution License, which permits unrestricted use, distribution, and reproduction in any medium, provided the original work is properly cited.

Nowadays, researchers have been on the lookout for eco-sustainable additives such as agro/industrial waste in concrete in order to offset the carbon footprint created by cement manufacturing. However, it has been said that the use of agro/industrial-waste-based cementitious materials in concrete improves its quality. However, this study compared the performance of hydrated lime and cement concrete replaced with 5% and 10% *Costus englerianus* bagasse ash and bagasse fibre for determining the mechanical properties (compressive and flexural strength). Moreover, compressive strength was evaluated on cubical specimens and flexural strength was evaluated on beam samples at 7, 14, and 28 days, respectively. Results showed that the compressive strength and flexural strength of the concretes increased with an increase in the curing age. Also, the compressive and flexural strengths of cement concrete were recorded by 65.38 MPa and 10.86 MPa at 0% bagasse ash or fibre, which performed better than concrete replaced with 5% and 10% bagasse ash and fibre at 28 days, respectively. Besides, the compressive strength of concrete was noted by 53.85 MPa and 48.92 MPa at 10% bagasse ash and 10% bagasse fibre, respectively, while the flexural strength was calculated by 6.86 MPa and 5.54 MPa at 10% bagasse ash and 10% bagasse fibre, respectively, which were higher than that of concrete produced with hydrated lime alone at 28 days. Thus, bagasse ash performed better than bagasse fibre ash as a partial replacement of cement or hydrated lime in concrete production. Therefore, *Costus englerianus* bagasse ash or bagasse fibre improved the performance of hydrated lime concrete at 5–10% replacement, but higher concrete strength would be obtained in cement replacement than hydrated lime.

1. Introduction

Concrete is only second to water as the most widely used materials in the world, which was estimated at 30 billion tons per yearly consumption [1]. The demand for high-strength concrete in building infrastructures has been on the increase, but increasing the strength of concrete could equally increase its brittleness, which ultimately may lead to crack and

failure of concrete structures [2–6]. However, the development of new cementitious materials could improve the safety, durability, and sustainability of concrete [7–10]. The addition of pozzolan materials in cement enhanced the mechanical properties of concrete, such as compressive, tensile, and flexural strength [11, 12].

Lime, as binding material, yields concrete with low strength, which may not be useful in certain areas of

construction [13–17]. In a study by Salman and Muttar [18], the optimum compressive strength of Portland cement concrete obtained at 28 days of curing was 26.96 N/mm^2 , but just 6.12 N/mm^2 was recorded at 28 days of curing for lime concrete and only increased by 50% (13.15 N/mm^2) when the curing period was increased to 90 days. However, Awodiji et al. [14] recommended the addition of pozzolanic materials in lime concrete to increase the lime concrete strength designed for construction purposes. Brzyski [19] reported an increase in the strength of concrete by adding 10% meta-kaolinite, micro silica, and zeolite, independently, in lime concrete, which doubled the strength by 20%.

The use of agricultural waste ash as a cement substitute is gaining popularity among academics owing to its eco-friendliness, sustainability, and economic benefits [20–22]. Portland cement (PC) concrete is utilized in a wide variety of structural applications, and modern and complex designs need a substantial amount of PC [23]. But PC production is one of the most energy-intensive processes in concrete [24–27], and it also produces carbon dioxide which has been a cause of discomfort for the atmosphere. PC manufacturing accounts for between 5% and 7% of industrial carbon dioxide emissions [28–31]. Additionally, affordable housing has grown more difficult to get for many low-income workers in a number of developing nations owing to the high cost of construction ingredients, notably cement. Without impacting the performance of concrete buildings, the amount of Portland cement must be lowered to help limit emissions of carbon dioxide and offer sustainable building materials [32, 33]. However, a partial replacement of PC using combined cement replacing materials (CRMs) is favorable in terms of economics, mechanical properties, and microstructure. There are various commonly produced CRMs that could be used in concrete. Millet husk ash (MHA), sugarcane bagasse ash (SCBA), coconut shell ash (CSA), groundnut shell ash (GSA), silica fume (SF), maize cob ash (MCA), wheat straw ash (WSA), and rice husk ash (RHA) are among the most commonly used products [34, 35]. Reusing these CRMs offers a practical solution to contamination, waste management, and excessive cement costs. Therefore, *Costus englerianus* bagasse ash and bagasse fibre are used as cementitious material in this experimental work. Moreover, *Costus englerianus* bagasse is a family of sugarcane bagasse that mostly grows in the bush with stronger fibres than sugarcane bagasse. *Costus englerianus* bagasse has not attracted wide attention as a partial replacement of cement in concrete production. On the other hand, sugarcane bagasse ash as pozzolan materials has shown effectiveness in the enhancement of mechanical properties and durability of concrete [36–38]. Malyadri and Supriya [39] reported a 5% increase in concrete strength using sugarcane bagasse ash as a partial substitute for cement. A similar observation was also reported by Mangi et al. [40]. Between 5% and 20% sugarcane bagasse ash replacement, an acceptable strength of concrete can be obtained [41, 42]. Other studies have shown that sugarcane bagasse is a good replacement material for concrete production [43, 44]. Also, 5 to 15% sugarcane bagasse ash increased the compressive strength and workability of concrete [45–47],

while other authors have recorded compressive strength produced from sugarcane bagasse ash that was higher than cement concrete alone at 5% replacement or more [48–51]. An excessive increase in the percentage replacement of bagasse ash could result in reduced strength of concrete [52–55].

Furthermore, some studies were performed on the concrete blended with cement and lime as cementitious material. But no experiments were performed on concrete incorporating the combining influences of PC and lime replaced with *Costus englerianus* bagasse ash and fibre for determining the mechanical properties of concrete. Therefore, this research is performed to determine the mechanical properties of concrete blended with PC and lime replaced with *Costus englerianus* bagasse ash and fibre in the mixture, respectively.

2. Materials and Methods

2.1. Materials. The materials used in the study include hydrated lime and limestone cement (Dangote cement) as the binder, *Costus englerianus* bagasse ash and bagasse fibre as pozzolan materials, granite chipping as coarse aggregates, river sand as fine aggregates, clean tap water, and superplasticizer. However, the stems of *Costus englerianus* bagasse were collected from bushes in the Odiokwu community, Ahoada West Local Government Area of Rivers State, Nigeria, and sundried for 72 hours at atmospheric temperature to remove the moisture content. Parts of the dried samples were burnt to ashes in open air and sieved to remove the carbonaceous material. The free carbonaceous burnt ashes (bagasse ash) were ground to fine particle sizes, while the remaining parts of the dried samples (bagasse fibre) were also ground to fine particle sizes. The ground fine particles of the bagasse ash and bagasse fibre were sieved to $90 \mu\text{m}$ uniform sizes and stored in airtight containers. The limestone cement (Grade 42.5R) and hydrated lime were purchased from a building material shop in Port Harcourt, Rivers State. The chemical composition and properties of cement, bagasse ash, and bagasse fibre are shown in Table 1. River sand was collected from the Sombrero River in Ahoada East Local Government Area of Rivers State and poorly graded to $<5 \text{ mm}$ in size which was used for this research. Besides, granite chippings were used as coarse aggregates (CA) having 20 mm in size which were bought from a retailer in Rivers State. In addition, polycarboxylate polymer superplasticizer (SP) (Auracast 200) was obtained from a building material store in Port Harcourt, while tap water was collected from the laboratory.

2.2. Mix Proportions. The bagasse ash and bagasse fibre were prepared at replacement percentages of 5% and 10% and mixed with cement, fine and coarse aggregates. Concrete cubes including 0% bagasse content (with only cement or hydrated lime) from the mix proportions were cast with the following dimensions: $150 \text{ mm} \times 150 \text{ mm} \times 150 \text{ mm}$ to test for compression strength, while the test for flexural strength was conducted on casted beams (including sample with only

TABLE 1: Chemical and physical properties of lime and *Costus englerianus* bagasse.

Composition (%)	Limestone cement	Bagasse ash	Bagasse fibre
SiO ₂	20.36	64.85	56.78
Al ₂ O ₃	5.15	5.36	6.73
Fe ₂ O ₃	2.98	4.72	7.52
CaO	64.07	1.78	5.31
MgO	1.33	1.23	4.65
K ₂ O	0.52	6.41	8.92
Na ₂ O	0.2	1.02	4.17
MnO	—	0.05	0.94
TiO ₂	0.22	—	—
H ₂ O	0.52	0.2	3.76
SO ₃	2.03	0.18	1.03
LOI	2.76	10.48	7.4
SiO ₂ + Al ₂ O ₃ + Fe ₂ O ₃	—	74.93	71.03
Density (g/cm ³)	3.11	2.16	2.25
Specific surface area (cm ² /mg)	3586	4727	2850.8

cement or hydrated lime) with the following dimensions: 500 mm × 100 mm × 100 mm. The samples were mixed at a water binder ratio of 0.32 and cement content of 550 kg/m³. The cubes and beams were cured for 7, 14, and 28 days by immersion in a water tank at room temperature. The mix proportions of concrete are shown in Table 2.

2.3. Testing Methods. The mechanical properties are in terms of compressive and flexural strength. However, the compressive strength test was carried out according to BS EN 12350-3:2009 [56], in which the specimens were crushed at a 15 N/mm² constant rate increase in stress using the universal crushing machine. The cubes were centrally placed on the crushing machine with a smooth surface and allowed to fail under direct axial compressive load. Similarly, the flexural strength test was carried out according to BS EN 12390-5:2009 [57]. The load under which the specimen failed was recorded from which the flexural strength was calculated. All these tests were cured at 7, 14, and 28 days respectively.

3. Results and Discussions

The comparative results obtained for compressive and flexural strength of cement and hydrated lime concrete replaced at 5% to 10% *Costus englerianus* bagasse ash and bagasse fibre are presented and discussed in this section.

3.1. Compressive Strength. The comparative analysis of compressive strength of concrete produced from the bagasse ash and bagasse fibre as partial replacement of cement and hydrated lime was investigated at curing age of 7, 14 and, 28 days with a percentage replacement of 5%, 10%, 15%, and 20% bagasse ash and bagasse fibre. It has been observed that the experimental work is performed by using cement and hydrated lime as binders, and these binders are replaced with various proportions of bagasse ash and bagasse fiber for determining the compressive strength of concrete respectively. The profiles of the compressive strength of concrete produced from the two types of binders are shown in Figures 1–4. Figure 1 shows the profiles for compressive strength comparison of cement and lime concretes

produced at 5% bagasse ash and bagasse fibre between the curing age of 7 and 28 days. The profiles showed that the compressive strength of bagasse ash at 5% replacement was higher than that of bagasse fibre at 5% replacement for both cement and lime concretes. Also, the compressive strength of 0% bagasse (cement only) concrete was greater than the strength of concretes produced with 5% bagasse ash and bagasse fibre, while the strength of concrete with 5% bagasse ash was higher than that of 0% bagasse lime (lime alone) concrete. Furthermore, compressive strength at 5% bagasse ash and bagasse fibre increased with an increase in curing age. Thus, compressive strength between 7 and 28 days increased from 56.74 to 65.38 N/mm² for concrete with cement only, while with only lime or zero per cent bagasse, the compressive strength ranged from 38.01 to 46.47 N/mm². Similarly, the compressive strength between 7 and 28 days increased from 53.86 to 63.95 N/mm² at 5% cement replacement with bagasse ash compared to 39.12–44.87 N/mm² increase in lime concrete with 5% bagasse ash content. Also with 5% bagasse fibre, compressive strength ranged from 51.08 to 59.65 N/mm² and 37.19 to 45.53 N/mm² for cement and lime concretes, respectively.

Similarly, the profiles comparing the compressive strength of cement and lime concrete replaced with 10%, 15%, and 20% bagasse ash and bagasse fibre are shown in Figures 2–4, respectively. The analysis showed that compressive strength increased with an increase in curing age. In addition, the compressive strengths of cement and lime concrete replaced with bagasse ash were higher than those replaced with bagasse fibre. Again, the compressive strengths of cement concrete replaced with bagasse ash and bagasse fibre were higher than those produced with lime concrete at any percentage replacement (see Figures 2–4). This implied that cement is a better binding material for concrete compared to hydrated lime. Previous investigations on the performance of cement and hydrated lime concrete or mortar also showed that the compressive strength of cement concrete performed better than lime concrete [14, 15, 18], which was attributed to the slow rate of the hydration process in lime concrete [15].

The study also showed that the compressive strength of hydrated lime was improved when 10% to 15% bagasse ash and bagasse fibre was added to the mix. Ordinarily, the

TABLE 2: Mix proportions of concrete.

Mix ID	Cement	Lime (%)	Ash (%)	Fibre (%)	Sand (%)	CA (%)	Water/cement ratio	SP (%)
Cement	100	0	0	0	100	100	0.32	1
5% A-Cem	95	0	5	0	100	100	0.32	1
10% A-Cem	90	0	10	0	100	100	0.32	1
15% A-Ceme	85	0	15	0	100	100	0.32	1
20% A-Ceme	80	0	20	0	100	100	0.32	1
5% F-Cem	95	0	0	5	100	100	0.32	1
10% F-Cem	90	0	0	10	100	100	0.32	1
15% F-Cem	85	0	0	15	100	100	0.32	1
20 F-Cem	80	0	0	20	100	100	0.32	1
Lime	0	100	0	0	100	100	0.32	1
5% A-Lime	0	95	5	0	100	100	0.32	1
10% A-Lime	0	90	10	0	100	100	0.32	1
15% A-Lime	0	85	15	0	100	100	0.32	1
20% A-Lime	0	80	20	0	100	100	0.32	1
5% F-Lime	0	95	0	5	100	100	0.32	1
10% F-Lime	0	90	0	10	100	100	0.32	1
15% F-Lime	0	85	0	15	100	100	0.32	1
20 F-Lime	0	80	0	20	100	100	0.32	1

Note: A = ash, F = fibre, CA = coarse aggregates, and SP = superplasticizer.

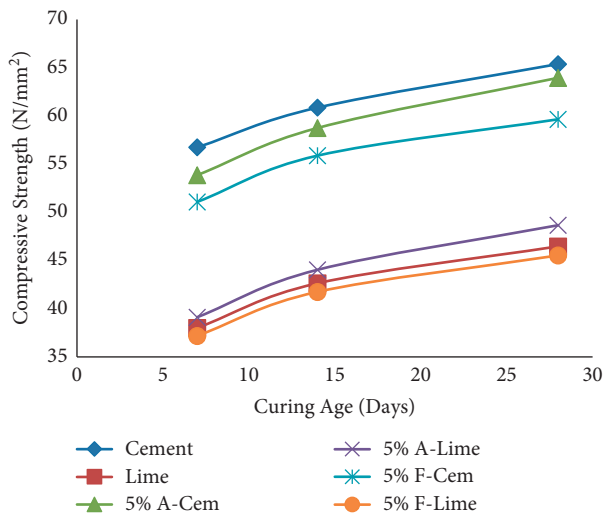


FIGURE 1: Compressive strength of cement and lime with 5% bagasse ash and fibre.

compressive strength of the lime concrete would result in low compressive strength that may not be suitable for structures that require high-strength concrete, but with the addition of other pozzolan materials [18, 58] or inclusion of superplasticizer [59–61], the compressive strength of lime concrete can be improved significantly. Thus, the compressive strengths recorded in this study were very high compared to other studies using sugarcane bagasse ash [2, 49, 51], which is attributed to the addition of a superplasticizer.

3.2. Flexural Strength. The flexural strength of concrete produced from limestone cement and hydrated lime was also investigated at only 5% and 10% bagasse ash and bagasse fibre replacement. The test results are presented for 5% and 10% bagasse ash and fibre as shown in Figures 5 and 6,

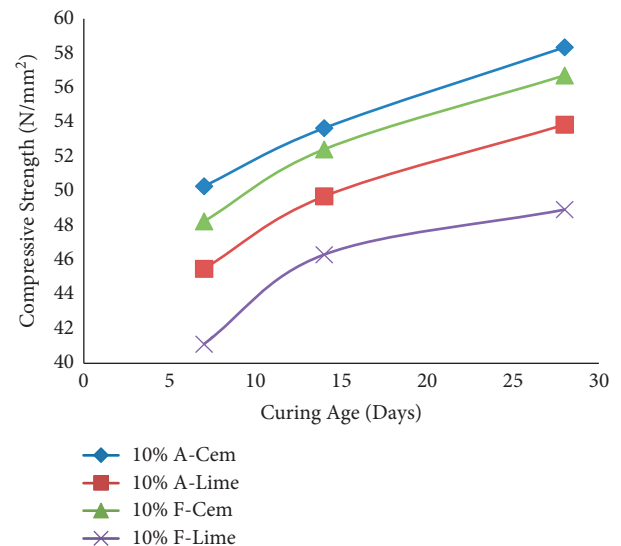


FIGURE 2: Compressive strength of cement and lime with 10% bagasse ash and fibre.

respectively. However, Figure 5 shows the flexural strength of cement and hydrated lime concretes produced with 5% bagasse ash and bagasse fibre replacement for 7, 14, and 28 days of curing age, while Figure 6 shows 10% bagasse ash and bagasse fibre replacement. Similar to compressive strength, the flexural strength of concrete increased with an increase in curing age. Also, the flexural strength of cement concrete with 0% bagasse ash or bagasse fibre (cement only) was more than that of concrete mixed with 5% bagasse ash or bagasse fibre. On the contrary, the flexural strength of lime concrete with 0% bagasse ash or bagasse fibre (lime only) was less than that of concrete mixed with 5% bagasse ash and slightly greater than concrete with 5% bagasse fibre replacement. Thus, between 7 and 28 days of the curing age, the flexural strength obtained for concrete mixed with cement ranged from 9.64–10.86 N/mm² compared to 3.15–5.31 N/mm²

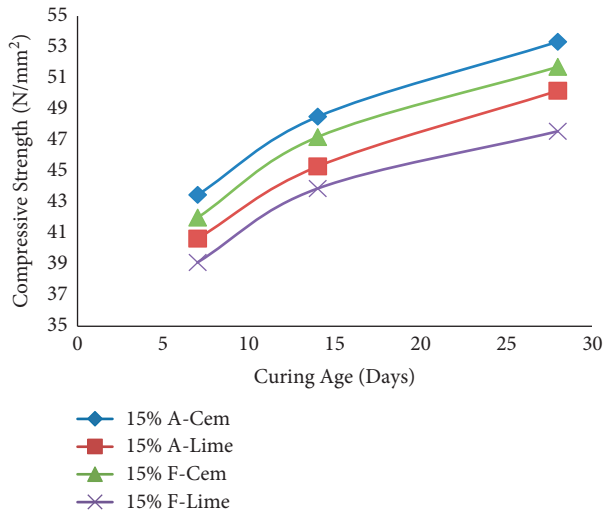


FIGURE 3: Compressive strength of cement and lime with 15% bagasse ash and fibre.

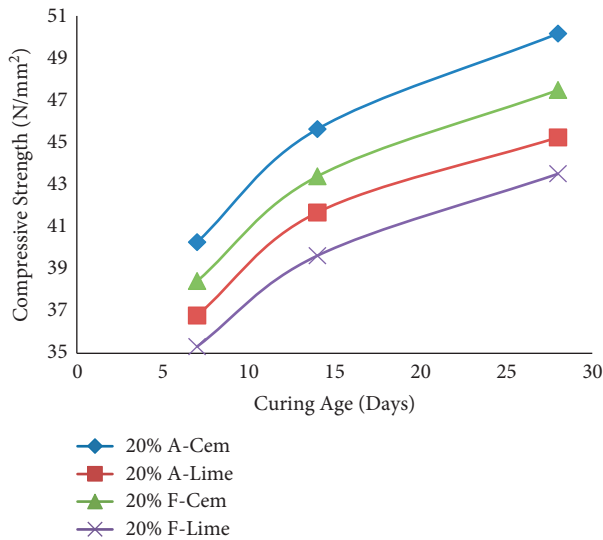


FIGURE 4: Compressive strength of cement and lime with 20% bagasse ash and fibre.

recorded for the mix with lime only. Also at 5% bagasse ash replacement, the flexural strength ranged from 9.29 to 10.55 N/mm² for cement and 3.76 to 5.94 N/mm² for hydrated lime. Similarly, at 5% bagasse fibre replacement, the flexural strength ranged from 7.58 to 8.68 N/mm² for cement and 2.88 to 4.85 N/mm² for hydrated lime.

Similarly, the flexural strength of concrete with cement only was more than that of concrete replaced with 10% bagasse ash and bagasse fibre, but the flexural strength of lime concrete replaced with 10% bagasse ash or bagasse fibre was greater than the flexural strength produced from concrete with lime only (Figure 6). Again, the flexural strength of concrete with bagasse ash performed better than bagasse fibre. The flexural strength obtained for limestone cement replaced by *Costus englerianus* bagasse ash or fibre was within the range reported in previous studies for sugarcane bagasse ash [2, 51, 61–63].

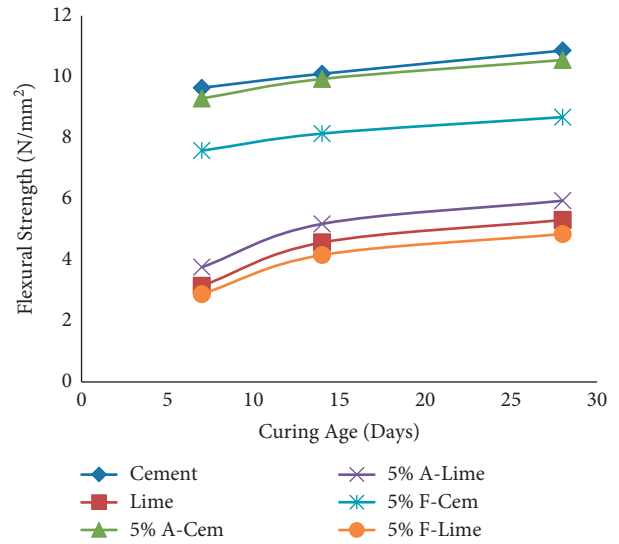


FIGURE 5: Flexural strength of bagasse ash concrete at 5% replacement.

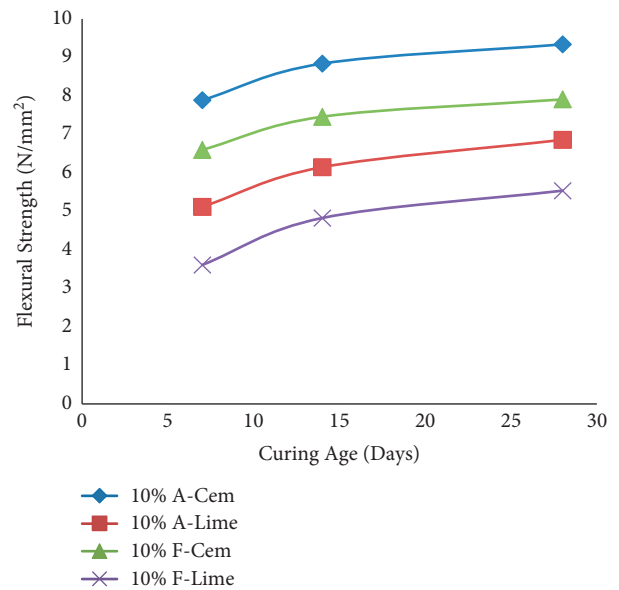


FIGURE 6: Flexural strength of bagasse ash concrete at 10% replacement.

4. Conclusion

The following conclusions were observed from the comparison of the performance of *Costus englerianus* bagasse ash and bagasse fibre as a partial replacement of cement and hydrated lime for the production of concrete suitable for use in the construction industry [63].

- (i) The compressive strengths of concrete were measured by 63.95 MPa, 58.34 MPa, 53.34 MPa, and 50.15 MPa at 5%, 10%, 15%, and 20% of PC replaced with *Costus englerianus* bagasse ash while the compressive strength of concrete was noted by 59.65 MPa, 56.71 MPa, 51.72 MPa, and 47.48 MPa at 5%, 10%, 15%, and 20% of *Costus englerianus*

bagasse fibre as the cementitious material at 28 days, respectively.

- (ii) The compressive strengths of lime concrete were measured by 48.66 MPa, 53.85 MPa, 50.18 MPa, and 45.24 MPa at 5%, 10%, 15%, and 20% of lime replaced with *Costus englerianus* bagasse ash at 28 days, respectively. Besides, the compressive strength of lime concrete was noted by 45.53 MPa, 48.92 MPa, 47.57 MPa, and 43.51 MPa at 5%, 10%, 15%, and 20% of *Costus englerianus* bagasse fibre as the cementitious material at 28 days, respectively.
- (iii) The flexural strengths of concrete were measured by 10.55 MPa and 9.34 MPa at 5% and 10% of PC replaced with *Costus englerianus* bagasse ash while the flexural strength of concrete was noted by 8.68 MPa and 7.91 MPa at 5% and 10% of *Costus englerianus* bagasse fibre as the cementitious material at 28 days, respectively.
- (iv) The flexural strengths of lime concrete were measured by 5.94 MPa and 6.86 MPa at 5% and 10% of lime replaced with *Costus englerianus* bagasse ash at 28 days, respectively. Besides, the flexural strength of lime concrete was noted by 4.85 MPa and 5.54 MPa at 5% and 10% of *Costus englerianus* bagasse fibre as the cementitious material at 28 days, respectively.
- (v) Compressive and flexural strengths of concrete replaced with 5% and 10% bagasse ash and 10% bagasse fibre were higher than the compressive strength obtained from concrete produced with hydrated lime alone. Bagasse ash performed better than bagasse fibre ash as a partial replacement material for concrete production.
- (vi) Based on the compressive flexural strengths results, *Costus englerianus* bagasse ash or bagasse fibre proved to be a promising partial replacement material for cement and hydrated lime in concrete. However, the performance of *Costus englerianus* bagasse ash or bagasse fibre will be enhanced as a partial replacement of cement than hydrated lime. Therefore, it has been recommended that the use of *Costus englerianus* bagasse ash or bagasse fibre up to 10% in the cement concrete or lime concrete provides good results for application in civil engineering.

Data Availability

The datasets produced during the proposed investigation are accessible from the authors upon request.

Conflicts of Interest

The authors declare that they have no conflicts of interest.

References

- [1] H. Klee, *The Cement Sustainability Initiative: Recycling concrete*, World Business Council for Sustainable Development (WBCSD), Geneva, Switzerland, 2009.
- [2] M. N. Amin, M. Ashraf, R. Kumar et al., "Role of sugarcane bagasse ash in developing sustainable engineered cementitious composites," *Frontiers in Materials*, vol. 7, no. 4, pp. 65–76, 2020.
- [3] V. Lesovik, A. Tolstoy, R. Fediuk et al., "Four-component high-strength polymineral binders," *Construction and Building Materials*, vol. 316, Article ID 125934, 2022.
- [4] M. A. Gad, A. M. Riad, E. Nikbakht, M. Ali, and G. M. Ghanem, "Structural behavior of slender reinforced concrete columns wrapped with fiber reinforced polymers subjected to eccentric loads," in *Proceedings of the 2020 Second International Sustainability and Resilience Conference: Technology and Innovation in Building Designs*, pp. 1–5, IEEE, Sakheer, Bahrain, November 2020.
- [5] M. Ali, S. Abbas, A. R. G. de Azevedo et al., "Experimental and analytical investigation on the confinement behavior of low strength concrete under axial compression," *Structures*, vol. 36, pp. 303–313, 2022.
- [6] M. Ali, S. Abbas, M. I. Khan, M. A. Gad, S. Ammad, and A. Khan, "Experimental validation of mander's model for low strength confined concrete under axial compression," in *Proceedings of the 2020 Second International Sustainability and Resilience Conference: Technology and Innovation in Building Designs*, pp. 1–6, IEEE, Sakheer, Bahrain, November 2020.
- [7] V. C. Li, C. Wu, S. Wang, A. Ogawa, and T. Saito, "Interface tailoring for strain-hardening polyvinyl alcohol-engineered cementitious composites (PVA-ECC)," *ACI Materials Journal*, vol. 99, pp. 463–472, 2002.
- [8] V. C. Li, "Tailoring ECC for special attributes: a review," *International Journal of Concrete Structures and Materials*, vol. 6, no. 3, pp. 135–144, 2012.
- [9] S. Room, M. Ali, M. A. Alam, U. Khan, S. Ammad, and S. Saad, "Assessment of lightweight Aggregate concrete using textile washing stone," in *Proceedings of the 2021 Third International Sustainability and Resilience Conference: Climate Change*, pp. 327–333, IEEE, Sakheer, Bahrain, November 2021.
- [10] A. Nafees, M. F. Javed, M. A. Musarat, M. Ali, F. Aslam, and N. I. Vatin, "FE modelling and analysis of beam column joint using reactive powder concrete," *Crystals*, vol. 11, no. 11, 1372 pages, 2021.
- [11] A. N. S. Al Qadi and S. M. Al-Zaidyeen, "Effect of fibre content and specimen shape on residual strength of polypropylene fibre self-compacting concrete exposed to elevated temperatures," *Journal of King Saud University - Engineering Sciences*, vol. 26, no. 1, pp. 33–39, 2014.
- [12] E. D. S. Barreto, K. V. Stafanato, M. T. Marvila et al., "Clay ceramic waste as pozzolan constituent in cement for structural concrete," *Materials*, vol. 14, no. 11, 2917 pages, 2021.
- [13] C. T. G. Awodiji, "Experimental study on the elastic properties of lime-cement concrete," *International Journal of Engineering Science*, vol. 9, no. 1, pp. 79–85, 2020.
- [14] C. T. G. Awodiji, O. O. Awodiji, and D. O. Onwuka, "Re-Investigation of the compressive strength of ordinary Portland cement concrete and lime concrete," *International Journal of Geology, Agriculture and Environmental Sciences*, vol. 4, no. 1, pp. 12–15, 2016.
- [15] P. O. Awoyera and I. I. Akinwumi, "Compressive strength development for cement, lime and termite-hill stabilised lateritic bricks," *International Journal of Engineering Science*, vol. 3, no. 2, pp. 37–43, 2014.
- [16] Z. Ying, Y. J. Cui, N. Benahmed, and M. Duc, "Changes of small strain shear modulus and microstructure for a lime-treated silt subjected to wetting-drying cycles," *Engineering Geology*, vol. 293, Article ID 106334, 2021.

- [17] X. Bian, L. Zeng, X. Li, X. Shi, S. Zhou, and F. Li, "Fabric changes induced by super-absorbent polymer on cement-lime stabilized excavated clayey soil," *Journal of Rock Mechanics and Geotechnical Engineering*, vol. 13, no. 5, pp. 1124–1135, 2021.
- [18] M. M. Salman and A. A. Muttar, "The mechanical properties of lime concrete," *Journal of Engineering and Sustainable Development*, vol. 21, no. 2, pp. 180–190, 2017.
- [19] P. Brzyski, "The effect of pozzolan addition on the physical and mechanical properties of lime mortar," *E3S Web of Conferences*, vol. 49, Article ID 00009, 2018.
- [20] A. R. de Azevedo, M. T. Marvila, M. Ali, M. I. Khan, F. Masood, and C. M. F. Vieira, "Effect of the addition and processing of glass polishing waste on the durability of geopolymeric mortars," *Case Studies in Construction Materials*, vol. 15, Article ID e00662, 2021.
- [21] M. Imran Khan, M. H. Sutanto, M. B. Napiyah et al., "Investigating the mechanical properties and fuel spillage resistance of semi-flexible pavement surfacing containing irradiated waste PET based grouts," *Construction and Building Materials*, vol. 304, Article ID 124641, 2021.
- [22] A. M. Memon, M. H. Sutanto, M. Napiyah et al., "Physico-chemical, rheological and morphological properties of bitumen incorporating petroleum sludge," *Construction and Building Materials*, vol. 297, Article ID 123738, 2021.
- [23] S. W. M. Supit and F. U. A. Shaikh, "Durability properties of high volume fly ash concrete containing nano-silica," *Materials and Structures*, vol. 48, no. 8, pp. 2431–2445, 2015.
- [24] N. Bheel, S. A. Abbasi, P. Awoyera et al., "Fresh and hardened properties of concrete incorporating binary blend of metakaolin and ground granulated blast furnace slag as supplementary cementitious material," *Advances in Civil Engineering*, vol. 2020, pp. 1–8, 2020.
- [25] M. A. Keerio, A. Saand, R. Chaudhry, N. Bheel, and N. ul Karim Bhatti, "The Effect of Local Metakaolin Developed from Natural Material Soorh on Selected Properties of concrete/mortar," *Silicon*, vol. 14, no. 4, pp. 1807–1816, 2021.
- [26] A. Kumar, N. Bheel, I. Ahmed, S. H. Rizvi, R. Kumar, and A. A. Jhatial, "Effect of silica fume and fly ash as cementitious material on hardened properties and embodied carbon of roller compacted concrete," *Environmental Science and Pollution Research*, vol. 29, no. 1, pp. 1210–1222, 2022.
- [27] N. Bheel, P. Awoyera, T. Tafsirojjaman, N. Hamah Sor, and S. sohu, "Synergic effect of metakaolin and groundnut shell ash on the behavior of fly ash-based self-compacting geopolymer concrete," *Construction and Building Materials*, vol. 311, Article ID 125327, 2021.
- [28] N. Bheel, P. O. Awoyera, and O. B. Olalusi, "Engineering properties of concrete with a ternary blend of fly ash, wheat straw ash, and maize cob ash," *International Journal of Engineering Research in Africa*, vol. 54, pp. 43–55, 2021.
- [29] N. Bheel, M. O. A. Ali, Y. Liu et al., "Utilization of corn cob ash as fine aggregate and ground granulated blast furnace slag as cementitious material in concrete," *Buildings*, vol. 11, no. 9, 422 pages, 2021.
- [30] S. H. Channa, S. A. Mangi, N. Bheel, F. A. Soomro, and S. H. Khahro, "Short-term analysis on the combined use of sugarcane bagasse ash and rice husk ash as supplementary cementitious material in concrete production," *Environmental Science and Pollution Research*, vol. 29, no. 3, pp. 3555–3564, 2022.
- [31] M. A. Keerio, S. A. Abbasi, A. Kumar, N. Bheel, and K. U. Rehaman, "Effect of Silica Fume as Cementitious Material and Waste Glass as fine Aggregate Replacement Constituent on Selected Properties of concrete," *Silicon*, vol. 14, pp. 165–176, 2020.
- [32] F. Ma, A. Sha, P. Yang, and Y. Huang, "The greenhouse gas emission from Portland cement concrete pavement construction in China," *International Journal of Environmental Research and Public Health*, vol. 13, no. 7, 632 pages, 2016.
- [33] L. Hanle, "Understanding CO2 emissions," *World Cement*, vol. 37, no. 4, 2006.
- [34] M. V. Madurwar, R. V. Ralegaonkar, and S. A. Mandavgane, "Application of agro-waste for sustainable construction materials: a review," *Construction and Building Materials*, vol. 38, pp. 872–878, 2013.
- [35] A. Nafees, M. N. Amin, K. Khan et al., "Modeling of mechanical properties of silica fume-based green concrete using machine learning techniques," *Polymers*, vol. 14, no. 1, 30 pages, 2021.
- [36] S. Rukzon and P. Chindaprasirt, "Utilization of bagasse ash in high strength concrete," *Materials & Design*, vol. 34, pp. 45–50, 2012.
- [37] R. Somna, C. Jaturapitakkul, P. Rattanachu, and W. Chalee, "Effect of ground bagasse ash on mechanical and durability properties of recycled aggregate concrete," *Materials and Design*, vol. 36, pp. 597–603, 2012.
- [38] A. Akkarapongtrakul, P. Julphunthong, and T. Nochaiya, "Setting time and microstructure of Portland cement-bottom ash-sugarcane bagasse ash pastes," *Monatshefte für Chemie - Chemical Monthly*, vol. 148, no. 7, pp. 1355–1362, 2017.
- [39] T. Malyadri and J. Supriya, "Experimental study on bagasse ash in concrete by partially replacement with cement," *Int. J. of Comput. Eng. Res. Tre.* vol. 2, pp. 995–1001, 2015.
- [40] S. A. Mangi, N. Jamaluddin, M. H. Wan Ibrahim et al., "Utilization of sugarcane bagasse ash in concrete as partial replacement of cement," *IOP Conference Series: Materials Science and Engineering*, vol. 271, Article ID 012001, 2017.
- [41] U. R. Kawade, V. R. Rathi, and V. D. Girge, "Effect of use of bagasse ash on strength of concrete," *International Journal of Innovative Research in Science, Engineering and Technology*, vol. 2, no. 7, pp. 2997–3000, 2013.
- [42] N. Shafiq, A. A. E. Hussein, M. F. Nuruddin, and H. AlMatarneh, "Effects of sugarcane bagasse ash on the properties of concrete," *Proceedings of the Institution of Civil Engineers - Engineering Sustainability*, vol. 171, no. 3, pp. 123–132, 2018.
- [43] J. E. Edeh, M. Joel, and A. Abubakar, "Sugarcane bagasse ash stabilization of reclaimed asphalt pavement as highway material," *International Journal of Pavement Engineering*, vol. 20, no. 12, pp. 1385–1391, 2018.
- [44] E. Bachtiar, I. Darwan, A. Marzuk, A. M. Setiawan, A. I. Yunus, and S. Gusty, "Potency of sugarcane bagasse ash partial substitution of cement in concrete," *Adv. Eng. Res.* vol. 165, pp. 27–31, 2019.
- [45] A. Dhengare, S. Amrodita, M. Shelote et al., "Utilisation of sugarcane bagasse ash as supplementary cementitious material in concrete and mortar – a review," *International Journal of Civil Engineering & Technology*, vol. 15, no. 6, pp. 94–106, 2015.
- [46] S. Srivastava, P. K. Shukla, K. Kumar, and P. Kumar, "Studies on partial replacement of cement by bagasse ash in concrete," *International Journal for Innovative Research in Science & Technology*, vol. 2, pp. 43–45, 2015.
- [47] P. D. Prasanna, B. S. Maneeth, B. Bhushan, and R. S. Gurav, "Experimental investigation on partial replacement of cement by sugar cane bagasse ash in cement concrete," *Int. J. Adv. Sci. Res. Dev.* vol. 3, pp. 550–554, 2016.

- [48] N. Nagpal and A. K. Saxena, "Effect of partial replacement of cement by SCBA on workability of concrete," *International Journal of Scientific Research*, vol. 4, pp. 19–23, 2015.
- [49] Q. Xu, T. Ji, S. J. Gao, Z. Yang, and N. Wu, "Characteristics and Applications of sugar cane bagasse ash waste in cementitious materials," *Materials*, vol. 12, no. 1, pp. 39–57, 2018.
- [50] R. Seyoum, B. B. Tesfamariam, D. M. Andoshe, A. Algahtani, G. M. S. Ahmed, and V. Tirth, "Investigation on control burned of bagasse ash on the properties of bagasse ash-blended mortars," *Materials*, vol. 14, no. 17, pp. 4991–5002, 2021.
- [51] P. G. Quedou, E. Wirquin, and C. Bokhoree, "Sustainable concrete: potency of sugarcane bagasse ash as a cementitious material in the construction industry," *Case Studies in Construction Materials*, vol. 14, no. 4, Article ID e00545, 2021.
- [52] A. K. Jha, A. Bariya, T. Panwar, G. Krishnatre, and S. Sharma, "Preliminary investigations on the partial replacement of cement with sugarcane bagasse ash," *Int. J. Creat. Res. Thou.* vol. 6, pp. 737–740, 2018.
- [53] R. Lathamaheswari, V. Kalaiyarasan, and G. Mohankumar, "Study on bagasse ash as partial replacement of cement in concrete," *International Journal of Engineering Research and Development*, vol. 13, pp. 1–6, 2017.
- [54] P. G. Quedou, H. Hoolaus, and Y. Ramdhony, "Experimental study of sugarcane bagasse ash as a supplementary cementitious material in concrete," *Int. J. Enhan. Res. Sci. Technol. Eng.* vol. 7, pp. 12–17, 2018.
- [55] P. V. Rambabu, K. D. Gupta, and G. V. Ramarao, "Sugarcane bagasse ash as a pozzolana," *International Journal of Engineering and Applied Sciences*, vol. 3, pp. 21–25, 2016.
- [56] B. S. En 12350-3, *Testing Hardened concrete: Compressive Strength of Test Specimens*, BSI, London, USA, 2009.
- [57] B. S. En 12390-5, *Testing Hardened concrete: Flexural Strength of Test Specimens*, BSI. British Standard Institute, London, USA, 2009.
- [58] A. C. Velosa and B. Paulo, "Hydraulic-lime based Concrete: strength development using a pozzolanic addition and different Curing condition," *Construction and Building Materials*, vol. 23, pp. 2111–2119, 2017.
- [59] P. Mishra and R. C. Singh, "Effect of super plasticizer for improvement of concrete strength: a review," *International Journal of Advanced Research and Innovative Ideas in Education*, vol. 4, no. 2, pp. 321–324, 2018.
- [60] W. Xun, C. Wu, X. Leng, J. Li, D. Xin, and Y. Li, "Effect of functional superplasticizers on concrete strength and pore structure," *Applied Sciences*, vol. 10, pp. 3496–3511, 2020.
- [61] I. Akijje, "Characteristic and effects of a superplasticizer quantity variation in some concrete strengths optimization," *Nigerian Journal of Technology*, vol. 38, no. 1, pp. 81–92, 2019.
- [62] N. Bheel, A. S. Memon, I. A. Khaskheli, N. M. Talpur, S. M. Talpur, and M. A. Khanzada, "Effect of sugarcane bagasse ash and lime stone fines on the mechanical properties of concrete," *Engineering, Technology & Applied Science Research*, vol. 10, no. 2, pp. 5534–5537, 2020.
- [63] N. Bheel, S. Khoso, M. H. Baloch, O. Benjeddou, and M. Alwetaishi, "Use of waste recycling coal bottom ash and sugarcane bagasse ash as cement and sand replacement material to produce sustainable concrete," *Environmental Science and Pollution Research*, pp. 1–13, 2022.

Research Article

An Experimental Study on the Strength and Crack Healing Performance of *E. coli* Bacteria-Induced Microbial Concrete

Md. Mahfuzul Islam, Nusrat Hoque , Moinul Islam , and Imteaz Ibney Gias

Department of Civil Engineering, CUET, Chattogram 4349, Bangladesh

Correspondence should be addressed to Nusrat Hoque; nusrat_hoque@cuet.ac.bd

Received 18 January 2022; Revised 6 March 2022; Accepted 29 March 2022; Published 15 April 2022

Academic Editor: Qian Chen

Copyright © 2022 Md. Mahfuzul Islam et al. This is an open access article distributed under the Creative Commons Attribution License, which permits unrestricted use, distribution, and reproduction in any medium, provided the original work is properly cited.

The most commonly used building material in the construction industry is concrete. However, the weak features of concrete are its low ductility and limited tension capacity and hence crack development with the increase in load. These cracks get more worsened by the intrusion of water and salt present in the composition and hence causing deterioration and reducing the longevity of the material. This study focuses on an innovative approach to mitigate concrete's fractures and flaws by utilizing microbiologically induced calcite (CaCO_3) precipitation (MICP) excited by *Escherichia coli* (*E. coli*) bacteria to improve the performance of cementitious building materials. The study investigated the development of microbiological concrete in plain water using only one culture density ($\text{OD}_{600} 0.5 \pm 0.1$). In this study, two water-to-bacterial mix ratios (75 : 25 and 50 : 50) were used and compared to the conventional concrete (100 : 0). 100-mm cube-sized specimens cured for a period of 7, 28, 90, and 365 days were tested for compressive strength, water absorption capacity, ultrasonic pulse velocity (UPV), and SEM analysis, which were performed on the samples at regular intervals. According to the results of these experiments, microbial concrete with the 50 : 50 ratio exhibited the highest strength for all curing times. From the water absorption test of samples, it is found that the absorption of the materials got reduced due to the infusion of microorganisms in concrete. On the other hand, the UPV test showed high velocity than the control samples for specimens with an $\text{OD}_{600} 0.5 \pm 0.1$. Scanning electron microscope (SEM) analysis performed on distinct concrete groups at the age of 28 days showed fewer voids in the concrete lumps due to the increase in water substitution rate caused by microbial culture.

1. Introduction

Concrete is recyclable, and it is a widely accepted and universally used construction material. It is a durable, strong, locally available, versatile, and has superb resistance to compressive loads until a limit. However, the cracking load in concrete is lower than the failure load [1], and it is acceptable until a certain limit [2]. The reinforcement is used in concrete to transmit the strength, and if the crack is present, it causes corrosion [3,4]. In practice, cracks in concrete also reduce the durability, permeability, and strength of the concrete. In the extreme winter situation, the situation also gets deteriorated as water seeps through these cracks and freezes, and causes a widening of gaps [3]. It is always necessary to repair those cracks because tiny little

cracks can lead to massive-sized shots and shorten the concrete's serviceability limit. Fixing problems can be complicated if damage occurs in places, which is difficult to reach. For repairing cracks in concrete, several traditional repairing systems are introduced, but they are very costly and not naturally available.

Self-healing concrete is a new type of concrete that has the ability to repair its cracks automatically. It is like healing of body wounds by secretion of some sort of body fluid. Among various methods of self-healing, the most common methods are biological self-healing, natural self-healing, and chemical self-healing process. Biological self-healing can be achieved by adding bacteria to the concrete. In self-healing concrete, bacteria are used along with calcium nutrients known as calcium lactate. This product is then added while

preparing the concrete mix in wet condition. These induced bacteria can be in inactive stages for up to 200 years and become active as soon as it comes in contact with water seeping through the cracks in concrete. This initiates the germination of bacterial spores, which feeds on the calcium lactate consuming oxygen. This process transforms the soluble calcium lactate into insoluble limestone. When this limestone gets hardened, the crack is being filled up [4]. This method of adding bacteria to concrete is known as direct method and is the most common method of preparing self-healing concrete. This is the easiest and cheaper method compared to other methods, namely, encapsulation method, although the cost of self-healing concrete is usually high; however, concrete with self-healing mechanisms can minimize costing by eradicating the need for either costly repair of concrete or new concrete and increase the structure's durability. Various physical and chemical treatments have been experimented so far to protect the concrete from damage, but very few of them proved to be fully compatible in terms of nonreversible action and sustainability. Therefore, the use of biological techniques could be focused on [5]. Microbiologically induced calcite precipitation (MICP) is a method that could be adopted to solve the cracking problem, which can help to get long-lasting and eco-friendly concrete [6].

Figure 1 shows the actual imagery with a different interval of the crack healing process, which shows a gradual reduction of crack width with the time (0 day, 1 week, 2 weeks, etc.) reported by Wang et al. [7]. The crack had nearly healed fully by 3 weeks. Cracks up to 1 mm width can be independently screened, depending on the dose of bacteria and lactate-based nutrients. The autonomous waterproofing of 0.4-mm large cracks is sufficient for a dose of 15 kg/m^3 of the auto-healing agent per m^3 of the concrete mix (Figure 2).

Self-healing concrete can be illustrated as concrete, which has the capability of repairing itself back to the original state. It is a green technology that embeds self-activating bacteria into concrete and fixes its cracks. Since the material used for this technique can be grown in the laboratory, it does not pose a risk to natural resources. Hence, this method can be an effective technology for the improvement of the strength of concrete [9].

Bacterial impacts on the crack and self-healing treatment offer cleaner, more sustainable, longer-lasting material and reduce the cost of repairing the cracks in long term. By reducing absorption, permeability, and diffusion as the key mechanisms for carrying concrete, the durability of concrete can be increased [10]. Several studies have documented the effect of bio-based healing agents on the permeability and water absorption of concrete. Cracks in concrete structures can be reduced by the presence of bacteria as can be seen from previous literature as described later. Sarker et al. [11] used *E. coli* bacterial strain on concrete mix and suggested from the mortar test that it enhances concrete strength and the cement quantity can be reduced by using microbes without compromising the strength.

Safiuddin et al. [12] studied the effect of mixing *Bacillus subtilis* and *Escherichia coli* on the time required for crack

the mitigation and mechanical properties of concrete by mixing them with a percentage by weight of cement. The result shows that 3% *Bacillus subtilis* is the optimum dosage for self-healing of concrete, whereas *Escherichia coli* mixed at the dose of 3% by weight of cement can increase the strength up to 60%.

The application of microbial concrete has been a research issue since long [13–15]. Xu et al. [16] used porous ceramsite particles as microbial carrier applying heat treatment and NaOH soaking and found that heat treatment can improve the loading content of ceramsite without reducing the concrete strength.

Zhang et al. [17] studied the concrete crack healing capacity using two microbial consortia under anaerobic (MC-Aa) and anoxic (MC-Ao) conditions and neurolytic pure-culture bacteria (*Bacillus cohnii*). Feng et al. [18] performed 3-point bending test by forming 0.3 mm width cracks on the beam bottom and found that the microcracks were healed by calcite precipitation due to the bacterial metabolic activity. Mondal and Ghosh [19] studied different levels of bacterial concentration of *Bacillus subtilis* and concluded that as the bacterial dose increases, crack healing also improved. Algiafi et al. [20] studied the factors influencing urea hydrolysis and bacterial growth so that the calcium carbonate precipitation inside concrete fissures can be modeled exactly. The authors also concluded that self-healing bacteria can be a future sustainable strategy to extend concrete life span. Vijay and Murmu [21] studied the effect of *Bacillus subtilis* strain bacterial concrete on the addition of calcium lactate. Nirala et al. [22] used *Escherichia coli* bacteria with 5%, 10%, and 15% by mass and observed a healing of fissures and improvement in compressive and tensile strength at the curing period of 7 days. Sumathi et al. [23] achieved a notable amount of healing in cracks at the age of 1 month using *Bacillus subtilis* bacteria. On the contrary, Balam et al. [24] achieved about 90 percent of surface healing at the age of 28 days using *Bacillus cohnii* culture by at the rate of 105 cells/mL. Vahabi et al. [25] used higher grade concrete with *Bacillus subtilis* bacteria with a concentration of 10 ml, 20 ml, and 30 ml and observed healing properties of concrete. Xu et al. [26] used *Sporosarcina pasteurii* at the concentration of 105 cells/ml and showed that the water absorption is reduced by four times when *S. pasteurii* is present. Bacterial calcite deposition resulted in a roughly eightfold reduction in chloride permeability, extending the life of concrete. Xu et al. [27] studied the effect of crack healing potential of reinforced concrete incorporated with ureolytic microbial self-healing agents immobilized in porous ceramsite particles and found that bacteria can heal up to $450 \mu\text{m}$ cracks within 120 days.

In microbially induced calcium carbonate precipitation (MICCP) or microbiologically induced calcite precipitation (MICP) via urea hydrolysis, substantial amounts of carbonates are produced rapidly through ureolytic microbes. Urea hydrolysis via the enzyme urease inside a calcium-rich atmosphere is investigated commonly because of its simplicity.

The decomposition of urea into carbonate and ammonium is amplified by the microbial enzyme going through

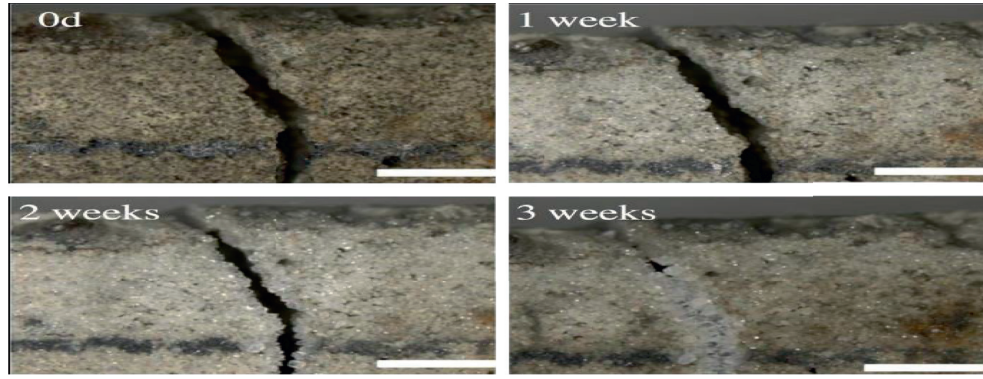


FIGURE 1: Phase of crack healing with respect to time [7].

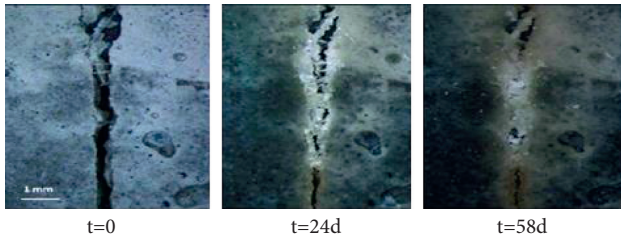
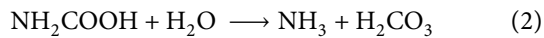


FIGURE 2: Self-healing of a 0.8 mm wide crack in concrete [8].

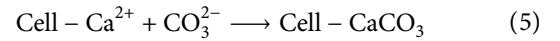
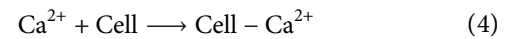
the chemical process as in equations (1) and (2). It is obvious from the chemical reaction that one mole of urea is hydrolyzed intracellularly to produce one mole of ammonia and one mole of carbamate, which then hydrolyzes naturally to generate one mole of ammonia and carbonic acid.



When it comes in contact with water, the pH levels increase as these molecules then split into bicarbonate and hydroxide ions:



The series of events occurring during this ureolytic calcification was observed by Hammes and Verstraete [28] and emphasized more on the role of pH and calcium metabolism. Various physiological processes [28] create an alkaline atmosphere by the stimulation of the bacteria. Figure 3 depicts the series of events occurring throughout microbially induced carbonate precipitation (MICP). Positively charged cations (e.g., Ca^{2+} and Mg^{2+}) get adsorbed upon the cell surface due to the nucleating area created by the heterogeneous electronegativity loaded bacterial cell membrane. Neutral pH environments facilitate the presence of various anionic (negative charge) groups, and these anionic charges get dominant over the bacterial cell surface resulting in the secretion of divalent cations (positively charged) on interaction. As shown by Eqs 4-5, the bacterial cell membrane plays a vital role in the CaCO_3 precipitation like a nucleation site.



The microbes serve as a nucleation site, assisting in the formation of calcite that can gradually seal cracks and pores throughout concrete, improving its durability. This microbially induced calcite precipitation (MICP) is the product of a complicated sequence of biological processes. This process leads to the formation of CaCO_3 crystal form, which expands and develops as the bacteria produce calcium lactate nutrition. The crystal formation grows until the entire void is filled. Hence, this natural and biochemical method increases the sustainability of concrete.

However, the subject of bacterial precipitation is still dubious. Several researchers argue that precipitation is indeed the by-product of metabolism that happened accidentally. Wherever others consider, this is a distinct environmental phenomenon that can be beneficial for humans [29, 30].

Nevertheless, based on the past studies as summarized earlier, the current study presents the crushing of concrete with the results obtained from UPV and water absorption test including SEM analysis for *E. coli* microbial culture ratio mixed with water in comparison with normal water. In direct application method of bacteria, bacterial spores and calcium lactate are added into concrete directly when mixing of cement is completed. The utilization of these microorganisms and calcium lactate does not change the typical properties of cement. At the point when water interacts with these microscopic organisms, they develop and feed on calcium lactate and deliver limestone. Consequently, the cracks are fixed. But in the case of an encapsulation method, bacterial spores are added with encapsulated nutrients in a concrete matrix. Hence, direct application method is chosen for this study for its easiness in use.

On the other hand, *Escherichia coli*, otherwise called *E. coli*, is a micrometer Gram-negative, non-spore-forming bacteria that are ordinarily found in the lower digestive tract of warm-blooded life forms. The primary benefit of inserting *E. coli* bacteria in concrete is that it continually hastens CaCO_3 . Positive increments in compressive strength test results due to the addition of *E. coli* in concrete were also

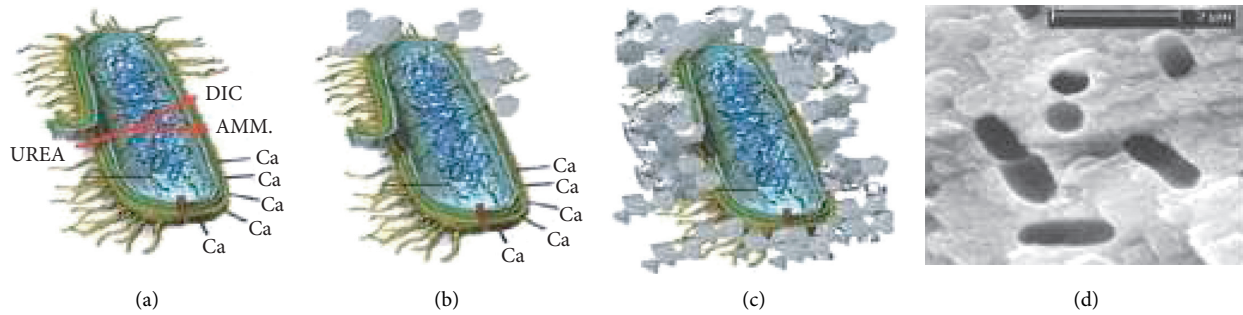


FIGURE 3: Key roles of pH and calcium metabolism in microbial carbonate precipitation [16].

reported by past researchers including Vijay et al. [3]. Hence, *E. coli* bacteria are used in this study and two arbitrary ratios (75 : 25 and 50 : 50) of plain water to microbial culture were chosen to find out the effectiveness of *E. coli* bacteria in concrete. The study aims to see the effect of bacterial injection in concrete to improve cracks and to maintain good compressive strength.

2. Materials

Ordinary Portland cement (OPC) ASTM type 1 complying with ASTM C-150 has been chosen as the cementitious material in the experimental work. Locally available natural sand passing through 4.75-mm sieve and retaining on 0.075-mm sieve has been used as a fine aggregate, and crushed stone with a nominal size of 12.5 mm has been chosen as a coarse aggregate in this experiment.

This study uses *Escherichia coli* (*E. coli*) bacteria that feed on carbon dioxide instead of traditional feed like sugar and other organic matter. *E. coli* is a well-known bacterium which has many other uses in the real world like synthesizing useful chemicals such as insulin, creating synthetic forms of human growth hormone. This bacterium can intrude into concrete cracks and can remain dormant for many years even at high temperatures. It is a nontoxic bacterium that reproduces quickly by splitting method, according to research. Therefore, one of the advantages of this bacterium is its easy culture within a short time. Plain water with a pH value of 7 and zero turbidity was used for the study. Sylhet sand with an absorption capacity of 2.78% and specific gravity of 2.51 is used as fine aggregates, whereas locally available stones with a specific gravity of 2.74 and absorption capacity of 2.33% are used as coarse aggregates.

3. Experimental Procedure

3.1. Preparation of Bacterial Culture. *Escherichia coli* bacteria had been used in this experiment, which was collected from the Microbiology Department of another local university. The media used was nutrient broth, which was made from peptone, beef extract, and a slight amount of NaCl. All composition materials were taken in a 300 ml conical flask in proper quantity and then mixed with water and stirred slowly for the preparation of nutrient broth. To make the media germ free, the media was sterilized for

exactly two hours in sterilization autoclaves. *Escherichia coli* spores were then injected into the prepared media by using a needle. The spore-injected media was then settled in the refrigerator by maintaining an ambient temperature. This process allows the bacteria to germinate in a binary fission manner. The growth period of bacteria and germination time helps to determine the bacterial concentration.

The next stage was to investigate different bacterial groups. However, before those steps, the properties of these prepared samples had been determined. Optical density (OD) measurement of bacterial cultures is a common technique used in microbiology. Spectrophotometers are used typically to measure the optical density, which actually measures how much light is scattered by the culture. Previous literature indicated that the concrete with a bacterial culture having an optical density of OD₆₀₀ 0.5 ± 0.1 yields better strength [31]. Based on those studies, this research work used an OD value of 600 0.5 ± 0.1 .

Generally, in spectrophotometer, the wavelength can be set from 420 to 660 nm. In this study, a wavelength of 600 nm has been set to track the growth of *E. coli*. It is crucial that the cells are in an excellently physiological process of growth. The estimated relationship between absorbance and colony-forming units (CFU) (the number of viable bacteria within a sample) may differ as the cell size differs with growth phase (lag, log, and stationary). The concentration of cells differs from the optical density and was therefore estimated using the following relation:

$$Y = 8.59E10^7 X^{1.362}, \quad (6)$$

where X is reading at optical density 600 nm, and Y is cell concentration per ml.

Figure 4 represents the whole procedure related to preparation of the bacterial culture.

3.2. Concrete Specimen Preparation. Cube samples of size 100 mm \times 100 mm \times 100 mm were made following ASTM standard procedure using the mix proportions as obtained from the proper mix design. Mix design was performed for two strength requirements: 25 MPa and 35 MPa. Cement: fine aggregate: coarse aggregate ratios for the two-strength category are 1 : 2.091 : 2.276 and 1 : 1.43 : 1.8 with water cement ratios of 0.5 and 0.395, respectively. Bacterial culture media containing the required number of microorganisms

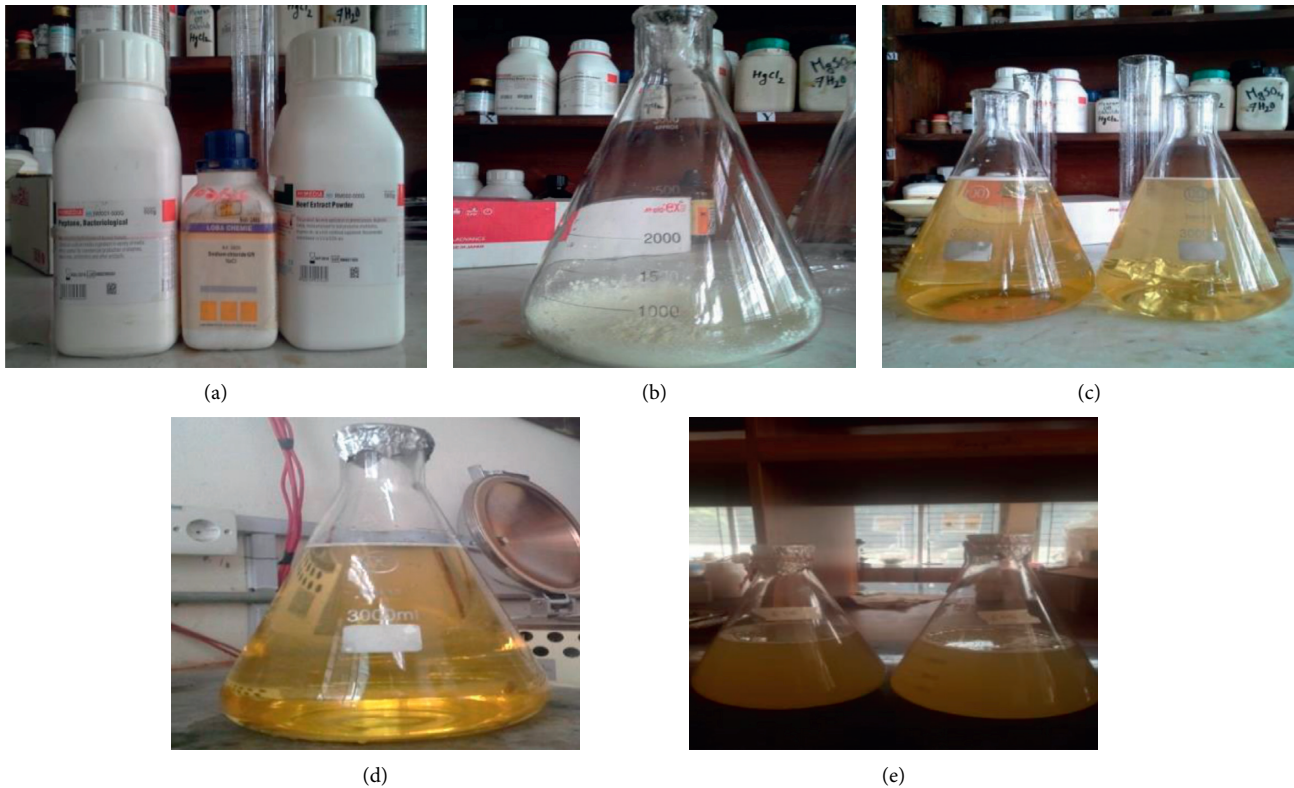


FIGURE 4: Preparation of the bacterial culture. (a) Materials. (b) Materials poured into flask for Luria-Bertani media. (c) Preparation of media for sterilization. (d) Media kept in refrigerator for germination. (e) Prepared bacterial solution.

mixed with water were used as the liquid substance. Two water: microbial culture ratios were 75 : 25 (75% of water and 25% of microbial culture) and 50 : 50 (50% of water and 50% of microbial culture). Prepared concrete is poured into mold for casting and removed from the mold after 24 hours. After preparing the samples, they were cured in plain water for various time spans.

3.3. Concrete Strength Using Ultrasonic Pulse Velocity (UPV) Measurement. The interior quality of concrete samples can be assessed using the UPV test. High velocity indicates strong concrete consistency, which can be attributed to density, uniformity, homogeneity, and other factors. On cube specimens, the UPV test was performed by putting a pulse transmitter on one side of the cube and a receiver on the other. Conventional relation between speed, distance, and time as shown below is used to compute the ultrasonic pulse velocity

$$UPV = \frac{L}{T}, \quad (7)$$

where L is distance between transducers, and T is transit time.

3.4. Absorption of Water by Immersion Method. Water absorption tests of concrete samples were measured using ASTM C1585 and ASTM C642 method.

$$\text{water absorption in percentage} = \left[\frac{(W_1 - W_2)}{W_2} \right] * 100, \quad (8)$$

where W_1 is SSD weight of the sample, and W_2 is oven-dry weight.

3.5. Analysis Using Scanning Electron Microscopy (SEM). SEM analyses were performed to observe and analyze the microstructural changes between conventional concrete and *E. coli* generated concrete. Powdered samples were taken from the core of each sample for SEM examination. The SEM analysis was carried out according to the guideline. The interfacial transition zone (ITZ) was utilized in SEM research to observe bacterial mineral formation, which creates a filler effect in the concrete mixture.

4. Results and Discussion

4.1. Compressive Strength Test Result. Compressive strength results of various concrete mixes at different curing ages are presented in Figure 5(a).

The compressive strength test results at various ages show the trend as expected where compressive strength increases with ages. This strength gain may be attributed to the formation of more hydration products as the time progresses, which improves the bonding between the particles. But the rate of strength gain is not same for all

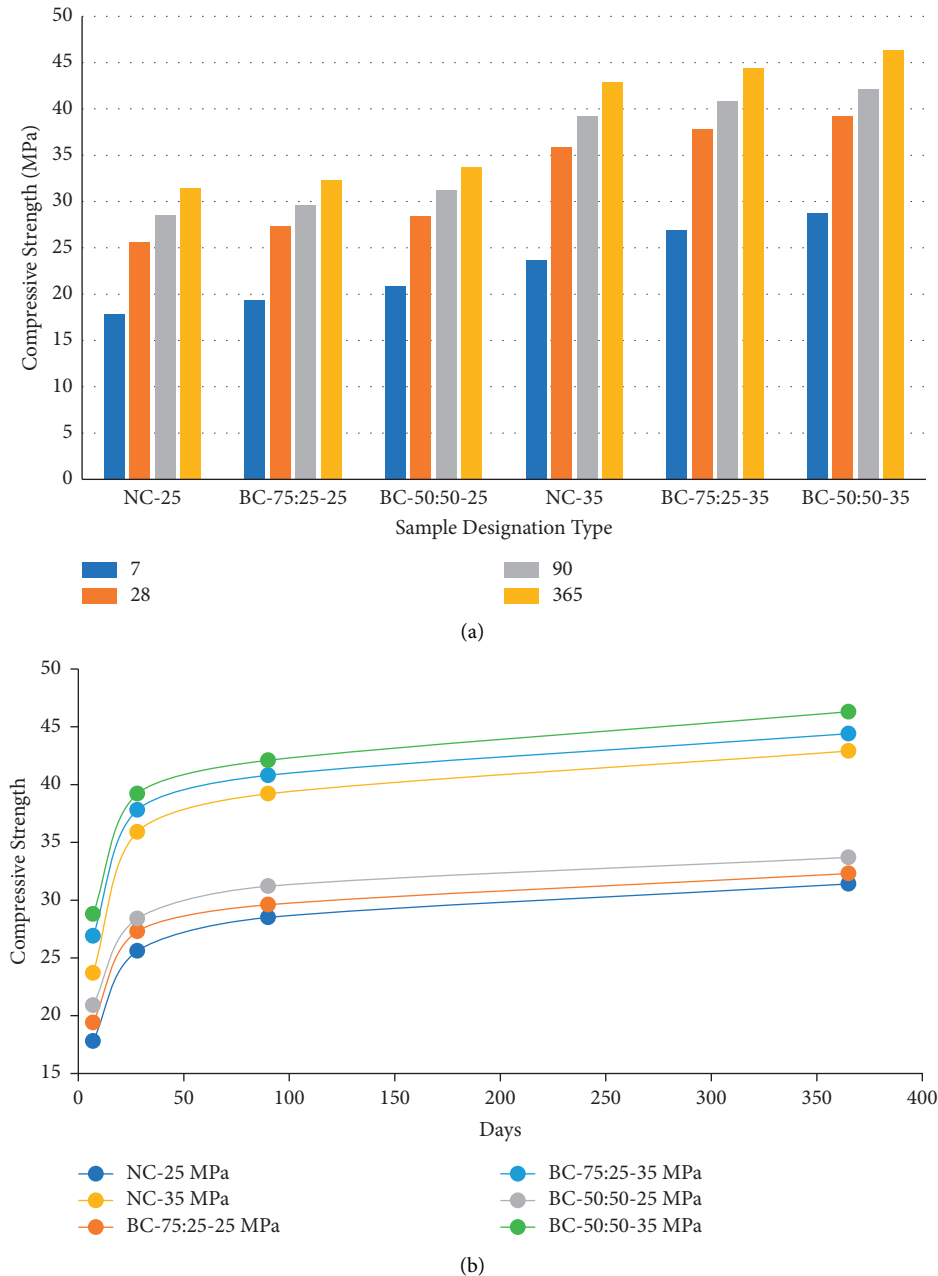


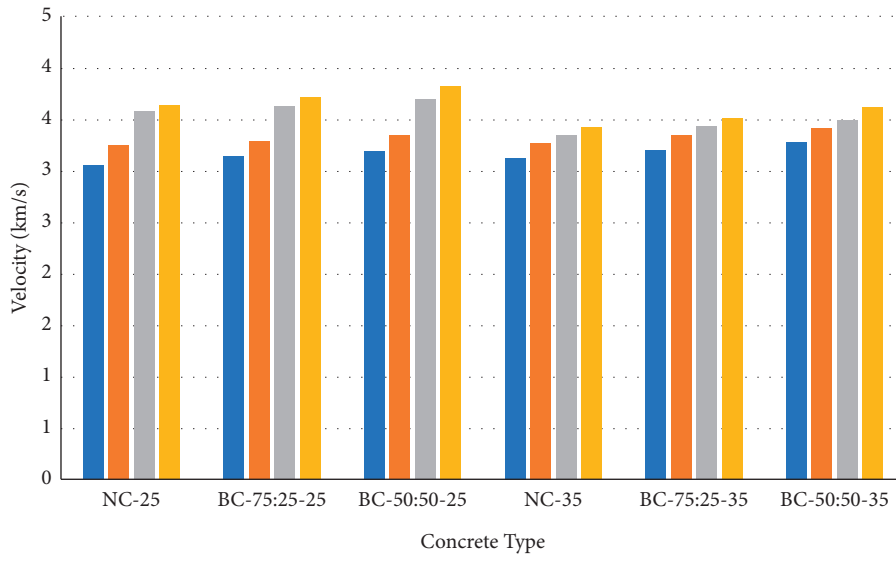
FIGURE 5: Variation of compressive strength for various concrete under increasing curing period.

specimens and variation is obvious since the design and material proportions are not same.

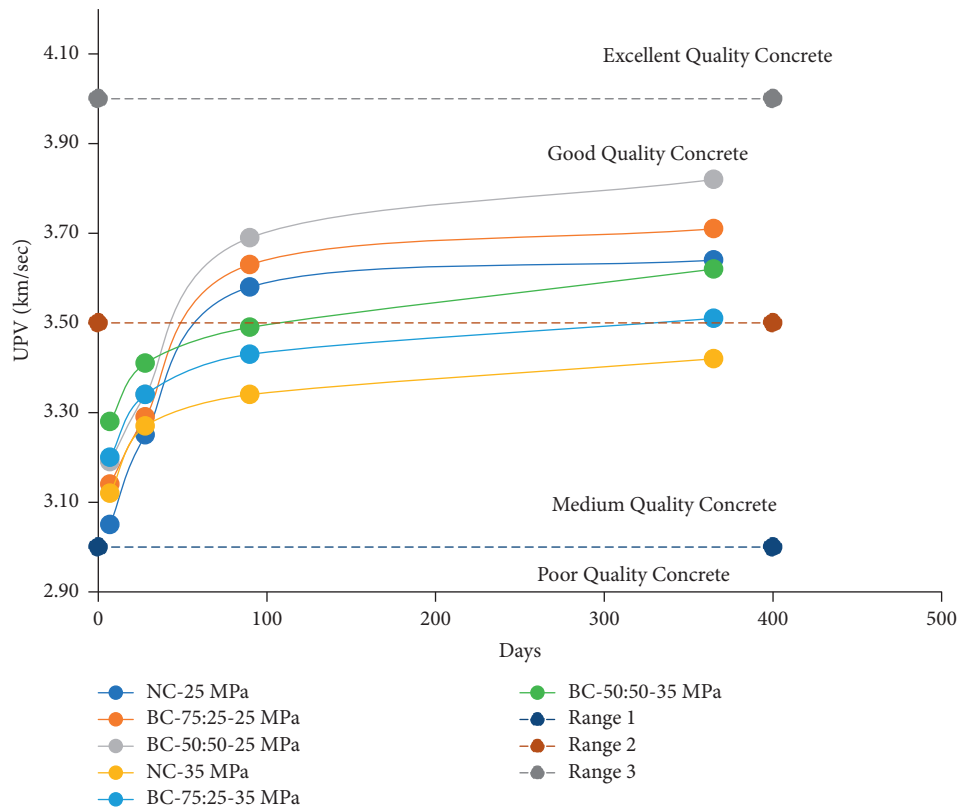
As obvious from the plot in Figure 5(b), the highest strength gain is observed in between 7 and 28 days. Subsequently, the strength increment becomes gradual. The graph also implies that the strength of 25 MPa concrete increases more than the 35 MPa concrete. However, when the concrete samples were cured for 90 or 365 days of curing, the strength of 35 MPa concrete increases more than the 25 MPa concrete. For 35 MPa grade, the compressive strength increases up to 21.5% for *Escherichia coli* (50% bacterial culture). On the other hand, the strength increase is higher for water: bacterial media ratio of 50:50 than water: bacterial media ratio of 75:25 concrete.

However, in all cases, the strength of bacterial concrete is higher than normal concrete, which most probably is the result of the filling of the pores inside the concrete matrix by the precipitation of calcite due to the bacterial injection.

4.2. Ultrasonic Pulse Velocity Test. Figure 6(a) shows UPV results on different curing ages for designed concrete strength of 25 MPa and 35 MPa. Similar to compressive strength, UPV values of all specimens rise with increase in age irrespective of the bacterial doses. As such, the average gain in UPV values at 365 days curing corresponding to its value at 28 days varies from 6.15 to 16.21%



(a)



(b)

FIGURE 6: Variation of UPV test results and curing periods for 25 MPa concrete and 35 MPa concrete.

for control specimen. In bacterial concrete, the long-term UPV improvement varies from 4.49 to 16.49% for C25 concrete, whereas it is 3.81–9.39% for C35 concrete at 365 days compared with 28-day UPV values. For samples with longer curing period, the concrete mix is filled with more hydration products, C-S-H, and this leads to more solid and compact internal structures.

This in turns increases the velocity since the time required to travel the pulse is decreased.

According to the guideline of concrete quality, UPV above 4.5 km/sec implies excellent quality concrete, whereas UPV ranging 3.5–4 km/sec specifies good quality; UPV ranging 3–3.5 km/sec specifies medium quality; and below that value concrete is of doubtful quality.

From Figure 6(b), it is obvious that concrete samples are of medium quality for normal as well as microbial concrete for curing ages of 7 days and 28 days. On the other hand as the curing age increased (90 days and 365 days), the concrete quality raises from medium to good quality concrete for 25 MPa concrete group. However, for 35 MPa concrete, it remains still in the medium-quality range except for BC 50:50–35 MPa at the age of 365 days. Another trend that is observed is that the UPV value of microbial concrete is higher than normal concrete, which implies the dense nature of microbial concrete than normal one.

4.3. Water Absorption Capacity Test by Immersion Method. Test results of water absorption are shown in Figure 7.

From Figure 7(a), it can be said that the use of microorganisms in concrete reduces the absorption of the material. When the water absorption rate is observed as a function of curing days as in Figure 7(b), it can be said that the water absorption decreases as the time increases. The lowest water absorption is observed for BC 50:50 35 MPa concrete, which suggested that as the bacterial concentration increases, there is a reduction in water absorption. That means microorganisms help concrete make more durable. The maximum reduction in water absorption is found to be 17.60% for *Escherichia coli* (50% bacterial culture).

4.4. Analysis of Scanning Electron Microscope (SEM).

Changes in the microstructure of concrete due to the addition of *E. coli* bacteria can be studied by SEM analysis caused. Concrete specimens with a standard curing period of 28 days were taken from all types of samples (with and without culture for 25 MPa and 35 MPa mix) and studied at various magnifications. Figures 8 and 9 show the SEM morphology of the three concrete groups at 28 days. It shows that the bacterial inclusion has a significant impact on the microstructure of concrete. Conventional concrete (Figure 8) shows significant amounts of voids among the concrete samples. Voids decreased as the rate of water substitution by microbial culture rises.

The intrusion nature of bacterial concrete might be attributed to the compact microstructure. And it is obvious that the microstructure of concrete had a considerable impact on the hardness and durability properties of the material. Reduction in voids in microbial strain-infused

concrete mixtures was indeed the primary cause for its better strength and durability properties when compared to the plain concrete group.

The cause for the high compactness of concrete containing microbial strains was also validated by SEM analysis. It exhibited the presence of calcite precipitation in bacterial concrete, which implies the presence of fewer cavities and more compact concrete. Calcite precipitation was detected as the white patches of areas in these images. The density of white patches seen in these photographs increased as the concentrations of microbes increased. As a result, it can be stated that the denser microstructure of concrete mixture is primarily responsible for the increase in strength and durability of concrete with the inclusion of microbial strain.

4.5. Comparison between Destructive and Nondestructive Testing Results.

The common destructive test to determine the strength of concrete is the crushing of sample. On the other hand, UPV is the easiest nondestructive test to determine the compressive strength. The comparison in strength obtained from these two methods is presented in this section.

The test results show that the UPV and compressive strength of concrete mix are significantly affected by bacterial doses and curing age. The experimental investigation was carried out at curing ages of 7, 28, 90, and 365 days. To establish the relationship between UPV and compressive strength, all the data points are merged together and plotted as shown in Figure 10. Plotting of test results shows that compressive strength is linearly correlated with UPV. The coefficient of determination R of general relationships was 0.88 for both C25 and C35 concrete mix proportions. This represents that the variation in compressive strength with UPV is accounted well by linear relationship.

4.6. Prediction Model for Compressive Strength.

A nonlinear regression analysis with 95% confidence level was carried out to determine the strength of concrete specimens for various ages and for different ratios of water to bacterial media.

The empirical relation found from the analysis is as follows:

$$z = a + bx + c \ln(y) + dx \ln(y) + e \ln(y)^2, \quad (9)$$

where z is compressive strength in MPa, x is the ratio of water to bacterial media, and y is the age of the specimen in days. Since there are two different types of mix design, the analysis is carried out for two sets of data separately and the coefficients are $a = 2.84$, $b = 7$, $c = 9.18$, $d = -0.395$, and $e = -0.754$ for 25 MPa concrete and $a = 2.25$, $b = 12.03$, $c = 13.4$, $d = -1.16$, and $e = -1.11$ for 35 MPa concrete. The percent of error is found to be 1.6%, which is clearly below 5%. The actual vs predicted strengths for both cases are shown in Figure 11. Figure 12 shows the response surface for both cases, which has been developed using MATLAB software.

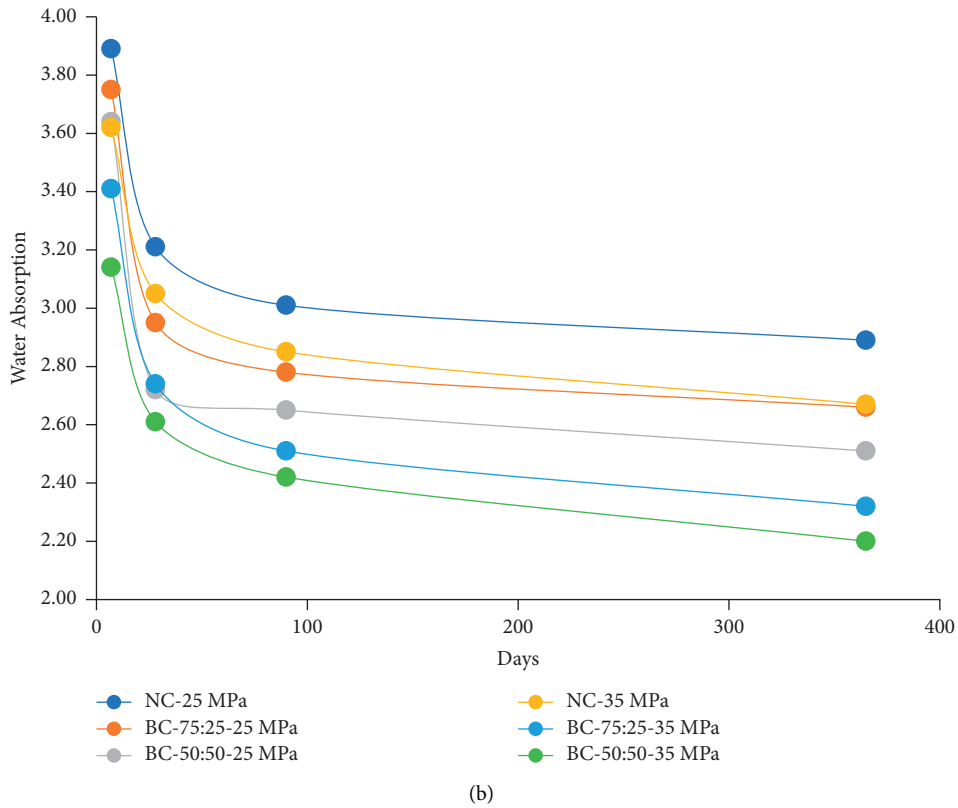
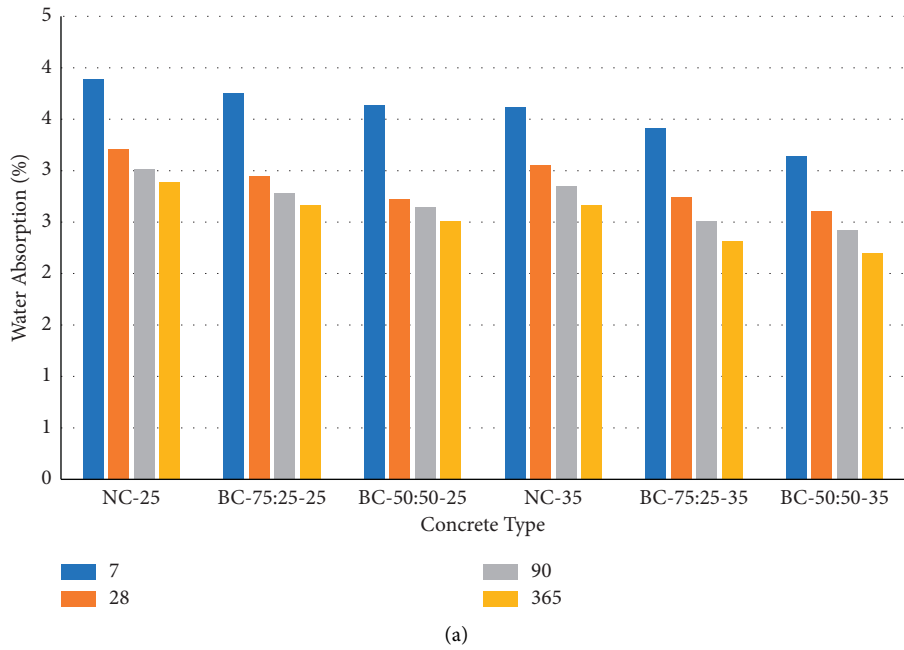


FIGURE 7: Variation of water absorption test results for various curing periods for 25 MPa concrete and 35 MPa concrete.

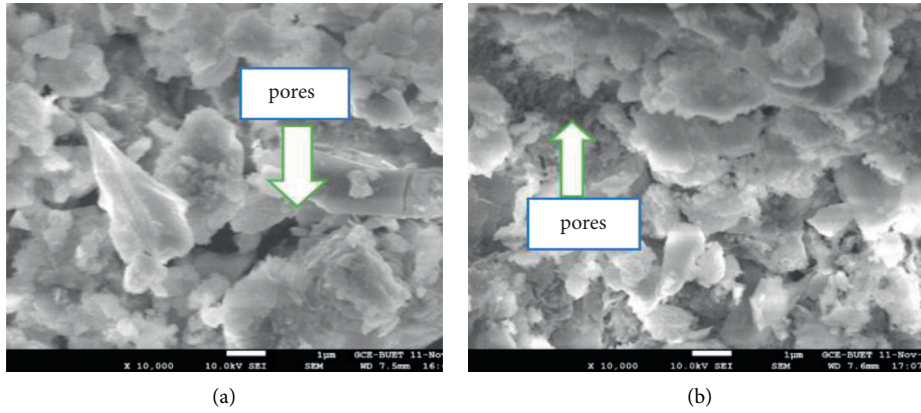


FIGURE 8: SEM imaging of conventional concrete. (a) 25 MPa plain concrete. (b) 35 MPa plain concrete.

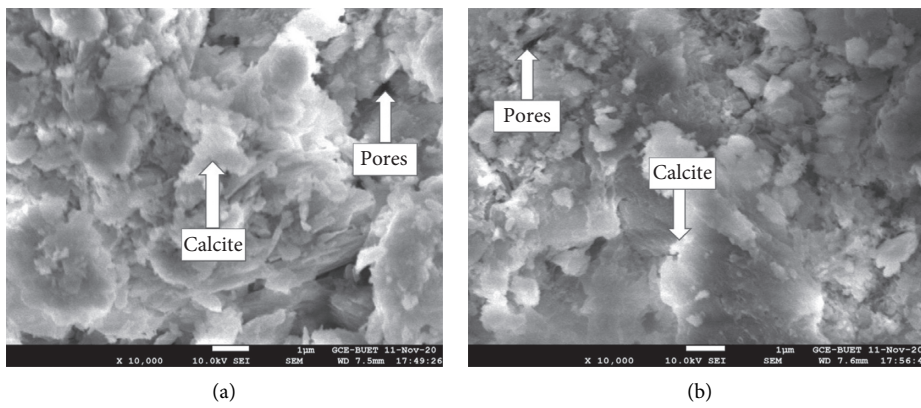


FIGURE 9: SEM imaging of E coli-induced concrete. (a) 25 MPa microbial concrete. (b) 35 MPa microbial concrete.

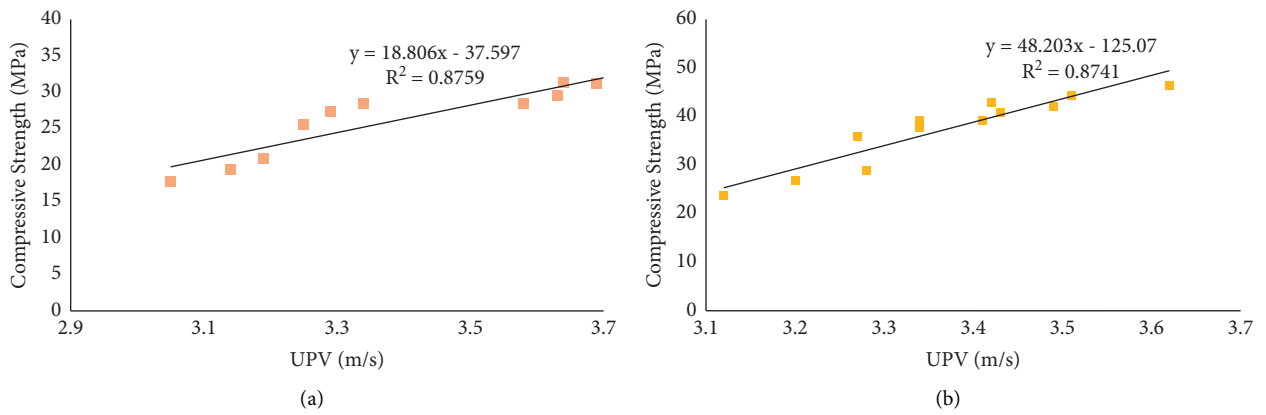


FIGURE 10: Relationship between compressive strength and UPV.

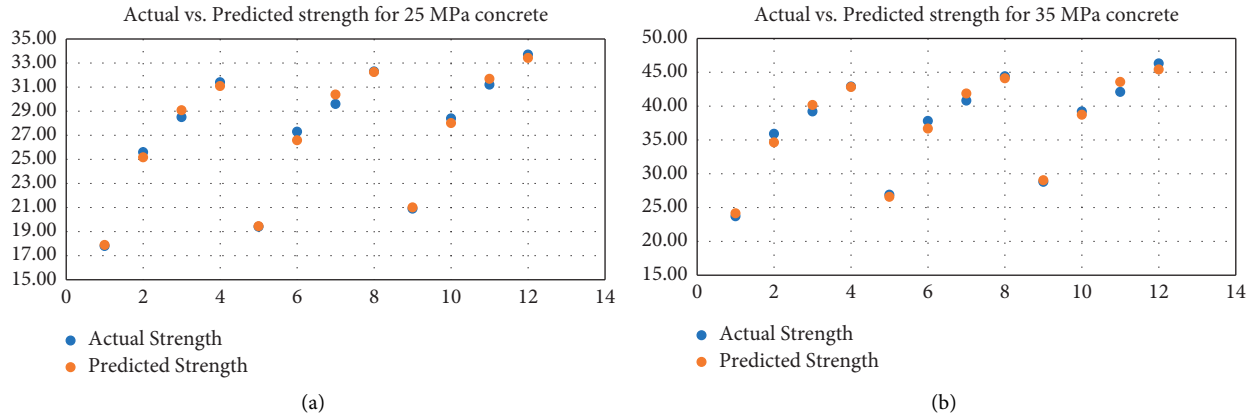


FIGURE 11: Plot of actual vs predicted strength.

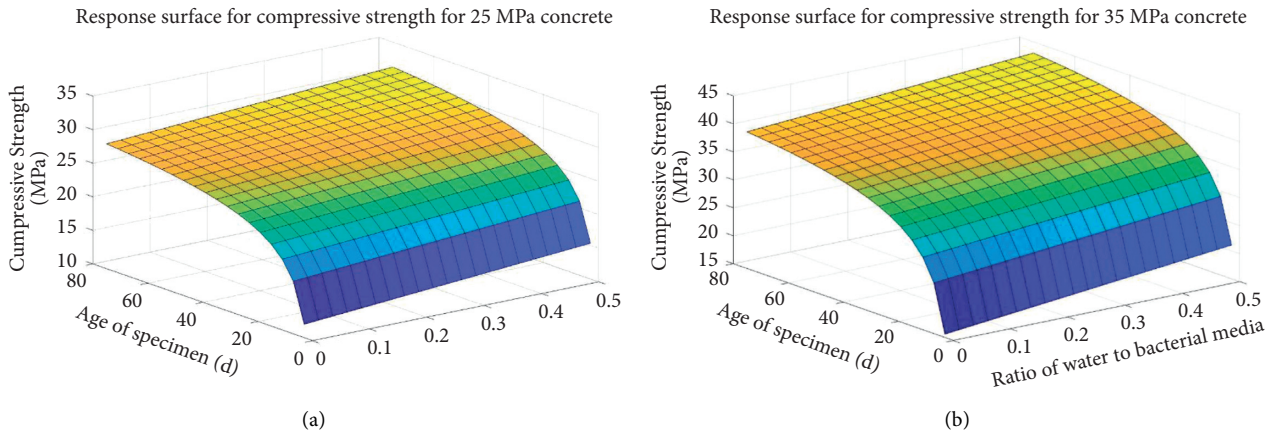


FIGURE 12: Response surface for concrete.

The goodness of fit of the model can be accessed by accessing the coefficient of determination (COD), that is, R squared (R^2) value.

If a data set has n values marked y_1, \dots, y_n (collectively known as y_i) and each of them is associated with a predicted value f_1, \dots, f_n (known as f_i), then the residual can be written as

$$r_i = y_i - f_i \tag{10}$$

The mean of the observed data \bar{y} is

$$\bar{y} = \frac{1}{n} \sum_{i=1}^n y_i \tag{11}$$

Then, R^2 value can be obtained using the following formula:

$$R^2 = 1 - \frac{\sum_i (y_i - f_i)^2}{\sum_i (y_i - \bar{y})^2} \tag{12}$$

The COD value is found to be 0.99 for the fit, and a value close to 1 indicates the higher efficiency and low discrepancy of the model from the actual.

Residual sum of squares (RSS) is another measure for the good of a regression curve. It is the sum of the squared

estimates of errors [21] or the difference between the actual data and an estimation model as expressed in (13). A small RSS refers to the tight fit of the model.

$$RSS = \sum_i (y_i - f_i)^2 \tag{13}$$

For the current prediction model, the average value of RSS (5.4) confirms that the model is effective in predicting the compressive strength.

5. Conclusions

The main aim of this study was to study the properties of microbial concrete using *E. coli* bacteria in the concrete mixture, which has self-healing capacity and hence can be a good solution for durable concrete.

The inclusion of bacterial cultures did not show any adverse effect on the crushing compressive strength as they were found higher than normal concrete in the current study for the investigated parameters. In terms of the optimum ratio of water to bacterial culture media, it is found that the higher the amount of bacterial dose, the better the performance and 50% bacterial culture media exhibits better results than 25% bacterial culture.

On the other hand, the nondestructive UPV test also indicates that microbial groups are more compact than normal concrete, which means the microorganism was effective in producing dense concrete structures. The results obtained from water absorption test also supported this finding, which shows that the use of microorganisms in concrete reduces the absorption of the material, which means less porosity and hence denser concrete structures. The calcium carbonate formed due to chemical action precipitated in the voids making the surface more compact, and hence, this also improves the stability of the structure since the liquid and ion absorption causing reinforcement corrosion were prevented.

The SEM test also exhibited less voids in the microstructure for concrete with high bacterial culture media.

A linear relationship is established between the compressive strength found from destructive test and the velocity found from nondestructive UPV test. From the results of the two proportions of bacterial injections, it can be said that the use of *Escherichia coli* (50% bacterial culture) having OD600 0.5 ± 0.1 has performed better and the use of this ratio will facilitate the production of durable concrete, which in turn can minimize the cost as it eliminates the need for casting new concrete. The investigational data for strength are supported through a prediction model and the fit of the model is found to be acceptable for practical purposes.

Data Availability

The data will be available upon request from the authors.

Disclosure

The abstract of this manuscript was presented at ACI concrete competition project 2021.

Conflicts of Interest

The authors declare that they have no known competing financial interests or personal relationships that could have appeared to influence the work reported in this paper.

Acknowledgments

The authors are grateful for the financial support toward this research by Chittagong University of Engineering and Technology, Directorate of Research and Extension under Grant No: CUET/DRE/2021-22/CE(041).

References

- [1] S. Dinesh, R. Shanmugapriyan, and S. N. Sheen, "A review on bacteria-based self-healing concrete," *Imperial Journal of Interdisciplinary Research*, vol. 3, no. 1, pp. 2454–1362, 2017.
- [2] H. M. Jonkers, "Bacteria-based self-healing concrete," *Genium*, 2021.
- [3] K. Vijay, M. Murmu, and S. V. Deo, "Bacteria based self healing concrete - a review," *Construction and Building Materials*, vol. 152, pp. 1008–1014, 2017.
- [4] S. Luhar and S. Gourav, "A review paper on self-healing concrete," *Journal of Civil Engineering Research*, vol. 5, no. 3, pp. 53–58, 2015.
- [5] J. Bashir, I. Kathwari, A. Tiwary, and K. Singh, "Bio concrete-the self-healing concrete," *Indian Journal of Science and Technology*, vol. 9, no. 47, 2016.
- [6] S. Soundharya and K. Nirmalkumar, "Study on the effect of calcite-precipitating bacteria on self-healing mechanism of concrete," *International Journal of Engineering Research & Management Technology*, vol. 1, no. 4, p. 202, 2014.
- [7] J. Wang, J. Dewanckele, V. Cnudde, S. Van Vlierberghe, W. Verstraete, and N. De Belie, "X-ray computed tomography proof of bacterial-based self-healing in concrete," *Cement and Concrete Composites*, vol. 53, pp. 289–304, 2014.
- [8] V. Wiktor and H. M. Jonkers, "Bacteria-based concrete: from concept to market," *Smart Materials and Structures*, vol. 25, no. 8, Article ID 084006, 2016.
- [9] M. S. Vel, S. Balamurugan, and B. Navaneetha, "Experimental study on self healing concrete by using bacteria(*Escherichia coli*)," *International Journal of Scientific Engineering and Research*, vol. 10, no. 3, 2019.
- [10] E. Benhelal, G. Zahedi, E. Shamsaei, and A. Bahadori, "Global strategies and potentials to curb CO₂ emissions in cement industry," *Journal of Cleaner Production*, vol. 51, pp. 142–161, 2013.
- [11] M. Sarkar, N. Alam, B. Chaudhuri, B. Chattopadhyay, and S. Mandal, "Development of an improved E. coli bacterial strain for green and sustainable concrete technology," *RSC Advances*, vol. 5, no. 41, pp. 32175–32182, 2015.
- [12] M. Safiuddin, S. Ihteshaam, R. A. Kareem, and Shalam, "A study on self-healing concrete," *Materials Today Proceedings*, vol. 52, pp. 1175–1181, 2021.
- [13] E. Stanaszek-Tomal, "Bacterial concrete as a sustainable building material?" *Sustainability*, vol. 12, no. 2, p. 696, 2020.
- [14] P. Kaur, V. Singh, and A. Arora, "Microbial concrete—a sustainable solution for concrete construction," *Applied Biochemistry and Biotechnology*, vol. 194, no. 3, pp. 1401–1416, 2021.
- [15] J. Zhang, X. Shi, X. Chen, X. Huo, and Z. Yu, "Microbial-induced carbonate precipitation: a review on influencing factors and applications," *Advances in Civil Engineering*, vol. 2021, Article ID 9974027, 16 pages, 2021.
- [16] J. Xu, X. Wang, J. Zuo, and X. Liu, "Self-healing of concrete cracks by ceramsite-loaded microorganisms," *Advances in Materials Science and Engineering*, vol. 2018, Article ID 5153041, 8 pages, 2018.
- [17] J. Zhang, C. Zhao, A. Zhou, C. Yang, L. Zhao, and Z. Li, "Aragonite formation induced by open cultures of microbial consortia to heal cracks in concrete: insights into healing mechanisms and crystal polymorphs," *Construction and Building Materials*, vol. 224, pp. 815–822, 2019.
- [18] J. Feng, B. Chen, W. Sun, and Y. Wang, "Microbial induced calcium carbonate precipitation study using *Bacillus subtilis* with application to self-healing concrete preparation and characterization," *Construction and Building Materials*, vol. 280, Article ID 122460, 2021.
- [19] S. Mondal and A. Ghosh, "Investigation into the optimal bacterial concentration for compressive strength enhancement of microbial concrete," *Construction and Building Materials*, vol. 183, pp. 202–214, 2018.
- [20] H. A. Algaifi, S. A. Bakar, A. R. M. Sam et al., "Insight into the role of microbial calcium carbonate and the factors involved in self-healing concrete," *Construction and Building Materials*, vol. 254, Article ID 119258, 2020.

- [21] K. Vijay and M. Murmu, "Effect of calcium lactate on compressive strength and self-healing of cracks in microbial concrete," *Frontiers of Structural and Civil Engineering*, vol. 13, no. 3, pp. 515–525, 2019.
- [22] S. Nirala, P. Kumar, J. Kumar, K. Paul, and D. Prasad, "Developing bio-concrete in laboratory and investigating its mechanical, structural and self-healing properties," in *Proceedings of the International Conference on Innovative Trends in Civil Engineering for Sustainable Development (ITCSD - 2019)*, Warangal, India, September 2019.
- [23] A. Sumathi, G. Murali, D. Gowdhaman et al., "Development of bacterium for crack healing and improving properties of concrete under wet-dry and full-wet curing," *Sustainability*, vol. 12, no. 24, Article ID 10346, 2020.
- [24] N. H. Balam, D. Mostofinejad, and M. Eftekhari, "Use of carbonate precipitating bacteria to reduce water absorption of aggregates," *Construction and Building Materials*, vol. 141, pp. 565–577, 2017.
- [25] A. Vahabi, A. A. Ramezani-pour, and K. A. Noghabi, "A preliminary insight into the revolutionary new line in improving concrete properties using an indigenous bacterial strain *Bacillus licheniformis* AK01, as a healing agent," *European Journal of Environmental and Civil Engineering*, vol. 19, no. 5, pp. 614–627, 2015.
- [26] J. Xu, W. Yao, and Z. Jiang, "Non-ureolytic bacterial carbonate precipitation as a surface treatment strategy on cementitious materials," *Journal of Materials in Civil Engineering*, vol. 26, no. 5, pp. 983–991, 2014.
- [27] J. Xu, Y. Tang, X. Wang, Z. Wang, and W. Yao, "Application of ureolysis-based microbial CaCO_3 precipitation in self-healing of concrete and inhibition of reinforcement corrosion," *Construction and Building Materials*, vol. 265, Article ID 120364, 2020.
- [28] F. Hammes and W. Verstraete, "Key roles of pH and calcium metabolism in microbial carbonate precipitation," *Reviews in Environmental Science and Biotechnology*, vol. 1, no. 1, pp. 3–7, 2002.
- [29] H. V. Knorre and W. E. Krumbein, "Bacterial calcification," in *Microbial Sediments* Springer, Berlin, Germany, 2000.
- [30] H. L. Ehrlich, "How microbes influence mineral growth and dissolution," *Chemical Geology*, vol. 132, no. 1–4, pp. 5–9, 1996.
- [31] S. Priyom, M. Islam, and S. Islam, "An experimental investigation on the performance of bacterial concrete," in *Proceedings of the 4th International Conference on Advances in Civil Engineering 2018 (ICACE 2018)*, Chittagong University of Engineering & Technology (CUET), Chattogram, Bangladesh, December 2018.

Research Article

Shrinkage and Mechanical Properties of Fibre-Reinforced Blast Furnace Slag-Steel Slag-Based Geopolymer

Shengtang Xu ^{1,2}, Chaofan Wu ³, Jinchao Yue ¹ and Zikai Xu ^{1,4}

¹School of Water Conservancy Engineering, Zhengzhou University, Zhengzhou 450001, Henan, China

²Xinyang Highway Development Center, Xinyang 464000, Henan, China

³Xi'an Changda Highway Maintenance Technology Co. Ltd, Xi'an 710000, Shanxi, China

⁴College of Highway, Chang'an University, Xi'an, 710064, Shanxi, China

Correspondence should be addressed to Zikai Xu; xuzikai@chd.edu.cn

Received 13 December 2021; Accepted 21 March 2022; Published 8 April 2022

Academic Editor: Md. Akter Hosen

Copyright © 2022 Shengtang Xu et al. This is an open access article distributed under the Creative Commons Attribution License, which permits unrestricted use, distribution, and reproduction in any medium, provided the original work is properly cited.

Geopolymer materials have several obvious advantages such as energy conservation, emission reduction, and waste reuse, so they can become substitutes for cement materials. In this study, geopolymer mortars made from blast furnace slag and steel slag reinforced by basalt fibre and polyvinyl alcohol (PVA) fibre were prepared to explore the effect on their strength and shrinkage properties. Scanning electron microscopy (SEM) was employed to characterize the reaction mechanism of the geopolymer mortars. The results show that both PVA fibre and basalt fibre can improve the mechanical properties of geopolymer mortars during the late curing period. The geopolymer reinforced by basalt fibre manifested a better toughness. A proper content of PVA fibres and basalt fibres can effectively reduce the drying and autogenous shrinkage of geopolymer mortars. The optimal content of basalt fibres and PVA fibres to reduce the drying shrinkage was 0.4%. The SEM results show that the fibres can effectively alleviate the stress concentration and prevent crack propagation.

1. Introduction

In recent years, cement mortar has been widely used in concrete repair and reinforcement materials due to its advantages of low cost, convenient construction, and stable properties. However, the large-scale use of cement has produced increasingly serious problems such as energy consumption, resource consumption, and environmental pollution. Geopolymers are a new type of nonmetallic material prepared from natural Si-Al-containing materials or industrial slags such as slag, fly ash, and steel slag [1–3]. Geopolymers exhibit excellent characteristics including high strength, low CO₂ emissions, excellent corrosion resistance, and durability compared to traditional cementitious binders [4–6].

Therefore, many researchers have used geopolymer materials to prepare mortars and made great efforts to improve their properties. Helmy [7] suggested that intermittent curing proved an increase in compressive strength of

all geopolymer mortars prepared by fly ash at the end of each curing step. Atis et al. [8] believed that an increase in heat curing temperature and heat curing durations was beneficial to enhance the compressive strength of geopolymers. Fly-ash-based geopolymer pastes reached 120 MPa when activated with 14% NaOH and cured at 115°C for 24 h. Ilkentalpar et al. [9] found that the water absorption of fly ash-based geopolymer mortars increased with increasing heat curing duration. An extra rest period of curing after heat curing increases the water absorption. Yang et al. [10] found that the substitution of fly ash decreased the reactivity of the solid precursors of metakaolin-based geopolymer mortars, which resulted in a lower reaction rate, a longer reaction time, and an obstruction of water evaporation from pore networks. Elyamany et al. [11] explored the effect of sodium hydroxide molarity on the setting time of geopolymer mortars. Some results showed that the setting time decreased with increasing NaOH solution molarity possibly because increasing the NaOH molarity can improve the dissolution

rate of the aluminosilicate precursors and enhance the geopolymerization process. Chen et al. [12] revealed that when the replacement ratio of GGBS reached 30%, the mortar had better compressive strength (75.9 MPa), flexural strength (12.2 MPa), and bond strength (6.4 MPa) than many pavement repair materials.

However, geopolymer mortars have disadvantages of high brittleness, low toughness, and low deformation resistance, which is similar to cement mortars. However, the addition of various fibres can significantly improve these properties. For example, Zhang et al. [13] experimentally concluded that the compressive strength and fracture energy of geopolymer mortars could be improved by mixing a certain amount of PVA fibre. Malik [14] suggested that the structural properties and durability of geopolymers were improved by incorporating 5% PVA fibres. Microstructural studies confirmed that PVA fibres in geopolymer matrices were well distributed to develop a fibre-bridging texture with improved performance. Guo [15] found that basalt fibres could also significantly improve the 28-d compressive and flexural strength of geopolymer mortars and effectively prevent cracking and crack propagation, as shown in scanning electron micrographs. Punurai [16] found that basalt fibre could make geopolymer pastes more uniform and denser with a smaller total porosity. Therefore, PVA fibres or basalt fibres can be used to enhance the toughness and durability of geopolymer mortars.

The obvious shrinkage during the setting and hardening processes is another important factor that affects the wide-area applications of geopolymers [17, 18]. Excessive shrinkage will result in cracking, which further reduces the strength, stiffness, and service life of the structure [10, 19, 20]. Much effort has been made by scholars to study the shrinkage properties of geopolymers. Studies have shown that an increase in the addition of fly ash can significantly reduce the drying shrinkage of geopolymers due to the microaggregate filling effect of fly ash [21, 22]. In addition, the NaOH concentration has a serious effect on the drying shrinkage of geopolymers. The geopolymers prepared by a higher NaOH molarity showed a lower drying shrinkage and a higher autogenous shrinkage [23]. Ridditirud et al. [24] found that the curing temperature and solid/liquid ratio played key roles in determining the drying shrinkage of fly-ash-based geopolymers. Duan et al. [25] believed that the incorporation of TiO₂ nanoparticles into geopolymers could improve the carbonation resistance of geopolymers and reduce drying shrinkage.

In this article, steel slag and slag are used as raw materials to prepare geopolymer mortar. Steel slag and slag can promote each other under the action of an alkaline exciter due to the difference in activity. Due to the rapid reaction in the early stage and lack of Ca²⁺ in the later stage, while the steel slag has a high CaO content, Ca(OH)₂ generated by the reaction can be absorbed by the slag to promote the hydration of the slag. The absorption of Ca²⁺ by the slag promotes the dissociation hydration of the steel slag and generates products such as hydrated calcium aluminosilicate and zeolite to fill the pores, which form in the early stage of

the reaction. In addition, mixing the fibre material is expected to improve the toughness and reduce the shrinkage of the geopolymer. Thus, further research on restricting the shrinkage of geopolymer mortars by adding PVA fibre or basalt fibre is meaningful, but relevant research remains insufficient. Geopolymers made from slag and steel slag with various mixed volume ratios of PVA fibres and basalt fibres are prepared to explore the effect on the shrinkage and mechanical properties of geopolymer mortars.

2. Experimental

2.1. Materials. Blast furnace slag and steel slag were used as the raw materials to prepare geopolymer binders, and quartz sand with a particle size of 40–70 mm was used as the fine aggregate. The specific surface area of the blast furnace slag powder is 436 m²/kg. The blast furnace slag mainly consisted of 37.2% CaO, 30.0% SiO₂, and 16.6% Al₂O₃, as shown in Table 1. Steel slag is a type of solid waste discharged from steelmaking, and its chemical composition is affected by factors such as the iron ore source, slagging material, and steelmaking methods. The chemical composition of steel slag in this study is mainly composed of 30.1% CaO, 15.3% SiO₂, 33.2% Fe₂O₃, and 15.0% MgO, as shown in Table 1, with a specific surface area of 420 m²/kg.

The chosen modulus of the sodium silicate solution ($M = n(\text{SiO}_2)/n(\text{Na}_2\text{O})$) was 3.2, which was adjusted by NaOH and used as a composite alkali activator. The modulus of the composite alkali activator was 1.2. The solid contents of Na₂O and SiO₂ were 8.5% and 26.8%, respectively.

Polyvinyl alcohol fibres (PVA fibres) 12 mm in length and 15 μm in diameter and basalt fibres (BF) 12 mm in length and 13 μm in diameter were used. Their technical indicators are shown in Table 2.

2.2. Mix Proportions of Geopolymer Mortars. Table 3 presents the mix proportions of the geopolymer mortars. The ratio of water to binder was 0.55 (including the water in activator), the ratio of binder to sand was 0.60, and the equivalent of Na₂SiO₃ in activator to the binder material was 22%. The addition of 0.1%, 0.2%, 0.3%, and 0.4% PVA fibres (PVA-1, PVA-2, PVA-3, and PVA-4, respectively) was selected for comparison with the control sample (PVA-0), and all proportions were expressed in volume ratio (%). Samples mixed with a 0.1–0.4% volume ratio of basalt fibres (named BF-1, BF-2, BF-3, and BF-4) were also prepared.

2.3. Preparation of Geopolymer Mortars. The geopolymer mortars had a similar preparation process to cement pastes. First, the fibres were put into activators and mixed to be well distributed, and the mixture was poured into a cement mortar mixer with water, blast furnace slag, steel slag, and quartz sand. Then, the mixture was stirred for 120 s at low speed in the mixer prior. After 180 s of stirring at high speed, the geopolymer mortars were poured into moulds with dimensions of 70.7 × 70.7 × 70.7 mm and 40 × 40 × 160 mm.

TABLE 1: Chemical composition of blast furnace slag and steel slag.

Materials	Chemical composition (wt%)					
	CaO	SiO ₂	Al ₂ O ₃	MgO	SO ₃	Fe ₂ O ₃
Blast furnace slag	37.20	30.03	16.58	9.17	3.92	0.76
Steel slag	30.12	15.32	3.80	15.00	1.09	33.24

TABLE 2: Technical indexes of PVA and basalt fibre.

Type	Length (mm)	Diameter (μm)	Tensile modulus (MPa)	Initial modulus (GPa)	Density (g/cm^3)
PVA fibre	12	15	1830	40	1.29
Basalt fibre	12	13	4500	101	2.64

TABLE 3: Mix proportions of geopolymers mortars.

Samples	Slag (%)	Steel slag (%)	Activator modulus	Activator concentration (%)	Water binder ratio	Binder sand ratio	Fibre content (%)
PVA-0	70	30	1.2	22	0.50	0.60	0
PVA-1	70	30	1.2	22	0.50	0.60	0.1
PVA-2	70	30	1.2	22	0.50	0.60	0.2
PVA-3	70	30	1.2	22	0.50	0.60	0.3
PVA-4	70	30	1.2	22	0.50	0.60	0.4
BF-1	70	30	1.2	22	0.50	0.60	0.1
BF-2	70	30	1.2	22	0.50	0.60	0.2
BF-3	70	30	1.2	22	0.50	0.60	0.3
BF-4	70	30	1.2	22	0.50	0.60	0.4

2.4. Testing Methods

2.4.1. Mechanical Properties. According to the standard of cement test methods to determine the strength (ISO 679: 2009), the compressive strength ($70.7 \times 70.7 \times 70.7$ mm) and flexural strength ($40 \text{ mm} \times 40 \text{ mm} \times 160$ mm) of the specimens were tested at curing ages of 3 d, 7 d, and 28 d in a microcomputer-controlled pressure testing system. The samples were cured in a standard curing box (20°C and $>95\%$ RH) until the specified age was reached. The compressive strength and flexural strength were the averages of six separate tests. Data deviating by more than 10% of the mean were eliminated.

2.4.2. Drying Shrinkage. According to the standard test method (JC/T 603–2004), the drying shrinkage was reported by measuring three specimens to obtain an average value. After demoulding, the samples were further cured in a 20°C water bath for 2 days and subsequently removed. The water on the surface of the specimens was wiped, and the initial length was measured with an accuracy of 0.001 mm, as shown in Figure 1. Afterwards, the samples were put into a drying and shrinking box to cure at a temperature of $20 \pm 2^\circ\text{C}$ and a relative humidity of $60 \pm 5\%$. The length of the samples after curing was tested with an accuracy of 0.001 mm. Drying shrinkage is determined as follows:

$$\varepsilon = \frac{L_0 - L_d}{L_0} \times 100\%, \quad (1)$$



FIGURE 1: Comparator and dial indicators.

where ε is the drying shrinkage, L_0 (mm) is the demoulded length, L_d (mm) is the measured length, and 160 (mm) is the effective length of the specimens without two head nails.

2.4.3. Autogenous Shrinkage. The autogenous shrinkage test was performed using a beam specimen with a size of $40 \times 40 \times 160$ mm. After 24 h of moulding, the specimens were removed from the mould, immediately sealed with polyethylene film, and wrapped with a layer of self-adhesive tin foil. Autogenous shrinkage is determined as follows:

$$\sigma = \frac{L_1 - L_t}{L_1} \times 100\%. \quad (2)$$

The initial length L_1 was measured with a length-ratio metre, and L_t was measured after setting to the specified age.

2.4.4. Mass Loss. The mass loss rate was used to measure the mass change under identical curing conditions to the drying shrinkage test. The mass loss is determined as follows:

$$\Delta m = \frac{W_s - W_t}{W_s} \quad (3)$$

Here, Δm (wt%) is the mass loss, W_s is the initial weight of the specimens, and W_t is the measurement weight of the specimens at t days.

3. Results and Discussion

3.1. Compressive and Flexural Strength of Basalt Fibre-Reinforced Geopolymer Mortars. The compressive strengths of geopolymer mortars with different basalt fibre contents after 3 d, 7 d, and 28 d of curing are shown in Figure 2(a). The compressive strength of the samples at 3 d and 7 d slightly decreased after basalt fibres was added. The compressive strength was higher than that of the control group only when the fibre content was 0.3%. After 28 d of curing, the compressive strength first increased and subsequently decreased with the increase in the fibre content, and all strengths were higher than that of the control group. The compressive strength of the mortars reached a maximum of 41.1 MPa when 0.2% fibre was added, which is 11.7% higher than that of the control group.

Figure 2(b) shows the flexural strength of geopolymer mortars with different basalt fibre contents at curing ages of 3 d, 7 d, and 28 d. The flexural strength of geopolymer mortars increased when the basalt fibre content increased from 0.1% to 0.3%. When the basalt fibre content further increased, the flexural strength slightly decreased, and the compressive strength remained higher than that of the control group. The optimal content of basalt fibre is approximately 0.2%, and the early flexural strength reached a maximum of 5.4 MPa and 6.1 MPa for 3 d and 7 d of curing. If the content of basalt fibre was 0.3%, the flexural strength at 28 d of curing age reached the maximum of 7.4 MPa and increased by 17.4% compared to the control sample. The optimal basalt fibre content for compressive strength development is 0.2-0.3%.

The basalt fibre can be uniformly dispersed in specimens to form a mesh structure, which effectively resists crack extension and enhances the structural toughness [26]. Adding a proper content of fibres is beneficial to energy absorption and strength development. However, too many fibres are difficult to mix well in mortars, which results in an uneven structure with excessive porosity defects [27].

3.2. Compressive and Flexural Strength of PVA Fibre-Reinforced Geopolymer Mortars. The compressive strength of geopolymer mortars at 3 d, 7 d, and 28 d of curing with different PVA fibre contents is shown in Figure 3(a). The incorporation of PVA fibres reduced the compressive strength of mortars at 3 d of curing except when 0.2% of PVA fibres was added. The 7-d compressive strength appeared to decrease with the increasing incorporation of PVA fibres. If the content of PAV fibres was less than 0.2%,

the compressive strength at 28 d of curing age obviously improved. However, if the content was higher than 0.2%, the compressive strength at 28 d of curing decreased. This strength was even lower than that of the control group, while the content was 0.4%. The highest 28-d compressive strength of geopolymer mortars (prepared with 0.2% content of PVA fibres) was 41.8 MPa, which is 13.6% higher than that of the control sample.

Figure 3(b) shows the flexural strength of geopolymer mortars with different PVA fibre contents at 3 d, 7 d, and 28 d of curing ages. The results show that the 3-d flexural strength reached a maximum value of 4.3 MPa at a PVA fibre content of 0.2%. The 7-d flexural strength at various PVA fibre contents was slightly higher than that of the control group. The reinforcing effect of PVA fibres on geopolymer mortars was obvious at 28 d of curing. The optimal content of PVA fibres for 28 d flexural strength gain was 0.2%, and the corresponding strength reached 7.6 MPa, which is 20.6% higher than that of the control sample. Similar to the trends of the compressive strength, an excessive content (>0.2%) is expected to weaken the reinforcing effect of PVA fibres.

The PVA fibre significantly contributed to the compressive and flexural strength gain at the later curing age (28 d), which is consistent with the report in [15]. The optimal PVA fibre content is 0.2-0.3%. In addition, basalt fibres have a higher reinforcing effect on geopolymer mortars than PVA fibres at an early age. The reason can be the higher elastic modulus of basalt fibres, which benefits the stress dispersion and withstands part of the stress.

3.3. Drying Shrinkage of Geopolymer Mortars. Figure 4 shows the influence of the content of basalt fibres and PVA fibres on the drying shrinkage of geopolymer mortars. The shrinkage can be attributed to the internal water that evaporates from the pore network of the binder to the external environment at a relatively low level of humidity. Capillary stresses from the evaporation of capillary water during the drying process result in shrinkage strain. Most of the drying shrinkage occurs on the first day because of the rapid loss of internal water from freshly formed surfaces.

Figure 4(a) shows that the drying shrinkage of geopolymer mortars reinforced by basalt fibre experiences two stages. The drying shrinkage geopolymer mortars rapidly increase at the initial stage and subsequently level off. The drying shrinkage first increases and subsequently decreases with increasing fibre content. The drying shrinkage was minimal when the basalt fibre content was 0.4% at 56 d. The 14-d drying shrinkage was 410×10^{-5} for the control group, which accounts for 92.5% of the 56-d drying shrinkage. For geopolymer mortars prepared with 0.4% basalt fibres, the 56-d drying shrinkage was 361×10^{-5} for mortars reinforced with 0.4% basalt fibres, which is a decrease of 18.5% compared to the control group. The high elastic modulus of basalt fibres increases the tensile strength of composites at the initial stage of plasticity and hardening and resists the deformation of matrices due to dehydration and drying. A proper content of basalt fibres can reduce the drying shrinkage and improve the volume stability of the material.

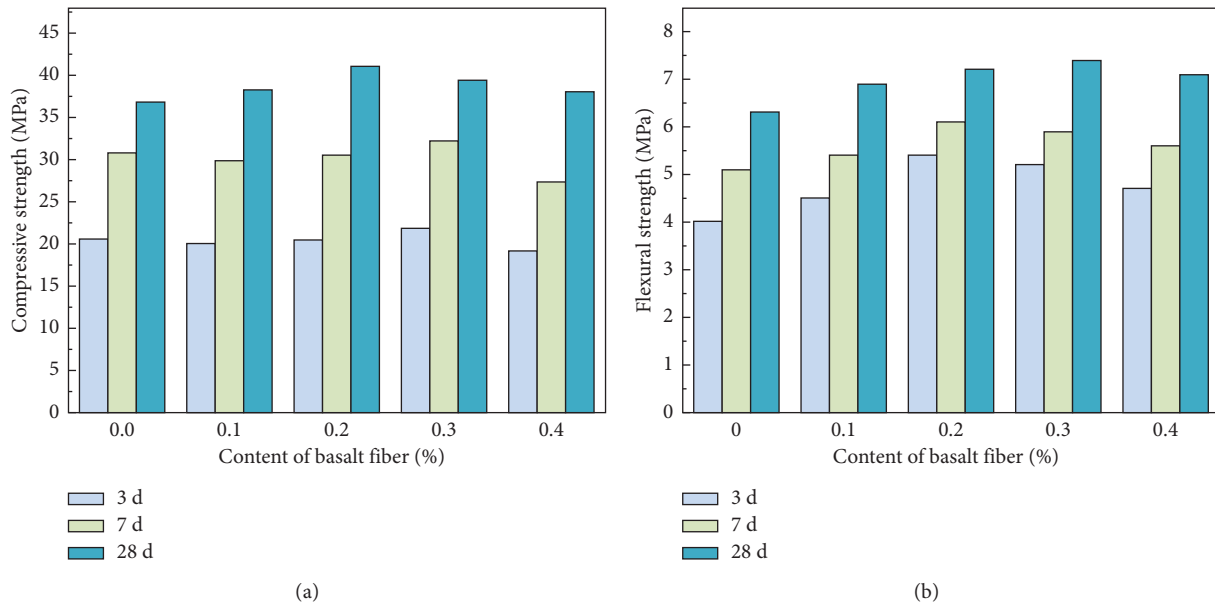


FIGURE 2: Strength of geopolymers mixed with different basalt fibre contents. (a) Compressive strength and (b) flexural strength.

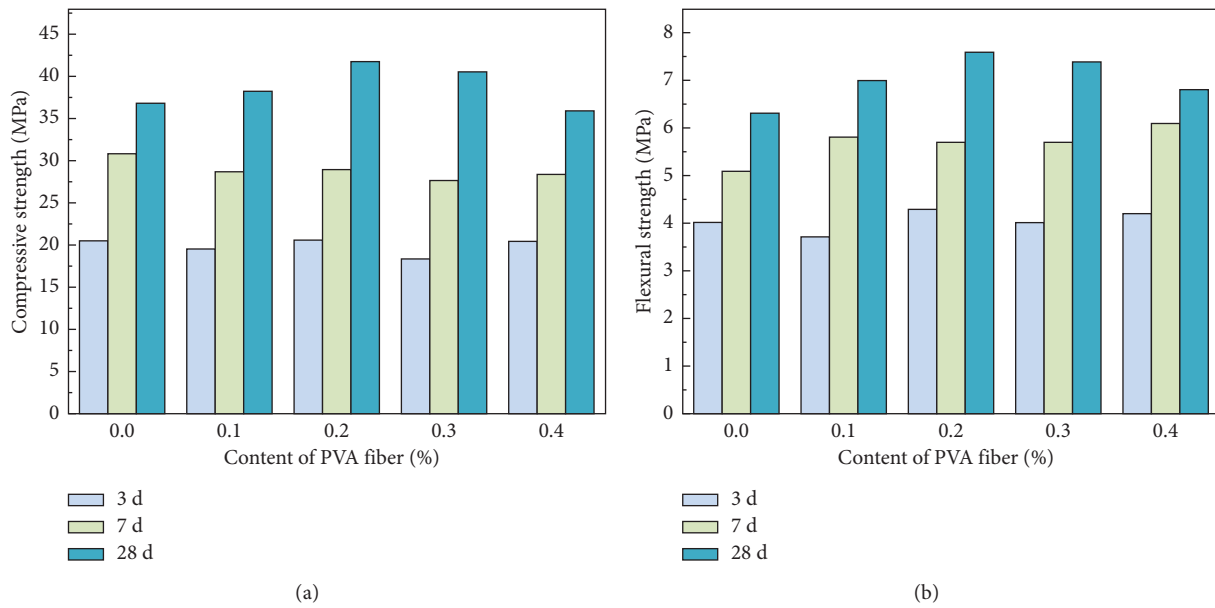


FIGURE 3: Strength of geopolymers with different PVA fibre contents. (a) Compressive strength and (b) flexural strength.

Figure 4(b) shows the influence of the PVA fibre content and drying age on the drying shrinkage of geopolymer mortars. The drying shrinkage of samples prepared with PVA fibres appeared to rapidly increase in the early stage and levelled off after 28 d of curing. A more obvious drying shrinkage appeared when the PVA fibre content was less than 0.3% compared to the control group. For example, the 56-d drying shrinkage of samples prepared at 0.2% volume fractions of PVA fibres was 540×10^{-5} , which is an increase of 21.9% compared to the control group. In contrast, the 56-d drying shrinkage was subject to an obvious limitation when the PVA fibre content increased to 0.4%, which is a

decrease of 4% compared to the control group. Basalt fibres have a better effect on the drying shrinkage of geopolymer mortars than PVA fibres. The optimal content of fibres to inhibit drying shrinkage is different from that for the compressive strength. The 56-d drying shrinkage was maximal when 0.2% content of basalt fibres and PVA fibres was added, reaching 458×10^{-5} and 540×10^{-5} , respectively. Adding fibres with 0.4% volume fractions has the optimal reinforcing effect for drying shrinkage of geopolymer mortars. The fibres restrain the expansion and extension of the microcracks and disperse the stress caused by shrinkage, which reduces the shrinkage strain of the materials.

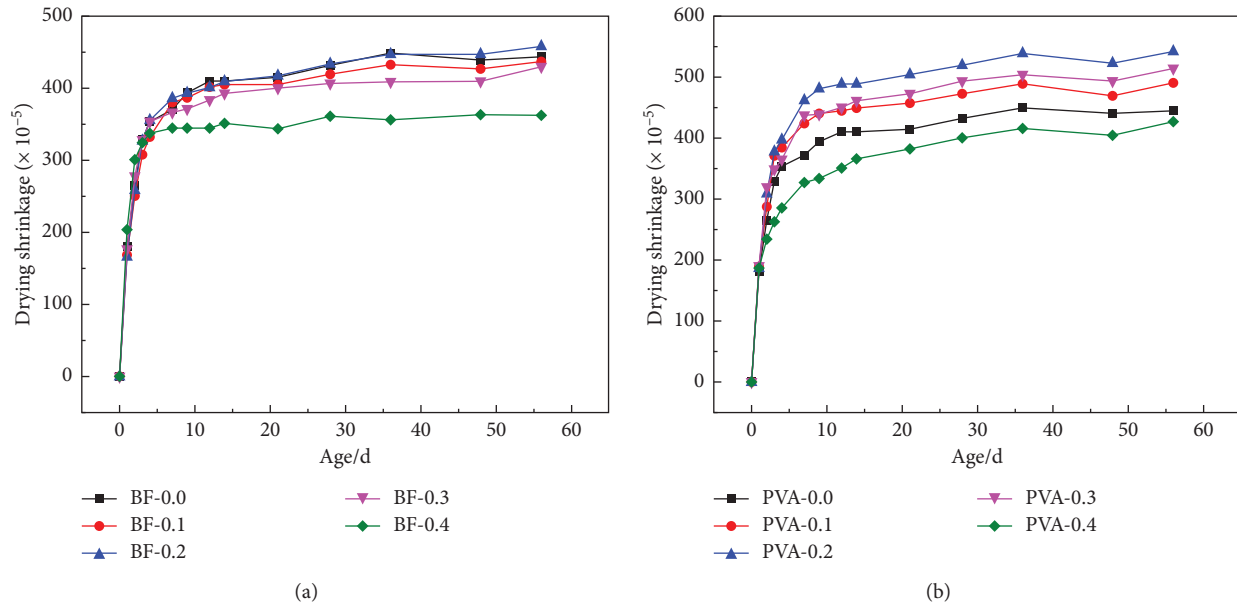


FIGURE 4: Effect of the content of (a) basalt fibre and (b) PVA fibre on drying shrinkage of geopolymer mortars.

Figure 5 shows the mass loss rate of geopolymer mortars in the drying process. Similar to the drying process, the mass loss rate of geopolymers increased with longer drying age. A more obvious mass loss occurred in the early stage. The relatively stable mass loss rate in the late stage is positively correlated with the drying shrinkage; that is, greater drying shrinkage corresponds to a greater water loss rate. Adding basalt fibres with appropriate content can effectively reduce the porosity of geopolymers and limit the internal water release from geopolymers. The geopolymer mortars have a lower early mass loss rate than the control group when the PVA fibre content is 0.4% but increases to become higher than that of the control group after 56 d of drying.

3.4. Autogenous Shrinkage of Geopolymer Mortars. Autogenous shrinkage of geopolymers derives from self-desiccation and chemical shrinkage, which reduces the volume. In this study, the autogenous shrinkage of geopolymers is measured after 24 h of moulding. Chemical shrinkage mainly occurs in the fresh state, so it will not be discussed in the following section. The autogenous shrinkage curves of the pastes evolve in two distinct stages: (1) the expansion behaviour during the initial curing age and (2) the shrinkage behaviour due to the further increase in shrinkage strain.

Figure 6(a) shows the influence of basalt fibres on the autogenous shrinkage of geopolymer mortars. The autogenous shrinkage increased with increasing setting age. The autogenous shrinkage of geopolymer mortars reinforced by the basalt fibres with 0.3% content was the minimum (278×10^{-5}) at 56 d, which decreases by 15.3% compared to the control group. The 14-d autogenous shrinkage reached 188×10^{-5} when the basalt fibre content was 0.4%, which accounted for 65.7% of the drying shrinkage at 56 d. Adding 0.3–0.4% volume fractions of basalt fibres has a relatively obvious inhibiting effect on autogenous shrinkage.

The influence of PVA fibres on the autogenous shrinkage of geopolymer mortars is different from the drying shrinkage, as shown in Figure 6(b). The autogenous shrinkage of geopolymer mortars decreased with increasing fibre content up to 0.3% volume fractions and subsequently increased. All contents of PVA fibres effectively reduced the autogenous shrinkage. The autogenous shrinkage of the geopolymer mortars increased with increasing setting age. Adding 0.3% content of PVA fibres mostly reduced the 56-d autogenous shrinkage. It reached 240×10^{-5} and decreased by 26.8% compared to the control group.

3.5. SEM Analysis. Figure 7 shows the SEM images of geopolymer mortars after 28 d of curing. Mass flocculent phases without regular shapes were found in all specimens. This is expected to be amorphous phases formed by the alkali-activated reaction and to form C–S–H gel and/or N–A–S–H [28, 29]. The alkali-activated reaction can generate C–S–H gels with smaller gel particles to fill the pore structure. Furthermore, gel phases can generate a three-dimensional network structure via a polymerization process [30, 31]. However, a few unreacted steel slag particles remain due to their low activity. Pores and cracks in geopolymer mortars can also be observed, as shown in Figure 7(a), which can be caused by shrinkage and water loss [32]. Single independent fibres can be observed and appear as a strong bond with the surrounding geopolymer mortar, which can effectively resist the crack extension and disperse the stress, as confirmed by Figure 7(b) [33]. Therefore, when the fibre content of both is 0.4%, the drying shrinkage is minimal. At this content, the fibres can effectively improve the mechanical properties and reduce drying shrinkage. However, comparing Figures *b* and *c*, PVA fibres will exhibit agglomeration phenomena due to better hydrophilicity, and there are microcracks at the combination surface of PVA fibres and ground poly. The gel and fibre fail to be closely

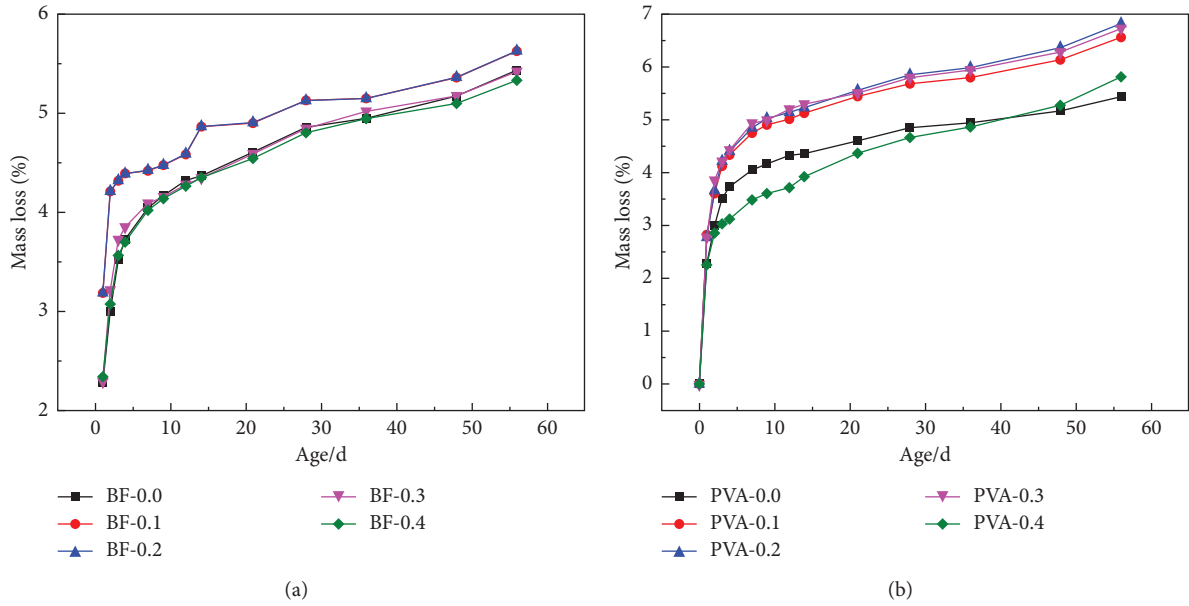


FIGURE 5: Effect of content of (a) basalt fibres and (b) PVA fibres on water loss rate of geopolymer mortars.

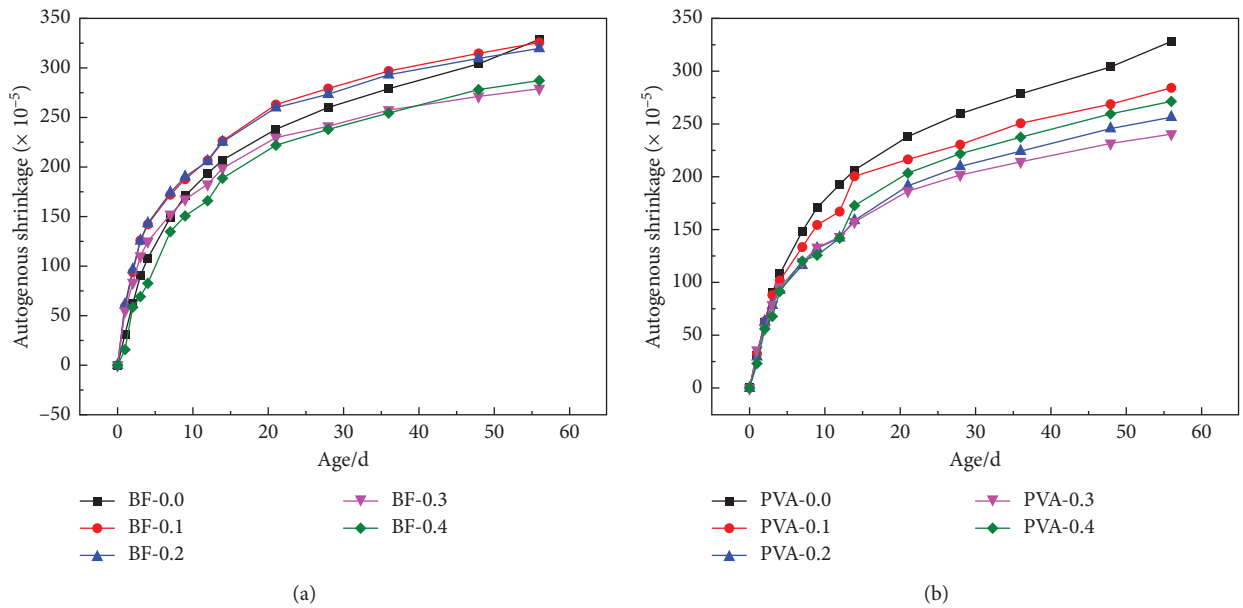


FIGURE 6: Effect of content of (a) basalt fibres and (b) PVA fibres on the autogenous shrinkage rate of geopolymer mortars.

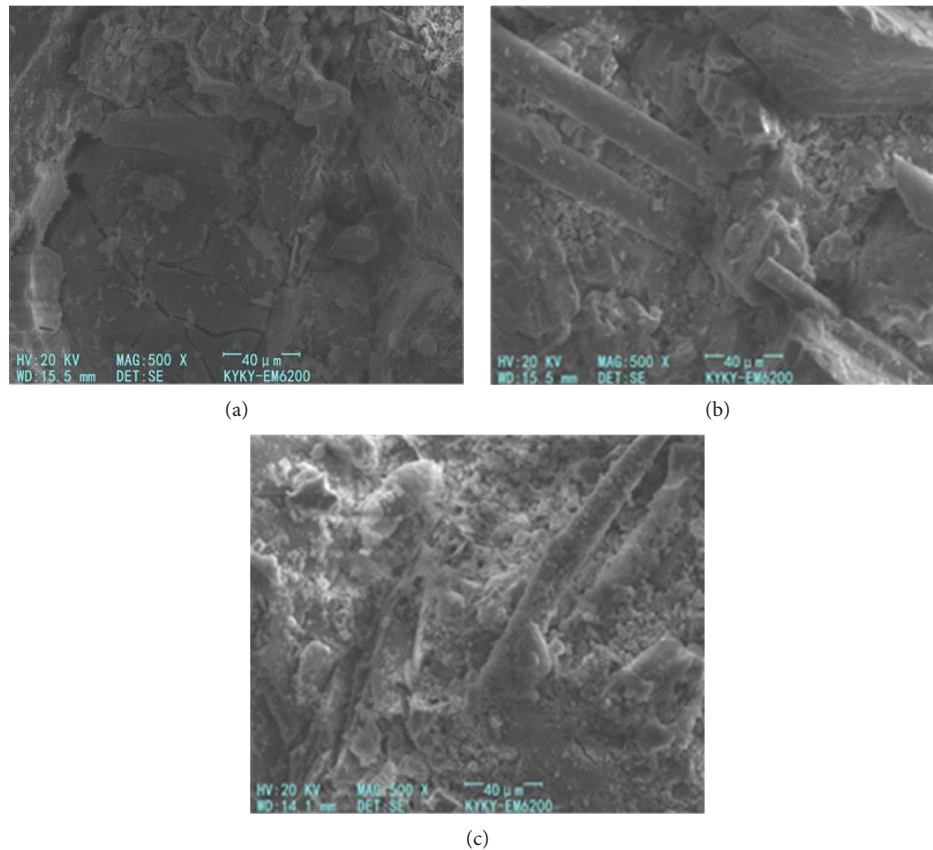


FIGURE 7: SEM images of geopolymer mortars to represent the dispersibility of fibres. (a) Blank sample. (b) Basalt fibres (0.4%). (c) PVA fibres (0.4%).

combined, the surrounding structure is looser, and more water is lost, so when PVA fibre doping is 0.4%, the drying shrinkage value is greater than that of basalt fibres.

4. Conclusions

In this article, the shrinkage and strength properties of geopolymer mortars made from blast furnace slag and steel slag reinforced by basalt fibre and polyvinyl alcohol (PVA) were studied. The main conclusions are as follows:

- (1) After PVA fibres and basalt fibres have been added, the compressive strength and flexural strength of geopolymer mortars are improved. The flexural and compressive strengths first increase and subsequently decrease. The optimal content of basalt fibre and PVA fibre is 0.2–0.3%, and basalt fibre has a better toughening effect than PVA fibres.
- (2) The drying shrinkage of geopolymer mortars first increases and subsequently decreases with increasing basalt fibre and PVA fibre contents. The mass loss rate shows the same trend as the drying shrinkage. The optimal content of basalt fibres and PVA fibres to limit drying shrinkage is 0.4%. PVA fibres will increase shrinkage due to their hydrophilicity compared to basalt fibres.

- (3) The autogenous shrinkage test shows that when the content of both fibres is 0.3%, the self-shrinkage is minimal. SEM testing shows that the addition of fibres can effectively alleviate the stress concentration of geopolymer mortars and prevent crack propagation. However, excessive fibres can agglomerate, which results in a loss of strength.

Data Availability

The data used to support the findings of this study are included within the article.

Conflicts of Interest

The authors declare that they have no conflicts of interest.

Acknowledgments

This work was financially supported by the Project of Science and Technology of Henan Transportation Department (Grant no. 2018J4).

References

- [1] G. Liang, H. Zhu, H. Li, T. Liu, and H. Guo, "Comparative study on the effects of rice husk ash and silica fume on the freezing resistance of metakaolin-based geopolymer,"

- Construction and Building Materials*, vol. 293, Article ID 123486, 2021.
- [2] W. Long, J. Peng, Y. Gu, and J. Li, "Recycled use of municipal solid waste incinerator fly ash and ferronickel slag for eco-friendly mortar through geopolymer technology," *Journal of Cleaner Production*, vol. 307, Article ID 127281, 2021.
 - [3] K. Sedić, N. Ukrainczyk, V. Mandić, and N. Gaurina Međimurec, J. Šipušić, Carbonation of Portland-Zeolite and geopolymer well-cement composites under geologic CO₂ sequestration conditions," *Cement and Concrete Composites*, vol. 111, Article ID 103615, 2020.
 - [4] P. Zhang, Y. Zheng, K. Wang, and J. Zhang, "A review on properties of fresh and hardened geopolymer mortar," *Composites Part B: Engineering*, vol. 152, pp. 79–95, 2018.
 - [5] C. Suksiripattanapong, S. Horpibulsuk, P. Chanprasert, P. Sukmak, and A. Arulrajah, "Compressive strength development in fly ash geopolymer masonry units manufactured from water treatment sludge," *Construction and Building Materials*, vol. 82, pp. 20–30, 2015.
 - [6] S. S. Hossain, P. K. Roy, and C.-J. Bae, "Utilization of waste rice husk ash for sustainable geopolymer: a review," *Construction and Building Materials*, vol. 310, Article ID 125218, 2021.
 - [7] A. I. I. Helmy, "Intermittent curing of fly ash geopolymer mortar," *Construction and Building Materials*, vol. 110, pp. 54–64, 2016.
 - [8] C. D. Atiş, O. E. B. Görür, and C. Karahan, "Very high strength (120MPa) class F fly ash geopolymer mortar activated at different NaOH amount, heat curing temperature and heat curing duration," *Construction and Building Materials*, vol. 96, pp. 673–678, 2015.
 - [9] S. İlkentapar, C. D. Atiş, O. Karahan, and E. G. Avşaroğlu, "Influence of duration of heat curing and extra rest period after heat curing on the strength and transport characteristic of alkali activated class F fly ash geopolymer mortar," *Construction and Building Materials*, vol. 151, pp. 363–369, 2017.
 - [10] T. Yang, H. Zhu, and Z. Zhang, "Influence of fly ash on the pore structure and shrinkage characteristics of metakaolin-based geopolymer pastes and mortars," *Construction and Building Materials*, vol. 153, pp. 284–293, 2017.
 - [11] H. E. Elyamany, A. E. M. Abd Elmoaty, and A. M. Elshaboury, "Setting time and 7-day strength of geopolymer mortar with various binders," *Construction and Building Materials*, vol. 187, pp. 974–983, 2018.
 - [12] K. Chen, D. Wu, M. Yi, Q. Cai, and Z. Zhang, "Mechanical and durability properties of metakaolin blended with slag geopolymer mortars used for pavement repair," *Construction and Building Materials*, vol. 281, Article ID 122566, 2021.
 - [13] P. Zhang, K. Wang, J. Wang, J. Guo, and Y. Ling, "Macroscopic and microscopic analyses on mechanical performance of metakaolin/fly ash based geopolymer mortar," *Journal of Cleaner Production*, vol. 294, Article ID 126193, 2021.
 - [14] M. A. Malik, M. Sarkar, S. Xu, and Q. Li, "Effect of PVA/SiO₂ NPs additive on the structural, durability, and fire resistance properties of geopolymers," *Applied Sciences*, vol. 9, no. 9, p. 1953, 2019.
 - [15] X. Guo and X. Pan, "Mechanical properties and mechanisms of fiber reinforced fly ash-steel slag based geopolymer mortar," *Construction and Building Materials*, vol. 179, pp. 633–641, 2018.
 - [16] W. Punurai, W. Kroehong, A. Saptamongkol, and P. Chindapasirt, "Mechanical properties, microstructure and drying shrinkage of hybrid fly ash-basalt fiber geopolymer paste," *Construction and Building Materials*, vol. 186, pp. 62–70, 2018.
 - [17] R. Si, Q. L. Dai, S. C. Guo, and J. Wang, "Mechanical property, nanopore structure and drying shrinkage of metakaolin-based geopolymer with waste glass powder," *Journal of Cleaner Production*, vol. 242, Article ID 118502, 2019.
 - [18] I. Khan, T. Xu, A. Castel, R. I. Gilbert, and M. Babae, "Risk of early age cracking in geopolymer concrete due to restrained shrinkage," *Construction and Building Materials*, vol. 229, Article ID 116840, 2019.
 - [19] D. S. Perera, O. Uchida, E. R. Vance, and K. S. Finnie, "Influence of curing schedule on the integrity of geopolymers," *Journal of Materials Science*, vol. 42, no. 9, pp. 3099–3106, 2007.
 - [20] R. J. Thomas, D. Lezama, and S. Peethamparan, "On drying shrinkage in alkali-activated concrete: improving dimensional stability by aging or heat-curing," *Cement and Concrete Research*, vol. 91, pp. 13–23, 2017.
 - [21] Y. Ling, K. Wang, and C. Fu, "Shrinkage behavior of fly ash based geopolymer pastes with and without shrinkage reducing admixture," *Cement and Concrete Composites*, vol. 98, pp. 74–82, 2019.
 - [22] P. Kamhangrittirong, P. Suwanvitaya, W. Witayakul, P. Suwanvitaya, and P. Chindapasirt, "Factors influence on shrinkage of high calcium fly ash geopolymer paste," *Advanced Materials Research*, vol. 610, pp. 2275–2281, 2013.
 - [23] K. Mermerdaş, Z. Algin, and Ş Ekmen, "Experimental assessment and optimization of mix parameters of fly ash-based lightweight geopolymer mortar with respect to shrinkage and strength," *Journal of Building Engineering*, vol. 31, Article ID 101351, 2020.
 - [24] C. Rıdtirud, P. Chindapasirt, and K. Pimraksa, "Factors affecting the shrinkage of fly ash geopolymers," *International Journal of Minerals, Metallurgy, and Materials*, vol. 18, no. 1, pp. 100–104, 2011.
 - [25] P. Duan, C. Yan, W. Luo, and W. Zhou, "Effects of adding nano-TiO₂ on compressive strength, drying shrinkage, carbonation and microstructure of fluidized bed fly ash based geopolymer paste," *Construction and Building Materials*, vol. 106, pp. 115–125, 2016.
 - [26] A. Saloni, A. Parveen, and M. Thong, "Enhanced properties of high-silica rice husk ash-based geopolymer paste by incorporating basalt fibers," *Construction and Building Materials*, vol. 245, Article ID 118422, 2019.
 - [27] A. Noushini, M. Hastings, A. Castel, and F. Aslani, "Mechanical and flexural performance of synthetic fibre reinforced geopolymer concrete," *Construction and Building Materials*, vol. 186, pp. 454–475, 2018.
 - [28] Z. Xu, J. Yue, G. Pang, R. Li, P. Zhang, and S. Xu, "Influence of the activator concentration and solid/liquid ratio on the strength and shrinkage characteristics of alkali-activated slag geopolymer pastes," *Advances in Civil Engineering*, vol. 2021, Article ID 6631316, 11 pages, 2021.
 - [29] J. Xu, A. Kang, Z. Wu, P. Xiao, and Y. Gong, "Effect of high-calcium basalt fiber on the workability, mechanical properties and microstructure of slag-fly ash geopolymer grouting material," *Construction and Building Materials*, vol. 302, Article ID 124089, 2021.
 - [30] S. Saxena and A. R. Tembhurkar, "Developing biotechnological technique for reuse of wastewater and steel slag in bio-concrete," *Journal of Cleaner Production*, vol. 229, pp. 193–202, 2019.
 - [31] X. Guo and G. Xiong, "Resistance of fiber-reinforced fly ash-steel slag based geopolymer mortar to sulfate attack and

- drying-wetting cycles,” *Construction and Building Materials*, vol. 269, Article ID 121326, 2021.
- [32] C. Seneviratne, C. Gunasekara, D. Law, S. Setunge, and D. Robert, “Creep, shrinkage and permeation characteristics of geopolymer aggregate concrete: long-term performance,” *Archives of Civil and Mechanical Engineering*, vol. 20, no. 4, pp. 1–15, 2020.
- [33] S. Samal and I. Blanco, “An application review of fiber-reinforced geopolymer composite,” *Fibers*, vol. 9, no. 4, p. 23, 2021.

Research Article

Impacts of Addition of Palm Kernel Shells Content on Mechanical Properties of Compacted Shale Used as an Alternative Landfill Liners

Clement A. Amagu ¹, Beatrice O. Enya,² Jun-ichi Kodama,¹ and Mostafa Sharifzadeh³

¹Rock Mechanics Laboratory Graduate School of Engineering, Hokkaido University, Kita-ku 0608628, Sapporo, Japan

²Department of Geology, University of Ibadan, Ibadan, Nigeria

³Key Laboratory of Ministry of Education for Safe Mining of Deep Metal Mines, Northeastern University, Shenyang 110819, China

Correspondence should be addressed to Clement A. Amagu; amaguclementglk@gmail.com

Received 3 November 2021; Revised 7 January 2022; Accepted 17 January 2022; Published 21 February 2022

Academic Editor: Md. Akter Hosen

Copyright © 2022 Clement A. Amagu et al. This is an open access article distributed under the Creative Commons Attribution License, which permits unrestricted use, distribution, and reproduction in any medium, provided the original work is properly cited.

The design of landfill liners of waste disposal to reduce migration of leachate containment, low swelling, and shrinkage and ensure sufficient shear strength to resist bearing capacity and instability of the landfill has been a major challenging task to landfill engineers. Over the last decade, there has been an increase in research on the stability of substitute materials as liners that are environmentally friendly, cost-effective, and socially beneficial due to the growing cost of traditional landfill liners. In this regard, geotechnical tests were conducted on shale samples treated with 0–12% (increment of 2%) of palm kernel shell ash (PKSA) and pulverized palm kernel shell (PPKS) to evaluate their suitability as alternative landfill liners using West African Standard (WAS) and Modified AASHTO Standard (MAS) for compactive energy. The shale has more percentage of finer fractions, thus classified as poorly graded soil (A-7-5). The Atterberg limit tests show that liquid and plastic limits decrease with an increase in plasticity index as the percentage of addition of PKSA and PPKS content increases. The results also established that the maximum dry density (MDD), volumetric shrinkage strain (VSS), and hydraulic conductivity significantly decrease, while the optimum moisture content (OMC) increases as the content of PKSA and PPKS increases at both compactive efforts. The maximum strengths of 380.30 and 448.70 kPa were obtained at 4% of both stabilizers. From the results, it can therefore be concluded that the treated compacted shale meets the condition of the suitability of landfill liners. Furthermore, with the use of industrial and agricultural wastes such as palm kernel shells as replacement materials with natural soils used as liners, significant social, economic, and environmental impact of landfills and reduction in wastes can be achieved. The research results can provide a reference for similar conditions of landfill liners worldwide.

1. Introduction

To date, there is a global increase in waste generation as a result of growth in population and income, changing lifestyles, increase in industrialization and use of disposable materials, excessive packaging of items, and consumer's habits. Daily, domestic and industrial wastes are generated in large quantities and the safe disposal of these waste materials is increasingly becoming a major concern around the world. Currently, waste is becoming more serious than ever as there are lots of environmental problems related to its management.

Further, landfilling of wastes has been the final stage of many municipal wastes in many countries [1, 2]. It confines the waste to the available area, thereby reducing the waste to the minimum practical volume. Despite that, the problem of waste management is still a big social and environmental issue complying with the shortage of landfill capacity, a result of doubt to the environmental soundness of landfills and reject to unpleasant landfills [3], mainly because the waste in a landfill often reacts to release leachate, which poses a threat to the surrounding environment and humans [3]. Hence, the environmental impacts of landfills are

numerous, including the contamination of surface water and groundwater by leachate, pollution of soil by direct contact with wastes or leachate percolation, spreading of diseases and foul odours in landfill areas, and uncontrolled release of methane by anaerobic decomposition of deposited wastes [4, 5].

To overcome these problems, waste disposal of landfills should be packaged and placed in an underground vault surrounded by thick liners to provide a certain degree of redundancy for leachate containment [1]. In particular, Kayabaly [6] and Cazaux and Didier [7] reported that liners are required to minimize pollutant migration over the long term, low swelling and shrinkage, and resistance to shearing. As a matter of fact, landfill liners must have a large attenuation capacity to prevent seepage of leachate into the surrounding groundwater and subsequent contamination of the groundwater system [7].

For these reasons, liners must be designed to accommodate the landfill settlement, lower the hydraulic conductivity, and have sufficient shear strength to resist bearing capacity and slope failure [8]. Over the last decades, compacted clay liners, bentonite, or bentonite-bearing mixtures have been used extensively in constructing landfills due to their cost-effectiveness and large capacity of attenuation [6, 8]. In spite of that, these barriers contain appreciable swelling clay minerals, e.g., smectites; thus, they have high shrinkage and high expansive potential causing instability problems [9]. Additionally, geosynthetic clay liners, geomembranes, geonets, and geotextiles are often used to construct liners in developed countries, even though they are more expensive [10–12].

From the above discussions, it can be said that the sustainability of clay liners may be significantly affected by their long-term sealing capabilities, resulting from the hydraulic conductivity after compaction, swell-shrinkage characteristics, resistance to cyclic drying and rewetting, and desiccation cracking [1]. Notwithstanding, the aforementioned liners are very uncertain in the design of landfills in low- and medium-income countries, such as Nigeria, mainly because there might be a possibility of social unacceptability and lack of technological know-how to achieve the desired purposes. Therefore, the stabilization of natural soils used as liners with recycled or waste materials, such as oil palm ash, shell and clinker, rice husk ash [13], coconut shells [14], iron ore tailings, and blast furnace slags [15], has been a way to forward alternative solutions in the landfill engineering to ensure the significant social, economic, and environmental impact of landfills, consequently ensuring that the high mechanical strength, impermeability to water, stability, and great durability of the landfills are also achievable. Therefore, the investigations of the stabilizing potential of industrial and agricultural waste in soils have become the focus of research globally. Hence, the need for the use of palm kernel shell, which is relatively inexpensive and readily available locally through the burning and grinding of palm kernel shell as a stabilizing agent to enhance the mechanical properties of natural soils used as landfill liner, has become very significant [16].

In Nigeria, approximately 64% of palm kernel shell is generated as waste per year [17]. The palm kernel shell is

regarded as waste from oil processing, which is either burnt to supply energy at palm oil mills or left in piles to compost. This in turn pollutes the environment. Thus, it is greatly required to consider the use of palm kernel shell in improving the engineering properties of natural soil liners in landfill sites. Thus, the main aim of this study is to evaluate the suitability of compacted shale treated with palm kernel shell ash (PKSA) and pulverized palm kernel shell (PPKS) as an alternative material for landfill liners. The hydraulic conductivity, swell-shrink characteristics, and geotechnical properties of the compacted shale samples treated with the two selected stabilizers were examined using West African Standard (WAS) and Modified AASHTO Standard (MAS) for compactive efforts to ascertain their potential usage as an engineered barrier in waste containment applications. This approach can also serve as an alternative disposal means of palm kernel shells in Nigeria.

2. Environmental Issues of Open Dumping Site in Nigeria

Over the decades, prevention, reuse, recycling, recovery, and disposal of waste in the practice of collecting, treating, and managing waste in Nigeria have been a challenging task as a result of the unchecked rapid growth of urban population, unplanned urbanization, changing lifestyles, increase in the use of disposable materials, lack of training in modern solid waste management practices, lack of awareness on the dangers of unsustainable waste management practices, poverty, illiteracy, and poor government policies [1, 18]. In Nigeria, the generation, disposal, or management of waste has proved to be a major environmental and public health issue. Waste is often dumped on the major streets and several open spaces and left unattended for long periods (Figure 1), which encroach on the roads, thereby limiting road users access, generate serious air pollution issues, constitute a significant nuisance when blown over by the wind, and distort the aesthetic view of the metropolis [19]. Environmental and health issues arising from the unsustainable management of those open dumping waste sites have consequently resulted in runoff of toxic compounds into surface water and groundwater, which contaminates the water due to the percolation of leachate [20]. To overcome this problem, there is a need for sophisticated landfill technology to ensure that the waste is disposed of in a landfill, which is the simplest, cheapest, and most cost-effective method of disposing of waste [21]. Thus, the utilization of waste such as palm kernel shells to stabilize natural soil used as landfill liners is a priority because it is not only a cost-effective and already available material but also an alternative disposal means of palm kernel shells in Nigeria.

3. Geological Characteristics of the Study Area

The study area is located at Nguzu Edda in Afikpo South Local Government Area, Ebonyi State. Geographically, the area is bounded by longitude 7°49' E to 7°54' E and latitude 5°45' N to 5°50' N, as depicted in Figure 2. The area lies within the Afikpo Subbasin, which is regarded as the



FIGURE 1: Picture of the open dumping site at Nguzu Edda.

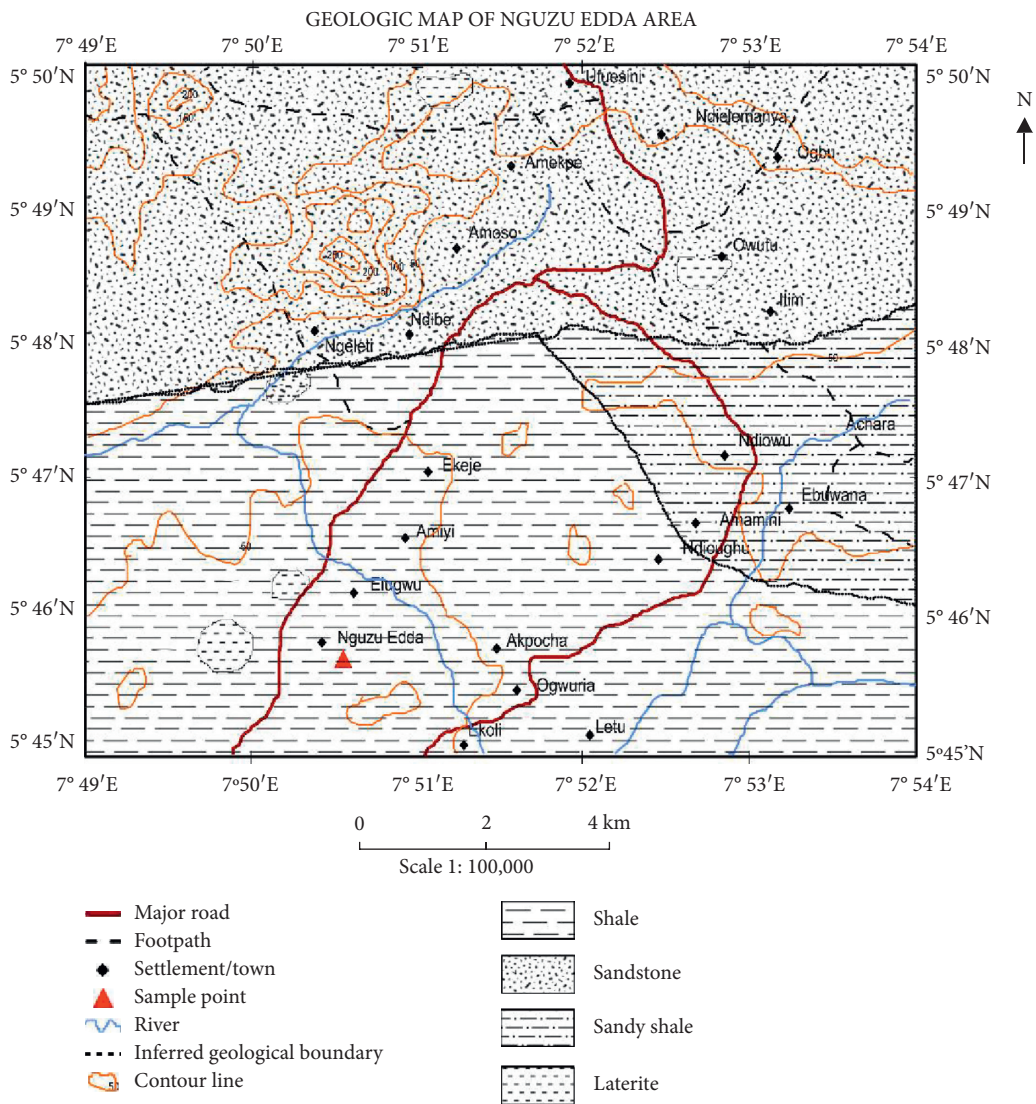


FIGURE 2: Geological map of the study area.

southeastern depression of the Anambra Basin [22]. Stratigraphically, the study area is predominantly composed of the sediments of the Upper Campanian-Maastrichtian identified as the Afikpo sandstone, Nkporo, and Mamu Formation [23], which consists mainly of fine to very coarse ferruginized sandstone and shale with intercalations of sandstone and shale and laterite. The shale is soft and there is a precipitate of ironstone and sandstone interbeds on the shale. It has a thick pile of clay minerals, most likely to be kaolinite. The laterite of the area has been used for construction purposes mostly as fillings, both as subgrade for road and pavement construction and as filling in roads, buildings, and dam fillings.

4. Materials and Methods

The shale employed for this study were taken along Nguzu Edda road within longitude $7^{\circ}50' 38.3''$ E and latitude $5^{\circ}45'48.29''$ N using both disturbed and undisturbed sampling methods at a square meter of 3×3 at 1 m depth. The palm kernel shells (PKS) were sourced from the local milling farm at Ugwuegu village. It was sorted and air-dried sufficiently. To generate palm kernel shell ash (PKSA), some of the palm kernel shells were burnt in a blast furnace to about 900°C , whereas others were grounded as pulverized palm kernel shell (PPKS). The air-dried samples were sieved through a sieve aperture of $4.76 \mu\text{m}$, while the palm kernel shell contents were sieved through a sieve aperture of $75 \mu\text{m}$. Index properties of both the natural and shale-palm kernel shell mixtures were determined in accordance with British standard BS 1377 [24]. Two compaction energy levels, West African Standard (WAS) and Modified AASHTO Standard (MAS), were used for comparison purposes. The engineering tests such as optimum moisture content (OMC), maximum dry density (MDD), volumetric shrinkage strain (VSS), compressive strength, and hydraulic conductivity (k) were carried out at the Soil Laboratory, Department of Geology, Federal University of Technology, Akure, Nigeria, to determine the suitability of the treated samples as landfill liners. The Atterberg limits, grain size distribution test, specific gravity, and natural moisture content tests were carried out on the natural shale samples at the laboratory of the Civil Engineering Department, University of Ibadan. The sieved air-dried soil samples were batched using 0, 2, 4, 8, and 12% PKSA and PPKS by dry weight. Rigid wall permeameter under falling head condition was used for hydraulic conductivity, the samples for compressive strength test were cured for 3 days prior to the test, while the samples for drying shrinkage test were cured for a day, thereafter, extruded, and cured for a period of 30 days. The measurements of diameters and heights for each specimen were taken with the aid of a vernier caliper of accuracy of ± 0.03 mm.

5. Results and Discussion

5.1. Analysis of the Index Properties of the Untreated Shale. The results of index tests such as Atterberg limits (liquid and plastic limits), particle size distribution, natural moisture

content, specific gravity test, compressive strength, hydraulic conductivity, and volumetric shrinkage strain carried out on the shale sample are presented in Table 1 for comparison with the treated shale samples as described in the later sections. Figure 3 shows the grading curve of the particle size distribution of the shale. As can be seen from Figure 3, there is clear evidence that the shale had more fine fractions than the coarse fractions. From Table 1 and Figure 3, the results showed that the shale samples have more percentage of finer fractions that pass 0.075 mm sieve, <35% with LL of 56.60% and PI of 21.29%. Overall, the shale has significant constituent materials, mainly clay, silty clay, gravel, and sand. From this point of view, the shale was classified as poorly graded soil (A-7-5) and MH according to the American Association of State Highway Transportation Officials (AASHTO M 145) [25] and Unified Soil Classification System (USCS), respectively. Figure 4 shows the Casagrande chart of the shale, which indicates that the samples are widely distributed in the region of high plasticity below the A line of the Casagrande chart. The high plasticity could be explained by the presence of the fine fraction, which tends to reduce the interconnected pores. Consequently, the high plasticity index can reduce hydraulic conductivity, implying that the shale can withstand volumetric shrinkage on drying and exhibit a low to medium swelling potential when wet. It is worth noting that the fine fractions are expected to help in the workability, while the coarse fractions enhance the mechanical strength of the shale. Hence, the shale is expected to resist an increase in hydraulic conductivity that may be caused by the contaminant and also retard the migration of contaminants through sorption [26].

5.2. Atterberg Limits Test. Atterberg limit tests were conducted to determine the liquid limit (LL), plastic limit (PL), and plasticity index (PI) of shale treated with 0, 2, 4, 8, and 12% of palm kernel shell ash (PKSA) and pulverized palm kernel shell (PPKS) by dry weight of the samples. Figure 5 shows the effects of the addition of PKSA and PPKS on the Atterberg limits of the samples. From Figure 5, it is observed that LL and PL decrease, whereas PI increases almost linearly with an increase in the percentage of addition of PKSA and PPKS content. This demonstrates that the palm kernel shell, either in ash or pulverized, has similar effects on the Atterberg limits of the shale sample.

It can be seen from Figure 5 that the liquid limit (LL) decreases slightly from 56.6 to 53.43% and 56.4% at 0–12% of PPKS and PKSA, respectively. The plastic limit (PL) also decreases slightly from 35.31 to 32.39% and 32.1%, with a corresponding increase in PI from 21.29 to 23.31% and 21.44% at 0–12% of PPKS and PKSA, respectively. The reduction in the LL and plastic limit (PL) of the shale could be explained by the cementitious properties of PKSA and PPKS content, which resulted from the initial flocculation agglomeration between the clay particles present in the shale-PKS mixtures. These aggregation and cementation properties of the shale-PKSA and PPKS matrix lead to the closure of interconnected pores, thereby decreasing the void ratio.

As seen in Figure 5, the results demonstrate that the values of LL and PL of the treated shale sample are higher

TABLE 1: Geotechnical properties of the untreated shale.

Parameters	Values
Natural moisture content (%)	20.00
Specific gravity (g)	2.24
Liquid limit, LL (%)	56.60
Plastic limit, PL (%)	35.31
Plasticity index, PI (%)	21.29
AASHTO classification	A-7-5
Unconfined compressive strength, UCS (kPa)	375.10 ^a , 426.20 ^b
Hydraulic conductivity (m/s)	5.24 × 10 ^{-7a} , 0.43 × 10 ^{-7b}
Volumetric shrinkage strain, VSS (%)	14.93 ^a , 16.03 ^b
Maximum dry density (Mg/m ³)	1.45 ^a , 1.51 ^b

^aResults from West African Standard (WAS). ^bResults from Modified AASHTO Standard (MAS).

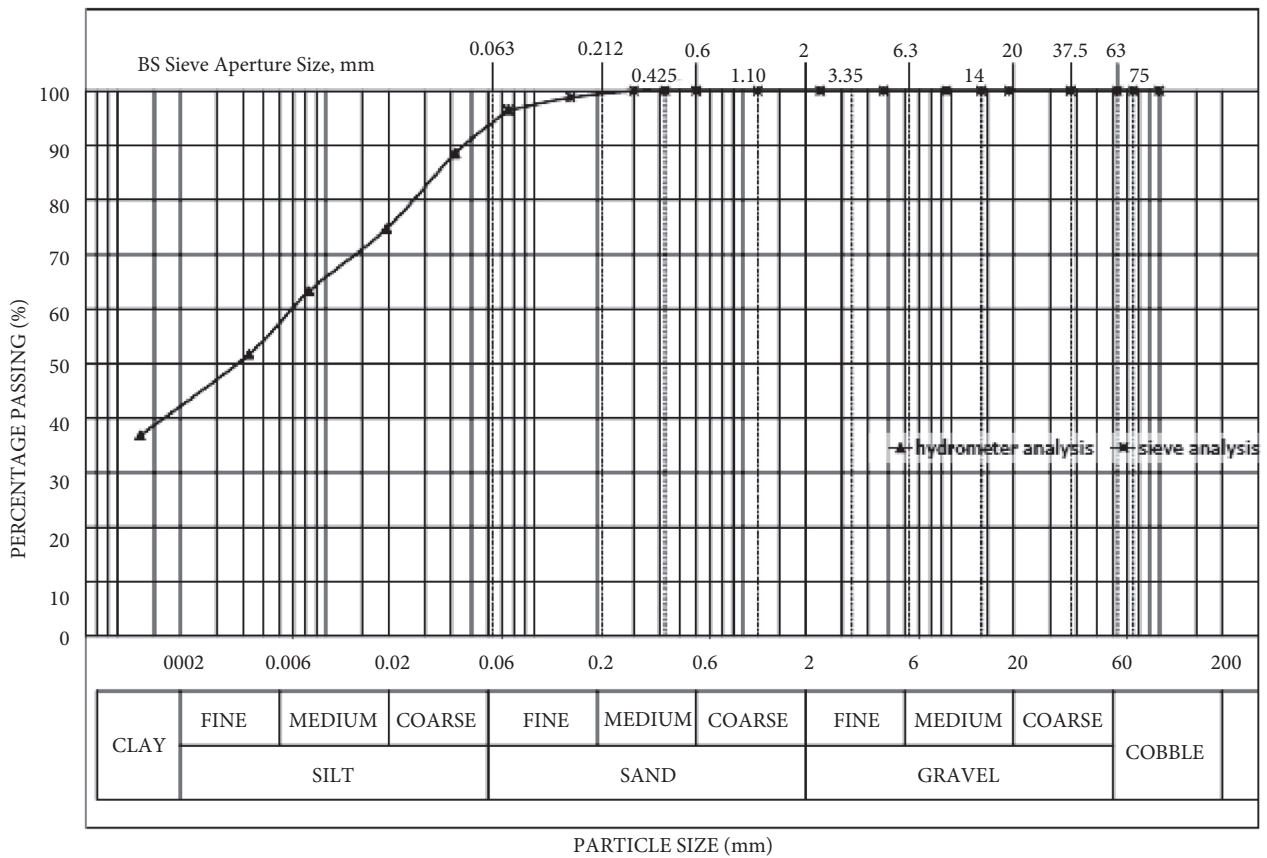


FIGURE 3: The particle size distribution of the sampled shale.

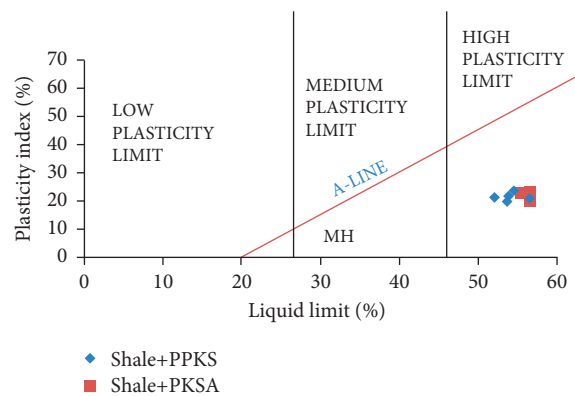


FIGURE 4: The Casagrande chart of the sampled shale.

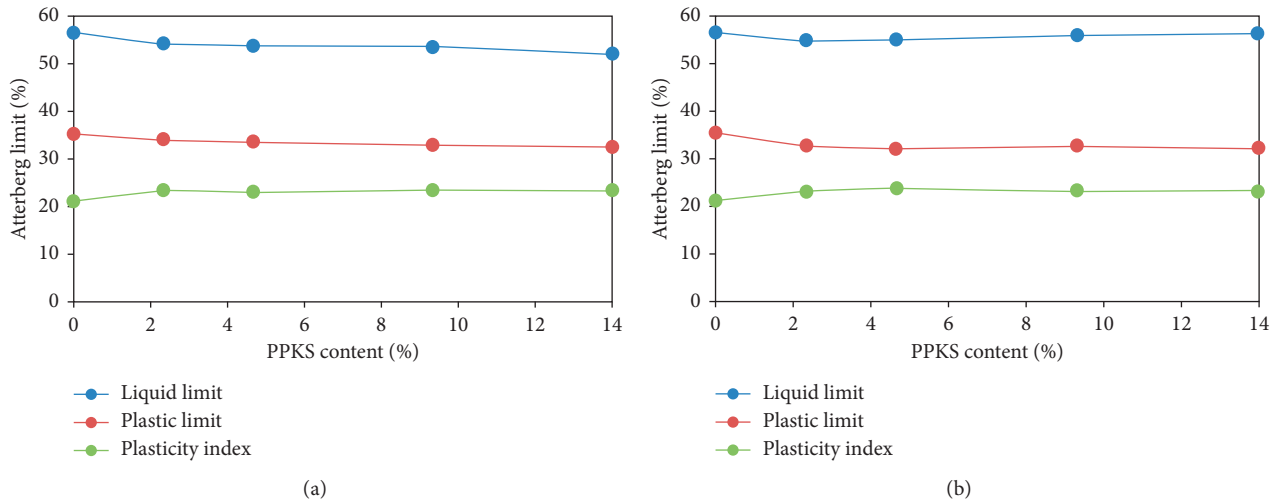


FIGURE 5: Atterberg limits versus PPKS and PKSA for the treated shale.

than $LL \geq 30\%$ and $PL \geq 15\%$ as recommended by TCEQ [27]. Significantly, the plasticity index of the treated shale sample is also higher than 7%, therefore meeting the condition of the suitability of soils as landfill liners (Hamdi and Srasra [28]).

5.3. Compaction Characteristics. Figure 6 shows the maximum dry density (MDD) of shale samples containing 0%, 2%, 4%, 8%, and 12% of PPKS and PKSA. As can be seen from Figure 6, there is clear evidence that MDDs of the soil-PPKS and PKSA matrix compacted at the MAS and WAS compactive efforts decrease almost linearly with an increase in the percentage of addition of the stabilizers. Significantly, the MDD of each stabilizer falls within a small range for each compactive energy. In the case of MAS compactive energy, the MDD at 0% of PKSA and PPKS content was 1.51 Mg/m^3 , which increased to 1.53 and 1.51 Mg/m^3 (at 2% of both stabilizers), respectively, and then decreased constantly as the content of PKSA increases. Conversely, the MDD of the treated shale decreases constantly with an increase in the stabilizer content for WAS compactive energy. Figure 7 shows the relationship between the optimum moisture content (OMC) and PKSA and PPKS of the compacted shale samples. From Figure 7, it can be seen that the results exhibited general trends of increase in OMC with an increase in the percentage of addition of PPKS and PKSA for both compactive energies. The optimum moisture content (OMC) for WAS ranges from 20.7 (at 0% of the stabilizers) to 33.3 and 26.0% at 12% of PKSA and PPKS, respectively, whereas the OMC for MAS ranges from 19.92% (at 0% of the stabilizers) to 24.68 and 24.51% at 12% of PKSA and PPKS, respectively. However, WAS compactive effort shows a more pronounced increase in OMC for both stabilizers.

As described above, the initial increase in MDD could be attributed to the pozzolanic effect of the stabilizers and probably due to the initial flocculation and agglomeration of shale particles caused by a possible cation exchange reaction between the shale-PKSA and PPKS matrix. Thus, these

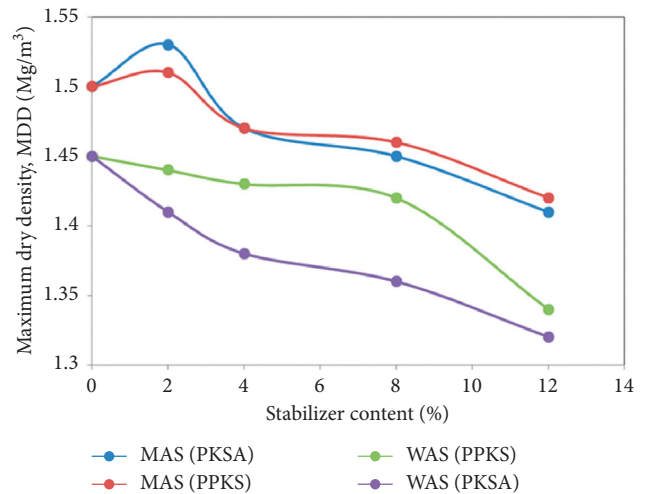


FIGURE 6: Maximum dry density (MDD) versus PKSA and PPKS for the treated shale at MAS and WAS methods.

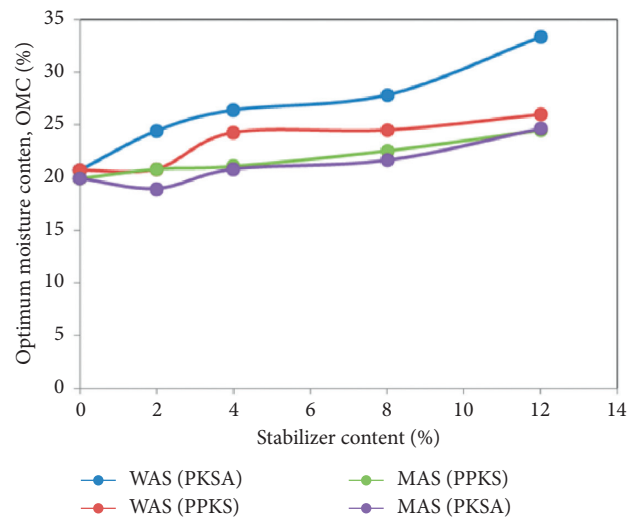


FIGURE 7: Optimum moisture content (OMC) versus PKSA and PPKS for the treated shale at MAS and WAS methods.

effects lead to an increase in volume and a decrease in dry density. The constant decrease in MDD after 2% addition of the stabilizers is owing to the effects of coating the shale sample with PKSA and PPKS, which consequently increases the voids and density, as confirmed by Ako and Yusuf [16]. It was also possible due to the low specific gravity of PKSA and PPKS of 1.19 and 1.22, respectively, which may have substituted the high absorption rate of the soil and the addition of finer particles, which requires more water to hydrate [29, 30].

The corresponding increase in OMC could be a result of an increase in the surface area of particles caused by an increase in the volume of PKSA and PPKS content in the mixture, which required more water to lubricate the entire mix matrix to enhance compaction, due to hydration reactions of the matrix as explained by Ako and Yusuf [16]. The increase in OMC and its corresponding decrease in MDD with the increase in the percentage of addition of the stabilizers have significant geotechnical effects as compaction can easily be achieved with wet shale. Consequently, there is less need for the shale to be dried to lower moisture content prior to compaction in the landfill. However, a mixture of 2% of the stabilizers, mostly at MAS compactive effort, satisfied the criteria for landfill liner as Amadi et al. [31] and Tunçan et al. [32] recommended soils with MDD $\geq 1.50 \text{ Mg/m}^3$ to be applied as landfill liner.

5.4. Hydraulic Conductivity (k). It is well known that when clay-shale soil is used as liners subjected to water pressure in the landfills, it causes an increase in hydraulic conductivity as time passes, which in turn may lead to instability as a result of the excessive expansion. For this reason, the choice of adequate natural soil with a hydraulic conductivity of the order of 10^{-7} – 10^{-9} ms^{-1} for attenuation is needed for the construction of a landfill [1]. Therefore, the hydraulic conductivity of the shale samples treated with PKSA and PPKS compacted using the WAS and MAS compactive energy was determined based on ASTM D5084-1991 procedures as described by Hamdi and Srasra [28]. The hydraulic conductivity k was calculated using the following equation:

$$k = 2.303 \frac{aL}{At} \log \frac{h_1}{h_2}, \quad (1)$$

where k is the hydraulic conductivity (ms^{-1}), A is the cross-sectional area of the specimen (m^2), a is the cross-sectional area of the standpipe (m^2), L is the length of the specimen (m), and h is the head difference (m), at time t .

Figure 8 shows the relationship between the hydraulic conductivity of compacted shale samples and varying percentages of PKSA and PPKS content. As presented in Table 1, the hydraulic conductivities of the untreated sample compacted by WAS and MAS compactive energy were $5.24 \times 10^{-7} \text{ m/s}$ and $2.43 \times 10^{-7} \text{ m/s}$, respectively. In contrast, the hydraulic conductivity of the shale samples treated with PKSA ranged from 1.51×10^{-7} at 2% to $1.25 \times 10^{-7} \text{ m/s}$ at 12% under WAS and 3.91×10^{-7} at 2% to $9.91 \times 10^{-8} \text{ m/s}$ at 12% for MAS. In contrast, the hydraulic conductivity of the

compacted shale samples treated with PPKS varies from 2.05×10^{-7} at 2% to $1.18 \times 10^{-7} \text{ m/s}$ at 12% for WAS and 1.64×10^{-7} at 2% to $8.47 \times 10^{-8} \text{ m/s}$ at 12% for MAS.

As shown in Figure 8, the hydraulic conductivity of the samples treated with PPKS decreases gradually with an increase in the percentages of the stabilizer content. The decrease in the hydraulic conductivity could be explained by reducing the pore size. Conversely, the hydraulic conductivity of the samples treated with PKSA stabilizer increased slightly higher than that of untreated shale sampled at 2% for MAS and 4% for WAS. These slight increases may result from the porous nature of the PKSA particles, which in turn lead to a high specific surface, consequently resulting in the adsorption of a large number of hydrated cations and water molecules, thereby contributing to the increase in hydraulic conductivity. Moreover, the excessive PKSA content can change the soil matrix, which also can cause an increase in flocculation, as established by Osinubi and Eberemu [15]. It can also be seen that the treated sample (Figure 8) has lower values of hydraulic conductivity than those of the untreated sample, as presented in Table 1. As seen in Figure 8, the results demonstrate that the hydraulic conductivity of treated samples with 4% of the PPKS stabilizer and above falls within $\leq 1 \times 10^{-7} \text{ ms}^{-1}$ [1]; therefore, it meets the condition of the suitability of soils as landfill liners. This proves that the addition of PKS to the soil used as a landfill liner will resist an increase in the hydraulic conductivity caused by contaminants, as it positively influences the suitability of the soil as a landfill liner. Moreover, it functions as an attenuating layer enabling the leachate to percolate slowly downwards, simultaneously undergoing attenuation by precipitation, adsorption, and exchange processes within the landfill [26].

5.5. Compressive Strength of the Treated Shale. The standard uniaxial compression tests were performed on shale samples containing 0%, 2%, 4%, 8%, and 12% of PPKS and PKSA cured for 3 days to determine the compressive strength of the treated shale using West African Standard (WAS) and Modified AASHTO Standard (MAS) compactive energy level. The relationship between the compressive strength of the shale and the percentage of addition of PPKS and PKSA content is shown in Figure 9. Figure 9 shows that the strength of the compacted shale was enhanced by adding 4% of PKSA and PPKS contents and a further increase in the addition of PPKS and PKSA contents beyond 4% tends to reduce the strength of the compacted samples steadily. It is also observed, in Figure 9, the strengths of the treated shale compacted at MAS were generally 50 times greater than those of the WAS. Therefore, it is noted that the maximum strengths of 380.40 and 448.70 kPa were recorded at 4% of PKSA with MAS and WAS compactive efforts, respectively. The subsequent increase in the strength of the treated shale at 4% can be attributed to the pozzolanic effect of the PKSA and PPKS in which the lime provides a conducive environment for the dissolution of silicates and aluminates in the soil, hence reacting with Ca^{+2} cations to form the cementation process through the hydration process [33]. The

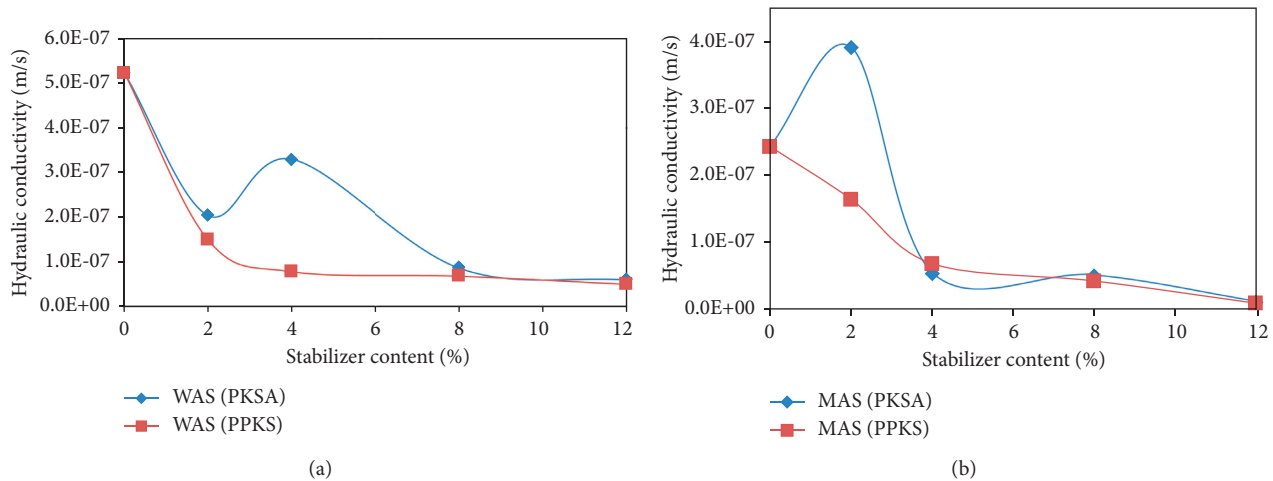


FIGURE 8: Hydraulic conductivity versus PKSA and PPKS for the treated shale at MAS and WAS methods.

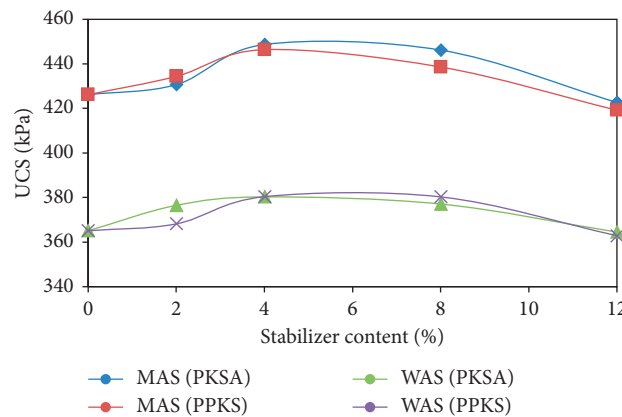


FIGURE 9: Compressive strength of the treated shale samples at MAS and WAS compactive efforts.

decline in the strength by a further increase in the addition of PPKS and PKSA contents is owing to the dilution influence of the stabilizers on the shale, which reduces the pozzolanic reactions. In a related study, the use of a PKSA has proved to be highly effective for cementitious application in the soil, as reported by Ako and Yusuf [16]. Significantly, the result showed that the strength of the treated shale at both compactive efforts is greater than 200 kPa, maximum bearing strength of a landfill liner as proposed by Daniel and Wu [34]; therefore, it satisfied the condition of the suitability of soils as landfill liners.

5.6. Volumetric Shrinkage Strain (VSS). In landfill engineering, it is essential to understand the shrinkage characteristics of liner material in order to control cracks. Desiccation cracking is often a problem in landfills, which in turn can cause an increase in hydraulic conductivity [35]. Therefore, it is essential to prevent excessive shrinkage cracking due to changes in moisture content that occur during the lifetime of the landfill. This is mainly because the presence of cracks in landfill cover provides potential pathways for water infiltration, increasing the generation of

waste leachate and eventually increasing the risk of soil and groundwater contamination, as demonstrated by Miller et al. [35]. To overcome this problem, there is a need to ensure sufficient strength for the stability of engineering projects worldwide [36], including landfills during their construction and operation stage [37].

Consequently, the drying shrinkage test was performed on shale samples with the addition of containing 0%, 2%, 4%, 8%, and 12% of PPKS and PKSA contents. Prior to the test, the shale-PPKS and PKSA matrix were cured for a day, thereafter, extruded from the compaction molds, and then allowed to air-dry for a period of 30 days in the laboratory to assess the effect of desiccation-induced shrinkage on the material used as a landfill liner. The volumetric shrinkage upon drying was measured by extruding cylindrical specimens and then compacted using the WAS and MAS energy levels. Measurements of diameter and heights for each specimen were taken with the aid of a vernier caliper accurate to ± 0.03 mm. The average diameter and heights were used to compute the volumetric shrinkage strain.

Figure 10 describes the effect of PKSA and PPKS as cementitious material on the drying shrinkage of the mixture at 0, 5, 10, 15, 20, 25, and 30 days, respectively. It can be

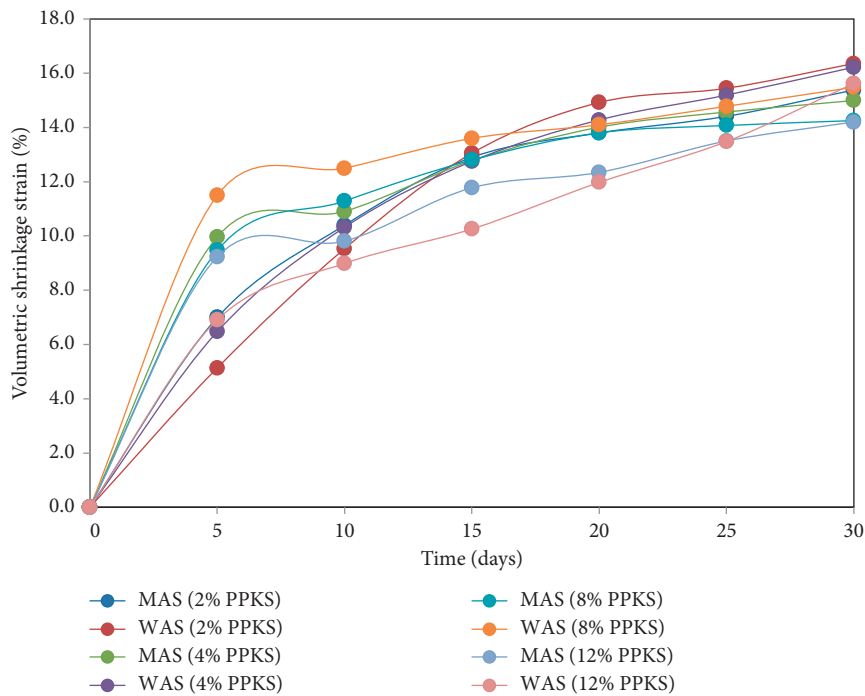
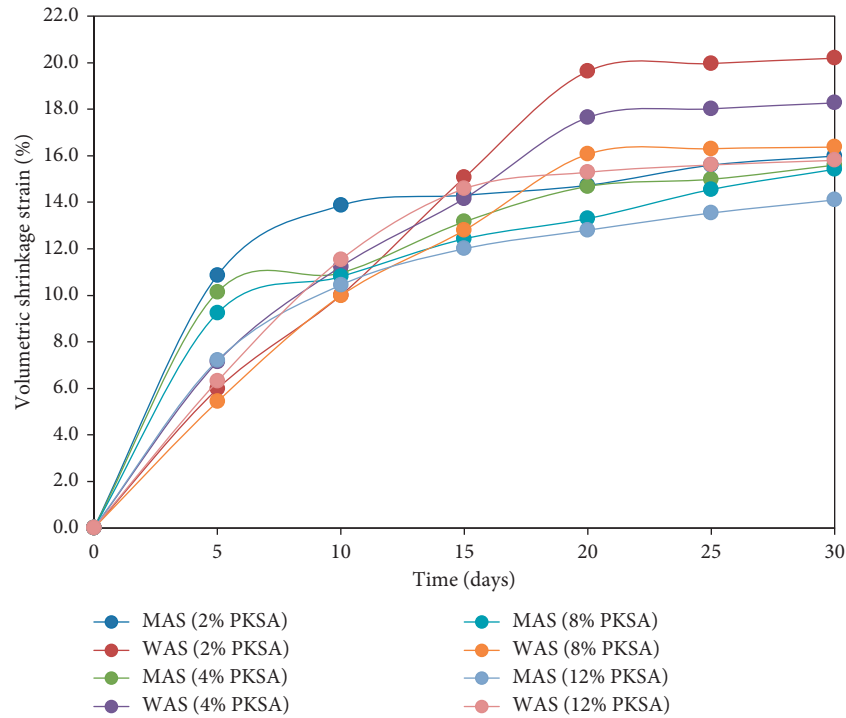


FIGURE 10: Volumetric shrinkage strain with time.

seen that there is a sharp increase in VSS within the first five to fifteen days of drying, mostly with WAS compactive energy level. Thereafter, the trends of increment become more or less constant with time. Figure 11 shows

correlations between mass of the shale-PPKS and PKSA matrix and time at 30 days. As shown in Figure 11, the mass of the treated shale decreases gradually as PKSA and PPKS contents increase with time of drying. The decreases in the

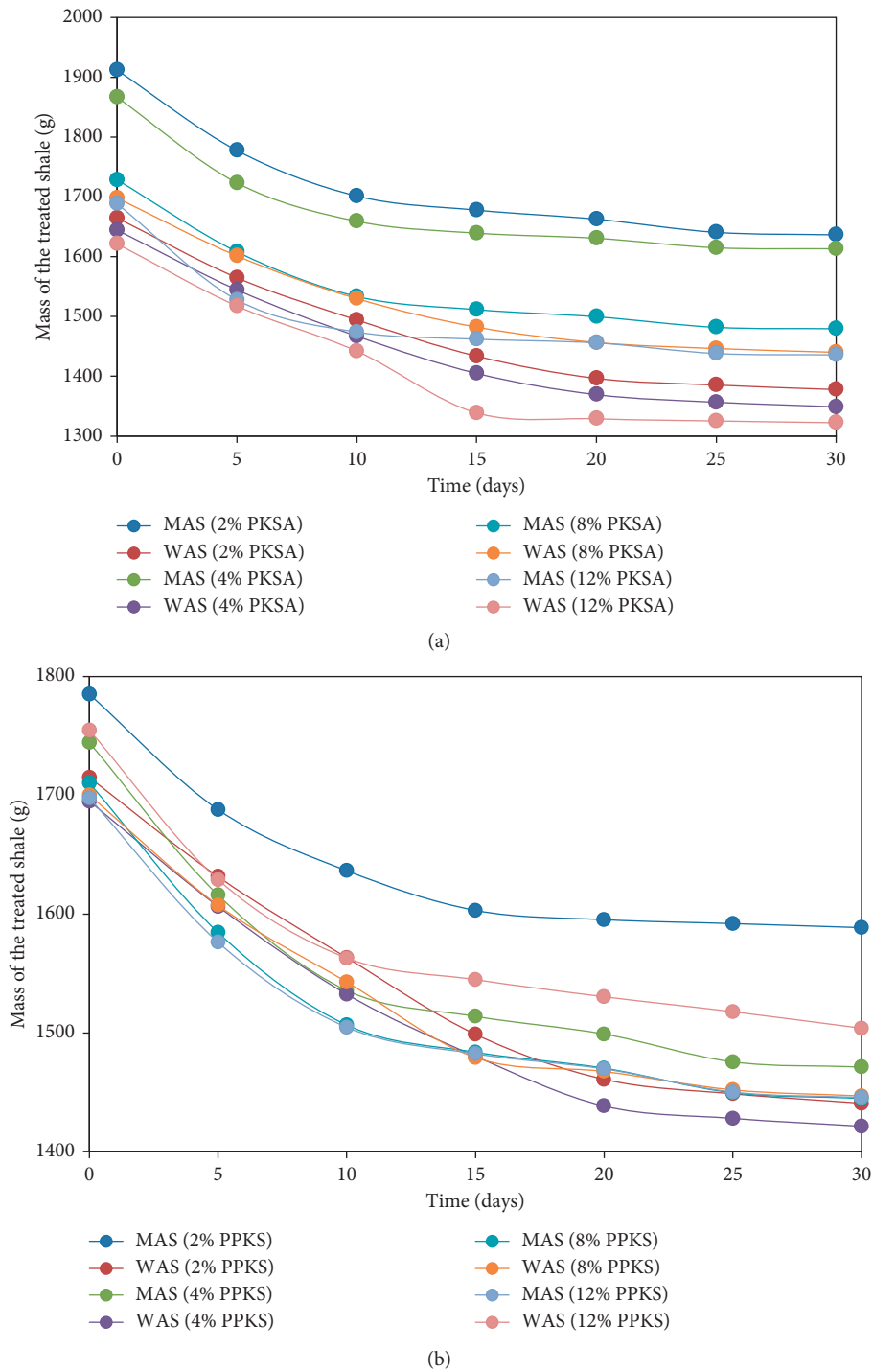


FIGURE 11: Relationship between the mass of the treated shale and time.

trends of mass are similar for each compactive energy level. Clearly, drying shrinkage is proportional to the molding water content.

The relationship between VSS and varying percentages of PKSA and PPKS for the two compactive efforts was shown

in Figure 12. From Figure 12, it can be observed that the shrinkage of the shale decreases with the rising content of PKSA and PPKS. Although the decreasing trends were more clear for MAS compactive effort, the decrease in drying shrinkage is owing to the finer particles of PKSA and PPKS,

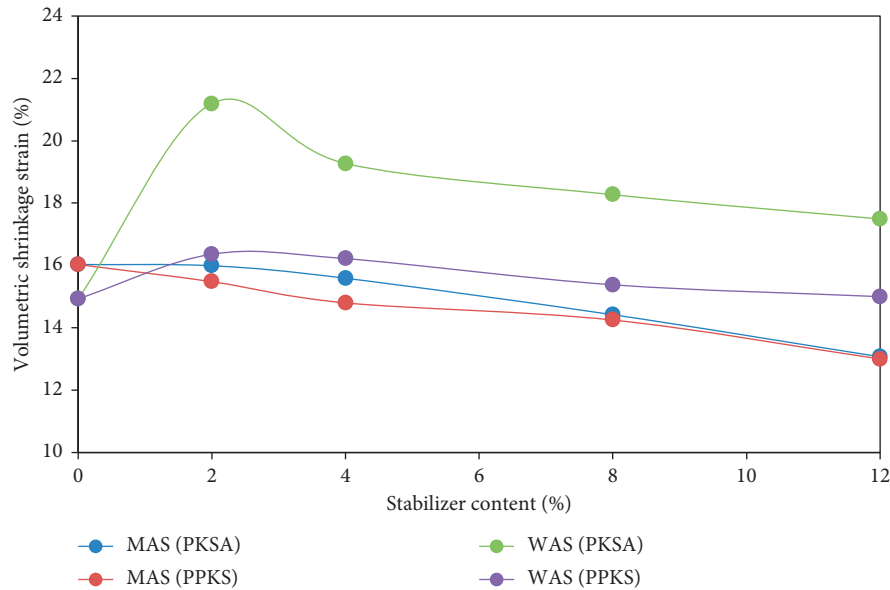


FIGURE 12: Volumetric shrinkage strain of the treated shale at MAS and WAS compactive efforts.

which act as a filler and interlocked the pores, which consequently slow the rate of shrinkage in the treated shale. According to Tay et al. [37], shrinkage decreases as the amount of cement replacement material (such as ash), which builds up the mechanical interlocking in the pores, increases.

6. Conclusions

This study determined the mechanical properties of compacted shale treated with varying percentages of palm kernel shell ash (PKSA) and pulverized palm kernel shell (PPKS) using West African Standard (WAS) and Modified AASHTO Standard (MAS) for compactive efforts to ascertain their stability as landfill liners barrier in waste containment applications. Thus, the following conclusions were drawn from the study:

- (1) From the grain size analysis and the Atterberg limit, the shale was classified as A-7-5, with percentage finer grains, which constituted materials, mainly clay, silty, and sand. The Atterberg limit tests revealed that the liquid limit (LL) and plastic limit (PL) decrease with an increase in plasticity index (PI) as the percentage of addition of PKSA and PPKS content increases.
- (2) The results also revealed that an optimum moisture content (OMC) value increases, whereas the maximum dry density (MDD) and hydraulic conductivity decrease with rising in the percentage of addition of PKSA and PPKS content for both compactive efforts.
- (3) The drying shrinkage of the treated shale samples reduced with an increase in the percentage of addition of PKSA and PPKS content. Overall, the experimental results infer that the blend of the compacted shale-PPKS matrix, mostly 4% of the stabilizer at MAS compactive effort, satisfied the

condition of the suitability of soils as landfill liners for both compactive energy levels. Therefore, it can be concluded that the addition of 4% of PPKS to the compacted shale sample is the optimum replacement. Moreover, the addition of palm kernel shells to the compacted shale used as landfill liners can also serve as alternative means of reducing wastes generated from the local milling industry to ensure the significant social, economic, and environmental impact of the waste.

Data Availability

The data used in supporting the results of our study are included within the manuscript.

Conflicts of Interest

The authors declare that there are no conflicts of interest regarding the publication of this article.

Acknowledgments

The authors wish to acknowledge the efforts of the staff at the Laboratory of Civil Engineering Department, University of Ibadan and Soil Laboratory, Department of Geology, Federal University of Technology, Akure, Nigeria, in conducting the experiments for this study.

References

- [1] A. Allen, "Containment landfills: the myth of sustainability," *Engineering Geology*, vol. 60, pp. 3–19, 2000.
- [2] J. Wagner, "Incentivizing sustainable waste management," *Ecological Economics*, vol. 70, no. 4, pp. 585–594, 2011.
- [3] M. El-Fadel, E. Bou-Zeid, W. Chahine, and B. Alayli, "Temporal variation of leachate quality from pre-sorted and





- bated municipal solid waste with high organic and moisture content,” *Waste Management*, vol. 22, no. 3, pp. 269–282, 2002.
- [4] M. A. Warith and R. N. Yong, “Landfill leachate attenuation by clay soil,” *Hazardous Waste and Hazardous Materials*, vol. 8, no. 2, pp. 127–141, 1991.
- [5] U. N. Ngoc and H. Schnitzer, “Sustainable solutions for solid waste management in Southeast Asian countries,” *Waste Management*, vol. 29, no. 6, pp. 1982–1995, 2009.
- [6] K. Kayabaly, “Engineering aspects of a novel landfill liner material: bentonite amended natural zeolite,” *Engineering Geology*, vol. 46, pp. 105–114, 1997.
- [7] D. Cazaux and G. Didier, “Field evaluation of hydraulic performances of geosynthetic clay liners by small and large-scale tests,” *Geotextiles and Geomembranes*, vol. 18, no. 2–4, pp. 163–178, 2000.
- [8] E. A. M. Yahia, A. A.-R. Amer, Y. A. L.-A. Mohammed, Q. Ahmed, and Al-R. Abdul-Hamid, “Assessment of crushed shales for use as compacted landfill liners,” *Engineering Geology*, vol. 80, pp. 271–281, 2005.
- [9] C. Di Maio, L. Santoli, and P. Schiavone, “Volume change behaviour of clays: the influence of mineral composition, pore fluid composition and stress state,” *Mechanics of Materials*, vol. 36, no. 5, pp. 435–451, 2004.
- [10] L. A. Guerrero, G. Maas, and W. Hogland, “Solid waste management challenges for cities in developing countries,” *Waste Management*, vol. 33, no. 1, pp. 220–232, 2013.
- [11] M. K. Widomski, W. Stepniewski, and R. Horn, “Sustainability of compacted clays as materials for municipal waste landfill liner,” *Middle Pomeranian Scientific Society of the Environment Protection*, vol. 18, pp. 439–454, 2016.
- [12] D. Q. Zhang, S. K. Tan, and R. M. Gersberg, “Municipal solid waste management in China: status, problems and challenges,” *Journal of Environmental Management*, vol. 91, no. 8, pp. 1623–1633, 2010.
- [13] M. O. A. Mtalib and G. M. Bankole, “The improvement of the index properties and compaction characteristics of lime stabilized tropical lateritic clays with rice husk ash (RHA) admixtures,” *EJGE*, vol. 16, pp. 983–996, 2011.
- [14] J. R. Oluremi, S. I. Adedokun, and O. M. Osuolale, “Stabilization of poor lateritic soils with coconut husk ash,” *International Journal of Engineering Research and Technology*, vol. 1, no. 8, 2012.
- [15] K. J. Osinubi and A. O. Eberemu, “Hydraulic conductivity of lateritic soil treated with blast furnace slag,” *Electronic Journal of Geotechnical Engineering*, vol. 11, pp. 1–16, 2006.
- [16] T. Ako and I. T. Yusuf, “Utilization of palm kernel shell ash as a stabilizer of lateritic soil for road construction,” *Epistemic in Science, Engineering and Technology*, vol. 6, no. 1, pp. 423–433, 2016.
- [17] K. Obeng, K. AG. Ocran, and D. Anaba, “Palm Kernel Shell as fuel for burning bricks,” *Building Resources Information*, vol. 2, no. 5, pp. 131–136, 1997.
- [18] I. N. Ali and U. M. Umar, “An appraisal of spatial distribution of solid waste disposal sites in kano metropolis, Nigeria,” *Journal of Geoscience and Environment Protection*, vol. 5, pp. 24–36, 2017.
- [19] K. A. Ayuba, L. A. Manaf, A. H. Sabrina, and S. W. N. Azmin, “Current status of municipal solid waste management practise in FCT abuja,” in *Research Journal of Environmental and Earth Sciences*, F. C. T Abuja, Ed., vol. 5, no. 6, pp. 295–304, 2013.
- [20] C. M. A. Iwegbue, G. E. Nwajei, J. E. Ogala, and C. L. Overah, “Determination of trace metal concentrations in soil profiles of municipal waste dumps in Nigeria,” *Environmental Geochemistry and Health*, vol. 32, no. 5, pp. 415–430, 2010.
- [21] A. R. Allen, “Sustainability in landfilling: containment versus dilute and disperse,” in *8th Congress of the International Association of Engineering Geologists*, D. P. Moore and O. Hungr, Eds., vol. 4, pp. 2423–2431, Vancouver, Canada, 1998.
- [22] C. S. Nwajide, *Geology of Nigeria’s Sedimentary Basins*, p. 565, CSS Bookshops, Lagos, 2013.
- [23] A. C. Amagu, S. N. Eze, J. Kodama, and M. O. Nweke, “Geological and geotechnical evaluation of gully erosion at Nguzu Edda, Afikpo Sub-basin, southeastern Nigeria,” *Journal of Environment and Earth Science*, vol. 8, no. 12, pp. 148–158, 2018.
- [24] BSI 1377-1, *Methods of Test for Soils for Civil Engineering Purposes (BS 1377: 1990, Parts 1 to 9)*, p. 406, British Standards Institute, London, 1990.
- [25] AASHTO M145-91, *Standard Specifications for Classification of Soils and Soil-Aggregate Mixtures for Highway Construction Purposes*, American Association of State Highway and Transportation Officials, Washington, Wash, USA, 1991.
- [26] L. Y. Li and F. Li, “Heavy metal sorption and hydraulic conductivity studies using three types of bentonite admixes,” *Journal of Environmental Engineering*, vol. 127, no. 5, pp. 420–429, 2001.
- [27] Texas Commission on Environmental Quality Tceq, *Guidance for Liner Construction and Testing for a Municipal Solid Waste Landfill*, p. 37, Waste Permits Division, Municipal Solid Waste Permits Section, Texas, 2017.
- [28] N. Hamdi and E. Srasra, “Hydraulic conductivity study of compacted clay soils used as landfill liners for an acidic waste,” *Waste Management*, vol. 33, no. 1, pp. 60–66, 2013.
- [29] N. N. Nik Daud, A. S. Muhammed, and A. M. Kundiri, “Hydraulic conductivity of compacted granite residual soil mixed with palm oil fuel ash in landfill application,” *Geotechnical & Geological Engineering*, vol. 35, no. 5, pp. 1967–1976, 2017.
- [30] O. Adewale, A. Segun, and A. Ariyo, “Structural evaluation of the effect of pulverized palm kernel shell (PPKS) on cement-modified lateritic soil sample,” *American Journal of Civil Engineering*, vol. 5, no. 4, pp. 205–211, 2017.
- [31] A. N. Amadi, I. A. Okunlola, C. J. Eze, M. O. Jimoh, C. Unueho, and F. Abubakar, “Geotechnical assessment of clay deposits in Minna, North-Central Nigeria for use as liners in sanitary landfill design and construction,” *American Journal of Environmental Protection*, vol. 3, no. 3, pp. 67–75, 2015.
- [32] A. Tuncan, M. I. Onur, K. Akpınar, and M. Tuncan, “Use of sepiolite and zeolite mixtures as a landfill liner,” *International Journal of Wine Research*, vol. 6, no. 1, p. 197, 2016.
- [33] M. Alhassan, “Potentials of rice husk ash for soil stabilization,” *AUJ T*, vol. 11, no. 4, pp. 246–250, 2008.
- [34] D. E. Daniel and Y. K. Wu, “Compacted clay liners and covers for arid sites,” *Journal of Geotechnical Engineering*, vol. 119, no. 2, pp. 223–237, 1993.
- [35] C. J. Miller, H. Mi, and N. Yesiller, “Experimental analysis of desiccation crack propagation in clay liners,” *Journal of the American Water Resources Association*, vol. 34, no. 3, pp. 677–686, 1998.
- [36] C. A. Amagu, C. Zhang, J. Kodama et al., “Displacement measurements and numerical analysis of long-term rock slope

deformation at higashi-shikagoe limestone quarry, Japan,” *Advances in Civil Engineering*, vol. 2021, Article ID 1316402, 15 pages, 2021.

- [37] Y. Y. Tay, D. I. Stewart, and T. W. Cousens, “Shrinkage and desiccation cracking in bentonite-sand landfill liners,” *Engineering Geology*, vol. 60, no. 1-4, pp. 263–274, 2001.

Research Article

Force-Deformation Study on Glass Fiber Reinforced Concrete Slab Incorporating Waste Paper

S. Praburanganathan ¹, N. Sudharsan,² Yeddula Bharath Simha Reddy,¹
Chukka Naga Dheeraj Kumar Reddy ³, L. Natrayan ⁴, and Prabhu Paramasivam ⁵

¹School of Civil Engineering, REVA University, Bengaluru, India

²Department of Civil Engineering, Vidya Jyothi Institute of Technology, Hyderabad, India

³Department of Civil Engineering, Aditya College of Engineering and Technology, Surampalem, India

⁴Department of Mechanical Engineering, Saveetha School of Engineering, SIMATS, Chennai, Tamil Nadu 602105, India

⁵Department of Mechanical Engineering, College of Engineering and Technology, Mettu University, Mettu, Ethiopia

Correspondence should be addressed to S. Praburanganathan; praburanganathan.s@reva.edu.in, Chukka Naga Dheeraj Kumar Reddy; dheerukumbi@gmail.com, and Prabhu Paramasivam; prabhuparamasivam21@gmail.com

Received 11 November 2021; Revised 15 December 2021; Accepted 22 December 2021; Published 12 January 2022

Academic Editor: Md. Akter Hosen

Copyright © 2022 S. Praburanganathan et al. This is an open access article distributed under the Creative Commons Attribution License, which permits unrestricted use, distribution, and reproduction in any medium, provided the original work is properly cited.

This study inspects the viability of engaging the discarded paper wastes in concrete by varying the volume proportions from 0%–20% with each 5% increment in replacement of the weight of cement. A biomechanical study was conducted, and the results were presented. A glass fiber reinforced rectangular slab with a longer span (l_y) to shorter span (l_x) ratio of ($l_y:l_x$) 1.16 was cast with optimum replacement of waste-paper mass and compared the force-deformation characteristics with the conventional concrete slab without waste paper. The optimum percentage of discarded papers for the replacement of cement is 5%. Also, the results imply that the compressive strength at the age of 28 days is 30% improved for the optimum replacement. Based on the outcomes of the investigation, it can be inferred that the compressive strength gets progressively reduced if the volume of the discarded paper gets increases. The incorporation of glass fibers improves the split and flexural strength of the concrete specimens considerably. The ultimate load-carrying capacity of the glass fiber reinforced waste paper incorporated concrete slab measured 42% lower than that of the conventional slab. However, development of the new type of concrete incorporating waste papers is the new trend in ensuring the sustainability of construction materials.

1. Introduction

Currently, a huge volume of concrete is used in construction due to its properties of easy molding, higher strength, and durability characteristics [1]. However, due to the usage of cement in concrete production, the emissions and carbon footprint are ever increasing [2]. Hence, concrete technology is under constant pressure to innovate novel concrete which has minimalistic emission properties. There are several new types of concrete under research. Also, the accumulation of waste materials from municipal and industrial sources is increasing day by day [3].

The disposal of these waste materials is a point of concern for every municipality or industry [4]. As per the

Central Pollution Control Board of India, the per capita production of solid waste is 0.26–0.85 kg/day [5]. Studies reveal that 70–80% of solid wastes are directly dumped as landfills [6]. Direct landfilling creates environmental issues and health hazards depending on the nature of the waste materials [7]. The optimum solution for this problem is to use the waste material in the construction products [8]. As per the Confederation of European Paper Industries, the paper industry waste is predominantly used in landfills [9], energy recovery, and is used on composting or land spreading [10]. As per the existing research of Agulló et al. [11] and Ahmadi and Al-Khaja [12], the paper pulp has been used as the replacement of mineral filler material in concrete mixes. As per the record, the world paper production is

around 400 million tons, and it can increase to another 100 million tons in the year 2050 [13]. The disposal of paper waste involves social and economic constraints [14]. The paper waste can be used in bioplastics [15], asphalt [16] and cement products [17], and adsorbent production [18]. As per the latest study of Karimi et al. [19], the paper mass can also be used as a viscosity modifying agent in cement-based materials [20]. Numerous studies are focusing on the energy management [21] and energy efficiency [22] of paper pulp-based products; however, the available literature on using paper waste in the production of concrete products is scarce [23]. Existing research focused towards the use of paper waste with the ordinary portland cement and water mix. This kind of product was termed "Paper Crete." With the use of this new material, blocks were manufactured and tested for the structural properties such as modulus of elasticity and thermal and bond characteristics [24, 25].

Also, Agulló et al. [11] conducted a study based on the incorporation of paper pulp sludge in plaster composite mixtures, and the authors concluded that the wet paper sludge needs to be dried for obtaining good mechanical and rheological characteristics. However, the discarded paper waste concrete is an innovative type of concrete manufactured with the basic ingredients of normal concrete with partial substitution of waste papers in place of cement [22]. It can be inferred from the earlier research that with the use of waste papers, the final product can be obtained with a reduced density [26], improved acoustic [27], and heat insulation characteristics [28]. The disadvantage reported by adding the paper mass is the higher water absorption. By adjusting the water-cement ratio, the concrete can be produced with an equal density as that of conventional concrete. Also, it is suggested to use this material as a roofing element with the addition of necessary reinforcement [29]. The strengthening may be of either (a) chicken wire mesh, (b) glass fibers, or (c) wooden fibers [30]. According to an earlier study, the waste paper mass was mixed with conventional concrete mixture with and without fly ash, kaolin, clay, Rice Husk Ash (RHA), SiO_2 , and Quartz powder, and physical and mechanical properties were studied, and it was determined that the use of paper induces the reduction in strength properties of concrete. Hence, it was advised to add reinforcements in any form to improve the strength of paper concrete [31]. In this paper, an attempt has been made to engage the glass fibers as reinforcement in the paper concrete. As per the study of Madhkhan and Katirai [32], the incorporation of glass fibers improves the mechanical properties of the final concrete. Waste papers are used as a partial replacement of cement, and the mechanical properties are assessed including the compressive strength, split tensile strength, and flexural strength. These results are compared with specimens containing the glass fibers.

2. Raw Materials and Brick Mixture Proportions

Portland cement of 53-grade cement as per BIS 1489 standards [33] is used for this investigation. Crushed stone aggregates with 20 mm passing and a 12.5 mm retaining on the Indian Standard (IS) sieve are used. The specific gravity

of the aggregate is recorded as 2.62. Natural sand with a specific gravity of 2.6 is engaged for the experimental investigations. The paper mass used for the study has undergone preprocessing stages obtained through several stages. Initially, the discarded waste paper was soaked in water for a minimum period of 72 hours. After obtaining the wet mass, it is ground into fine mass using the wet grinder. The paper mass was sun dried for 24 hours before obtaining the final product (Figure 1). Water-dispersible chopped glass fiber of density 2600 kg/m^3 has been used with the optimum volume proportion of 4%. Figure 2 shows the dispersing process of glass fibers in the concrete. Table 1 presents the properties of water-dispersible chopped glass fibers. Tables 2 and 3 present the physical and chemical properties of the waste paper used in the present investigation.

A concrete mix design of M25 grade corresponding to BIS 10262-2019 standards is engaged with a mix ratio of 1:1.12:2.746 and limited the water/cement ratio to 0.44. Table 4 shows the mix proportions for 1 cu.m. of concrete. Accordingly, the fine aggregate and coarse aggregate volume are fixed as 500 kg/m^3 and 1223 kg/m^3 .

3. Methods

To understand the mechanical properties of discarded waste paper concrete with and without glass fiber addition, specimens were cast by varying the paper residues of different percentages of 0%, 5%, 10%, 15%, and 20% of the weight of cement. After finding the initial set of outcomes, a constant 4% volume of glass fiber reinforcement has been added to all the different percentage paper residue mixes, and then, the strength properties have been analyzed.

The dry density of the concrete samples is found by heating the sample in the oven for 48 hours at the temperature of 90°C , and each sample was weighed for the dry weight. The saturated weight of the sample was found by immersing the specimens in the water tank for three complete days. After the soaking period, the specimens were removed and wiped with a dry cloth and weighed with a digital balance. From the saturated weight and the dry weight, the percentage of absorption was computed.

Compressive strength of the concrete cubes (150 mm) was found at the curing age of 28 days subject to the vertical load under the compression testing machine. The splitting tensile strength of the cylinder (150 mm diameter and 300 mm high) was obtained for each sample by placing the cylinder specimen horizontally and applying a compressive force on the specimen. The flexure strength of the prism ($100 \times 100 \times 410 \text{ mm}$) was obtained by testing a prism at the curing age of 28 days. The casting of the slab is shown in Figure 3.

Two numbers of two-way slabs of l_y/l_x ratio - 1.16 are cast, out of which one slab is cast with conventional mix and the other with optimum replacement of paper mass with water-dispersible glass fiber. The overall dimensions of the slab are $1200 \times 1400 \times 75 \text{ mm}$ with 6 mm diameter reinforcements at 150 mm C/C distance. The support edge condition is simply supported in all corners. The test is performed under a loading frame. A hydraulic loading Jack

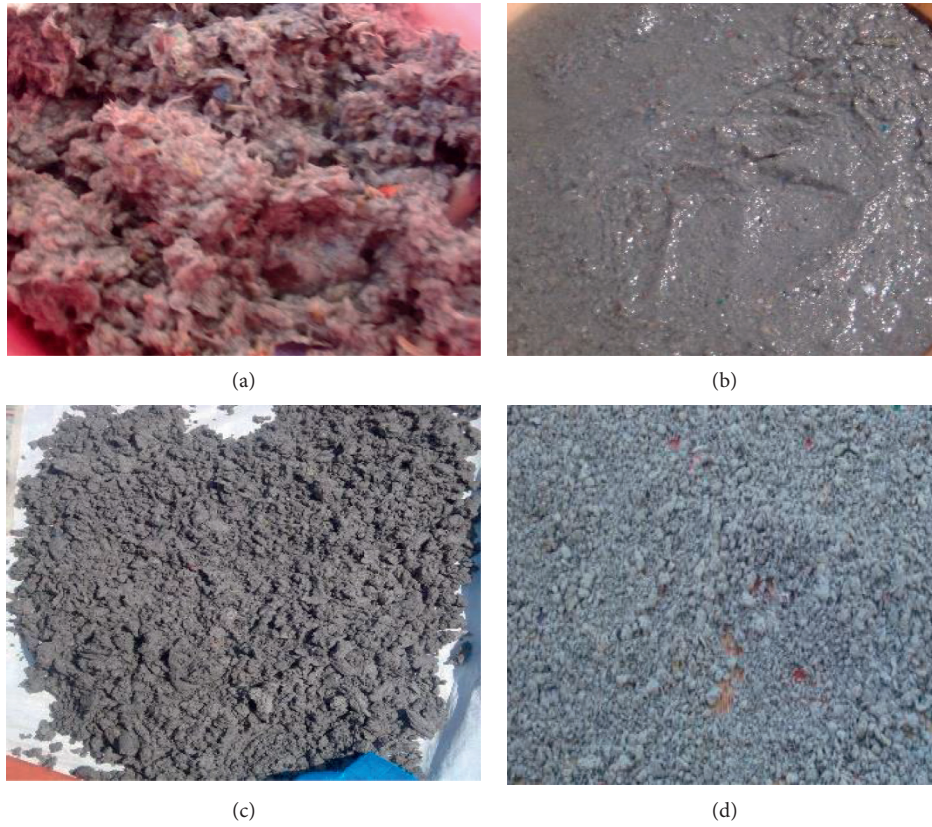


FIGURE 1: Preprocessing process of paper waste. (a) Wet mass. (b) After grinding. (c) During sun drying. (d) Final mass.

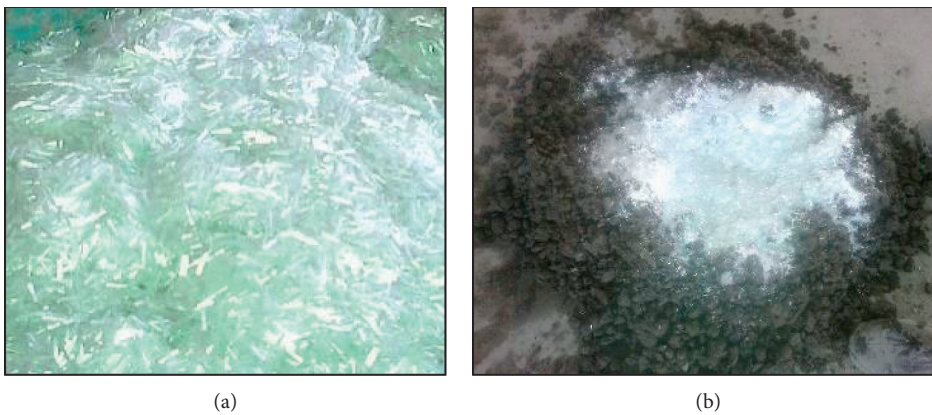


FIGURE 2: Glass fiber mixing procedure. (a) Dispersing of the glass fiber in the water; (b) mixing with concrete.

is fitted under the loading frame followed by a load spreader. Seven numbers of steel 'I' section are placed below the load spreader for load distribution. Ten numbers of mild steel rods larger than slab dimensions are placed in longitudinal and transverse directions. Slabs are positioned in an upright position so that the movement in horizontal and vertical directions is restricted. A linear variable differential transducer (LVDT) is fixed at the midpoint of the slab to observe the deformation of the slab during the vertical monotonic loading. The load is applied at each 4 kN increment. The displacement is noted in each load level. A load indicator is attached, and the corresponding deformation is measured

TABLE 1: Properties of glass fiber.

Description	Property
Type of glass fiber	Chopped strand
Fiber length	6 mm
Moisture (%)	0.2
Sizing/Coupling system	Starch-based
Loss on ignition (%)	0.7

through a data logger. Figure 4(a) presents the test setup of the slab under a loading frame. Figure 4(b) shows a view of LVDT placed at the middle of the slab.

TABLE 2: Physical Properties of waste paper mass.

Physical properties	Value
Density	798 (g/cu.m)
Absorption (%)	89%
Specific gravity	0.98

TABLE 3: Chemical properties of waste paper mass (XRF analysis).

Composition	%
Carbon-di-oxide	86.2
Silicon-di-oxide	5.6
Aluminium oxide	6.95
Magnesium oxide	1.25

4. Results and Discussion

4.1. Physical Properties

4.1.1. Percentage of Water Absorption. The test results of the water absorption test are shown in Figure 5. It is observed that if the percentage of paper mass gets increased, the water absorption also increased. This is due to the phenomenon of absorbing more water by the added paper mass. The results also implied that the addition of glass fiber reinforcement comparatively reduces the percentage of water absorption of the specimens. The maximum water absorption of 16.7% and 12.55% is observed in the cases with and without glass fiber addition, respectively. The reason for the higher absorption is due to the paper waste that contains the cellulose materials and thereby absorbs water and retains it for a longer time [34, 35].

4.1.2. Bulk Density. The results indicate that if the level of paper mass increases, the dry density gets reduced irrespective of with/without glass fiber addition. Figure 6 presents the test results of the concrete specimens at the age of 28 days. The density of the samples ranges between 2041 and 2548 kg/m³ with glass fiber reinforcement. The density of concrete specimens without glass fiber incorporation displayed higher values than the latter. The lower density of paper mass causes a decrease in density and higher incorporation of paper mass into the concrete mixes [34].

4.2. Mechanical Properties

4.2.1. Compressive Strength. Figure 7 presents the compressive strength test results at the age of 28 days. The results infer that the 5% replacement of paper mass showed enhanced compressive strength, and further replacement beyond this point tends to reduce the strength of the concrete specimens. In the case of the glass fiber added concrete specimens, the increased addition of waste paper gradually decreases the compressive strength. 5% replacement of paper mass provides 30.4% enhanced compressive strength at the age of 28 days than the conventional mix. However, 10%, 15%, and 20% replacement levels show 40%, 66.4%,

TABLE 4: Mix proportions for the waste paper concrete.

Substitution (%)	Paper (kg)	Cement (kg)	Sand (kg)	Coarse aggregate (kg)	Water (kg)
0	0	445			196
5	22	423			186
10	44	401	500	1223	176
15	66	379			166
20	89	356			156

and 93.6% reduction in strength. Therefore, it can be concluded that the 5% replacement of paper mass with cement is the optimum replacement. This might be due to its dense microstructure which is evident from the micrograph (Figure 8) [3]. Paper is a natural polymer, and it contains abundant wood cellulose. Also, cellulose is in the form of sugar. In the polymeric chain links, it contains several hydroxyl groups. The reason for the compressive strength enhancement at 5% replacement level is the hydrogen bonding that coated with the cement matrix. For higher replacement levels, by applying the load, the hydrogen bond among the molecules of cellulose and water got broken and the reduction in strength occurred. Also, up to the optimum level, the water absorption by the paper mass promotes the water supply internally to the concrete mix, and more water is available for the hydration process and thereby improving mechanical characteristics. [34].

4.2.2. Split Tensile Strength. Figure 9 presents the test results of the split tensile strength of concrete specimens. The maximum split tensile strength is achieved at 5% substitution of paper mass, and further increases in the paper mass decrease the strength. However, the addition of glass fiber reinforcement increases the split tensile strength in all the percentage replacement of paper mass. The replacement of 10,15, and 20% of paper mass provides a reduction in split tensile strength of 23%, 40%, and 83% at the age of 28 days compared to the conventional specimens. However, the addition of glass fibers increased the split tensile strength upto 15% replacement levels. An increase in the split tensile strength of 25%, 40%, and 60% was observed at 5,10, and 15% of glass fiber reinforcement addition. This increment in strength is due to the glass fibers that effectively filled the voids in the concrete and thereby interlocking of constituent materials of the concrete matrix. These results are in agreement with the previous work [34].

4.2.3. Flexural Strength. From Figure 10, it can be inferred that the addition of glass fiber reinforcement enhanced the 28-day flexural strength of concrete. The optimum percentage is observed at the 5% replacement. Further addition of glass fibers tends to reduce the flexural strength of specimens. It can be observed that the 5% replacement of paper mass showed an increased strength of 21.69% at the age of 28 days. The increased incorporation of paper mass tends to reduce the flexural strength after the optimum replacement level of 5%. An increase in the flexural strength



FIGURE 3: A view of making of waste paper concrete slab. (a) Conventional mix. (b) Glass-fiber reinforced mix.

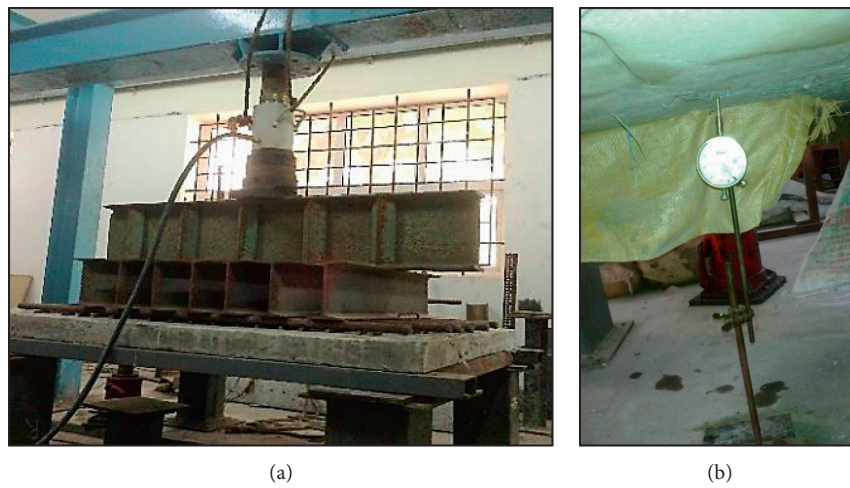


FIGURE 4: (a) Test setup of the slab under a loading frame. (b) LVDT at the middle of slab.

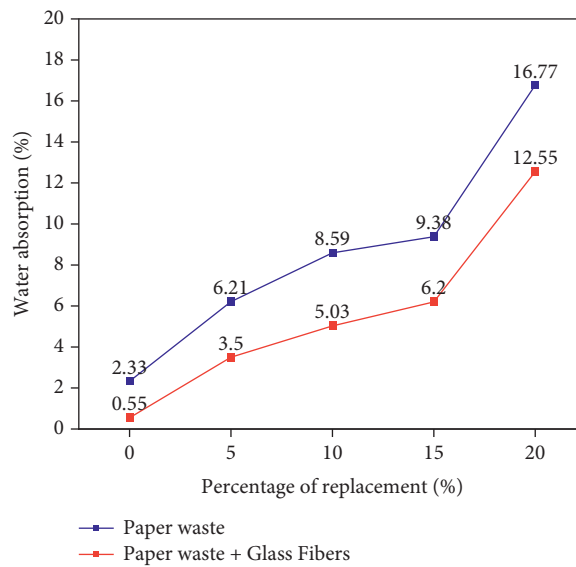


FIGURE 5: Water absorption test results.

of 13.36% is noted at the optimum replacement level. A reduction in the strength of 7.47%, 64.03%, and 87% was noted for the 10%, 15%, and 20% replacement levels. The

reason for this reduction in the flexural strength may be due to the higher porosity of the waste papers which leads to more void space inside the matrix. [34].

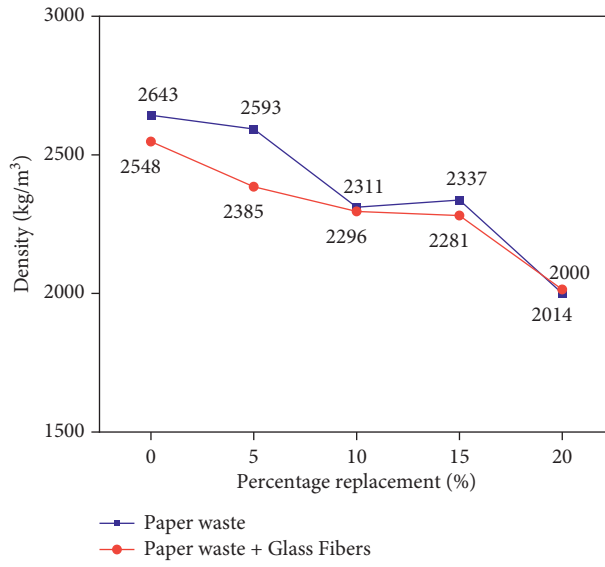


FIGURE 6: Bulk density results.

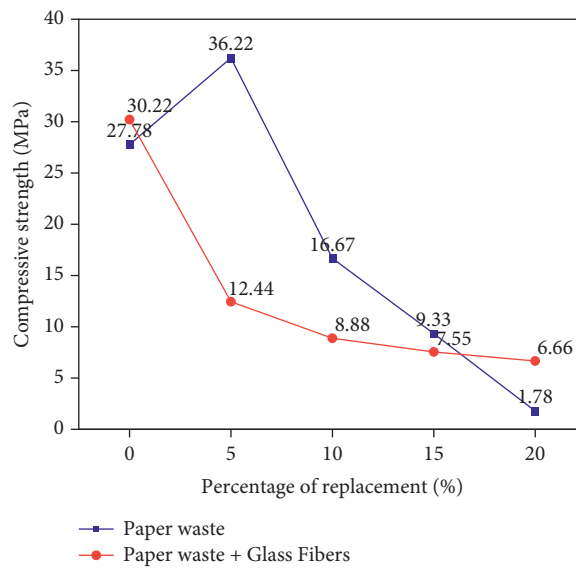


FIGURE 7: Test results of compressive strength.

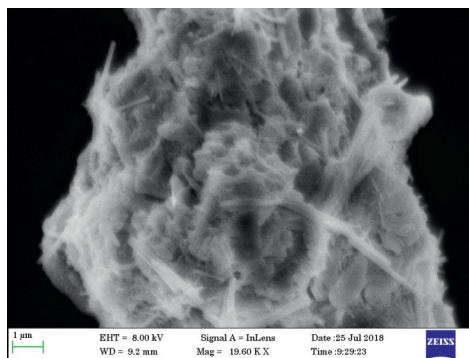


FIGURE 8: Micrograph of the optimum mix.

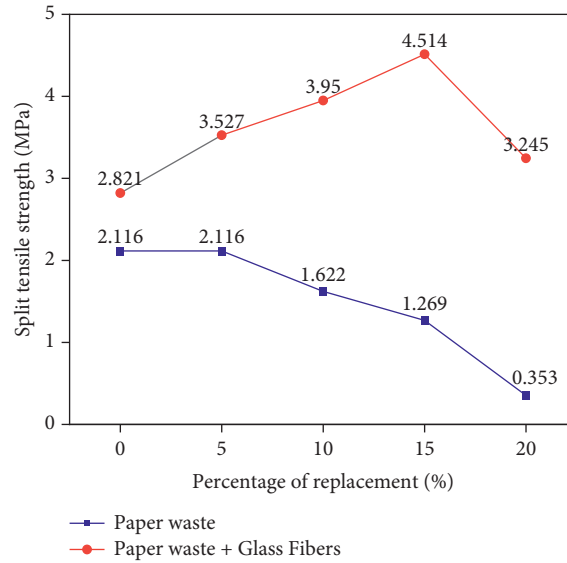


FIGURE 9: Split tensile strength results.

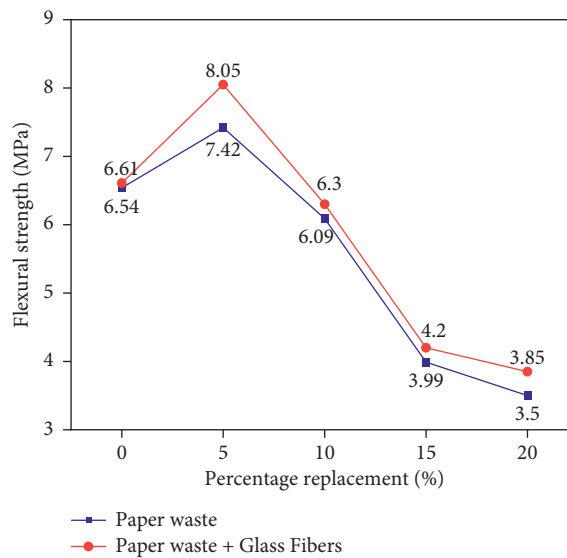


FIGURE 10: Flexural strength results.

4.2.4. Force-Deformation Characteristics of Slab Element.

A vertical monotonic load is applied through a pumping unit. The deformation of the slab is measured in each 4 kN load increment. The corresponding deformation properties are measured through the LVDT attached data acquisition system. Figure 11 presents the force-deformation characteristics of slab elements. The ultimate load-carrying capacity of the conventional slab without paper mass and glass fiber is 380 kN, whereas the slab which contains the paper mass sustains the ultimate load of 220 kN. Also, it is observed that the ultimate deflection corresponding to the ultimate load is 32.9 mm and 27.5 mm, respectively, for conventional and glass fiber reinforced paper concrete slabs.

Figure 12(a) represents the deflected configuration of the conventional slab, and Figures 12(b) and 12(c) represent the typical crack pattern observed along the breadth

and depth of the slab specimen, respectively. Figure 13 displays the brittle collapse of the glass fiber reinforced paper concrete slab. The stiffness of the glass fiber reinforced paper concrete slab is comparatively lesser than the conventional slab without paper mass addition. Also, in the higher magnitudes of load progresses, massive and wider cracks with large crack widths are observed in the glass-fiber reinforced paper concrete slab. However, in the conventional slab, the crack widths are less significant. The addition of waste paper mass disrupts the constituent materials in the concrete matrix. This makes the ingredients get weaker and loosen the compactness. Under the load increment, it magnifies the crack width and leads to enhanced and significant wide width of cracks. This phenomenon is comparatively lesser in the case of the conventional slab.

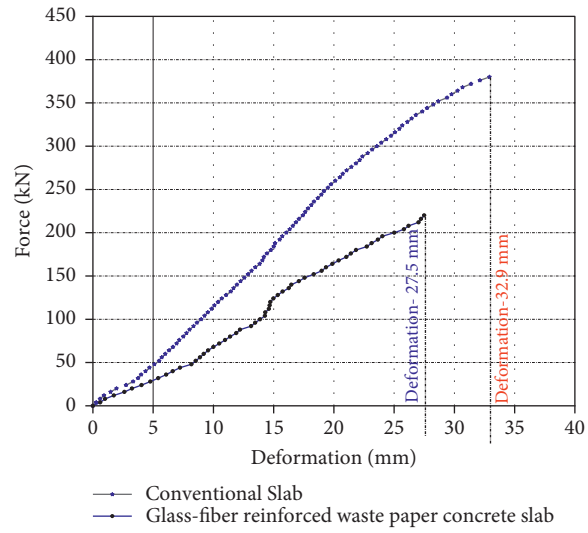


FIGURE 11: Force-deformation characteristics of the slab.

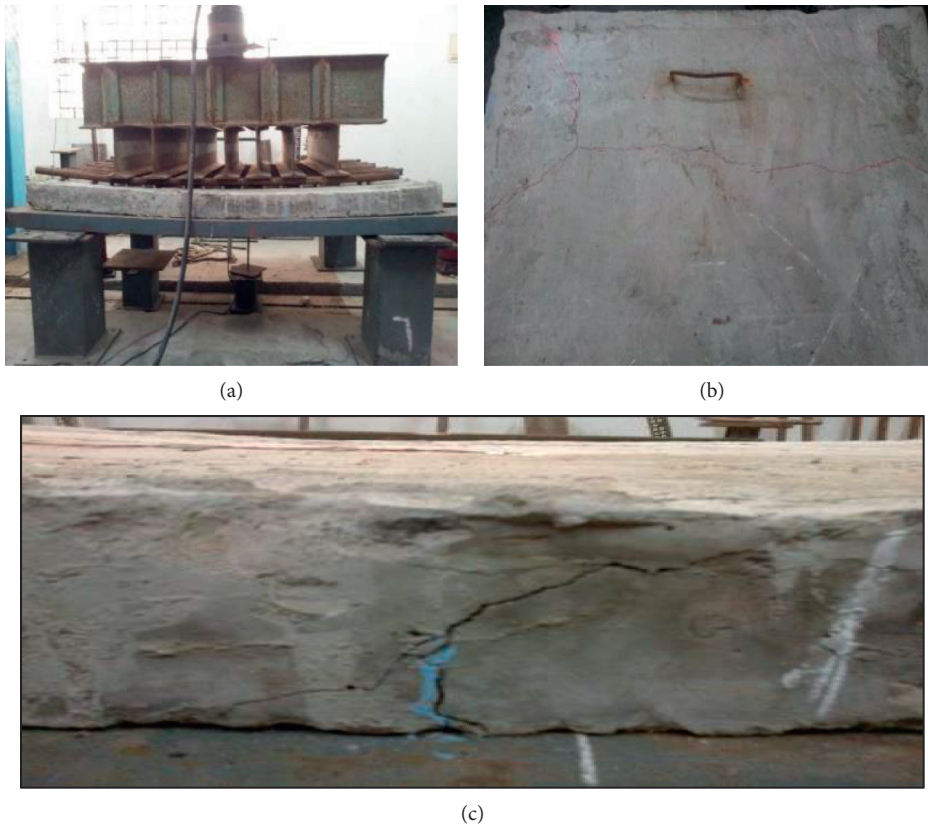


FIGURE 12: Failure pattern of the conventional slab. (a) Deflected configuration. (b) Crack propagation along the width. (c) Crack extension through the depth of the slab.



FIGURE 13: Final brittle collapse of glass fiber reinforced paper mass slab.

5. Conclusions

From the attained results, the following conclusions were drawn:

- (i) The increase in the incorporation of paper mass tends to increase the percentage of water absorption gradually. However, the addition of glass-fiber reinforcement minimizes the water absorption characteristics for all the mixes. With the 0, 5, 10, 15, and 20% of paper mass replacement, there is an increase of 2.33%, 6.21%, 8.58%, 9.37%, and 16.77% water absorption, respectively.
- (ii) The incorporation of paper waste in the specimen made it denser by nearly 21%.
- (iii) The addition of paper waste in the mix leads to the increase in strength of the specimen by 30.4%. The optimum value of the replacement is observed at 5%. A similar trend is observed in the tensile and flexural strength results.
- (iv) The addition of glass fibers upto 15% improves the split tensile strength of the mix.
- (v) Wider cracks and brittle types of failure are observed in the paper waste-based concrete slab. However, in the conventional slab, cracks along the width and depth of the specimens are noted. Though the first crack load is observed in an earlier stage in the conventional slab than the paper concrete slab, the load-deformation analysis implies that the paper waste-based concrete slab sustains a lower ultimate load than the conventional slab.
- (vi) Therefore, it is concluded that the addition of paper waste in the structural elements such as slab is not recommended for the usage of high load scenarios.

Data Availability

The data used to support the findings of this study are included within the article.

Conflicts of Interest

The authors declare that there are no conflicts of interest regarding the publication of this paper.

Acknowledgments

The authors thank REVA University, Bengaluru, for the technical assistance. The authors appreciate the support from Mettu University, Ethiopia. It was performed as a part of the Employment of Mettu University, Ethiopia.

References

- [1] B. Ali, L. A. Qureshi, and S. U. Khan, "Flexural behavior of glass fiber-reinforced recycled aggregate concrete and its impact on the cost and carbon footprint of concrete pavement," *Construction and Building Materials*, vol. 262, Article ID 120820, 2020.
- [2] G. K. Gupta and P. Shukla, "Insights into the resources generation from pulp and paper industry wastes: challenges, perspectives and innovations," *Bioresource Technology*, vol. 297, Article ID 122496, 2020.
- [3] A. Ahmad, "Paper sludge, an environmentally sound alternative source of MK-based cementitious materials. A review," *Construction and Building Materials*, vol. 22, no. 7, pp. 37–48, 2008.
- [4] R. Joshi and S. Ahmed, "Status and challenges of municipal solid waste management in India: a review," *Cogent Environmental Science*, vol. 2, no. 1, pp. 1139434–1139518, 2016.
- [5] Akhilesh Kumar and Avlokita Agrawal, "Recent trends in solid waste management status, challenges, and potential for

- the future Indian cities–A review,” *Current Research in Environmental Sustainability*, vol. 2, p. 100011, 2002.
- [6] I. J. Ahluwalia and U. Patel, “Working paper No . 356 solid waste management in India an assessment of resource recovery and environmental impact isher judge ahluwalia,” *Indian Counc. Res. Int. Econ. Relations*, vol. 356, pp. 1–48, 2018.
 - [7] A. Kumar and A. Agrawal, “Recent trends in solid waste management status, challenges, and potential for the future Indian cities - a review,” *Current Research in Environmental Sustainability*, vol. 2, Article ID 100011, 2020.
 - [8] A. Gholampour, T. Ozbakkaloglu, O. Gencel, and T. D. Ngo, “Concretes containing waste-based materials under active confinement,” *Construction and Building Materials*, vol. 270, no. xxxx, Article ID 121465, 2021.
 - [9] N. M. Ngwabie, Y. L. Wirten, G. S. Yinda, and A. C. VanderZaag, “Quantifying greenhouse gas emissions from municipal solid waste dumpsites in Cameroon,” *Waste Management*, vol. 87, pp. 947–953, 2019.
 - [10] F. N. Andrés, L. B. Beltrami, A. G. Guillarducci, M. S. Romano, and N. O. Ulibarrie, “Lightweight concrete: an alternative for recycling cellulose pulp,” *Procedia Materials Science*, vol. 8, pp. 831–838, 2015.
 - [11] L. Agulló, A. Aguado, and T. Garcia, “Study of the use of paper manufacturing waste in plaster composite mixtures,” *Building and Environment*, vol. 41, no. 6, pp. 821–827, 2006.
 - [12] B. Ahmadi and W. Al-Khaja, “Utilization of paper waste sludge in the building construction industry,” *Resources, Conservation and Recycling*, vol. 32, no. 2, pp. 105–113, 2001.
 - [13] P. Faubert, S. Barnabé, S. Bouchard, R. Côté, and C. Villeneuve, “Pulp and paper mill sludge management practices: what are the challenges to assess the impacts on greenhouse gas emissions?” *Resources, Conservation and Recycling*, vol. 108, pp. 107–133, 2016.
 - [14] M. Likon, F. Cernec, J. Saarela, T. F. Zimmie, and J. Zule, “Use of paper mill sludge for absorption of hydrophobic substances,” in *Proceedings of the 2nd International Conference on New Developments in Soil Mechanics and Geotechnical Engineering*, pp. 526–533, Lefkosa, North Cyprus, 2009.
 - [15] J. Soucy, A. Koubaa, S. Migneault, and B. Riedl, “The potential of paper mill sludge for wood-plastic composites,” *Industrial Crops and Products*, vol. 54, pp. 248–256, 2014.
 - [16] M. Pervaiz and M. Sain, “Recycling of paper mill biosolids: a review on current practices and emerging biorefinery initiatives,” *Clean - Soil, Air, Water*, vol. 43, no. 6, pp. 919–926, 2015.
 - [17] S. Yan, K. Sagoe-Crentsil, and G. Shapiro, “Reuse of de-inking sludge from wastepaper recycling in cement mortar products,” *Journal of Environmental Management*, vol. 92, no. 8, pp. 2085–2090, 2011.
 - [18] W. Li, Q. Yue, P. Tu et al., “Adsorption characteristics of dyes in columns of activated carbon prepared from paper mill sewage sludge,” *Chemical Engineering Journal*, vol. 178, pp. 197–203, 2011.
 - [19] H. Karimi, F. Gauvin, H. J. H. Brouwers, R. Cardinaels, and Q. Yu, “On the versatility of paper pulp as a viscosity modifying admixture for cement composites,” *Construction and Building Materials*, vol. 265, Article ID 120660, 2020.
 - [20] S. Haider, M. S. Danish, and R. Sharma, “Assessing energy efficiency of Indian paper industry and influencing factors: a slack-based firm-level analysis,” *Energy Economics*, vol. 81, pp. 454–464, 2019.
 - [21] F. Corcelli, J. Vehmas, and S. Ulgiati, “Energy efficiency and environmental assessment of papermaking from chemical pulp - a Finland case study,” *Journal of Cleaner Production*, vol. 198, pp. 96–111, 2018.
 - [22] V. S. Nadh, C. Krishna, L. Natrayan et al., “Structural behavior of nanocoated oil palm shell as coarse aggregate in lightweight concrete,” *Journal of Nanomaterials*, vol. 2021, Article ID 4741296, 7 pages, 2021.
 - [23] N. D. K. R. Chukka, L. Natrayan, and W. D. Mammo, “Seismic fragility and life cycle cost analysis of reinforced concrete structures with a hybrid damper,” *Advances in Civil Engineering*, vol. 2021, Article ID 4195161, 17 pages, 2021.
 - [24] B. Fuller, A. Fafitis, and J. Santamaria, “Structural properties of a new material made of waste paper,” *Build. Integr. Solut.*, vol. 3, 2006.
 - [25] S. A. S. I. N. Gorgis, “Properties of papercrete,” *ARN J. Eng. Appl. Sci.* vol. 12, no. 24, pp. 7401–7411, 2017.
 - [26] A. Lawrence, T. Nehler, E. Andersson, M. Karlsson, and P. Thollander, “Drivers, barriers and success factors for energy management in the Swedish pulp and paper industry,” *Journal of Cleaner Production*, vol. 223, pp. 67–82, 2019.
 - [27] P. Bajpai, “Uses of recovered paper other than papermaking,” *Recycling and Deinking of Recovered Paper*, vol. 16, pp. 283–295, 2014.
 - [28] D. Gavrilescu, “Energy from biomass in pulp and paper mills,” *Environmental Engineering and Management Journal*, vol. 7, no. 5, pp. 537–546, 2008.
 - [29] Z. Yuan and Y. Jia, “Mechanical properties and microstructure of glass fiber and polypropylene fiber reinforced concrete: an experimental study,” *Construction and Building Materials*, vol. 266, Article ID 121048, 2021.
 - [30] T. Simões, H. Costa, D. Dias-da-Costa, and E. Júlio, “Influence of fibres on the mechanical behaviour of fibre reinforced concrete matrixes,” *Construction and Building Materials*, vol. 137, pp. 548–556, 2017.
 - [31] N. M. Ayash, A. M. Abd-Elrahman, and A.-E. Soliman, “Repairing and strengthening of reinforced concrete cantilever slabs using Glass Fiber-Reinforced Polymer (GFRP) wraps,” *Structures*, vol. 28, pp. 2488–2506, 2020.
 - [32] M. Madhkhan and R. Katirai, “Effect of pozzolanic materials on mechanical properties and aging of glass fiber reinforced concrete,” *Construction and Building Materials*, vol. 225, pp. 146–158, 2019.
 - [33] BIS:1489 (Part 1), *Portland-pozzolana Cement-Specification*, Bur. Indian Stand., New Delhi, India, 1991.
 - [34] S. R. Ahmedizat, A. B. Al-Zubaidi, and A. A. Al-Tabbakh, “Fabrication green concrete by Recycled wastepaper,” *IOP Conference Series: Materials Science and Engineering*, vol. 870, no. 1, Article ID 012146, 2020.
 - [35] T. Cardinale, M. D’Amato, R. Sulla, and N. Cardinale, “Mechanical and physical characterization of papercrete as new eco-friendly construction material,” *Applied Sciences*, vol. 11, no. 3, pp. 1011–11, 2021.